Winter 2-24-2016

Field Geology and Petrologic Investigation of the Strawberry Volcanics, Northeast Oregon

Arron Richard Steiner
Portland State University

Field Geology and Petrologic Investigation of the Strawberry Volcanics, Northeast Oregon

by

Arron Richard Steiner

A dissertation submitted in partial fulfillment of the
requirements for the degree of

Doctor of Philosophy
in
Environmental Sciences and Resources: Geology

Dissertation Committee:
Martin J. Streck, Chair
Michael L. Cummings
Jonathan Fink
John A.Wolff
Dirk Iwata-Reuyl

Portland State University
2016

ABSTRACT

The Strawberry Volcanics of Northeast Oregon are a group of geochemically related lavas with a diverse chemical range (basalt to rhyolite) that erupted between 16.2 and 12.5 Ma and co-erupted with the large, (~200,000 km^3) Middle Miocene tholeiitic lavas of the Columbia River Basalt Group (CRBG), which erupted near and geographically surround the Strawberry Volcanics. The rhyolitic lavas of the Strawberry Volcanics produced the oldest $^{40}Ar/^{39}Ar$ ages measured in this study with ages ranging from 16.2 Ma to 14.6 Ma, and have an estimated total erupted volume of 100 km^3. The mafic and intermediate lavas of the Strawberry Volcanics include both tholeiitic and calc-alkaline compositions; calc-alkaline andesite is the dominant type by volume. $^{40}Ar/^{39}Ar$ ages of the mafic and intermediate lava flows range from 15.6 Ma to 12.5 Ma, and volume estimates of the intermediate lavas are approximately 1,100 km^3. The magmas that gave rise to the Strawberry Volcanics traveled to the surface through numerous dikes, some of which have been exposed at the surface and supplied lava to fissure – style eruptions and/or shield volcanoes. Herein, we show that the Strawberry Volcanics are related to the CRBG in both time and space and share a chemical affinity, specifically to the Steens Basalt. Chemical similarities are observed in normalized trace element patterns, selected trace element ratios, and radiogenic isotopes. Comparison of the Strawberry Volcanic rhyolites to the other Middle Miocene rhyolites of eastern Oregon associated with the initiation of the Yellowstone – Snake River mantle plume reveals similar eruption ages, trace element compositions, including the rare earth elements (REEs), and “A-type”

rhyolite characteristics. These data suggest that the Strawberry Volcanics are part of the regional volcanism (basalt to rhyolite) of the Columbia River Basalt Province. The petrogenesis of the Strawberry Volcanics can be explained as follows: 1) The tholeiitic, intermediate magmas were produced by fractional crystallization of mafic magmas, which have a commonality with the surrounding Columbia River Basalt Group; 2) The calc-alkaline magmas are a result of mixing between tholeiitic basalt, rhyolite, and crust. The arc-like signature of the calc-alkaline lavas (elevated large ion lithophiles) is a result of both the melting source region and the end-members with which the mafic magmas mixed/contaminated. Other authors have produced similar findings from within the Basin and Range/Oregon-Idaho graben and CRB province. The difference at the Strawberry Volcanics is that there is no need for a primitive calc-alkaline magma or extensive fractional crystallization to generate the calc-alkaline andesite series. Alternatively, the calc-alkaline magmas of the Strawberry Volcanics were generated by a more primitive tholeiitic magma than erupted at the surface, which interacted with crustal melts and assimilated crustal lithologies from the complex zone of assimilated terranes that make up the basement of eastern Oregon.

ACKNOWLEDGMENTS

The author would like to express a sincere appreciation of gratitude to the academic committee members: Martin Streck, Michel Cummings, Jonathan Fink, John Wolff and Dirk Iwata-Reuyl. I would like to further thank Martin Streck for providing opportunities to study at Portland State University and working tirelessly with me on edits for this dissertation. The work for Chapters 1, 2 and 3 were supported by: NSF-EAR grant #1220676; PSU Faculty Enhancement grant to Streck; and 2011 GSA research grant # 9579-11. I would also like to thank Mark Ferns for our discussions of eastern Oregon geology, Richard M. Conrey, Charles M. Knaack and Scott Boroughs at Washington State University for their assistance in whole rock geochemical XRF and ICP-MS analysis; Frank Ramos at New Mexico State University for Isotope analysis, Frank Tepley and Dale Burns at Oregon State University for the EMP analysis, Bob Duncan, Anthony Koppers and Dan Miggins for age analysis at Oregon State University, Dale Burns for his thoughtful insights, excellent field company and stimulating conversation regarding this research and including all geology. And to Ashley Van Hoose/Steiner, thanks for excellent field assistance and superior editing and comments along the way. Thank you for supporting me in every way. I would also like to thank Eric Christiansen and Esteban Gazel for their comments and edits that helped to improve the final published manuscript of Chapter 1, along with Arturo Gomez-Tuena for his editorial handling and additional comments towards the publishment of Chapter 1. Lastly, I would like to thank my family. Without their love and support this could not have happened. Thank You.

TABLE OF CONTENTS

LIST OF TABLES

LIST OF FIGURES

CHAPTER 1

*THE STRAWBERRY VOLCANICS: GENERATION OF 'OROGENIC' ANDESITES FROM THOLEIITE WITHIN AN INTRA-CONTINENTAL VOLCANIC SUITE CENTERED ON THE COLUMBIA RIVER FLOOD BASALT PROVINCE, USA.

Abstract

The widely distributed, mid-Miocene lavas of the Strawberry Volcanics of NE Oregon are compositionally diverse ranging from basalt to rhyolite. They are mainly composed of calc-alkaline and mildly tholeiitic basaltic andesite and andesite. Ar-Ar dating and stratigraphic relationships indicate that the volcanic field was active from >16 Ma to ~12 Ma and thus is coeval for the first 1-2 m.y. with strongly tholeiitic flood basalts of the Columbia River Province that encircle the Strawberry Volcanics. Tholeiitic and calc-alkaline compositions develop subtle but noticeable differences towards higher silica contents. At silica contents of <55 wt.% SiO_2, calc-alkaline and tholeiitic lavas are essentially indistinguishable. Trace element constraints among Strawberry Volcanics and crustal rocks indicate that open-system processes such as assimilation or magma mixing are responsible for evolution along a calc-alkaline trend leading to 'orogenic' andesites from tholeiite. Exclusively tholeiitic basalts carrying evidence for a metasomatized mantle source erupted during the mid-Miocene of eastern Oregon. Consequently, tholeiite imparted the "subduction signals" and crustal processing generated the calc-alkaline

* Steiner, A.R., and Streck, M. J., 2013, The Strawberry Volcanics: generation of 'orogenic'andesites from tholeiite within an intra-continental volcanic suite centred on the Columbia River flood basalt province, USA, *Geological Society, London, Special Publications*, v. *385*(1), 281-302.

$^{40}Ar/^{39}Ar$ ages analysis presented here are slightly different than the published paper and recalibrated using FCT-NM (R98) (4E36-14) (28.201±0.003 Ma)

character to end up with compositions of typical ‘orogenic’ andesites at the Strawberry Volcanics. No primitive calc-alkaline basalt from the mantle is needed as parental magma here and possibly at other similar intra-continental calc-alkaline suites.

Introduction

Magmas of calc-alkaline affinity (see Arculus, 2003) are the typical magmas of subduction zone settings, yet they occur in other tectonic regimes. Because of their prevalence at active plate margins, the generation of the calc-alkaline trend has been closely tied to processes that occur as a consequence of the subduction of hydrated oceanic lithosphere. Key parameters that drive magmas toward calc-alkaline evolution are higher water content and higher degree of oxidation, which researchers have pointed out for many years (e.g., Hora et al., 2009; Zimmer et al., 2010 and references therein). At subduction zones, these two conditions likely exist at primary magma generation in the mantle wedge although this has been recently questioned (Lee et al., 2005). In regions without active subduction (i.e. intra-continental or anorogenic settings), explanation of magmas with calc-alkaline character is more challenging, as there is no dehydrating slab that can introduce fluids to the overlying mantle. However, in such settings, partial melting of mantle that was previously affected by subduction zone magmatism during an earlier stage is thought to be the principal control (e.g., Hawkesworth et al. 1995, Hooper et al., 1995, Christiansen and McCurry, 2008). Thus, even in such non-subduction settings, most workers would argue that primitive calc-alkaline basalts originating from the melting of a subduction modified (i.e. metasomatized) mantle is required in order to generate the calc-alkaline trend with andesite as their intermediate magmas. In this study, we address this issue and present data on generating voluminous calc-alkaline ‘orogenic’ andesites from tholeiitic parents instead of primitive mafic parents that already are calc-

alkaline. Our case study is centered on a volcanic field located in NE Oregon, USA called the Strawberry Volcanics and which consists of a diverse suite of calc-alkaline and mildly tholeiitic lavas (Figs. 1.1, 1.2). The Strawberry Volcanics are coeval with flood basalts of the Columbia River Basalt Group (CRBG) that were issued from vents geographically encircling the Strawberry Volcanics (Robyn, 1977, this study) documenting that the prevalent magmas from the mantle during activity of the Strawberry Volcanics were tholeiitic. Our primary focus in this contribution is to document the distribution, age, and composition of mafic to intermediate lavas of the Strawberry Volcanics followed by a discussion of likely petrogenetic causes.

Methods

Major and selected trace elements were analyzed using an X-ray fluorescence spectrometer (XRF) at Washington State University (WSU). Sample preparation followed the analytical procedures of the WSU geochemical lab. Beads were fused at 1000ºC using a 2:1 dilithium tetraborate ($Li_2B_4O_7$) flux to powered sample. Selected trace elements and rare earth elements (REEs) were analyzed using inductively-coupled plasma mass spectrometry (ICP-MS) at WSU. Samples were analyzed following standard analytical procedures at the geochemical lab at WSU: samples are ground into fine powder and mixed with an equal amount of dilithium tetraborate flux and fused at 1000°C. The beads are then re-ground to a fine grained powder and dissolved for final analysis.

$^{40}Ar/^{39}Ar$ analyses were conducted on fresh groundmass samples which were handpicked after crushing and sieving whole rock samples at the Noble Gas Mass Spectrometry Lab at Oregon State University. All samples were washed in a solution of diluted HCL (<5 %) for approximately 10 minutes to remove any secondary carbonation. All samples with small quantities of mineral monitor FCT-3 biotite (28.030 ± 0.003 Ma , Renne et al., 1998) were loaded in quartz vials and irradiated at the OSU TRIGA research reactor. All samples were recalculated using FCT-NM (R98) (4E36-14) (28.201 ± 0.023 Ma, Kuiper et al., 2008). $^{40}Ar/^{39}Ar$ analysis was performed on samples using an MAP 215-50 gas mass spectrometer using the incremental heating method. Starting temperature of 400°C was followed by 100°C incremental increases until significant ^{39}Ar

was released. Thereafter, temperature was increased in 50 to 100°C steps until reaching 1400°C. We reduced the isotopic data and made age calculations using the ArArCALC software provided by Koppers (2002) using the currently accepted ^{40}K decay constant (Steiger and Jäger, 1977). Further details of the analytical procedures are described in Duncan and Keller (2004) and on the laboratory website (http://www.coas.oregonstate.edu/research/mgg/chronology.html).

Five samples were chosen to represent the large area of the Strawberry Volcanics. One sample from each cardinal direction (N, E, S and W) along with a central location was chosen for $^{40}Ar/^{39}Ar$ analysis (Table 1.1). All samples were basaltic andesite to andesite in composition (53-58 wt. % SiO_2) and field studies indicate that they represent the upper stratigraphy of the Strawberry Volcanics.

Results

The lavas of the Strawberry Volcanics are distributed over 3,600 km^2 and make up a diverse volcanic suite which spans the range of compositions from basalt to rhyolite (Figs. 1.1, 1.2). Below, we present our current data on field relationships of the Strawberry Volcanics, when and for how long volcanic activity occurred, and the erupted magma types.

Stratigraphy and new ages of the Strawberry Volcanics

Field Relationships

The Strawberry Volcanics were named after Strawberry Mountain located along the southeastern margin of the John Day Valley in NE Oregon (Fig. 1.1) (Thayer, 1957). There, uplift and glaciation produced the largest continuously exposed sections consisting of 30 or more, mostly conformably overlying lava flows (Figs. 1.3, 1.4). Lava flow sections can reach thicknesses of approximately 1000 m. Where large continuous sections are exposed, thickness of individual lava flows varies dramatically from the lower to upper sections. Near the base of the Strawberry Volcanics lava thickness can reach > 40 m while the upper sections thicknesses decrease to no greater than 15 m (Fig. 1.3). Independent of thickness, individual lava flow thickness appears nearly constant for the length of exposed section which can reach several kilometers along fault blocks (Fig. 1.3). At Strawberry Mountain, andesitic lava flows dominate and are typically phenocryst poor (<3%) to essentially aphyric. The groundmass includes microphenocrysts of

plagioclase and pyroxene. Phenocrysts occasionally occur as crystal clots instead of single crystals of ~1-3 mm dominated by plagioclase, orthopyroxene and minor clinopyroxene. Xenoliths >3 cm of the same mineral assemblage with plutonic textures have also been observed. Strawberry Volcanics are emplaced on top of pre-Tertiary accreted terranes of the Blue Mountain Province (Thayer, 1957), Mesozoic plutonic rocks, and older Tertiary volcanic rocks thought to be mostly Oligocene of age (Thayer et al., 1967). More specifically, Strawberry Volcanics overlie Oligocene volcanic rocks to the north and east of Strawberry Mountain, and Paleozoic marine sediment (Izee terrane) and ophiolitic sequences (Baker terrane) to the south and west (Fig. 1.1b). Oligocene volcanic rocks are typically phenocryst-rich and display large phenocrysts (>0.5–3 mm). This lithological contrast has been used to differentiate Strawberry Volcanics from older intermediate volcanic rocks. Silica undersaturated alkali basaltic lavas erupted within the area of this study and overlie Strawberry Volcanics in the southern portion and are thought to be late Miocene/Pliocene in age (Fig. 1.1b). In addition, several regional ignimbrites reach into the area. The 9.7 Ma Devine Canyon Tuff and the 7.1 Ma Rattlesnake Tuff (cf., Streck and Grunder, 1995, Green, 1972, Jordan et al., 2004) overlie the Strawberry Volcanics. The 15.9-15.4 Ma Dinner Creek Tuff (Streck et al., 2011) is also mid-Miocene and clear stratigraphic relationships are found only in one area where the tuff is intercalated between thick Strawberry Volcanics lava flows (Fig. 1.4). Lavas with characteristic Strawberry Volcanics lithology have a wide distribution and are at least distributed over an area of 40 x 90 km centered 20 km SW of Strawberry Mountain proper (Fig. 1.1b). The more mafic flows locally exhibit inflated pahoehoe and a’a

features. Lavas with characteristics similar to Strawberry Volcanics occur south of 44ºN and north of 44º30'N (Fig. 1.1b) but our investigation does not go past these 2 limits. Massive rhyolites (~ 300 m) are exposed mainly along the western flank (Fig. 1.1b) and underlie the intermediate composition lavas. Because of the proximity to Strawberry Mountain proper, we group these rhyolites with the Strawberry Volcanics as was done by earlier investigators for the northernmost rhyolites (Thayer et al., 1967; and Robyn, 1977). These rhyolites are phenocryst-poor (≤1%) and range from obsidian to devitrified flows. We previously named them Strawberry Rhyolites (Steiner and Streck, 2011) whereas Thayer (1967) and Robyn (1977) referred to them as the Wildcat Rhyolite Member of the Strawberry Volcanics. Other rhyolites that also appear slightly older than intermediate lavas of the Strawberry Volcanics crop out along the NE near the town of Unity (Fig. 1.1b). This location is where a series of other rhyolite occurrences are found nearby as well (Fig. 1.1b). These rhyolites are more phenocryst rich (>10%) and include mineral phases of plagioclase, quartz, biotite, and occasional amphibole. Mafic lavas of the Strawberry Volcanics occur sporadically throughout the area but are concentrated in the northeast where mostly basaltic andesites have been called Slide Creek Basalts (Robyn, 1977, Goles et al.,1989) and this is also the area where lava flows of the Strawberry Volcanics interfinger with flows of the CRBG (Picture Gorge Member) (Thayer, 1957). These basalts have an ophitic texture dominated by plagioclase, clinopyroxene, and olivine.

Eruption sites have locally been identified either by the accumulation of near vent pyroclastic material or by intrusive rocks and contacts. The most prominent occurs at

Strawberry Mountain where an elongated intrusion >500 m wide cross cuts more than 1000 m of lava flows (Fig. 1.1b). The intrusions are fine-grained with interlocking crystal boundaries. Similar but smaller vent structures appear throughout the area (Fig. 1.1b). In addition, numerous NW-SE trending dikes accompany these volcanic intrusions (Fig. 1.1b, 1.3b and c).

$^{40}Ar/^{39}Ar$ ages of Strawberry Volcanics and stratigraphic relationships to mid-Miocene flood basalts and other regional rock units

New $^{40}Ar/^{39}Ar$ ages indicate calc-alkaline and tholeiitic basaltic andesites to andesites of the Strawberry Volcanics erupted from 14.87 ± 0.13 Ma (2σ) to 12.52 ± 0.12 Ma (2σ) (Table 1.1, Fig. 1.5). This demonstrates magmatism of the Strawberry Volcanics was ongoing during the eruptions of the Wanapum Basalt (15-14.5 Ma) and the Saddle Mountain Basalts (13-6 Ma) of the CRBG (Table 1.1, Fig. 1.5). We expect to extend this range to older ages as our last field work revealed a regional stratigraphic marker bed intercalated with the Strawberry Volcanics. This maker bed (Fig. 1.4) consists of two ignimbrites that we tentatively correlate with the 15.9-15.4 Ma Dinner Creek Tuff (Streck et al., 2011). The sample southwest of Strawberry Mountain, AS-SV-156, gave the oldest date of 14.87 ± 0.13 Ma (2σ) while to the southeast, AS-SV-82 yielded the second oldest date of 14.21 ± 0.26 Ma (2σ) (Table 1). The sample to the north of Strawberry Mountain (the Slide Creek Basalt member) yielded an age of 13.76 ± 0.16 Ma (2σ) and the sample to the east yielded an age of 13.53 ± 0.24 Ma (2σ) (Table 1.1). The sample directly from Strawberry Mountain (AS-SV-192) is a micronorite volcanic neck/plug with the youngest

age of 12.52 ± 0.12 Ma (2σ) (Table 1.1). Previously, the eruption period of the Strawberry Volcanics was bracketed by K-Ar ages of 19.8 ± 0.38 Ma (2σ) and 12.4 ± 0.41 Ma (2σ) (Robyn, 1977). Robyn considered dacites that were dated at 19.8 ± 0.38 Ma (2σ) and 18.1 ± 0.50 Ma (2σ) to be part of the Strawberry Volcanics. These dacites underlie the Strawberry Volcanics and we argue that they are not likely part of them because they are texturally and compositionally distinct. Other reported ages (Robyn, 1977) are 14.9 ± 0.85 Ma (2σ) on a basalt and 12.4 ± 0.41 (2σ) Ma on basaltic andesite. Both of these ages closely correspond with our new Ar-Ar ages.

Geochemistry

Based on the discrimination scheme by Miyashiro (1974) and Arculus (2003), mafic to intermediate magmas of the Strawberry Volcanics are both tholeiitic and calc-alkaline (Fig. 1.2). All basalts of the Strawberry Volcanics are tholeiitic whereas lavas of intermediate compositions are either tholeiitic or calc-alkaline (Fig. 1.2). As compositions become more evolved, the range in tholeiitic vs. calc-alkaline character increases with transitional samples in between (Fig. 1.2). Continuous ranges from tholeiite to calc-alkaline similar to those of the Strawberry Volcanics have been observed in other magma series (e.g., Arculus, 2003; Hora et al., 2009, Brueseke and Hart, 2009).

Tholeiitic lavas of the Strawberry Volcanics

The tholeiitic lavas of the Strawberry Volcanics comprise compositions ranging from basalt (49-50 wt.% SiO_2) to andesite (57-60 wt.% SiO_2) (Table 1.2). All tholeiitic

lavas have high Al_2O_3 ranging from 16–17 wt.%. MgO decreases from 8.9–5.9 wt.% in the basalts to 2.5 wt.% in the andesites. As MgO decreases FeO* decreases as well yet not as fast and it is more variable. FeO* values range from 9.9–13.7 wt.% in basalts to 7.4 wt.% in andesites (Table 1.2). Consequently, the range in terms of FeO*/MgO generally becomes wider towards higher SiO_2 contents (Fig. 1.2b). In a total alkalies vs. SiO_2 diagram, tholeiitic lavas plot on or very near the subalkaline/alkaline divide (Fig. 1.2a).

Select incompatible element ranges are as follows: Rb (4-37 ppm), Ba (408-929 ppm), La (18-34 ppm), Th (1.2-3.5 ppm), U (0.33-2.10 ppm) and K_2O (1.80–0.45 wt.%) with the basalts being the least enriched (Table 1.2). The high field strength (HFS) trace elements (Nb, Ta, Zr, Hf) display near constant or slightly decreasing concentrations towards andesitic compositions (Fig. 1.6). There are no Eu anomalies. Rare earth element (REE) patterns have negative slopes with $(La/Yb)_N$ values ranging from 4.9-7.4, $(La/Sm)_N$ from 2.1-2.9, and $(Gd/Yb)_N$ from 2.1-1.7 (Fig. 1.7). Incompatible trace element concentrations of the tholeiitic lavas of the Strawberry Volcanics indicate elevated concentrations at 20 to 100 times primitive mantle with the most incompatible elements being most enriched (Table 1.2, Figs. 1.8, 1.9). Normalized incompatible trace element patterns indicate distinct spikes at Ba, Pb, and in some samples Sr and K (Figs. 1.8, 1. 9). Ta and Nb have small troughs relative to neighboring elements.

The calc-alkaline suite of the Strawberry Volcanics

The calc-alkaline lavas (excluding rhyolites) mostly consist of basaltic andesite and andesite (53-63 wt.% SiO_2). Only a few dacitic lavas and no calc-alkaline basalt have been found (Fig. 1.2). All calc-alkaline compositions plot in the sub-alkaline field and contain generally less total alkalies than tholeiitic samples. Al_2O_3 is similar to tholeiitic lavas with a range of 16.0–17.9 wt.%. MgO and FeO* decrease with increased silica ranging from 6.2–2.0 wt.% and 9.2–5.2 wt.%, respectively. FeO*/MgO ratios display no increase to a slight increase and trend horizontally from the tholeiitic/calc-alkaline dividing line towards higher SiO_2 to straddling it (Table 1.2, Fig. 1.2).

Normalized incompatible trace element patterns indicate similar enrichment levels and patterns as tholeiitic samples (Table 1.2, Figs. 1.6, 1.8). Select element ranges for samples of the calc-alkaline suite are: Rb (10.8–42.0 ppm), Ba (550–1124 ppm), Th (0.8–4.0 ppm), U (0.3–2.3), and K_2O wt.% (0.9–2.8) (Table 1.2). Typical incompatible elements during evolution from basaltic andesite to andesite behave variably within the calc-alkaline suite of the Strawberry Volcanics. Incompatible elements that do increase include Rb, Ba, Th, U, those that are nearly constant include Zr, Hf, and others decrease including Nb, Ta. Another noteworthy feature is that Sr also stays constant. $(La/Yb)_N$ values of the calc-alkaline lavas range from 5.6–9.0, $(La/Sm)_N$ from 2.4–3.5 and $(Gd/Yb)_N$ from 1.5–1.9 (Fig. 1.7). Some of the more evolved samples indicate small negative Eu anomalies.

Compositional difference between tholeiitic and calc-alkaline suite

The calc-alkaline suite strongly overlaps with the tholeiitic suite in regards to most major elements (Table 1.2). Both suites are medium to high K lavas (Le Bas et al. 1986) and normalized trace element patterns are comparable and similar to the most Mg-rich basalt (Fig. 1.8). Despite these similarities, there are distinct compositional differences – albeit some are quite small – between calc-alkaline and tholeiitic samples. Differences become more notable the more evolved samples are and the greater their relative difference in FeO*/MgO (Figs. 1.8, 1.9). Tholeiitic samples are generally lower in the LILE elements (e.g. Rb, Ba, Th, U and K) and tend to be higher in HFSE (Figs. 1.6, 1.8, 1.9). There is also a difference in the slope of the REE pattern. The slope of LREE-MREE is generally steeper and slope of MREE-HREE shallower in calc-alkaline samples than in tholeiitic samples (Fig. 1.7). And finally, Ti and P are lower in calc-alkaline than in tholeiitic samples (Table 1.2, Fig. 1.8).

The range in FeO*/MgO at any given SiO_2 concentration among lavas of the Strawberry Volcanics allows to investigate whether the mentioned differences change progressively from samples with highest to lowest tholeiitic index. Using a series of samples at 55-62 wt.% SiO_2 and comparing normalized trace element diagrams illustrates how observed changes correlate with tholeiitic index at a given SiO_2 (Fig. 1.9).

Discussion

Field interpretations

One question to answer is did lavas of the Strawberry Volcanics erupt from central vent volcanoes with a few localized general eruption sites or did eruptions occur from numerous vents widely distributed constituting a volcanic field without prominent topographic edifices. Evidence that bears on this question includes field data on thickness distribution of lava flows, on location of venting sites, and distribution of dikes. Erosional levels as encountered within the area of the Strawberry Volcanics are likely to be near (~< 1 km) of the original surface as judged from intrusive contact relationships and volcanic textures of intrusive magmas cooled in a subvolcanic environment. The exception may be recorded at Strawberry Mountain where rocks do begin to show interlocking plutonic textures. With this in mind, we have no evidence for the existence of a major volcanic edifice rising 1000-2000 m above its base existed anywhere in the area as could have been expected given the intermediate magma composition which is typical for volcanic arcs. To the contrary, equal thicknesses of single lava flows over considerable distances argue that original landscape was relatively flat for lava flows to spread out evenly with or without inflation. Dike patterns follow a regional NNW-SSE trend as seen, for example, by the nearby Monument dike swarms that gave rise to the Picture Gorge Basalt (Fig. 1.1) (Wilcox and Fisher, 1966) instead of radial arrangements characteristic for large composite volcanoes. These data point to the interpretation that a volcanic field with topographically subdued volcanic edifices in form of fissure eruptions

or small central vent volcanoes produced the lavas of the Strawberry Volcanics. A likely analogue to the Strawberry Volcanics is found in the Harney Basin of the eastern High Lava Plains, eastern Oregon where intermediate composition magmas erupted during the late Miocene from small, mostly low relief venting sites, as identified by agglutinates and other pyroclastic material, to form thin lava flows (Streck and Grunder, 2012).

The eruptions of lavas of the Strawberry Volcanics were not only coeval with the eruptions of the Wanapum member (15-14.5 Ma) but likely also with earlier units of the CRBG (Camp and Hooper, 1981; Baksi, 1989) because our oldest age of 14.8 Ma (Table 1.1) does not correspond with the activity onset of the Strawberry Volcanics. Onset must have been considerably earlier as approximately 850 m of lavas sit underneath the lava flow that yielded the oldest date reported here. The intercalated ash-flow tuffs (Fig. 1.4), that we correlate with the 15.4-15.9 Ma Dinner Creek Tuff (Streck et al., 2011), is found in the lower section, indicating some lavas flows of the Strawberry Volcanics are even older than Dinner Creek Tuff. Therefore, it is reasonable to infer that activity started around 16 Ma, if not before. The shallow intrusive andesite plug of Strawberry Mountain dated at 12.52±0.12 Ma is probably close to the terminal activity of the Strawberry Volcanics (Table 1.1).

Rhyolite lava flows subordinate in volume to basaltic and andesitic lava flows mainly crop out in the west and south of the area (southwest of Strawberry Mountain) (Fig. 1.1b). Field evidence suggests a stratigraphic level of the rhyolites below basalts and andesites and thus rhyolites constitute the first erupted phase of the Strawberry Volcanics. One date of 17.3 ± 0.36 Ma (Robyn, 1977) places these rhyolites at the very

onset of plume-head related rhyolites associated with the CRBG (Pierce and Morgan, 1992; Coble and Mahood, 2012). There is no evidence for a significant time hiatus, such as paleosol development, scouring, or reworking between the emplacement of rhyolite lavas and the basalt to intermediate flows of the Strawberry Volcanics. This suggests earliest eruptions of basalts and andesites closely followed those of rhyolite that in turn also suggests an onset of basaltic to andesitic volcanism of the Strawberry Volcanics at ≥ 16 Ma.

In summary, basaltic to andesitic magmas of the Strawberry Volcanics erupted over a period of ~3-4 million years from ≥16 to ~12 Ma and for the first 1-2 million years were coeval with the eruption of flood basalts of the Wanapum, Picture Gorge, and Grande Ronde members of the CRBG, and possibly even with Imnaha and Steens Basalt (Camp and Hooper, 1981; Baksi, 1989). The volcanic suite of the Strawberry Volcanics is surrounded by the voluminous (230,000 km^3) exclusively tholeiitic flood basalts and basaltic andesites of the CRBG (Fig. 1.1a). The upshot of the Strawberry Volcanics being in the center of and coeval to CRBG magmatism is that the melting anomaly responsible for the mid-Miocene Columbia River flood basalt province likely also caused magmatism at the Strawberry Volcanics, yet at the Strawberry Volcanics we observe calc-alkaline and mildly tholeiitic volcanism contrasting with CRBG magmas (Fig. 1.2).

Common parent for calc-alkaline and tholeiitic magmas

The calc-alkaline and tholeiitic rock suite of the Strawberry Volcanics and the tholeiites of the CRBG all converge towards higher Mg concentrations to a composition with about 8 wt.% MgO (Fig. 1.2c). This suggests the same parental basalt composition in terms of Fe/Mg ratio can lead to vastly different trajectories in a FeO* vs MgO diagram, leading to both tholeiitic and calc-alkaline compositions. This is not only observed for eastern Oregon during the mid-Miocene but has also been documented for a late Miocene/Pliocene basaltic suite from farther SSW along the High Lava Plains (Streck and Grunder, 2012). There, an evolved high-alumina olivine tholeiite gave rise to a strongly calc-alkaline suite – just like the calc-alkaline Strawberry Volcanics – as well as a ferrotrachytic suite (Streck and Grunder, 2012). Furthermore, there is trace element evidence that tholeiitic and calc-alkaline magmas of the Strawberry Volcanics developed from the same tholeiitic parent. Incompatible trace element and REE patterns among tholeiitic and calc-alkaline basaltic andesites ($\leq$ 53 wt.% SiO_2) are identical suggesting that both have a common parent (Fig. 1.8c). The mentioned subtle differences between tholeiitic and calc-alkaline compositions become only significant at higher silica contents (Fig. 1.8a) and are discussed in the next section but compositions are essentially indistinguishable at lower silica contents irrespectively whether tholeiitic or calc-alkaline in character. Some variations among Strawberry Volcanics basalts do exist but our current data also include compositions that are compatible with being parental to basaltic andesites, again judged from nearly identical trace element concentrations and REE patterns (Table 1.2, Fig. 1.8c). Furthermore, tholeiitic basalts of the Strawberry Volcanics

and lavas of the CRBG lavas overlap in some trace-element ratios (Fig. 1.10) and are otherwise similar in their incompatible trace element patterns (Fig. 1.11). This is testimony that Strawberry basalts are derived from a more or less similar mantle source as the flood basalts of the CRBG. The fact that all CRBG magmas and all basalts of the Strawberry volcanics are tholeiitic indicates that this mantle source apparently gave rise to only tholeiitic magmas during the mid Miocene in eastern Oregon. This is further supported by the fact that neither our study to date nor any other published data have revealed the existence of any calc-alkaline basalt among tholeiites. The mantle source for the tholeiites was metasomatized by subduction processes at some earlier point in time because all CRBG and Strawberry tholeiites show clear geochemical signs in form of elevated concentrations levels of e.g. Ba, Pb, Sr and lower Nb, Ta relative to similarly incompatible elements (Figs. 1.10, 1.11) (Brandon et al., 1993; Carlson, 1984, Wolff et al., 2008). It is such tholeiitic magma that is parental to the compositional intermediate, tholeiitic as well as the calc-alkaline suites of the Strawberry Volcanics as based on geological and geochemical arguments. There is no evidence for and no need to call upon an unseen calc-alkaline basalt magma from which calc-alkaline lavas evolved.

Compositional changes and petrogenesis associated with calc-alkaline and tholeiitic evolution

As Strawberry Volcanics magmas become more silica rich and more evolved their compositional diversity increases in terms of being less or more strongly calc-alkaline. Here we evaluate what compositional changes take place along with changes in the calc-alkalinity index of the magmas and use this in turn as constraints for the processes involved. Detailed modeling of these trends is beyond the scope of this paper but will the subject of subsequent work. The main changes between the strongest calc-alkaline and tholeiitic andesite of the Strawberry Volcanics is that tholeiitic andesites tend to be slightly richer in REE, P, Ti, Ta and Nb, (Figs. 1.7, 1.8, 1.9 Table 1.2). All other elements are practically indistinguishable. Also, calc-alkaline REE patterns have in general a steeper LREE-MREE (higher $(La/Sm)_N$ ratios) part and a shallower MREE-HREE portion (i.e. lower $(Gd/Yb)_N$ ratios) (Fig. 1.7). If these differences were to be explained by fractional crystallization processes then observed compositional systematics would be consistent with fractionating liquidus minerals for the calc-alkaline magmas that include more Ti-Fe oxides, apatite and silicates that preferentially uptake the MREE such as amphibole compared to tholeiitic magmas. However, near constant incompatible element concentrations going from basalt to silicic andesites as observed for example for Zr and La (Fig. 1.6b, c) are inconsistent with a dominant control by fractional crystallization except for some tholeiitic magmas (Fig. 1.6e). Even more striking are the generally decreasing Nb concentrations towards calc-alkaline andesite (Fig. 1.6a) that violates any reasonable fractional crystallization scenario (Fig. 1.6f). Consequently, evolution towards

calc-alkaline andesite must therefore be controlled by open-system processes either in form of crustal contamination, magma mixing processes, or a combination thereof. Contaminant or magma for magma mixing must be silicic in order to generate the more silicic compositions of the Strawberry Volcanics. Some of the Strawberry rhyolites have compositions that make them suitable for magma mixing as they have concentrations of incompatible elements as low, lower, or only slightly higher than basalt, which means concentrations around 8-9, 110, and 28 ppm for the key elements Nb, Zr, and La, respectively (Fig. 1.6, Table 1.3). Similarly our preliminary data on composition of crustal rocks also indicate low Nb, Zr, and La and thus they are permissive as contaminants in case of silicic bulk composition (>65 wt.% SiO_2) or suitable as source rocks to generate permissive silicic partial melts when crustal rocks are more mafic (Fig. 1.6, Table 1.3).

Implications for other intra-continental settings with calc-alkaline suites

Calc-alkaline suites of intra-continental settings are numerous. Examples from Oregon include the late Miocene Harney Basin suite (Streck and Grunder, 2012), other mid Miocene suites of the Powder River Volcanics (Hooper et al., 1995; Ferns and McClaughry, 2013) and of the Owyhee volcanic field (Camp et al., 2003; Ferns and McClaughry, in press), Oligocene suites of the Steens Mountain Volcanics (Langer, 1991) and Tower Mountain volcanic complex (Ferns et al., 2001). They are equally abundant throughout the western US, for example in the Basin and Range province (e.g. Hawkesworth et al., 1995) and elsewhere (Zielinski and Lipman, 1976; Ewart et al.,

1982; Lipman, 2000; Kürkcüoglu et al., 2001, Harangi et al., 2007). Some of the calc-alkaline centers that occur in an intra-continental setting have been interpreted to be due to very shallow subduction that caused volcanic-arc style volcanism much farther inward than is known from modern volcanic arc settings. This was championed by Lipman et al. (1972) for the Oligocene San Juan volcanic field. In fact, the occurrence of calc-alkaline suites of older age, where the original geotectonic setting is unsure, is traditionally used to argue for a subduction setting. Even in cases of calc-alkaline suites of young age where a non-subduction setting is unquestionable, a common precondition for the generation of calc-alkaline magmas is a mantle that has previously been metasomatized by earlier subduction processes from which first calc-alkaline basalt is generated (Hawkesworth et al., 1995; Hooper et al., 1995; Harangi et al., 2007). It is here where the record of the Strawberry Volcanics has implications. Calc-alkaline rocks of the Strawberry Volcanics indeed show evidence of this metasomatized mantle but this signal was most likely imparted by tholeiites and not by calc-alkaline basalt. Instead, as we discussed open-system processes in form of contamination and mixing facilitated the development along calc-alkaline evolution with the production of arc-like orogenic andesites from ambient tholeiitic magmas delivered from the mantle. The follow up question is how much of the other intra-continental calc-alkaline systems indeed require delivery of calc-alkaline basalt from the mantle that serves as parent to calc-alkaline intermediate lavas. Tholeiites carrying subduction signals as those of the mid-Miocene of eastern Oregon are able to spawn calc-alkaline andesites during crustal processing eliminating the need of a mantle derived calc-alkaline basalt. Our example of the Strawberry Volcanics calls into question

the general interpretation that a metasomatized mantle signal is imparted to the more evolved magmas by calc-alkaline basalts when the most mafic lavas are basaltic andesite or more silicic. In case of the Strawberry Volcanics, calc-alkaline basaltic andesites have undergone already some crustal processing despite that some are fairly mafic with MgO and Cr of around 6 wt.% and 200 ppm, respectively (Table 1.2). Such compositions are often the most mafic samples encountered at other intra-continental calc-alkaline systems (e.g., Zielinski and Lipman, 1976; Askren et al., 1997). The up-shot of this is that even though calc-alkaline basaltic andesites and andesites of intra-continental settings carry compositional evidence for being derived from a mantle that experienced some compositional overprint by subduction (e.g. high Ba/Zr), there it is no guarantee that parental mantle magmas were already calc-alkaline as tholeiitic magmas can be carrier of subduction signals just as well – as our study demonstrates. This challenges the *a priori* interpretation that when chemical subduction signals are observed in basaltic andesites and andesites that they are coming indeed from calc-alkaline basalt. Our study is showing that crustal interactions and/or magma mixing can solely be responsible for developing a calc-alkaline trend from tholeiite and therefore merging the subduction signals with calc-alkaline character.

Conclusions

The Strawberry Volcanics is a diverse group of lavas ranging from basalt to rhyolite and from tholeiitic to calc-alkaline. The most primitive lavas of the Strawberry Volcanics are tholeiitic basalts and are also the parent to the intermediate calc-alkaline lavas. Calc-alkaline and tholeiitic basaltic andesites show identical enrichment and depletion patterns on trace element normalization diagrams that are similar to the ones of basalts attesting to their common tholeiitic ancestry. Subtle differences show up as magmas evolve and acquire progressively stronger calc-alkaline or tholeiitic character. Decreasing, constant, or increasing incompatible element abundances along with increased silica contents among calc-alkaline compositions are un-reconcilable with fractional crystallization scenarios but instead require open-system processes in form of crustal contamination and magma mixing and are the main driver for developing a calc-alkaline suite. Preliminary evaluations indicate that observed rhyolites and nearby exposed crustal rocks have compositions suitable for magma mixing and/or contamination. Crustal interactions appear to be important for the early stage of the calc-alkaline liquid line in order to diverge from the regional tholeiitic trend.

Our study holds implications for intra-continental calc-alkaline suites where relationships to tholeiitic magma are equivocal or do not exist. When calc-alkaline basaltic andesites and andesites of intra-continental settings carry compositional evidence for being derived from a mantle influenced by subduction then this signal may also have been delivered by tholeiitic magmas that subsequently evolved a calc-alkaline suite

during open system processes in the crust. Therefore, the notion that chemical subduction signals as observed in evolved mafic magmas must come from calc-alkaline basalt is to be reevaluated. Subsequent crustal processing can solely be responsible for developing a calc-alkaline trend including ‘orogenic’ andesites and therefore merging the subduction signals and calc-alkaline character – just as observed at volcanic arcs.

CHAPTER 2

THE VOLUMINOUS AND COMPOSITIONALLY DIVERSE, MID-MIOCENE STRAWBERRY MOUNTAIN VOLCANICS OF NORTHEASTERN OREGON AND THEIR RELATIONSHIPS TO BASALTIC AND RHYOLITIC VOLCANISM OF THE COLUMBIA RIVER BASALT PROVINCE.

Abstract

The Strawberry Volcanics of northeastern Oregon play an important role in our understanding of the intra-continental mid-Miocene volcanic history of the Pacific Northwest. Because of the timing, location and diversity of these erupted units. The Strawberry Volcanics may hold valuable information about the role that crustal modification has during large volcanic events such as hot-spot volcanism. Here we determine the eruptive sequence of events of the Strawberry Volcanics. The eruptions began at 16.2 Ma with low silica rhyolite, and high silica, A-type rhyolite eruptions followed at 15.3 Ma. The silicic eruptions continued until 14.6 Ma, with a estimated total volume up to ~100 km^3. The first eruptions of the intermediate lava flows occur at 15.6 Ma and continue with both tholeiitic and calc-alkaline and transitional lavas until 12.5 Ma. Volume estimates of the intermediate lavas are approximately 1,100 km^3. The mafic lavas are sparse (~2 % of total volume) and are distributed throughout the upper sequences and appear to be near-last to arrive at the surface. Here we show that the Strawberry Volcanics are not only related in time and space to the CRBG but also share a chemical affinity specifically to the Steens Basalt, such as overlapping normalized

incompatible trace element patterns, selected trace element ratios, and radiogenic isotopes. Furthermore, we compare the Strawberry Mountain rhyolites to the other mid-Miocene rhyolites of eastern Oregon associated with the inception of the Yellowstone – Snake River mantle plume and find similar eruption ages, trace and rare earth element composition and “A-type” rhyolite characteristics. Therefore, this research suggests that the Strawberry Volcanics are part of regional basalt to rhyolite magmatism of the Columbia River Basalt province.

Introduction

The name *Strawberry Volcanics* was given to a diverse group of volcanic rocks (Fig. 2.1, Thayer, 1957) that crop out along the southeastern margin of the John Day valley of NE Oregon and are mid-Miocene in age. Thayer (1957), Brown and Thayer (1966), and Robyn (1977) published the first works on the Strawberry Volcanic lavas providing data on their areal extent, geologic relationships to regionally occurring, stratigraphically younger and older units, and delineating their general geochemical and petrographic characteristics. These works established the overall calc-alkaline character and prevalence of andesitic lavas of this volcanic field (Fig. 2.2). It was also noted that these voluminous andesites are located in an intra-continental setting and not generated due to subduction processes (Robyn, 1979). The only subsequent work of note on the Strawberry Volcanics after the 1950s to '70s was that by Brandon and Goles (1988) who presented isotopic data for basaltic andesites of the Slide Creek member (Thayer, 1957), located in the NNE portion of the field. No more recent data exist on this enigmatic mid-Miocene calc-alkaline field. However, these earlier studies have brought to light aspects that make the Strawberry Volcanics an important field to understand and these include: 1) the petrogenetic evolution of a voluminous volcanic field dominated by intra-continental calc-alkaline andesites, 2) the relationship of mafic magmas to the surrounding contemporaneous tholeiitic flood basalts of the Columbia River Basalt Group (CRBG) and 3) the context of largely unknown rhyolites of the Strawberry Volcanics to other mid-Miocene silicic centers associated with the inception of the Yellowstone-Snake River Plain hotspot (Fig 2.3).

The goals of this paper are the following: 1) to establish units of the Strawberry Volcanics based on physical characteristics, mineralogy, geochemistry and geologic mapping; 2) to reconcile the timing and stratigraphy of the Strawberry Volcanics with $^{40}Ar/^{39}Ar$ age dates with particular emphasis on time and space relationships to CRBG magmas; 3) to investigate the relationships of mafic magmas of the Strawberry Volcanics to surrounding CRBG units, and 4) to describe the rhyolites of the Strawberry Volcanics and explore their association with other mid-Miocene rhyolites and the Yellowstone-Snake River Plain hotspot.

Geologic setting

Accreted Terranes (~320-220 Ma)

The lavas of the Strawberry Volcanics are underlain by the pre-Tertiary accreted terrane rocks of the Blue Mountain Province and Mesozoic sediments of the Izee terrane (Fig. 2.4, Robyn, 1977; Schwartz el al., 2010; LaMaskin et al,. 2011). A section of the Baker terrane, locally known as Canyon Mountain ophiolite, crops out immediately adjacent to Strawberry Mountain. The Canyon Mountain ophiolite represents part of an oceanic sea floor which was thrust onto the continent (Figs. 2.1, 2.4, Thayer, 1977). This terrane extends approximately 18 km southeast of John Day and dips to the south below a portion of the Strawberry Volcanics (Fig. 2.1, Thayer, 1977). Other portions of the Baker terrane are sections of dunites and pyroxenites, which crop out near Miners Ridge located north of Bull Run Mtn. and east of Strawberry Mountain which has not traditionally been part of the Canyon Mountain ophiolite (Fig. 2.1). Fine grained mudstone/siltstone, argillite and limestone of the Izee terrane crop out in areas southwest of Strawberry Mountain near the town of Seneca (Figs. 2.1, 2.4, Brown and Thayer, 1966). Southwest of Strawberry Mountain, these sedimentary rocks form discontinuous units. East of Strawberry Mountain, Jurassic argillite and limestone and Cretaceous intermediate to silicic dikes and sills are exposed near Bull Run Mountain and Ironside Mountain (Fig. 2.1, Thayer and Brown, 1967).

Clarno/John Day (~54-22 Ma)

Rocks of the Clarno formation are exposed north and northeast of Strawberry Mountain near highway 26 and northeast of Prairie City (Fig. 2.1, 2.4). The Clarno Formation is composed of non-marine volcanic and volcaniclastic units ranging from 54 – 39 Ma (Swanson and Robinson, 1968). These volcanic products are thought to be derived from subduction zone magmatism and are strongly calc-alkaline with hydrous minerals phases (amphibole and biotite) yet, some transitional tholeiitic compositions do occur (Rogers et al., 1977). Within the vicinity of the Strawberry Volcanics these units are mostly breccias and conglomerates from lahars and debris flows composed of andesite fragments (Rogers et al., 1977). Within the Strawberry Mountain range, previous geologic mapping by Robyn (1977) and Thayer (1977) identified andesite and dacite flows within the cirque walls at Strawberry Mountain underlying the Strawberry Volcanics to belong to the Clarno formation. Evidence for this should include textural features, erosional/age breaks, geochemical evidence, or ages determined by $^{40}Ar/^{39}Ar$. Our recent field work coupled with updated geochemical and geochronological data reveals that these lavas belong to the Strawberry Volcanics.

The John Day Formation is composed of volcanic units ranging from silicic to intermediate tuffs, lava flows, and domes and intermediate lava flows all ranging in age from 39 – 22 Ma (Rogers et al., 1977). Within the Strawberry Volcanics, exposures of the John Day Formation are minimal (Brown and Thayer, 1966). Such exposures are located in the cliffs west of Strawberry Mountain near Canyon Mountain, and volcanic plugs are

exposed at Bull Run Mountain (Figs. 2.1, 2.4). These exposed units are identified by large (>1cm) and abundant (>30%) phenocrysts, and geochemical data.

The Columbia River Basalt Group (~16.9 – 6.0 Ma)

The main outcrop area of the Strawberry Volcanics is bordered by units from the Columbia River Basalt Group (CRBG) – lavas of Picture Gorge Basalt to the west and northwest, lavas of the Grande Ronde to the north, lavas of the Imnaha Basalt to the east to southeast, and Steens Basalt lavas to the south (Fig. 2.1).The main pulse of the CRBG erupted tholeiitic mafic lava flows during the middle Miocene (~17 to 15 Ma), and the most widespread and voluminous Cenozoic geologic unit within the Pacific Northwest (230,000 km^3) (Camp and Hooper, 1981; Baksi, 1989; Camp and Ross, 2004; Barry et al., 2013; Camp et al., 2013; Reidel et al., 2013a). Specifically, the ages of the CRBG eruptions and duration are: Steens Basalt 16.9 to 16.6 Ma; Imnaha Basalt 16.7 to 16.0; Grand Ronde Basalt 16.0 to 15.6 Ma (or 16.54-15.95, Jarboe et al, 2010); Wanapum Basalt 15.6 to 15.0; and Saddle Mountains Basalt 15.0 to 6.0 Ma (Barry et al., 2013). These magmas erupted from fissures that are now preserved as dike swarms (Wilcox and Fisher, 1966; Swanson et al., 1975; Brown et al., 2014). Eruption sites include: northwest of the Strawberry Volcanics, the Monument dike swarm produced Picture Gorge lavas, the Chief Joseph dike swarm producing Imnaha and Grande Ronde to the northeast, and the Steens dike swarm to the south (Fig. 2.1). The main difference between the CRBG and the Strawberry Volcanics is the CRBG are dominated by tholeiitic basalt and basaltic andesite (Hooper and Hawkesworth, 1993; Hooper, 2002) while the Strawberry

Volcanics are mainly calc-alkaline basaltic andesites to andesites (Fig. 2.2) (Robyn, 1977, and this study).

Regional ignimbrites and younger units

Several regional ignimbrites reach into the area of the Strawberry Volcanics and are found either intercalated among intermediate or silicic units or overlie the Strawberry Volcanics. The Dinner Creek Tuff is found in a number of places (Fig. 2.4) and was co-eruptive with the rhyolitic and mafic/intermediate lavas of the Strawberry Volcanics. New ages of the Dinner Creek Tuff indicate that several flow units of the Dinner Creek Tuff range from ~16.2 to 14.9 Ma (Streck et al., 2015). The redefined distribution of the Dinner Creek Tuff covers an area of ~ 25,000 km^2 (Streck et al., 2015) The proposed eruption center is located along the eastern edge of the Strawberry Volcanics between Ironside Mountain in the north and Castle Rock in the south (Fig. 2.1) (Streck et al., 2015 and references therein). Dinner Creek Tuff outcrops found between lava flows of the Strawberry Volcanics are 5 - 10 m thick and can be identified in the field by its low phenocryst abundance (<1 – 5 %) and pumice ranging from 1 to 30 % (Streck et al., 2015). A further geochemical comparison is provided in the discussion herein.

Younger ignimbrites that reach into the area include the Devine Canyon Tuff and the Rattlesnake Tuff. The Devine Canyon Tuff is an alkali feldspar and quartz bearing, crystal rich (10-30 %) tuff. The areal extent is estimated at 18,600 km^2 stretching across eastern Oregon centered near Burns (Greene, 1973). Significant outcrops within the margins of the Strawberry Volcanics include the southwestern margin near Poison Creek

where a 30 m section of Devine Canyon Tuff is located (Greene, 1973). This tuff has an $^{40}Ar/^{39}Ar$ age of ~ 9.7 Ma (Jordan et al., 2004). The Rattlesnake Tuff erupted ~ 7 Ma and covered an area of ~ 30,000 to 40,000 km^2 of eastern Oregon (Streck and Grunder, 1995), again centered near Burns. This tuff is crystal poor and overlies the Strawberry Volcanics.

Methods

Field Methods and Sample Collection

Field observations and geologic mapping were conducted in the summers of 2010 to 2014. Numerous outcrops exist throughout the area of the Strawberry Volcanics yet exposures to establish stratigraphic relationships are limited to the Strawberry Mountain range. Access to the mountain range itself is limited to two main roads: from the north, Strawberry road (NF-6001) which ends at the 1750 m evaluation point near the base of the mountain and bottom of the cirque walls. Access in the range itself from that point is limited to hiking trails. From the South, road NF-1640 ends at the overview of High Mountain and Strawberry Mountain at 2400 m. From this elevation access to the mountain range follows hiking trails along the glacially carved walls cut into the Strawberry Volcanics. Outside of this range, forest and regolith cover a significant portion of the lavas. Geologic maps provided in this chapter are mainly focused on the rhyolitic sections of the Strawberry Volcanics and were created using field observations and analysis of aerial photography.

Whole Rock Geochemistry

Major and Trace Elements

All mafic, intermediate and silicic units of the Strawberry Volcanics are defined based on field relationships, major and trace element composition, and age determinations. 206 whole rock major, trace and REE analyses of the Strawberry Volcanics were conducted to produce a robust data set to answer research questions. Only fresh samples were collected and analyzed. Once the samples were selected for analysis they were chipped to < 1 cm and inspected for mineralization or alteration. A sample location map is provided in Figure 2.5.

Major and select trace elements were analyzed using a Wave Dispersive - X-ray fluorescence spectrometer (WD-XRF) at Washington State University (WSU). Sample preparation followed the analytical procedures of the WSU geochemical lab and can be found here: http://cahnrs.wsu.edu/soe/facilities/geolab/technotes/xrf_method/. Selected trace elements and rare earth elements (REEs) were analyzed using inductively-coupled plasma mass spectrometry (ICP-MS) at WSU. Samples were analyzed following standard analytical procedures at the geochemical lab at WSU: samples are ground into fine powder and mixed with an equal amount of dilithium tetraborate ($Li_2B_4O_7$) flux and fused at 1000°C. The beads are then re-ground to a fine-grained powder and dissolved for final analysis. A full detailed procedure of sample preparation and methodology can be found here: http://cahnrs.wsu.edu/soe/facilities/geolab/technotes/icp-ms_method/.

Radiogenic Isotopes

Sr, Nd, and Pb isotopic compositions were measured on 13 samples representing mafic, intermediate, and rhyolitic compositions. Sample dissolution and chemistry were performed at the radiogenic isotope clean lab and analyzed using thermal ionization mass spectrometry (TIMS) at New Mexico State University. Sample preparation methods for whole rock isotopic analysis can be found at: http://geology.nmsu.edu/framos/TIMS.html. Age corrections for Sr and Nd isotopic ratios were applied using the ratio of Rb and Sr whole rock element concentrations.

$^{40}Ar/^{39}Ar$ geochronology

$^{40}Ar/^{39}Ar$ geochronology was conducted at Oregon State University's Argon Geochronology Research Laboratory on a total of fifteen samples: ten groundmass concentrates, three plagioclase separates, one biotite, and one glass sample. Six rhyolitic samples (one of which was a repeat run of plagioclase separates) were collected from two main rhyolitic sections, one adjacent to Strawberry Mountain and the other south of Strawberry Mountain (Table 2.1). The remaining nine samples are from lava flows of calc-alkaline and tholeiitic composition, which were collected from various stratigraphic sections and locations (Table 2.1). All samples were loaded in quartz vials with small quantities of mineral monitor FCT-3 (28.030 ± 0.003 Ma, Renne et al., 1998) and irradiated at the OSU TRIGA research reactor. Obtained ages were later on recalculated using a Fish Canyon Tuff (FCT) age of 28.201 (Kuiper et al., 2008). All samples were analyzed by the furnace incremental heating age spectrum method using a Mass Analyzer

Products (MAP) Model 215-50 mass spectrometer and analyzing between eight and twelve heating steps (Table 2.1). Starting temperature of 400°C was followed by 100°C incremental increases until significant ^{39}Ar was released. Acquired isotopic data were reduced using the ArArCALC software provided by Koppers (2002) and age calculations were made using the currently accepted ^{40}K decay constant (Steiger and Jäger 1977). Further details of the analytical procedures are described in Duncan and Keller (2004) and on the laboratory website: http://www.coas.oregonstate.edu/research/mgg/chronology.html. All new age data cited in the text are quoted at 2σ (Table 2.1). This study produced age spectra that yield at least 6 consecutive heating steps, containing no less than 70% of the total ^{39}Ar released with the exception of two, which only 4 and 5 consecutive heating steps were produced and are in the processes of being re- analyzed (Table 2.1). These groundmass and mineral separate samples can be considered as “well behaved”, despite having some discordance for early and late heating steps. It is possible that the discordance could be related to geological effects (argon loss) or irradiation-induced artifacts (^{39}Ar recoil).

Radiometric ages

Previous ages of Strawberry Volcanics

Robyn (1977) determined a 7 million year long activity period for the Strawberry Volcanics from 19.8 ± 0.38 Ma (2σ) to 12.4 ± 0.41 Ma (2σ) based on 6 K/Ar age dates. Of the ages reported by Robyn (1977), a single basalt lava at 14.9 ± 0.85 Ma (2σ) and a basaltic andesite at 12.4 ± 0.41 (2σ) Ma. conform best with our geochronological study of the Strawberry Volcanics. On the other hand, the oldest ages of 19.8 ± 0.38, 19.1 ± 0.65, and 18.1 ± 0.50 Ma (2σ) that Robyn (1977) reports for lava flows are significantly older than any of our ages. Using latitude and longitude data, and descriptions of these dacite samples provided by Robyn (1977), we were able to locate units yielding these old ages. Field and lithological characteristics indicate that any of these old lavas are unlikely units of the Strawberry Volcanics. They are dacitic in composition and contain large phenocrysts of plagioclase and amphibole (~1-3cm) different than typical mineral assemblage of the Strawberry Volcanics. . Robyn (1977) also reported an age of 17.3 ± 0.36 Ma for a rhyolite within the Strawberry Mountain Range. This rhyolite is similar to other rhyolites found within the Strawberry Volcanics. We have not yet confirmed this age yet but, if correct, then this would be the oldest recorded Yellowstone-Snake River hotspot related rhyolite volcanism.

Summary of new $^{40}Ar/^{39}Ar$ results

New $^{40}Ar/^{39}Ar$ ages from this investigation indicate that basaltic andesite to rhyolite lavas of the Strawberry Volcanics erupted from 16.16 ± 0.17 Ma (2σ) to 12.52 ± 0.12 Ma (2σ, Fig. 2.6; Table 2.1). Rhyolites yielded the oldest ages ranging from 16.16 ± 0.17 Ma (2σ) to 14.70 ± 0.13 Ma (2σ), which is consistent with stratigraphic field observations described below (Fig. 2.6; Table 2.1). Among intermediate lavas, those of calc-alkaline affinity erupted over the longest duration as indicated by ages ranging from 15.59 ± 0.36 Ma (2σ) to 12.52 ± 0.12 Ma (2σ) (Fig. 2.6; Table 2.1). The tholeiitic lavas produced a slightly narrower range of ages of 15.57 ± 0.16 Ma (2σ) to 13.53 ± 0.24 Ma (2σ). This may not be significant but what is clear is that tholeiitic and calc-alkaline volcanism was coeval (Fig. 2.6; Table 2.1). One basalt sample yielded an age of 12.61 ± 0.08 Ma (Fig. 6; Table 1). Other basalts are intercalated near the middle of a stratigraphic sequence of lava flows at Strawberry Mountain and thus have ages within the range of intermediate lavas.

Stratigraphy and eruptive units

Rocks of the Strawberry Volcanics are dispersed over 3,600 km^2 from 44° 00” N to 44° 40’’ N and 119° 00” W to 118° 00” W. (Fig. 2.1). Due to the size of the area of the Strawberry Volcanic field and ability to finish in a timely manner, the southern boundary of the field area was placed along Forest Road 17 representing therefore an artificial cut-off rather than a natural boundary. Of the 3,600 km^2 approximately 200 km^2 (~ 6 %) is rhyolite and roughly 100 km^2 (~3 %) is basalt lavas. The rest of the volcanic field is basaltic andesite to andesite calc-alkaline and tholeiitic lavas. In this paper, we have divided the eruption history of the Strawberry Volcanics into 3 different eruption units based on field evidence and major-element geochemistry and include: 1) rhyolite lava flows and tuffs, 2) intermediate calc-alkaline lavas, and 3) tholeiitic basalt and intermediate tholeiitic lavas.

Rhyolite Volcanism

Rhyolite lavas of the Strawberry Volcanics erupted as lava domes and coulees, and fallout and ash-flow tuffs. In addition, far travelled ash-flow tuffs that erupted from centers ~80 km to the south and ~20 km to the southeast reach into the area. These include the late Miocene Devine Canyon and Rattlesnake Tuff (Greene, 1972; Streck and Grunder, 1995) and tuffs erupted from the mid-Miocene Dinner Creek Tuff Eruptive Center (Streck et al., 2015). Rhyolites are typically situated in the lower part of the stratigraphy and sit atop Izee terrane sediments or co-erupted with both calc-alkaline and

tholeiitic intermediate lavas. Where the rhyolites are in direct contact with the intermediate lavas, there is no evidence of a significant time gap (e.g. paleosol or unconformities). Dikes of mafic to intermediate composition crosscut these rhyolite lavas and tuffs. The volume is difficult to estimate because of outcrop exposure, erosion and the expected variability in thicknesses of domes and rhyolite flows at emplacement. Nevertheless, we estimate a total erupted rhyolite volume of between 40 and 100 km^3.

Locally erupted lava domes and flows can be separated into different rhyolite units based on location, petrography, and composition. The following is a description of these rhyolites that we discuss according to exposure area as “northern” and “southern” rhyolites. Detailed geologic field maps of these rhyolites and the surrounding units are located in figure 2.7, 2.8, and 2.9.

The northern rhyolites are located west of Strawberry Mountain and are phenocryst-poor lavas (<1% phenocrysts) of high-silica rhyolite composition (~76-78 wt% SiO_2) that often display flow banding textures. Northern rhyolites cover an area of approximately 55 km^2 and have a volume between 10 and 30 km^3 (Fig. 2.7). Phenocrysts are limited to plagioclase and quartz. Microphenocrysts are rare (<1%) but are seen on occasion and include plagioclase, quartz, and minor pyroxene. These lavas are often devitrified or include obsidian bands between devitrified sections. Ash-flow tuffs and fall out deposits, associated with vents proximal to this location, are dispersed throughout the area and intercalated among rhyolitic lavas or are stratigraphically younger.

The northern rhyolites are both peralkaline and peraluminous, high silica rhyolites and tend to be lowest in major elements oxides such as Al_2O_3, CaO, FeO* as are high-

silica rhyolites of the other area (Fig. 2.10). The peraluminous characteristic is likely due to minor loss of alkalies. Some of these rhyolites have increased REE and HFSE compared to other rhyolites (Fig. 2.11; Table 2.2). Another major difference between the northern Strawberry rhyolites (purple symbols in Figs 2.10 to 2.13) and the other rhyolites of the Strawberry Volcanics (red and blue symbols) is their wide range in Zr concentrations from 175 ppm to 450 ppm whereas the southern section ranges from 70 ppm to 240 ppm (Fig. 2.12; Table 2.2). The enriched northern rhyolites have Zr + Nb + Ce + Y (>600 ppm) and 10,000 x Ga/Al (>3) (Fig. 2.12; Table 2.2). These high values make them distinct among the rhyolites of the Strawberry Volcanics (Fig. 2.12; Table 2.2) and confirm as A-type magmas (cf. Whalen et al., 1987).

The second semi-continuous rhyolitic section is located south and southwest of Strawberry Mountain (Figs. 2.5, 2.8 and 2.9). This rhyolitic section covers an area of approximately 145 km^2 with a volume between 30 and 70 km^3 (Figs.2.8, 2.9). Structurally these lavas appear as large (up to 3 km long) coulees and are composed of generally two different geochemical and mineralogical types. The first type (red symbols in Figs. 2.8, 2.9, 2.10) are low-silica rhyolites ranging from ~70-74 wt. % SiO_2 and are dominated by a single mineral phase of plagioclase (~20 %) and minor amounts of amphibole (<1 %). They range considerably in texture with regards to flow banding, presence of mafic inclusions, vesicularity, and of being glassy or devitrified lavas. The second rhyolite type (light blue symbols) is a high-silica rhyolitic composition ~77-78 SiO_2 wt% (Fig. 2.8, 2.9, 2.10) and contains lesser amounts of plagioclase (~10 %) and occasional amphibole and biotite ($\leq$ 2 %).

The southern low silica rhyolites are metaluminous to peraluminous with the highest Al_2O_3 and CaO wt. % of 13.0 - 15.2 and 1.18 - 2.70 respectively (Fig. 2.10). FeO* (2.0-3.5), TiO_2 (0.26-0.60) wt. % and Cr (5-9) ppm are also elevated with respect to the other Strawberry rhyolites (Fig. 2.10; Table 2.2). Notable trace element concentration differences are the lowest Nb (8-12 ppm) and highest Sr (100-250 ppm) concentrations (Figs. 2.11, 2.12; Table 2.2). Overall, normalized to chondrite, REE multivariable diagrams show that the LREE (La through Sm) concentrations overlap the range of the other groups of rhyolites but the HREEs (Gd through Lu) generally have slight lower values and at higher concentrations overlap only with the other southern section (blue) (Fig. 2.11; Table 2.2).

The southern high-silica rhyolites have similar major element compositions as the high silica group in the north with comparable Al_2O_3, CaO, FeO*, and TiO_2 wt. % (Fig. 2.10; Table 2.2). Trace element concentrations are also comparable to northern rhyolites with the exception of lower Zr and Hf concentrations that range from 70 to 113 ppm (Figs. 2.11, 2.12; Table 2.2). In variation diagrams of Nb and 10,000 Ga/Al vs Zr, the trend of the northern and southern high silica rhyolites diverge with a positive correlation seen in the northern rhyolites and a negative correlation in the southern rhyolites (Fig. 2.12; Table 2.2). REE patterns of southern high silica rhyolites overlap with the southern low silica rhyolites and are generally less enriched in all REE relative to the northern high silica rhyolites (Fig. 2.11; Table 2.2).

In general, most rhyolites of the Strawberry Volcanics were likely metaluminous prior to alkali loss but some are mildly peralkaline (Fig. 2.10; Table 2.2). Trace elements

concentrations vary most in elements like Sr (9 - 250 ppm), Zr (66 - 450 ppm), Ti (300 - 3500 ppm), and Ba (350 - 1630 ppm) (Figs. 2.11, 2.12; Table 2.2). When normalized to upper crust values, rhyolites plot around 1 with significant troughs at Sr, P, and Ti, and minor troughs in Nb, Ta, and some samples with troughs and spikes in Zr (Fig. 2.11; Table 2.2). REE patterns indicate slight LREE enrichment with $(La/Yb)_N$ ranging from 2.5 to 8.9. $(La/Yb)_N$ values with weak positive correlations with elements that are sensitive to feldspar fractionation (i.e. Ba, Sr, Eu/Eu*) (Fig. 2.13; Table 2.2). This suggests that fractional crystallization may have played a minor role in the generation of these rhyolites. It does not appear that they were generated by a parental mafic or intermediate magma. Rather, it seems more likely that these magmas were formed by partial melting of country rocks. Figure 2.14 shows the path of fractionation from an intermediate magma composition. It is clear that fractional crystallization of an intermediate or mafic magma of the Strawberry Volcanics cannot result in the generation of these rhyolitic lavas (Fig. 2.14). Rhyolites of the Strawberry Volcanics all have low Nb concentrations (<25 ppm) comparable in concentrations to the intermediate lavas which may be the result of mixing between the mafic and silicic magmas.

Basaltic to intermediate lava flows

The Strawberry Volcanics primarily consist of lava flows of basaltic andesitic and andesitic composition (Fig. 2.2) that cover 3,600 km^2 of the Malheur National Forest and Strawberry Mountain Wilderness (Fig. 2.1). The best exposures of these lava flows are found in the vicinity of Strawberry Mountain, a glacially carved mountain with a maximum elevation of ~3,000 m, which the Strawberry Volcanics were named for (Fig. 2.1). Strawberry Mountain with its southern extension, High Mountain, and its eastern extension, Slide Mountain, make up the east/northeast-trending Strawberry Mountain range, extending approximately 15 km parallel to the John Day valley. Within this mountain range, the total thickness of numerous basaltic andesite and andesite lava flows is consistently about 1000 m. Across this range, individual lava flows show constant thicknesses of ~5-10 m with little columnar jointing but instead display a thin (~10s of cm), platy appearance. In contrast, the lavas of the CRGB are often the result of inflationary flows (Thordarson and Self, 1998) displaying columnar jointing. Volume estimates can be conservatively calculated by using the volume of a cone ($V = \pi r^2 \frac{h}{3}$; where r is the radius and h is the height of thickness) assuming that the lava thicknesses decrease from Strawberry Mountain towards the outer edges of the volcanic field. The result is approximately 1,100 km^3 if we use a radius of 32 km and a thickness of 1km. We are confident that this calculated volume is an underestimate as the thickness of lava flows do not decrease to the outer edges as a cone. Alternatively, we use a series of rectangles as a volume calculation with the Strawberry Mountain range being the thickest unit with 1 km and extending 75 km^2. To the east a safe estimate of 500 m thick units

covering 1875 km^2 and to the south of the Strawberry Mountain range is a thinner approximately 200m section extending 500 km^2. The total volume estimated this way is approximately 1,100 km^3 of erupted lava same as the cone.

Calc-Alkaline Intermediate Volcanism (15.60 to 12.5 Ma)

The oldest (15.59 ± 0.36 Ma (2σ)) intermediate lava of the Strawberry Volcanics is a calc-alkaline basaltic andesite and the youngest 12.52 ± 0.12 Ma (2σ) is a andesite vent plug located at High Mountain (based on discrimination schemes by Miyashiro (1974) and Arculus (2003)).

Calc-alkaline lavas range in SiO_2 (wt. %) from 52.7 % to 64.5 % and incompatible elements behave variably within the calc-alkaline suite of the Strawberry Volcanics from basaltic andesite to andesite to dacite (Fig 2.2, 2.15; Table 2.3). Trace elements that do increase include Rb, Ba, Pb, and U but all other trace elements including REEs are nearly constant or slightly decrease with increasing SiO_2 wt. % (Figs. 2.15, 2.16; Table 2.3).

Calc-alkaline lava flows and breccias vary from aphyric, to phenocryst-poor to containing 30 % phenocrysts. The dominate lava type are aphyric and contain < 5 % phenocryst. The aphyric type flows are best exposed along the lower section below 2000 m in the cirque walls of Strawberry Mountains near Strawberry Lake. The calc-alkaline lavas which show greater amounts of phenocrysts have glomerocrysts consisting of small (1-2 mm) plagioclase, pyroxene and minor olivine and oxides. The more phenocrystic rich calc-alkaline lavas are dispersed throughout the Strawberry Mountain vicinity.

Numerous dikes are exposed throughout the Strawberry Volcanic field and appear to be the main conduit system for magma extrusion at the surface through fissures or small scale central vent volcanoes (Figs. 2.1, 2.17) (cf. Chapter 1 –Steiner and Streck, 2013). These dikes are often represented by topographic highs and cross-cut lava flows of the Strawberry Volcanics and associated terranes (Fig. 2.1). Strawberry dikes mostly strike NNW-SSE similar to dikes of the nearby (~40 km) Monument Dike Swarm that gave rise to the Picture Gorge Basalt unit of the CRBG (Fruchter and Baldwin, 1975; Thayer, 1957). We identify these dikes as part of the Strawberry Volcanic field and not the Monument Dike Swarm based on geochemical and petrographic similarities to the lavas of the Strawberry Volcanics. Some vent site lavas have micro-plutonic textures (e.g. the micro-norite dikes and plugs of Strawberry Mountain and High Mountain) and were previously thought to be a feature related to a long-lived, strato-volcanic edifice, which supplied the lavas for the Strawberry Volcanics (Robyn, 1977). There is no evidence for large single composite volcanoes such as thickening of lava flows away from the vent locations throughout the Strawberry Volcanics. Rather, we see the lava flows extend in uniform thicknesses for 10s of km away from the vent.

Tholeiitic Basalt and Intermediate Volcanism (15.60 to 13.50 Ma)

The tholeiitic lavas of the Strawberry Volcanics are subalkaline and comprise compositions ranging from basalt to andesite with SiO_2 ranging from 47.5-60.4 wt. %. These lavas are relatively high in Al_2O_3 (15.4-18.2 wt. %), and vary in MgO (2.6-7.2 wt. %) (Fig 2.2; Table 2.3). Incompatible element ranges are comparable to calc-alkaline lavas although HFSE and REE tend to be higher in more evolved tholeiitic compositions (e.g. Figs. 2.15, 2.16; Table 2.3). Normalized incompatible trace element patterns indicate distinct spikes at Ba and Pb, and occasionally Ta and Nb have small troughs relative to neighboring elements (Fig. 2.16).

Tholeiitic lavas of both basaltic and andesitic composition are dispersed throughout the Strawberry Volcanic stratigraphy (Figs.2.4, 2.5). Lavas with tholeiitic affinity are minor in volume relative to calc-alkaline lavas. Tholeiitic intermediate lavas are phenocryst poor (<10%) similar to the phenocrystic poor calc-alkaline lavas making them indistinguishable in the field. We advise caution in identifying tholeiitic vs calc-alkaline lavas in the field based on field characteristics alone due to similar textures and modal mineral abundances. The eruption vents for tholeiitic lavas are assumed to have been similar to those for calc-alkaline lavas. Tholeiitic basalt lavas tend to be more massive and cohesive in texture and lack the platy texture of the calc-alkaline lava flows. These tholeiitic basalts have vesicles and display dixtytaxitic texture. Several tholeiitic basalts are located in the Strawberry/High Mountain cirque walls and can be distinguished from the calc-alkaline and tholeiitic intermediate lavas by a ophitic texture (i.e. AS-SV-287, 109 and 11). Tholeiitic, basalt to andesitic lavas are distributed

throughout the Strawberry Volcanic range and are associated with vent structures (e.g. dikes) nearby which were identified at the Strawberry Mountain Range and south to southwest of this range and east, near the town of Unity.

Mafic surge deposits are deposited on the top of lava flows near the glacier-carved walls of High Mountain and other similar peaks within the Strawberry Mountain range. These deposits contain scorriacous material set in a fine grained matrix of palagonite. Deposits are up to ~20 m thick and often contain pyroclasts ranging in size from ash and lapilli to ~0.5 m-diameter blocks or spherical and spindle bombs (Samples AS-SV-195 and 198). At the peak of High Mountain, ~ 20 m high pinnacles tower above the rest of the lavas and have been nicknamed the Rabbit Ears of Strawberry Mountain.

Discussion

Synopsis of emplacement history of the Strawberry Volcanics

The Strawberry Volcanics, spanning the compositional range from basalt to rhyolite (Fig. 2.2), have an eruption history that lasted ~4 m.y. (Fig. 2.6; Table 2.1). The first eruption of the Strawberry Volcanics began with the rhyolites of the southern section erupting at ~16.2 Ma (Fig.2. 6; Table 2.1). Succeeding eruptions of calc-alkaline and tholeiitic intermediate lavas started at approximately ~15.6 Ma (Fig. 2.5; Table 2.1). Activity continued with eruptions of dominantly intermediate calc-alkaline lavas, accompanied by tholeiitic basalt and intermediate tholeiitic lavas. Rhyolite volcanism of the northern rhyolites near the western margin of Strawberry Mountain began at ~15.3 Ma and continued up to ~14.8 Ma with eruptions of phenocrystic-poor lavas forming separate but overlapping domes, and emplaced as minor pyroclastic events (Fig. 2.6; Table 2.1). During this time, the eruption of the early southern rhyolites continued and appears to have stopped at ~14.7 Ma (Fig. 2.6; Table 2.1). Low-volume (<36 km^3), mafic tholeiitic eruptions appear sporadically in stratigraphic sections primarily consisting of calc-alkaline intermediate lavas. The youngest intermediate lava flow with tholeiitic affinity is 13.5 Ma and we take this as the time when tholeiitic volcanism ceased (Fig. 2.6; Table 2.1). Tholeiitic volcanism likely superseded eruptions of calc-alkaline lavas that possibly erupted last at ~13.8 Ma as suggested by our current age data (Fig. 2.6; Table 2.1). However, an intrusive calc-alkaline micro-norite dike at Strawberry Mountain

was dated at ~12.5 Ma, but it is unclear if any lava flows were produced at the surface (Fig. 2.6; Table 2.1).

Relationships of mafic Strawberry Volcanics to flood basalt magmatism of the CRBG

The close temporal and spatial relationships between the Strawberry Volcanics and units of the CRBG (Fig. 2.1) invite the question to what extent there is a petrogenetic relationship, despite the predominantly calc-alkaline nature of the Strawberry Volcanics. New ages presented herein demonstrate that silicic magmatism of the Strawberry Volcanics was ongoing during the eruptions of the Imnaha (16.7 – 16 Ma) and the mafic and intermediate Strawberry Volcanics erupted during the waning state of the Grand Ronde Basalt (16-15.6 Ma or 16.54-15.95) and during eruption of Wanapum Basalt (15.6-15 Ma), (Jarboe et al., 2008; Barry et al., 2013; Camp et al., 2013) (Fig. 2.6; Table 2.1). Field evidence has shown that the eruption style of the mafic to intermediate lavas of the Strawberry Volcanics is akin to the eruptions of the CRBs. Despite our noted compositional differences to CRB magmas, eruptions of Strawberry Volcanics were fed from dikes leading to fissure eruptions at the surface. In fact several authors (e.g. Camp and Ross, 2004; Brueseke et al., 2008; Wolff, 2008) have shown on maps that the Monument Dike Swarm of the CRBG reach into the area of the Strawberry Volcanics (Fig. 2.1). It is our conclusion based on geochemical data and geographical location that these shown dikes are dikes of the Strawberry Volcanics. As described herein, the tholeiitic and calc-alkaline intermediate lavas of the Strawberry Volcanics can easily be misinterpreted as lavas of the CRB in the field. Below we will discuss the geochemistry

of mafic lavas (≤56 SiO_2 wt. %) of the Strawberry Volcanics in regards to differences and similarities to the various units of the CRBG

We base our comparison of Strawberry Volcanics to the CRBG on select mafic (≤56 SiO_2 wt %) lavas that are the least modified by processes in the crust and thus are closest to what a mantle input looked like that gave rise to mafic to intermediate Strawberry Volcanic magmas. We use the data of Wolff et al. (2008) as representative of the CRBG magmas. Comparison of major element compositions shows overlap of basaltic lavas of the Strawberry Volcanics with CRBG lavas specifically with Steens and Imnaha Basalt (Fig. 2.18). The higher SiO_2 wt. % (52 to 56) lavas of the Strawberry Volcanics lie within the general trend of the CRB lavas in some elements but also trend away towards increased silica in other elements. They overlap with Grand Ronde Basalt in MgO, CaO, and TiO_2 wt. % but diverge in Al_2O_3, FeO* and P_2O_5 wt. % with showing notable higher Al and P and lower Fe concentrations (Fig. 2.18). This suggests that crustal evolution does have a significant impact on magmas within the basaltic andesites already, although incompatible trace element may be less affected than major elements and compatible trace elements.

On normalized incompatible trace element diagrams (spider diagrams) and REE diagrams the greatest overlap of lavas of the Strawberry Volcanics is observed with samples of Steens and Imnaha Basalt as all samples of the Strawberry Volcanics are within their ranges and have similar patterns to these groups (Fig.2.19). Comparing however the average Steens Basalt pattern (or Imnaha Basalt), a subtle difference appears in the range from Nd to Dy. Samples of the Strawberry Volcanics have distinct Zr-Hf and

Ti troughs whereas average Steens has only a minor trough in Zr-Hf but none in Ti and Imnaha does not have any of these troughs. Another difference is that some samples of the Strawberry Volcanics are enriched in P which could be due to select enrichment during crustal assimilation (cf. Streck and Grunder, 2012). Significant overlap of elemental ranges of samples of the Strawberry Volcanics occurs with the Imnaha and Grand Ronde lavas, yet more elements fall out of the range compared to Steens Basalt (Fig. 2.19). For example the Strawberry Volcanics are enriched in Ba, Nb, Sr, and P ppm and enriched in the LREE (La through Nd ppm) relative to the Imnaha (Fig. 2.19). Compared to the Grand Ronde Basalt, the Strawberry Volcanics are enriched in Nb, Sr and P ppm but significantly lower in Rb, Th, and U ppm (Fig. 2.19). Samples of the Strawberry Volcanics are distinctly different to Picture Gorge Basalt in most elements from Rb to Eu but Picture Gorge Basalt interestingly shows the same Ti troughs as samples of the Strawberry Volcanics (Fig. 2.19).

Diagrams with element ratios using incompatible trace elements (e.g. Ba/Zr, La/Y, U/Nb) show that the overlap of Strawberry Volcanics samples with Steens Basalt is again greater than with other groups (Fig. 2.20) and that magmas of the Strawberry Volcanics are clearly offset from magmas of Grande Ronde and Picture Gorge Basalt in plots with U/Nb or U/La (Fig. 2.20).

Whole rock radiogenic isotopic data for samples of the Strawberry Volcanics provide further evidence for similarity among the Strawberry Volcanics and CRBG units (Fig. 2.21). Isotopic data for the two basalt samples analyzed show that one sample overlaps with Imnaha and Grande Ronde while the other has much lower initial Nd and

higher initial Sr. Also, $^{206}Pb/^{204}Pb$ and $^{208}Pb/^{204}Pb$ are lower causing the sample to plot outside of the range of the CRBG but to overlap with or trend towards local crustal values suggesting that crustal contamination may be responsible for these isotopic values (Fig. 2.21). The uncontaminated basalt sample plots within the CRBG range overlapping in initial Sr vs initial Nd with Imnaha and Grande Ronde and have similar radiogenic Pb within the range of Grande Ronde (Fig. 2.21). If we include the intermediate lavas of the Strawberry Volcanics, the initial Sr and Nd values of Strawberry Volcanics are very similar to the Steens, Imnaha and Grand Ronde while the $^{206}Pb/^{204}Pb$ is similar to Steens, Grande Ronde, and Picture Gorge (Fig. 2.21). Furthermore, this basalt sample and the intermediate lavas of the Strawberry Volcanics, overlap with the Grande Ronde lavas in Pb isotopic ratios (Fig. 2.21) and plot between the three components mixture of the CRB plume described by Carlson (1984).

Based on the discussion above, we are proposing that mafic and intermediate lavas of the Strawberry Volcanics should also be considered part of CRBG volcanism as discrete unit – the *Strawberry Volcanics*. Differences that exist among formal members for the CRBG are greater than differences to the *Strawberry Volcanics*. The *Strawberry Volcanics* are not more silicic than Grande Ronde Basalt lavas and are at least contemporaneous to eruptions of Wanapum Basalt units but may even overlap in age with upper Grand Ronde Basalt lavas – as this is a matter of ongoing controversy and is currently unresolved. *Strawberry Volcanics* have the greatest similarity to Steens Basalt lavas but have retained some unique geochemical features that still set them apart. Some of these differences may be controlled by open system processes as silica increases and

may in turn be partly due to what ultimately causes most *Strawberry Volcanics* to develop calc-alkaline affinity such as melting of local basement lithologies and differentiation during AFC processes. Isotopic data argue for melting of a mantle similar to Steens and Imnaha Basalt in some respect and Picture Gorge Basalt in others (Fig. 2.21). It is surprising, however, that the *Strawberry Volcanics* have more geochemical commonalities with Steens Basalt than with the immediately neighboring (~40 km) Picture Gorge Basalt.

Context of the Strawberry Mountain rhyolites to the Mid-Miocene rhyolite flare-up

McDermitt caldera and other rhyolitic centers such as the Santa Rosa-Calico volcanic field and the High Rock caldera complex located near the Oregon-Nevada border have been viewed as the first centers of rhyolitic volcanism associated with the Columbia River-Steens flood basalts of the Pacific Northwest starting at 16.5 Ma (Pierce and Morgan, 1992; Brueseke et al., 2009 and 2014; Coble and Mahood, 2012). Recent age determinations of long known mid Miocene rhyolitic centers throughout eastern Oregon have yielded ages that are about as old as those along the Oregon-Nevada state boundary and that range from 16.5 to 15.9 Ma (Streck et al., 2015). These ages are from rhyolites of the Lake Owyhee volcanic field and periphery, the Dinner Creek Tuff, and also come from as far north as near Baker City (Streck et al., 2015). The Strawberry Mountain rhyolites until recently were largely unknown and thus were neither included as area of significant rhyolite volcanism nor as one of the "earliest" mid-Miocene rhyolite center related to Columbia River Basalt volcanism despite that there was a K-Ar age of

17.3 ± 0.36 Ma reported by Robyn (1977). Our currently oldest age of the Strawberry Mountain rhyolites is 16.2 Ma (Fig. 2.6, Table 2.1) and indicates that rhyolite activity at Strawberry Mountain indeed started at a time when CRBG volcanism was ongoing (Jarboe et al., 2010; Barry et al., 2013). For this reason, rhyolites of the Strawberry Volcanics also need to be counted among the earliest mid-Miocene rhyolite centers that could be viewed as "plume-head" related rhyolites. Thus the emerging picture is that mid Miocene rhyolitic activity in eastern Oregon (east of ~119^{o} West) started up between 16.5 and 16 Ma across a wide area. The area is bound by the following towns: Baker City, in the north, Ontario in the east, McDermitt in the south, Buchanan, in the east and John Day in the northeast.

The revised area of "early" rhyolite volcanism makes the plume impingement area focused on just the general McDermitt area unlikely (Fig. 2.3) as the center of rhyolite volcanism shifts northward away from McDermitt. This implies that the center of the mantle upwelling, assuming no deflection at the accreted terrane- craton lithospheric boundary occurred (e.g. Jordan et al., 2004), that produced the flood basalts of the CRBG was located further north than previously thought as has been discussed by various workers (Shervais et al., 2008; Camp et al., 2013).

All age data suggest a rhyolite activity period of ~1.5 million year from 16.2 to 14.7 Ma agreeing with similar activity periods for the Dinner Creek Tuff eruptive center (Streck et al., 2015) and other larger rhyolite centers such as Dooley Mountain (Large et al., 2015) in eastern Oregon.

Compositions of rhyolites of the Strawberry Volcanics are comparable to other mid-Miocene rhyolite centers in eastern Oregon including rhyolites of the Dinner Creek Tuff (Figs. 20-22). We highlight Dinner Creek Tuff in our comparison because: 1) this ash-flow tuff is a prominent unit in the area, 2) is coeval with Strawberry Mountain rhyolites and, 3) erupted from a nearby center located along the southeastern extent of the distribution area of the Strawberry Volcanics (Streck et al., 2015). Strawberry Mountain rhyolites range from compositions akin to I-type rhyolites to those with A-type affinities and this range is typical for rhyolites from eastern Oregon, particular mid-Miocene rhyolites (Streck, 2014). Specifically, the rhyolites of the Strawberry Volcanics are slightly higher in both Al_2O_3 and CaO wt. % and tend to be lower in FeO* wt. % than the Dinner Creek Tuff rhyolites and some other eastern Oregon A-type rhyolites (Fig. 2.22). Strawberry Mountain rhyolites mostly overlap with other mid-Miocene rhyolites and indicate overall very low concentrations of HFSE (Figs, 2.11, 2.12). For example, in diagrams with parameters used to distinguish A from I type silicic magmas such as, Zr + Nb + Ce + Y and 10,000 x Ga/Al (Whalen et al., 1987) Strawberry Mountain rhyolites are often among those that have the lowest concentrations (Fig. 2.22). There are however a limited number of Strawberry Mountain rhyolites that do fall into the A-type field.

Generation models for rhyolites are dominated by two different scenarios. In one, rhyolites are generated by partial melting of the crust (Clemens and Wall, 1984; Munksgaard, 1984; Pichavant et al., 1988a, 1988b, Gunnarsson et al., 1998; Smith et al., 2003); the second is an origin through fractional crystallization from mafic magmas (Michael, 1984; Bacon & Druitt, 1988; Mahood & Halliday, 1988; Hildreth et al., 1981;

DePaolo et al., 1992; Hildreth and Fierstein, 2000; Lindsay, et al., 2001; Clemens, 2003). Variants of the partial melting model include degrees of differentiation and/or mixing following melting of the crust. In contrast, variants of the fractional crystallization model involve variations in the initial composition of the parental magma (i.e. how mafic it is), which undergoes differentiation to yield rhyolites. In the case of the Strawberry Mountain rhyolites, low HFSE concentrations are key to narrow down possible generation scenarios. All rhyolites that have lower or equal low concentrations of Nb and Ta than intermediate or basaltic Strawberry magmas could not be generated via fractional crystallization from them (Fig. 2.14). Nb and Ta behave incompatibly throughout the compositional range from basalt to rhyolite. Therefore, differentiation dominated scenarios would inevitably raise Nb and Ta contents and would lead to concentration levels higher than observed in the low HFSE rhyolites. The only mineral that could fractionate Nb and Ta is titanite but titanite has not been observed either in andesites nor in rhyolites. Furthermore, titanite is only stable in high-fo_2 rhyolites and would produce high Nb/Ta given the partition coefficients are slightly higher in Ta which is not seen in our data. The same constraint could be formulated for the trace elements Zr and Hf but since zircon is a stable phase in more silicic magmas, it could have lowered Zr and Hf contents during a very late stage. Although a plausible scenario, it is not very likely because other trace elemental parameters that are typically affected by differentiation processes within the rhyolitic field do not carry a strong late fractionation signal. These parameters include Ba contents and Eu/Eu*; both are still high in most rhyolites, in other

words ≥1200 ppm Ba and ≥ 0.4 Eu/Eu* (Fig. 2.13). This makes a partial melting model to generate many of the Strawberry Mountain rhyolites compelling.

Conclusion

In this paper we have reconciled the various units of the Strawberry Volcanics along with establishing the timing and duration of eruptions. The following is a summary of volcanic events: 1) the southernmost silicic centers start erupting at 16.16 ± 0.17 Ma (2σ) producing plagioclase-rich, mostly metaluminous, low silica rhyolite lavas flows and lava domes, and ash-flow tuffs. High- and low-silica rhyolitic volcanism continues in this area until 14.62 ± 0.06 Ma (2σ) and is co-eruptive with other phases of the Strawberry Volcanics. At 15.30 ± 0.10 Ma (2σ) the northern rhyolites erupt aphyric, peralkaline/aluminous, A-type, high silica rhyolites co-eruptive with the southern rhyolites. Activity continues here until 14.79 ± 0.12 Ma (2σ). 2) Intermediate volcanism of calc-alkaline composition begins erupting through dikes starting at 15.59± 0.36 Ma (2σ). This activity continues through the duration of eruptions of the Strawberry Volcanics to 12.52± 0.12 Ma (2σ). 3) Intermediate and mafic tholeiitic eruptions start at 15.57± 0.16 Ma (2σ). The intermediate compositions erupt first, co-erupting with other intermediate and silicic eruptions, and is followed by eruptions of more mafic composition. These eruptions continue in the same style as the calc-alkaline eruptions until 12.61± 0.06 Ma (2σ).

Herein, we show that the intermediate and mafic eruptions of the Strawberry Volcanics co-erupted in part with the main-phase of the CRBG from an area surrounded by dikes swarms producing CRBG lavas. The most mafic magmas of the Strawberry Volcanics (≤54 SiO_2 wt. %) share geochemical signatures with lavas of the CRBGs

therefore strongly suggesting CRBG lavas and Strawberry Volcanics have a similar petrogenetic origin. Specifically, such mafic lavas of the Strawberry Volcanics are most similar to the Steens Basalt. At higher silica, magmas of the Strawberry Volcanic appear to be largely a product of open-system differentiation (AFC and magma mixing) processes. These processes will be addressed in the following chapter (Chapter 3).

A hallmark of continental large igneous provinces is that flood basalts are associated with voluminous rhyolite volcanism. Numerous mid-Miocene silicic centers have been documented throughout northwestern Nevada and eastern Oregon that nearly coincide with the inception of the Yellowstone-Snake River Plain Hotspot as marked by flood basalt volcanism. The Strawberry Volcanics also includes rhyolitic volcanism during the height of silicic flair up. These rhyolites are not fractionates of the mafic or intermediate lavas of the Strawberry Volcanics or CRB magmas but instead appear to be generated by partial melting of the crust. We have compared the rhyolites of the Strawberry Volcanics to other mid-Miocene rhyolites of Oregon that are associated with flood basalt volcanism. The rhyolites of the Strawberry Volcanics appear geochemically similar in composition and have significant overlap in major and trace element concentrations with these other rhyolites. Furthermore, some of the Strawberry Mountain rhyolites are considered to have A-type characteristic which typifies almost near all rhyolitic products of the Yellowstone hotspot track.

CHAPTER 3

THE MAKING OF INTRA-CONTINENTAL ANDESITES WITH ARC AFFINITIES: THE STRAWBERRY VOLCANICS OF NORTHEAST OREGON

Abstract

The Strawberry Volcanics provide a unique opportunity to study andesitic magma generation in an intra-continental setting located in the center of and co-erupting with units of the Columbia River flood Basalt Group (CRBG). The Strawberry Volcanics are an ideal setting to investigate how magmas may differentiate from parental basalt magmas to tholeiitic and calc-alkaline intermediate lavas. Within the Strawberry Volcanic area tholeiitic basalt, tholeiitic intermediate, calc-alkaline intermediate, and rhyolite lavas erupted, and ample crustal lithologies are exposed throughout the area to test closed and open system models. This provides the opportunity to investigate the petrogenesis of calc-alkaline andesites that have arc affinities but erupted in an intra-plate setting. Our results indicate that the magmas that generated both calc-alkaline and tholeiitic intermediate magma compositions were initially basaltic tholeiites similar to Imnaha or Steens basalts of the CRGB. The tholeiitic intermediate magmas were produced primarily by fractional crystallization of these mafic magmas while the calc-alkaline magmas are a result of mixtures of tholeiitic basalt, rhyolite, and crust. The arc-like signature of the calc-alkaline lavas (elevated LILs) is a result of both the melting source region and the end-members with which the mafic magmas mixed/contaminated. This research agrees with similar findings from others within the Basin and

Range/Oregon-Idaho graben and CRB province. The main difference between this research and others is that there is no need for a primitive calc-alkaline magma or extensive fractional crystallization to generate the calc-alkaline andesites.

Introduction

Melt generation in the mantle and its subsequent rise to and through the crust is a fundamental process to which igneous petrologists account the chemical variation in the volcanic products expressed at the surface. As magma ascends from the mantle to the crust, it may undergo dynamic changes, altering the melt composition by one or any combination of the following processes: 1) fractional crystallization (FC) of mantle derived melts (e.g. Grove and Baker, 1984, and Sisson and Grove, 1993); 2) partial melting of lower crust by mantle derived melts (e.g. Smith and Leeman, 1987; Tatsumi et al., 2008); and 3) open-system processes that differentiate the melt by assimilation and fractional crystallization (AFC) or magma mixing (Eichelberger, 1975; DePaolo, 1981; Hildreth and Moorbath, 1988; Clynne, 1999). These processes can ultimately lead to the generation of intermediate magmas that retain the petrogenetic history of both the mafic and silicic components and the processes that acted upon the original mantle melt (i.e. FC, AFC, mixing or a combination of all). These differentiation processes must occur very commonly as the Earth's crust is overall andesitic in composition (e.g. Rudnick, 1995; Taylor, 1995; Rudnick and Gao, 2003), and in turn, these intermediate magmas, when expressed as andesitic lavas at the Earth's surface, provide igneous petrologists with evidence of the specific differentiation processes that acted upon the volcanic system. It is this geochemical evidence with which the petrogenetic history of the volcanic system can be pieced together.

Andesitic lava is the dominant product in 80% of all volcanic arc systems (Gill, 1981; Tatsumi et al., 2008), but in intra-continental settings where hot-spot volcanism drives melt generation, intermediate lavas are minor in terms of volume (e.g. the strongly bimodal Yellowstone-Snake River Plain Hotspot province of the Pacific Northwest) (Hooper and Hawkesworth, 1993; Hooper et al., 2002). The proportion of andesitic lavas expressed at the surface in intra-continental settings, which are typically dominated volumetrically by bimodal (basalt and rhyolite) compositions (Hooper and Hawkesworth, 1993; Hooper, 2002), may be misleading and grossly underestimate the volume of un-erupted material that stalled during ascent and crystallized within the crust. The voluminous (~1000 km^3) intermediate lavas of the Strawberry Volcanics (Chapter 2) provide a rare and valuable opportunity to study such magmas in an intra-continental setting unaffected by subduction zone processes, and to thereby evaluate what crustal modifications have occurred as the mafic component transitions to intermediate.

Tholeiitic and calc-alkaline andesites

Andesites compositionally fall into two different groups based on the evolution of Fe concentration with silica enrichment during the development of the melt to its final composition (Bowen, 1928; Fenner, 1929). A magma series can lose Fe (i.e. calc-alkaline series; Bowen, 1928) or gain Fe (i.e. tholeiite series; Fenner, 1929) with increasing differentiation (Wager and Deer, 1939). In the past, the total alkali ($Na_2O + K_2O$), FeO*, and MgO wt % (AFM) (Irvine and Baragar, 1971) and FeO*/MgO wt % vs SiO_2 wt % (Miyashiro, 1974) diagrams were used to define the compositional ranges of each

andesite series. The AFM diagram indicates a tholeiitic series as the suite evolves towards the FeO* corner before trending to the alkali corner of the ternary while the calc-alkaline series plots in the middle of the diagram and trends straight to the alkali corner. The inclusion of the alkalis can produce a trend which can be misleading when defining calc-alkaline vs tholeiite lavas (Zimmer et al., 2010). The FeO*/MgO vs SiO_2 diagram of Miyashiro (1974) (e.g. chapter 1 Fig. 1.2b and chapter 2 Fig 2.2b) is a more effective way to evaluate these series because it provides quantitative measurements and ignores the alkalis (Tatsumi et al., 2008; Zimmer et al., 2010). Therefore, herein we use the Miyashiro (1974) definition to define tholeiite and calc-alkaline series. Further, a baseline requirement for the classification of tholeiites is that the samples have normative hypersthene to which the samples labeled tholeiite or tholeiitic herein are hypersthene normative (see electronic appendix).

Petrographic characteristics can often be supplementary to geochemical data of volcanic suites when defining a series as either calc-alkaline or tholeiitic. The presence of orthopyroxene in the groundmass of sub-alkaline volcanic rock can indicate calc-alkaline character, and its absence, tholeiitic character (Kuno, 1950; 1959; 1968), yet in the light of recent understandings of the evolution of magma (i.e. magma mixing and assimilation processes) series this can be an unsafe determination of either series Other mineral phases which are common in calc-alkaline lavas are hornblende and biotite (Kuno, 1950).

Arc volcanic settings have been well studied and are known for producing both calc-alkaline and tholeiitic magma types (Jakes and Gill, 1970; Plank and Langmuir, 1988; Grove and Baker, 1984; Sisson and Grove, 1993) with calc-alkaline lavas as the

prevailing magma type (Ewart, 1982). Experiments have shown that a water-rich basalt undergoing fractional crystallization processes can generate calc-alkaline magmas at arc settings (Grove and Baker, 1984; Sisson and Grove, 1993). Calc-alkaline magmatism generated at non-arc settings are typically less abundant but have been documented (e.g. Ewart, 1982; Hawkesworth et al., 1995; Hooper et al., 1995). Herein, we will be evaluating the development of the calc-alkaline trend in a non-arc setting using the Strawberry Volcanics (Fig.3.1).

Regional Geologic Setting

The basement rocks of eastern Oregon consist of pre-Tertiary accreted terranes. They crop out in the periphery of the Strawberry Volcanic exposures (Fig. 3.3) and also make up the basement to the Strawberry Volcanics. They consist of the following units: a) the Baker Terrane (ophiolitic, mafic to ultramafic sequences and associated sedimentary units); b) the Izee Terrane (Mesozoic clastic sediments (siltstones to greywackes) with a minor component of carbonate horizons); and c) the Olds Ferry Terrane (volcanic arc sequences) (Fig. 3.3. 3.2). Other components of the broader surroundings include granodioritic plutons of early Cretaceous age (LaMaskin et al., 2009a, b) and intrusive equivalents to mostly compositional intermediate magmas of precursory volcanism of Eocene (Clarno), Oligocene (John Day) and early Miocene age. Late Oligocene to Early Miocene age (19 Ma) volcanism is locally represented by phenocryst-rich dacitic and rare tholeiitic lavas found within the investigated area (Chapter 2). Magma conduits and reservoirs that gave rise to the Strawberry Volcanics passed through and developed within the crust that is made up by these rocks.

The main pulse of the CRBG (>200,000 km^3 of cumulative lavas) erupted from 16.8 to 15.9 Ma and thus slightly predated or erupted concurrently to the Strawberry Volcanics (Camp and Hooper, 1981; Baksi 1989; Camp and Ross, 2004, Jarboe et al., 2008, Barry et al., 2013). The Strawberry Volcanics are geographically located in the heart of flood basalts and are surrounded by CRBG dike swarms (Chapter 2). Simultaneously (~16.5 to 14.5 Ma), widespread silicic volcanism occurred across the

region stretching from northwest/northeast Nevada to the silicic lava flows and domes of north-central eastern OR, including those of the Strawberry Volcanics (Chapter 2) (Pierce and Morgan, 1992; Brueseke et al., 2009 and 2014; Coble and Mahood 2012).

Methods

Bulk rock analyses

Radiogenic isotope analyses

Sr, Nd, and Pb isotopic compositions were measured on 13 samples representing mafic, intermediate, and rhyolitic compositions. Additional 5 samples of the regional accreted terranes (Fig 3.3) within the vicinity and underlying the Strawberry Volcanics were analyzed using the same method described below. Sample dissolution and chemistry were performed at the radiogenic isotope clean lab and analyzed using thermal ionization mass spectrometry (TIMS) at New Mexico State University. Standard sample preparation procedures for whole rock isotopic analysis were performed, the details of which can be found at: http://geology.nmsu.edu/framos/TIMS.html. Age corrections for Sr and Nd isotopic ratios were applied using the ratio of Rb and Sr whole rock element concentrations.

Electron Microprobe Analysis

In situ major and minor element concentrations were determined via electron microprobe analysis (EMP) on select samples of lavas of the Strawberry Volcanics using a Cameca SX100 electron microprobe at Oregon State University (OSU) with five wavelength dispersive spectrometers, including two spectrometers outfitted with large format diffracting crystals for trace element measurements. A 15 keV accelerating voltage and 30 nA beam current (focused beam diameter 1 μm) was used on

clinopyroxene (cpx), orthopyroxene (opx), and olivine. Typical counting times were from 10 - 30 seconds. Instrument calibration was checked by running the NMNH 117733 natural diopside standard as an unknown.

Results

Petrography

The petrographic characteristics of the Strawberry Volcanic units will be addressed in this section.

Basalt Lavas

Basalt lava flows of the Strawberry Volcanics are characterized by the presence of plagioclase, cpx, olivine, and Fe-Ti oxide (Fig. 3.4a, b). The most prevalent petrographic texture of the basalt lavas is the ophitic texture. Plagioclase chadacrysts are the main mineral phase with a modal abundance of ~60%. These chadacrysts range in size from <1 mm to 2 mm and are often tabular and euhedral (Fig. 3.4a, b). Oikocrysts of clinopyroxene (augite) are the sole pyroxene phase present and have a modal abundance of ~30%, ranging in size from 1 mm to 3 mm (Figs. 3.4a, b). Small olivine crystals (~1 mm in size) account for up to 7%. Acicular Fe-Ti oxides (ilmenite) are approximately 1 mm in length and account for ~3% of the total visible crystals. Minor amounts of glass fill the intersertal zones between crystal laths. No major disequilibria, xenoliths, or glomerocrysts are present in basaltic thin-sections.

Intermediate lavas

Tholeiitic lavas

Intermediate lavas of tholeiitic composition are largely phenocryst-poor, containing groundmass plagioclase (65% modal abundance) + cpx (30% modal abundance) + oxides (≤3% modal abundance) and ± olivine (≤ 2% modal abundance) (Figs. 3.4c, d, g). The groundmass minerals are typically <1 mm in size and are euhedral (Fig. 3.4g). Groundmass textures can vary and can include ophitic groundmass much like the basalts, but minerals are smaller in size (<1 mm) (Fig. 3.4h). Although most of the intermediate lavas are phenocryst-poor, some contain plagioclase, cpx, olivine, or display a combination of all three, never exceeding >10% by volume (Figs. 3.4h, i). Plagioclase phenocrysts can be >3 mm in length and often anhedral to subhedral, zoned and display sieved and resorbed textures (Figs. 3.4h, i). When present, cpx and olivine phenocrysts range in sizes from 1 to 2 mm. No xenoliths or glomerocrysts have been observed in thin-sections (Fig. 3.4).

Calc-alkaline Lavas

Intermediate calc-alkaline lavas have a plagioclase + cpx ± opx + oxides ± olivine mineral assemblage and display two common petrographic textural features: 1) phenocryst-poor (<5%) lavas with groundmass minerals of plagioclase (80% modal abundance) + cpx (10% modal abundance) ± opx (5% modal abundance) + oxides (1-5% modal abundance) and ± olivine (≤2% modal abundance); and 2) porphyritic lavas with up to 35% phenocrysts and a groundmass mineral assemblage identical to the

phenocryst–poor lavas (Figs. 3.4e, f). The phenocryst-poor lavas are the predominant type. Plagioclase is the major phenocrystic phase accounting for up to 80 % of total phenocrysts. These plagioclase phenocrysts are often subhedral to anhedral and can be as large as 5 mm in length (Figs. 3.4e, f, j, k, l). These phenocrysts are often zoned and display sieved and resorbed textures (Figs. 3.4j, k, l). Olivine phenocrysts are typically ~1 mm in size and display embayments or otherwise resorbed textures (Fig. 3.4j). Porphyritic lavas often have glomerocrysts of plagioclase + pyroxenes ± olivine (Figs. 3.4e, f), which is supported by the presence of xenolithic inclusions in hand sample that can range in sizes from 1 to 10 cm. Flow banding is not uncommon within the intermediate lavas. No hornblende or biotite minerals are observed as phenocryst or groundmass phases, which are commonly present in most calc-alkaline magma series (Kuno, 1950).

Rhyolite Lavas

The rhyolites of the Strawberry Volcanics can be broken into two different types based on geographic location, physical characteristics, and major and trace element geochemistry: 1) the northern high-silica rhyolites; and 2) the southern rhyolites, which are further subdivided into high-silica and low-silica groups (Chapter 2). All northern high-silica rhyolites are phenocryst-poor (<1%) and are either glassy or devitrified. When present, phenocrysts include small, ~1 mm in size plagioclase and/or quartz. The southern high-silica rhyolites are porphyritic, glassy or devitrified with ~10%.phenocrysts of plagioclase (~60 % modal abundance), quartz (35 % modal

abundance) and amphibole and biotite (≤ 5 % modal abundance). At 25-30% phenocrysts dominated by plagioclase (~80% modal abundance) and quartz (~20% modal abundance) and minor amounts of amphibole and biotite (<1%), the southern low-silica rhyolites are significantly different. Dark flow bands and/or mingling textures with inclusions of less silicic melts or xenoliths appear in the low-silica rhyolites. Disequilibria textures are observed in the phenocrysts, including sieving and resorption of plagioclase phenocrysts.

Mineral Chemistry

Basalts

EMP analyses of basalt olivine crystals indicate intra- and inter-compositional variability. The forsterite content range from Fo_{44} to Fo_{72} with an average of Fo_{60} (Figs.3.5, 3.6a; Table 3.1). Two populations of olivine exist: one population has higher Mg in the cores, averaging Fo_{70}, and the second has cores with an average Fo_{56}. Olivine crystals with Fo_{70} cores substantially decrease in forsterite content towards the rim, with an average of Fo_{48}. Olivine crystals with cores of Fo_{56} show no zonation towards the rim. Furthermore, in many instances olivine crystals with ~Fo_{70} cores have cpx rims. EMP analyses of pyroxene crystals indicate that the sole pyroxene phase is augite with an average mineral composition of 44% En, 17% Fs, and 39% Wo (Fig. 3.8 and Table 3.1). Cpx crystals have magnesium numbers that range between Mg_{65} to Mg_{77}, have an average of Mg_{72} and are typically uniform in composition from core to rim with minor normal zonation (Fig. 3.7b). The maximum variation measured in one cpx showed a range of

Mg_{76} to Mg_{67} while the rest have little (~±2 Mg content) to no variation (Figs.3.5, 3.6b, 3.7b).

Intermediate lavas

Tholeiitic lavas

EMP analyses of tholeiite olivine crystals indicate a single common olivine type that typically displays normal zonation from core to rim (Fig. 3.9). Cores of olivine crystals range from Fo_{67} to Fo_{74} with an average of Fo_{71}, and the rims range from Fo_{59} to Fo_{64} with an average of Fo_{62} (Figs. 3.6a, 3.7a, 3.9; Table 3.1). Similar to the basalt olivine phenocrysts, cpx growths are present around the rims of tholeiitic olivine crystals. Pyroxene analyses indicate that the sole pyroxene phase is augite with an average mineral composition of 45% En, 15% Fs, and 40% Wo (Fig.3.8; Table 3.1). Magnesium numbers of the cpx crystals range from Mg_{68} to Mg_{78} with an average of Mg_{75} (Figs. 3.6b, 3.7b). Most cpx crystals appear uniformed from core to rim but can also display oscillatory zonation ranging from Mg_{71} to Mg_{76} (Fig. 3.7b).

Calc-alkaline lavas

EMP analyses of calc-alkaline olivine crystals indicate one common olivine type that shows minor compositional variability within single crystals from core to rim (Fig. 3.10). Forsterite content of olivine crystals vary between Fo_{78} and Fo_{84} with an average Fo_{82} (Fig. 3.6a; Table 3.1). Cores of olivine crystals average Fo_{83}, and rims average Fo_{78} (Fig. 3.7a). These analyses are from a single calc-alkaline andesitic lava (59 SiO_2 wt. %), which is representative of typical intermediate, calc-alkaline Strawberry Volcanics lavas. Interestingly, this andesite contains pyroxene with the highest Magnesium number and olivine with the highest forsterite content among all tholeiitic basalts to andesites) (Figs. 3.6, 3.7; Table 3.1). It is also noteworthy that olivine crystals observed in this thin section often have resorbed cores (Fig. 3.4). Unlike the basalts and the intermediate tholeiites, pyroxene analyses indicated that calc-alkaline lavas contain two phases of pyroxene: augite and orthopyroxene (Fig. 3.8 and Table 3.1). The average cpx mineral composition is 45% En, 13% Fs, and 42% Wo and the opx 75% En, 22% Fs, and 3% Wo (Fig. 3.8; Table 3.1). magnesium numbers of the cpx range between Mg_{72} and Mg_{83} with an average of Mg_{77}. Cores of cpx phenocrysts range from Mg_{78} to Mg_{83} while groundmass cpx range from Mg_{72} to Mg_{79} (Figs. 3.6b, 3.7b, 3.10; Table 3.1). Magnesium numbers of the opx range between Mg_{66} and Mg_{84} with an average of Mg_{78} (Figs. 3.6c, 3.10; Table 3.1). Opx phenocrysts have cores that range from Mg_{77} to Mg_{84} and rims can be as low as Mg_{66}, and groundmass opx range from Mg_{70} to Mg_{82} (Fig. 3.6c and 3.10; Table 3.1).

Summary of EMP Results

Overall, the olivine crystals in the basalts have the lowest forsterite content, but the upper range does overlap the range of the intermediate tholeiitic group (Fig. 3.6a). The olivine crystals in the calc-alkaline lava analyzed recorded the highest forsterite content (Fig. 3.6a). These crystals also appear to have higher NiO wt % concentrations than the other lavas analyzed (Fig. 3.6a). Core to rim analyses within olivine crystals show that both the basalts and the tholeiitic intermediate lavas are normally zoned while the calc-alkaline lavas have little to no zonation (Fig. 3.7a). Cpx analyses indicate that the basalts have the lowest magnesium numbers, yet the upper range overlaps with the intermediate tholeiites and calc-alkaline groups (Figs. 3.6b, c). The calc-alkaline lavas have the highest cpx magnesium numbers (Fig. 3.6b, c), and overall, the more tholeiitic lavas have lower magnesium numbers, and the more calc-alkaline lavas have higher magnesium numbers (Fig 3.6c). Cpx core to rim analyses indicate that the basalts have little to no zonation or are normally zoned, while the intermediate tholeiites display both normal and minor reverse zonation (Fig. 3.7b). Calc-alkaline varies from no zonation to reverse zonation (Fig. 3.7b). Lastly, opx is present only in the calc-alkaline and has high magnesium number as in the cpx phase (Fig. 3.7c). Opx core to rim analyses show that both normal and reverse zoning occurs within these pyroxenes (Fig. 3.7c).

Whole Rock Geochemistry

Whole rock major and trace element geochemistry

Major elements of the Strawberry Volcanic lavas when plotted against silica generally form linear or co-linear trends with typical increases or decreases as silica increases from basalt to rhyolite (Fig. 3.11). The exceptions are Al_2O_3, Na_2O and P_2O_5 (Fig 3.12). Little to no change in Al_2O_3 occurs during the transition from basalt to andesite, and the concentration is lowest in rhyolites. Na_2O values increase rapidly from basalt to basaltic andesite, but then remains between 3 to 4 wt.% (Fig. 3.12). The compositional data of the tholeiitic and calc-alkaline intermediate lavas strongly overlap in major elemental concentrations with some minor but important exceptions. Tholeiitic lavas are slightly lower in MgO and higher in P_2O_5 relative to the calc-alkaline magmas (Figs. 3.11, 3.12). Among tholeiitic intermediate compositions, Nb-rich (>14ppm) lavas have slightly higher Na_2O and distinctly higher P_2O_5 concentrations than the Nb-poor (<14ppm) lavas (Fig. 3.12).

Trace element concentrations of the Strawberry Volcanics show great variability within the suite. Decreasing or constant concentrations are observed among incompatible elements from basaltic to rhyolite (Fig. 3.13). Incompatible trace elements that do increase with increased silica content of the sample include Cs, Rb, Ba, and Pb, i.e. most of the large ion lithophile elements (LILEs). On the other hand, incompatible elements of the high field strength elements (HFSE) including Nb, Zr, Hf, Ta, and Y show different trends than the LILEs, and concentrations decrease or stay constant with silica enrichment. Th and U that have affinities with both element groups moderately increase.

All REEs, excluding Eu, either remain constant (La, Ce, Er, Tm, Yb, and Lu) or decrease (Pr, Nd, Sm Gd, Tb, Dy, and Ho) with increasing silica (Chapter2). Typically, compatible trace elements (Ni, Cr, Sc, Sr, and Eu) decrease, but the highest concentrations are observed in intermediate compositions (e.g. Sr).

Mafic to intermediate compositional groups (i.e. basalts, tholeiitic and calc-alkaline basaltic andesites and andesites) of the Strawberry Volcanics have strongly overlapping but sometimes gradational incompatible trace concentrations (Fig. 3.13). Differences among intermediate magmas are strongest between the high-Nb group relative to others, i.e. the low-Nb tholeiitic and calc-alkaline group (Fig. 3.13). The high-Nb tholeiitic group is more enriched in incompatible elements including Nb, Ta, P, and all LREE (La, Ce, Pr, Nd, Sm, Eu, and Gd) relative to the other groups. In general, the tholeiitic intermediate compositions are more enriched in the HREEs than the calc-alkaline ones (Fig. 3.14, Chapter 1). The intermediate groups have similar trace element concentrations to the basalts with the exception of higher concentrations in Th, U, K, and Pb. Lower concentrations of La and Ce are observed in the low-Nb tholeiites and calc-alkaline lavas have lower Ti and P than the other lava types (Fig. 3.14)

When these data are plotted on normalized incompatible trace and REE diagrams, some general observations can be made. When normalized to primitive mantle (Sun and McDonough, 1989) (Fig. 3.14) and C1 chondrite (Boynton, 1984) (Fig. 3.14), all of the intermediate lavas of the Strawberry Volcanics have a pattern similar to that of the Steens and Imnaha Basalts. The intermediate lavas have prominent spikes of Ba, U, K, and Pb, indicating significant enrichment of these elements relative to neighboring elements. A

minor spike of P is present in both tholeiitic groups but is more pronounced in the high-Nb group (Fig. 3.14). Significant troughs are present at Nb, Ta, and Ti (Fig. 3.14). A trough in P is observed in some of the calc-alkaline andesites. The chondrite normalized REE diagrams show overlap within groups and with Steens Basalt (Fig.3.14). Between groups, the most notable trend is that the high-Nb tholeiitic group is the most enriched in all REEs and the calc-alkaline group is the most depleted (Fig. 3.14).

Sr, Nd, and Pb radiogenic isotope composition

Figure 3.15 shows radiogenic isotopes of the various groups of lavas of the Strawberry Volcanics along with CRBG lavas and various basement lithologies surrounding and underlying the Strawberry Volcanics. The basalts have two different isotopic compositions (Fig. 3.15): one basalt sample is fairly radiogenic with initial $^{87}Sr/^{86}Sr$ (Sr_i) >0.7050 and $^{143}Nd/^{144}Nd$ (Nd_i) <0.5125; this basalt may have already experienced contamination from assimilation and or magma mixing processes during assent through the crust. This sample may have been affected by weathering as well given the low K, U, Th concentrations. Its isotopic concentration is similar to values of crustal materials surrounding the Strawberry Volcanics (Fig. 3.15). The other basalt type is similar in its isotopic ratios to the intermediate lava compositions. As silica increases, isotopic ratios undergo no to minor changes. Sr_i appears to decrease slightly and initial Nd_i slightly increases from basalt to andesite (Fig. 3.15). Isotopic ratios of Sr_i and Nd_i for the compositional intermediate groups (calc-alkaline and tholeiitic) largely overlap (Fig. 3.15). Lead isotopic ratios remain the same within analytical uncertainty for all mafic to

intermediate composition with the exception of the basalt mentioned above. Rhyolites of the Strawberry Volcanics are slightly more variable in their isotopic composition but there are rhyolites that are remarkably similar in all isotopic ratios to mafic to intermediate compositions (Fig. 3.15). The greatest isotopic variability is observed among samples of the surrounding basement, which is not surprising given the large range of compositions from ultramafic to silicic, argillitic lithologies (Chapter 2; Table 3.3; Fig. 3.15). What is noteworthy, however, is that there are mafic igneous to silicic sedimentary basement samples that have comparable ratios with Sr_i values lower and higher than Strawberry Volcanics, and Nd_i values overlapping on the lower end of volcanic rocks (Table 3.3).

Discussion

Common basalt for calc-alkaline and tholeiitic suites

The lavas of the Strawberry Volcanics are mostly, by volume, intermediate composition lavas (Fig. 3.2), yet this research has shown that basaltic lavas are dispersed throughout the geographic area and stratigraphy of the Strawberry Volcanics (Chapter 2). These basaltic lavas provide the opportunity to evaluate what mantle magmas were prior to the path of evolution to intermediate composition. In previous research (Chapters 1 and 2), we showed that the basalts of the Strawberry Volcanics are dispersed throughout the sequences of the volcanic stratigraphy and co-erupted during the period of intermediate lava production. We have also shown that the volcanic suite of the Strawberry Volcanics, as well as the tholeiites of the CRBG, all converge at high-Mg concentrations of approximately 8.0 MgO wt.%, pointing to a tholeiitic basalt as the parental magma from which different Fe/Mg trends develop (Chapter 1).

All basalts of the Strawberry Volcanics are tholeiitic and are compositionally similar to the least evolved, intermediate calc-alkaline and tholeiitic lavas of the Strawberry Volcanics (Figs. 3.12, 3.13, 3.14, Chapter 1). Normalized incompatible trace element diagrams show similar patterns that illustrate this similarity between the basalt and the intermediate lavas (Fig. 3.16). These diagrams show that basalts and intermediate magmas have overlapping ranges (Fig. 3.16). Based on these data, we argued in Chapter 1 for a common tholeiitic basalt parent that gave rise to all intermediate magmas and that

differences in evolved intermediate magmas are due to distinct differences in processes during magma evolution (Fig. 3.16).

Here we add whole rock radiogenic isotopes of the basalts and intermediate lavas of the Strawberry Volcanics as additional evidence for this common basalt leading to the intermediate lavas. Analyzed basalts vary in their isotopic characteristics and the more enriched values of sample AS-SV-287 are likely due to crustal assimilation or slight post-emplacement isotopic shifts due to alteration processes (Fig. 3.15). On the other hand, basalt sample AS-SV-11 falls among the least evolved intermediate magmas of tholeiitic and calc-alkaline character (Fig. 3.15). Specifically, these are samples AS-SV-39b and AS-SV-56 (Chapter 2). Using this basalt and these intermediate samples, a common basalt magma would have the following isotopic values; Sr_i 0.70441 ±0.0002, Nd_i 0.51279 ±0.0001, $^{208}Pb/^{204}Pb$ 38.512 ±0.0709, $^{207}Pb/^{204}Pb$ 15.598 ±0.0173, $^{206}Pb/^{204}Pb$ 18.856 ±0.0620 (error calculated is 2σ). These values are nearly indistinguishable from isotopic ratios of the lava flows of the Imnaha Basalt except for lead isotopes (Fig.3.15; Chapter 2). Lead isotopic values of the common mantle input for the Strawberry Volcanics are like the ones for the nearby Picture Gorge Basalt (Fig. 3.15; Chapter 2).

Further comparisons of the basalts and the intermediate lavas can be assessed by looking at the mineral chemistry between the basalts and intermediate magmas. The basalt cpx crystals have an average Mg_{72}, tholeiitic intermediate lavas average Mg_{75}, and calc-alkaline intermediate lavas average Mg_{77} (Fig 3.6, 3.7; Table 3.1). The olivine analyses indicate that the core average in the basalts Fo_{70}, the tholeiites Fo_{71}, and the calc-alkaline Fo_{83}. This shows that pyroxene mineral chemistry between the basalts and

the intermediate tholeiites and the calc-alkaline lavas are nearly identical in their magnesium content despite the calc-alkaline lavas being the most silicic (~62 SiO_2 wt %). The olivine data suggest that the basalt and the tholeiitic intermediate lavas share a common olivine type but the calc-alkaline lavas may be inheriting olivine from an outside source. The latter is consistent with disequilibrium textures of olivine crystals seen in thin section.

Enrichment and fractionation during tholeiitic evolution

From the previous section, we determined that the basalts are related to the intermediate lavas yet evolution from basalt can lead to different compositional trends (calc-alkaline or tholeiitic). Using this basalt composition, we can evaluate how magmas would evolve given this starting composition and using fractional crystallization (FC) and assimilation fractional crystallization (AFC) (DePaolo, 1981) models. Some intermediate tholeiitic lavas show distinct enrichments in the concentration of incompatible trace elements, particularly HFSE and REE, and we have referred to these as the high-Nb group, although other trace elements are comparably enriched as well (e.g. Ta, Zr, Hf, Ti, Y and nearly all REEs (Figs. 3.14a, b). There are several processes that could account for these high-Nb group signatures. Higher silica and lower Mg contents, low compatible trace elements (Ni, Cr), and especially normalized incompatible trace element patterns that resemble basalt samples argues that enrichments are not due to variations in the mantle input, but rather due to fractionation dominated processes (Fig. 3.17). FC and AFC models with a starting composition using the least contaminated basalt (AS-SV-11)

have been calculated to determine the projected incompatible trace element enrichment trends (Fig. 3.17, 3.18). A fractionating mineral assemblage based on abundances determined by CIPW normative calculations (similar to the observed thin-section) of 54% plagioclase, 29% cpx, 6% olivine, 6% magnetite, 5% K-feldspar, and 2% apatite were used to calculate bulk partition coefficients. Partition coefficients for the following elements in the specific mineral are listed in Table 3.2 and results in Table 3.4.

The FC models reproduce element trends which fit the data for the tholeiitic intermediate lavas (Fig. 3.18; Table 3.4). The spread of the observed data can be explained by fractionation amounts of up to 54% crystallization (Table 3.4). An AFC model, using an assimilation of a local lithology (Oligocene age / John Day dacite lava), and using the same parameters described above with an r value = 10% (ratio of assailant) produces a similar fit of the observed data but not required (Fig. 3.18; Table 3.4). Therefore, it appears that to generate the tholeiitic intermediate lavas, which are described as having higher overall incompatible trace element content than samples that straddle the tholeiitic/calc-alkaline divide or are calc-alkaline, an FC model is sufficient to explain observed data (Fig. 3.18; Table 3.4).

Further evidence which supports a component of FC involved in these lavas is provided by the aphanitic nature of these lavas and lack of disequilibrium features associated with them, such as mixing textures, xenoliths, or glomerocrysts present in thin-sections (Fig. 3.4). Furthermore, the similarity in the mineral chemistry between the parental basalt and these tholeiitic lavas with olivine Fo_{70} and cpx Mg_{72} and olivine Fo_{71} and cpx Mg_{75}, respectively (Table 3.1). The low Mg content and normal zonation in both

olivine and pyroxenes in the basalts and the tholeiitic intermediate magmas suggest that FC processes have been a dominant process in these lavas (Fig. 3.7; Table 3.1). In the case of the basalts, it appears that FC processes have occurred and suggests that these lavas may not represent the most primitive magmas of the Strawberry Volcanics. On the other hand, the calc-alkaline lavas do contain magnesium and forsterite content of >80. These high-Mg olivine and pyroxene crystals may represent residual material of more primitive basaltic magmas than erupted.

Generation of intra-continental calc-alkaline andesites

Evidence for open system processes

The clearest textural evidence for open system processes of the intermediate calc-alkaline and transitional tholeiites lavas is the presence of xenoliths of country rock and mingling textures of the rhyolite and intermediate magmas. The xenoliths in the intermediates lavas appear as gabbro, shale/argillite, sandstones and rhyolitic lava. Mixing textures appear in the low-silica rhyolites, which have elongated bands which appear more mafic composition. These bands hosting inclusion of a dark, oxidized, micro phenocryst rich mafic inclusions. Furthermore, plagioclase and pyroxene glomerocrysts of the calc-alkaline lavas commonly display disequilibrium textures (Fig. 3.4).

One key geochemical feature of intermediate calc-alkaline lavas is that as silica content of the sample goes up, highly incompatible trace elements do not increase in concentration, but instead remain consistent at concentration levels seen in more mafic

compositions or even slightly decline; both trends are inconsistent with FC scenarios (Fig. 3.13).

The variability observed in whole rock radiogenic isotopes (i.e. Sr_i, Nd_i, and Pb) of the Strawberry Volcanic lavas (Fig. 3.15; Chapter 2) could also be interpreted as evidence of open system processes. There is a slight decrease in Sr_i with little to no change in Nd_i and Pb as silica increases from basalt to andesite. These data trend towards the analyzed basement lithologies with low Sr_i (Fig. 3.15). It is therefore possible that contamination with these basement lithologies via open system processes is the cause of the observed isotopic shift. A mixing line between the basaltic and crustal composition end-member were calculated for the Sr_i vs Nd_i plot of Figure 3.15. Although the data of the intermediate lavas don't exactly fall on the line, the data do fall along the similar trend suggesting a slightly different but similar end-member might be responsible.

Mixing with silicic magmas vs contamination by crustal rocks

Our data here and in Chapters 1 and 2 have established that the calc-alkaline lavas are genetically related to the tholeiitic basalt and intermediates lavas. Two fundamental questions remain regarding the Strawberry Volcanics: 1) what causes the variability in the intermediate lavas; and 2) how/why do lavas transition from tholeiitic basaltic to intermediate calc-alkaline lavas?

The results of the EMP analyses of olivine and pyroxene show that the calc-alkaline lavas have higher forsterite and magnesium content than that of the intermediate tholeiites or basalts (Figs. 3.5-3.10; Table 3.1), which is an important result in

determining which end-member may be responsible for the formation of the calc-alkaline trend. As suggested above, the tholeiitic lavas, including the basalts, have been modified by FC processes, and therefore do not represent the true primitive magmas. The calc-alkaline lavas, however, contain minerals with high magnesium content(Mg and Fo>80) at high silica concentrations (>60 SiO_2 wt %), which can be the result of either: 1) residual olivine and pyroxenes from a more primitive magma that heated, melted and mixed with silicic crustal lithologies, in turn increasing the silica concentrations of the magmas and generating the calc-alkaline signature; or 2) mafic lavas of the Strawberry Volcanics incorporated some mafic/ultra-mafic country rock from the Canyon Mountain Ophiolite prior to mixing with silicic lithologies, forming the increased silica and calc-alkaline composition.

Both of the above situations are plausible but can be further evaluated to determine which event is the more likely scenario. If the high-Mg olivine and pyroxene crystals within the calc-alkaline lavas are a result from scenario 1), then a primitive basaltic magma not seen at the surface is required as the source for such minerals. All of the observed basaltic lavas and tholeiitic intermediate lavas have mafic silicates with much lower magnesium content (Mg and Fo <80) than observed in the calc-alkaline lava. These lavas also display normal zoning within the crystals, which would further suggest that they have undergone FC processes and that a more primitive magma generated these lavas but is unseen at the surface. Alternatively, situation 2) would not increase the silica concentration of the overall magma but produce a basaltic magma containing minerals with high magnesium number miner and thus would require further interaction with more

silicic country rocks/magmas to drive the silica content to the observed concentrations in the calc-alkaline lavas.

The second scenario is problematic given the trace element compositions observed in the calc-alkaline lavas. Melting and/or incorporating material from the Canyon Mountain Ophiolite (the only basement lithology that could contain high-Mg minerals) even at small degrees would increase the Cr and Ni concentrations of the bulk magma to levels unobserved with the calc-alkaline lavas. It is possible to reach these levels if the ophiolite-contaminated basaltic magma then mixed with a silicic magma with very low Cr and Ni concentrations (Table 3.5). The problem with this is that it would require a significant contribution of rhyolite ~80:20 rhyolite to basalt to generate the suitable Cr and Ni concentrations (58, 40 ppm respectively) yet the SiO_2 content would be much higher (~72%) than observed in the calc-alkaline lavas (~53-62 %) (Table 3.5). In addition, there is a problem with the potential volume of rhyolite with which to mix. In Chapter 2, we determined that the potential volume of the calc-alkaline lavas could total roughly 1,000 km^3. To create this volume it would require a minimum of~800 km^3 of rhyolite below the surface yet at the surface there is only ~100 km^3 (Chapter 2). These problems make the scenario for which the high-Mg mafic minerals are derived from the ophiolite an unlikely situation.

Alternatively, if the high-Mg mafic minerals within the calc-alkaline lavas are derived from a more primitive magma than observed at the surface, then it suggests that in order to form the calc-alkaline lavas, these primitive basalts must have an important role. From the geochemistry, it is already shown that these lavas have similar trace

element patterns to the basalts, yet the incompatible trace elements diverge away from FC models at higher silica and converge to basement and rhyolite compositions. In order for this to occur, there must be an open system process where hot basaltic primitive magmas (capable of producing olivine and pyroxene crystals with high magnesium contents) melts the silicic crust and mixes with the rhyolite. Greater melting can occur if the magma responsible for the melting is a high-temperature primitive basalt. The high-Mg olivine and pyroxenes contained within the calc-alkaline lavas are the residual minerals produced by high-temperature primitive magmas but the primitive magmas alone cannot generate the calc-alkaline lavas. It is this hot magma, which rose and effectively melted the crust, and in turn differentiated the magmas and drove the chemical signature of the calc-alkaline lavas.

In addition to FC and AFC model calculations illustrated in Figure 3.18, calculated mixing lines are plotted with select end-members along with probability density contours of the observed calc-alkaline data in Figure 3.19. These mixing lines represent a three-component mixture between the basalt (AS-SV-11), rhyolite (AS-SV-151), and a local crustal rock (12-46) as end-members and best explain the observed spread of Strawberry Volcanics data (Fig. 3.19; Table 3.6). Using these end-members in some proportion can explain the incompatible trace element concentrations, which FC and AFC modeled results cannot. A mixing line has been generated using a basalt end-member mixed with a rhyolite and shows that a ratio of ~55:45 rhyolite to basalt is required to reach the concentrations observed away from the FC line (Fig. 3.19; Table 3.6). At this mixing ratio, the bulk rock SiO_2 concentration is andesitic (~63 SiO2 wt. %),

matching the observed data (Fig. 3.19; Table 3.6). This mixing line alone cannot account for all of the observed data, but if we assume that FC processes occur with/after mixing, then the observed data to the right of the mixing line can be explained. The data to the left, however must involve a third component. Two mixing lines have been calculated to explain the data, which have incompatible trace element concentrations less than the calculated values from the mixing between basalt and rhyolite (Fig. 3.19; Table 3.6). One line is generated from the mixture described (55:45 ratio) mixing with a selected local crustal rock (12-46) and the other is a mixture of basalt and that same crustal sample (Fig. 19; Table 3.6). These mixing lines show that some proportion of crustal composition is required. The maximum mixing ratio varies with trace element selection but is near a ~ 60:40 ratio of crustal component to either basalt or a hybrid between basalt and rhyolite (Fig. 3.19; Table 3.6). A small component of fractional crystallization for transitional tholeiites and calc-alkaline lavas is permissive (Fig. 3.18, 3.19; Table 3.4, 3.6). It appears that, when mixed with a basalt, both rhyolite and local crustal rocks are required to generate the diverse volcanic suite of the Strawberry Volcanics. This mixing further facilitates the transition from tholeiitic to calc-alkaline composition (Fig. 3.19; Table 3.6). To bring this point further, Table 3.6 lists mixing results using specific observed end-member compositions discussed above to generate the intermediate calc-alkaline composition. We propose that the suite of data observed at the Strawberry Volcanics, including tholeiitic, transitional and calc-alkaline intermediate lavas are a result of mixing mafic magmas with rhyolites and local crusts and FC processes.

Our results show that the variability in the intermediate lavas leading to a tholeiitic or calc-alkaline intermediate composition magma is ultimately the result of either closed system FC or open system mixing processes (Figs. 3.5, 3.6, 3.13-15, 3.18,3.19). Both magma series were generated by ascending mafic magmas coeval with the Columbia River flood basalt event (Chapter 2). The generation of the tholeiitic magmas must have developed by FC of a primitive tholeiitic parental basalt perhaps while being stored within magma chambers within the crust (Figs. 3.5, 3.6). However, the calc-alkaline magmas required a hot, primitive, tholeiitic magma capable of producing high- magnesium numbers in the mafic minerals (Figs. 3.5, 3.6), which interacted with the basement rock and rhyolite (Figs. 3.13-15, 3.18, 3.19). We believe that the transition from tholeiitic to calc-alkaline intermediate magmas is a result of different differentiation paths of the basaltic magmas within the crust (Figs. 3.13-15, 3.18, 3.19). These differences are ultimately a response to closed-system FC and open-system mixing processes (Fig. 3.18). It is likely that initially the magmas rising from depth were minor in volume and FC dominated these magmas, forming the tholeiitic intermediate lavas. After some time, the mafic magmas continued to rise through and heat the crust enough to melt and mix this crust and mix with the rhyolite, while diluting the Fe-enrichment trend and forming the calc-alkaline magmas (Fig. 3.19).

Other calc-alkaline intermediate magma eruptions associated with the Mid-Miocene CRBG of the Pacific Northwest and Basin and Range area (Nevada –Oregon – Idaho graben) and have been documented (i.e. Venator Ranch, Tims Peak, Drinkwater, Voltage and Keeney sequence) and are attributed to various processes (Robyn, 1979;

Brandon and Goles, 1995; Hooper et al., 2002, Camp et al., 2003). These processes include: 1) decompression melting of a previously metasomatized mantle wedge, generating a calc-alkaline primitive basalt; 2) a tholeiite mafic magma assimilating (AFC) crustal rocks with low-Fe composition; 3) FC of hydrous mafic magmas; and 4) magma mixing between a mafic magma and a more silicic/evolved magma (Robyn, 1979; Grove and Baker, 1984; Hildreth and Moorbath, 1988; Sisson and Grove, 1993; Brandon and Goles, 1995; Hooper et al., 2002, Camp et al., 2003; Dungan and Davidson, 2004). The calc-alkaline lavas of Strawberry Volcanic require a situation where a tholeiitic primitive mafic magma mixes with rhyolite and Fe-poor crustal rocks in a tectonic environment unrelated to subduction processes. These calc-alkaline lavas, as well as the tholeiites and basalts, do have elevated concentrations of LILs (Chapter 1, 2; Figs. 3.12, 3.13), but don't require the generation of a calc-alkaline basaltic magma to form the calc-alkaline intermediate magmas as other have suggested within the area (Robyn, 1977; Robyn, 1979; Hooper et al., 1995; Hooper et al., 2002). These elevated LILs are already a feature of tholeiitic basalts that likely resulted from melting of a metasomatized mantle that were further enhanced by fractionation and incorporated crustal components. Instead, our results agree with Brueseke and Hart (2008), Brandon and Goles (1995), and Camp et al., (2003) who attribute the transition from tholeiitic to calc-alkaline to the incorporation/assimilation of Fe-poor crust/melts.

Conclusions

This research sheds light on the diversity of lavas of the Strawberry Volcanics that were derived from a parental magma of tholeiitic composition, that in turn generates different suite of lavas of both calc-alkaline and tholeiitic composition. Given this, we are able to describe the relationship of these magmas to each other and the processes that led to observed differences. Furthermore, this research has implications for our current understanding processes leading to intermediate calc-alkaline magmas in an intra-plate setting and thus serves as a model for other similar intraplate occurrences of arc-like andesites.

The series of events which lead to the diverse suite of lavas mentioned above can be summarized in the following three main events:

- The large Yellowstone-Snake River mantle plume and rising mafic magmas supplies enough heat to partially melt the crust, forming the rhyolites of Eastern Oregon and the rhyolites of the Strawberry Mountain Volcanics.
- Primitive melts to rise through the crust, forming discreet pods of magmas that undergo fractionation, generating the tholeiitic composition seen at the Strawberry Volcanics.
- Prolonged heat input from the underlying mantle plume head thermally matured the crust, allowing primitive melts to rise and mix with both the crust and the partial melts, generating the calc-alkaline magmas.

It appears that in a setting where a mantle plume is a source of heat and melt production, the thermal input into the crust can alter the composition of the magmas to form tholeiitic or calc-alkaline magmas. In most cases, an intra-plate volcanism setting is thought to produce mainly tholeiitic lavas. This research may add to the already known volumes of lava produced during flood volcanism by the addition of calc-alkaline volcanism. Furthermore, the understanding of the precise location and timing of the onset of the mantle plume that generated these lavas and the CRBG is not entirely known, and it is worth looking at the bimodal calc-alkaline and tholeiite lavas of the John-Day/Clarno as a similar scenario prior to the onset of tholeiitic flooding of the CRBG.

Table 1.1: $^{40}Ar/^{39}Ar$ geochronology

				Plateau					Isochron				
Sample	Location	Rock Type[a]	Material Dated[b]	Age (Ma)	± (2σ)	Steps Plateau	^{39}Ar, %	Plateau MSWD	Age (Ma)	± (2σ)	$^{40}Ar/^{39}Ar$ Intercept	± (2σ)	Isochron MSWD
AS-SV-156	44° 2'38.60"N, 118°45'49.50"W	A	GM	14.87	0.13	6	87.43	0.63	14.74	0.25	296.24	4.45	0.76
AS-SV-230	44°18'50.39"N, 118°17'16.61"W	BA	GM	13.53	0.24	5	70.78	2.25	14.01	0.48	288.61	5.50	0.99
AS-SV-82	44°15'55.50"N, 118°22'57.40"W	A	GM	14.21	0.26	-	88.91	4.34	13.94	0.29	301.10	41.01	2.76
AS-SV-14	44°37'13.70"N, 118°28'13.20"W	BA	GM	13.76	0.16	9	85.41	1.04	13.84	0.35	293.20	4.26	1.03
AS-SV-192	44°17'05.30"N, 118°41'6.60"W	A	GM	12.52	0.12	9	98.84	0.19	12.40	0.13	295.60	53.64	0.26

[a] A, andesite; BA, basaltic andesite

[b] GM, groundmass

J = 0.0014610 ± 0.0000056

FCT-3 = 28.030 ± 0.003 Ma

Table 1.2: Whole rock major and trace element analysis of mafic and intermediate lavas

AS-SV-	**171**	**11**	**217**	**14**	**230**	**82**	**192**	**159c**	**156**
*CA/TH	0.94	0.75	0.88	1.03	0.87	1.1	1.18	0.72	0.73
Wt.% normalized									
SiO_2	49.48	50.47	52.06	53.13	53.43	56.23	57.66	57.59	58.08
TiO_2	1.85	1.86	1.60	1.57	1.81	1.42	1.20	1.77	1.68
Al_2O_3	16.10	16.17	17.09	16.45	16.82	16.59	16.98	16.77	16.31
FeO*	9.91	10.65	9.61	9.11	9.59	8.19	7.66	8.53	8.76
MnO	0.16	0.19	0.167	0.16	0.16	0.16	0.14	0.133	0.12
MgO	8.91	6.69	5.82	5.83	5.00	4.29	3.90	2.65	2.67
CaO	8.74	9.52	8.41	8.51	8.26	7.28	6.92	6.42	6.47
Na_2O	3.34	3.09	3.27	3.44	3.27	3.75	3.72	4.15	3.51
K_2O	1.09	0.76	1.394	1.22	1.08	1.58	1.34	1.541	1.75
P_2O_5	0.42	0.59	0.581	0.56	0.60	0.51	0.48	0.464	0.64
ppm									
Ni	188	69	91.2	96	53	66	37	6.4	14
Cr	270	167	101.8	214	82	90	62	19.4	29
Sc	24	29	23.26	24	24	21	19	23.26	22
V	222	265	232.5	207	217	183	153	195.4	209
Ba	408	431	576.77	550	578	746	671	808.70	875
Rb	18	9	12.83	15	13	21	17	25.39	31
Sr	799	527	564.36	560	498	522	520	435.22	483
Zr	126	119	143.46	154	172	185	169	194.67	165
Y	21	26	24.58	26	30	27	26	32.53	30
Nb	16	12	10.64	16	15	15	13	14.45	11
Ga	19	18	19.3	19	20	20	19	21.1	19
Cu	64	50	71.6	56	33	52	39	24	22
Zn	96	102	101.5	96	107	102	94	108.4	102
Pb	3.1	3.5	5.15	4.8	5.4	6.7	6.1	8.03	7.0
U	0.6	0.4	0.43	0.6	0.6	0.7	0.7	1.13	1.0
Th	1.7	1.2	1.22	1.6	2.0	2.1	1.8	3.46	2.8
Cs	0.44	0.18	0.19	0.31	0.33	0.37	0.25	1.40	1.68
Hf	3.15	2.85	3.41	3.62	4.01	4.44	4.09	4.91	4.18
Ta	1.00	0.68	0.60	0.94	0.89	0.87	0.77	0.94	0.70
La	18.8	19.6	22.22	23.1	27.1	27.9	24.6	24.21	23.7
Ce	41.2	42.6	45.59	49.0	55.4	56.5	51.1	48.55	48.1
Pr	5.44	5.67	5.94	6.4	7.4	7.13	6.51	6.72	6.69
Nd	23.1	24.5	24.90	26.6	30.7	28.8	26.8	28.51	28.1
Sm	5.22	5.61	5.46	5.94	6.83	6.29	5.67	6.58	6.47
Eu	1.72	1.9	1.75	1.84	2.12	1.87	1.77	2.04	1.9
Gd	4.82	5.46	5.08	5.56	6.39	5.78	5.20	6.62	6.23
Tb	0.74	0.84	0.82	0.86	1.02	0.89	0.83	1.04	0.99
Dy	4.37	5.06	4.69	5.07	5.87	5.24	5.01	6.36	5.89
Ho	0.85	1.01	0.95	1	1.19	1.05	1.01	1.26	1.17
Er	2.2	2.68	2.53	2.6	3.09	2.76	2.66	3.36	3.09
Tm	0.3	0.38	0.36	0.37	0.43	0.4	0.38	0.47	0.44
Yb	1.82	2.29	2.22	2.31	2.68	2.46	2.4	2.92	2.72
Lu	0.27	0.35	0.35	0.37	0.42	0.41	0.38	0.46	0.42

*CA/TH<1 = tholeiitic, CA/TH>1 = calc-alkaline (cf. Hora et al., 2009)

Table 1.3a: Whole rock major and trace element analysis of rhyolite lavas

	Strawberry Mountain Rhyolites					
AS-SV-	**173**	**15**	**60**	**85**	**110a**	**144**
Wt.% normalized						
SiO2	73.33	73.19	77.71	77.36	77.95	72.99
TiO2	0.27	0.35	0.10	0.13	0.10	0.35
Al2O3	14.24	14.57	12.40	12.76	12.54	15.00
FeO*	2.02	2.23	0.85	1.39	0.74	2.29
MnO	0.05	0.05	0.03	0.02	0.01	0.04
MgO	0.57	0.23	0.08	0.06	0.03	0.25
CaO	2.21	1.99	0.68	0.63	0.63	2.03
Na2O	3.28	3.86	3.76	3.29	3.50	3.53
K2O	3.96	3.42	4.37	4.34	4.49	3.47
P2O5	0.08	0.10	0.02	0.02	0.02	0.05
ppm						
Ni	5	3	1	3	2	3
Cr	7	5	4	2	3	5
Sc	6	6	4	4	4	7
V	27	30	2	8	3	25
Ba	1192	1485	1445	1587	1417	1450
Rb	92	87	117	114	116	84
Sr	198	231	58	65	58	258
Zr	139	171	102	113	99	172
Y	25	18	23	20	18	19
Nb	8	9	9	9	9	9
Ga	16	16	14	13	15	15
Cu	6	7	1	2	2	3
Zn	42	49	25	19	20	43
Pb	13.3	13.9	16.1	17.7	17.6	13.7
U	4.7	3.7	4.6	4.1	4.2	3.4
Th	8.7	7.7	10.5	9.4	10.2	7.3
Cs	4.42	4.20	5.53	-	-	4.32
Hf	3.99	4.59	3.66	-	-	4.59
Ta	0.83	0.74	0.86	-	-	0.74
La	22.3	25.4	28.8	21.8	29.3	24.9
Ce	43.6	46.2	54.5	41.3	43.0	43.5
Pr	5.16	5.36	6.04	-	-	5.14
Nd	19.2	19.6	21.2	17.2	19.9	18.8
Sm	4.32	3.82	4.10	-	-	3.69
Eu	0.77	0.88	0.46	-	-	0.77
Gd	3.98	3.35	3.64	-	-	3.24
Tb	0.68	0.54	0.64	-	-	0.54
Dy	4.28	3.26	3.98	-	-	3.33
Ho	0.89	0.67	0.84	-	-	0.68
Er	2.55	1.88	2.42	-	-	1.95
Tm	0.39	0.29	0.37	-	-	0.30
Yb	2.61	1.93	2.49	-	-	2.02
Lu	0.42	0.32	0.41	-	-	0.33

Table 1.3b: Whole rock major and trace element analysis of crustal rock surrounding the Strawberry Volcanics.

Strawberry Mountain Basement Rocks					
AS-BASRX-	**1**	**2**	**3**	**7**	**9**
Wt.% normalized					
SiO2	67.85	67.24	66.48	74.97	69.49
TiO2	0.65	0.56	0.55	0.04	0.60
Al2O3	15.44	16.25	16.22	15.68	13.66
FeO*	3.67	3.61	3.48	0.97	5.58
MnO	0.07	0.07	0.08	0.05	0.05
MgO	2.46	1.90	2.18	0.14	3.12
CaO	3.86	3.95	4.48	1.61	3.37
Na2O	4.66	4.73	5.30	5.08	2.64
K2O	1.16	1.50	1.08	1.40	1.36
P2O5	0.17	0.19	0.15	0.07	0.14
ppm					
Ni	30	15	19	7	31
Cr	46	24	25	4	52
Sc	9	9	9	1	15
V	78	74	77	5	156
Ba	662	721	538	577	843
Rb	22	29	16	29	40
Sr	536	526	537	389	403
Zr	145	116	104	39	95
Y	16	13	16	16	21
Nb	9	5	4	9	5
Ga	17	19	18	20	15
Cu	5	10	31	5	81
Zn	41	57	172	49	71
Pb	8.9	8.2	12.2	10.8	4.8
U	0	0.3	0.0	1.0	1.8
Th	3.5	3.6	4.5	2.1	4.6
Cs	-	-	-	-	-
Hf	-	-	-	-	-
Ta	-	-	-	-	-
La	16.1	13.5	11.2	10.5	15.3
Ce	32.7	27.3	25.8	23.9	25.3
Pr	-	-	-	-	-
Nd	14.7	13.7	12.9	14.2	14.4
Sm	-	-	-	-	-
Eu	-	-	-	-	-
Gd	-	-	-	-	-
Tb	-	-	-	-	-
Dy	-	-	-	-	-
Ho	-	-	-	-	-
Er	-	-	-	-	-
Tm	-	-	-	-	-
Yb	-	-	-	-	-
Lu	-	-	-	-	-

Table 2.1: $^{40}Ar/^{39}Ar$ age analysis of the Strawberry Volcanics

			Plateau					Isochron				
Sample	Rock Type[a]	Material Dated[b]	Age (Ma)	± (2σ)	Steps Plateau	^{39}Ar, %	Plateau MSWD	Age (Ma)	± (2σ)	$^{40}Ar/^{39}Ar$ Intercept	± (2σ)	Isochron MSWD
AS-SV-151	R	GM	16.16	0.17	7	84.00	8.38	16.27	0.37	5.21	0.12	32.08
AS-SV-291	A	GM	15.59	0.36	4	72.07	4.56	16.18	0.98	5.46	0.33	4.00
*AS-SV-291	A	GM	-	-	-	-	-	15.29	0.06	5.43	0.005	-
AS-SV-159c	BA	GM	15.57	0.16	8	94.37	0.95	15.75	0.30	5.00	0.09	0.79
AS-SV-144	R	Plag	15.34	0.52	8	98.38	0.36	15.50	0.92	4.86	0.29	0.31
*AS-SV-144	R	GM	14.62	0.06	11	14.41	1.48	14.61	0.08	5.11	0.02	1.63
AS-SV-179	R	GM	15.30	0.1	7	89.20	1.85	15.27	0.16	5.23	0.05	2.17
AS-SV-156	A	GM	14.87	0.13	6	87.43	0.63	14.83	0.25	5.61	0.09	0.76
AS-SV-190	R	Glass	14.79	0.12	10	100.0	0.62	14.98	0.19	4.93	0.06	16.05
AS-SV-173	R	Biotite	14.70	0.13	8	89.22	2.16	14.78	0.18	4.81	0.04	1.89
AS-SV-188	A	GM	14.59	0.26	8	99.20	0.61	14.97	0.40	5.21	0.14	20.96
AS-SV-82	A	GM	14.21	0.26	-	88.91	4.34	14.03	0.29	5.23	0.10	2.76
AS-SV-14	BA	GM	13.76	0.16	9	85.41	1.04	13.92	0.35	5.13	0.12	1.03
AS-SV-230	BA	GM	13.53	0.24	5	70.78	2.25	14.10	0.48	5.50	0.18	0.99
AS-SV-109	B	GM	12.61	0.08	13	47.27	2.56	12.65	0.24	4.46	0.08	2.75
AS-SV-192	A	GM	12.52	0.12	9	98.84	0.19	12.48	0.13	4.79	0.03	0.26

* repeat

[a] A, andesite; BA, basaltic andesite, R, rhyolite

[b] GM, groundmass, Plag, Plagioclase

FCT-NM (R98) (4E36-14) = 28.201 ± 0.023 Ma

Table 2.2a: Whole rock XRF data of rhyolite lavas from the Strawberry Volcanics.

	Strawberry Mountain Rhyolites												
AS-SV-	66	144	151	173	263	175	63	133	190	98	60	179	37
XRF													
Wt.% normalized													
SiO_2	69.85	72.99	73.19	73.33	74.62	75.44	76.80	76.88	76.93	76.97	77.71	78.45	78.72
TiO_2	0.59	0.35	0.35	0.27	0.26	0.21	0.06	0.05	0.19	0.09	0.10	0.15	0.14
Al_2O_3	15.17	15.00	14.57	14.24	12.98	12.96	13.20	13.35	12.66	13.16	12.40	12.36	11.64
FeO*	3.46	2.29	2.23	2.02	1.97	1.89	0.80	0.78	1.19	0.93	0.85	0.30	0.84
MnO	0.04	0.04	0.05	0.05	0.05	0.02	0.04	0.04	0.04	0.04	0.03	0.00	0.00
MgO	0.53	0.25	0.23	0.57	0.72	0.00	0.03	0.02	0.13	0.08	0.08	0.00	0.04
CaO	2.70	2.03	1.99	2.21	1.77	0.06	0.53	0.52	0.81	0.69	0.68	0.45	0.06
Na_2O	4.45	3.53	3.86	3.28	3.27	5.20	3.93	3.52	4.12	3.33	3.76	3.99	4.28
K_2O	3.07	3.47	3.42	3.96	4.30	4.20	4.59	4.83	3.91	4.69	4.37	4.28	4.25
P_2O_5	0.15	0.05	0.10	0.08	0.05	0.03	0.01	0.01	0.02	0.02	0.02	0.02	0.03
ppm													
Ni	3.4	3	2.5	4.5	0.40	3.4	1.9	1.5	3	2.3	0.8	3.4	1.3
Cr	4.7	4.6	5.4	6.7	9.18	3.5	2.9	3.3	3.2	3.4	3.6	3.4	3.6
V	43.1	25	29.8	27.1	35.91	4.2	1.2	2.7	5.2	2.1	1.9	2.7	3.6
Ga	17.4	14.6	15.7	15.5	14.86	24.7	17.9	17	14.4	16.7	13.7	16	21.2
Cu	5.3	2.8	7.2	6.4	9.18	1.8	0.4	0	2.7	0.4	1.1	0.5	0.0
Zn	63.4	43.4	48.5	42.1	35.11	132.7	34.0	38.7	35.2	34.2	25.4	21.2	41.3

Table 2.2b: Whole rock ICP-MS data of rhyolite lavas from the Strawberry Volcanics.

	Strawberry Mountain Rhyolites												
AS-SV-	66	144	151	173	263	175	63	133	190	98	60	179	37
ICP-MS													
Sc	10.1	6.6	5.8	6.2	7.3	1.7	4.4	5.3	4.7	4.4	3.6	5.3	2.8
Ba	1283	1450	1485	1192	1342	1626	969	349	1255	1288	1445	1195	493
Rb	65.4	84.2	86.7	91.7	98.3	78.2	111.9	119.6	90.5	105.9	117.1	100.4	89.1
Sr	252	258	231	198	101	32	33	18	77	56	58	45	9
Zr	236	172	171	139	109	448	81	71	176	97	102	220	451
Y	28.75	19.14	17.93	24.79	23.31	61.17	36.42	45.95	35.96	33.14	22.89	43.88	52.60
Nb	11.89	9.16	8.78	8.28	8.32	25.23	19.27	23.39	12.29	15.57	8.88	13.62	23.99
Pb	11.75	13.68	13.91	13.30	13.62	14.02	15.50	15.42	13.10	14.49	16.11	14.31	7.11
U	2.43	3.42	3.67	4.70	3.72	3.49	4.42	4.79	3.42	4.43	4.58	4.04	1.85
Th	5.91	7.35	7.70	8.74	8.61	7.82	10.80	10.44	8.46	10.88	10.50	8.89	9.41
Cs	1.59	4.32	4.20	4.42	4.50	1.54	3.96	4.82	3.32	4.30	5.53	4.27	1.34
Hf	5.93	4.59	4.59	3.99	3.57	10.87	3.57	3.60	5.38	3.77	3.66	6.37	11.14
Ta	0.82	0.74	0.74	0.83	0.78	1.57	1.79	2.15	1.01	1.46	0.86	1.02	1.68
La	29.40	24.86	25.41	22.27	25.11	49.89	27.72	17.84	29.51	37.87	28.82	36.91	42.57
Ce	55.22	43.51	46.23	43.55	47.22	87.43	55.33	38.55	59.07	69.36	54.48	70.96	79.27
Pr	6.88	5.14	5.36	5.16	5.43	12.49	6.81	5.02	7.04	8.73	6.04	8.95	11.51
Nd	26.16	18.81	19.62	19.21	19.38	48.20	25.38	19.95	26.15	31.35	21.18	33.40	43.85
Sm	5.39	3.69	3.82	4.32	4.03	10.60	5.62	5.62	5.67	6.25	4.10	7.12	9.78
Eu	1.30	0.77	0.88	0.77	0.61	1.82	0.66	0.42	0.80	0.89	0.46	0.66	1.12
Gd	5.11	3.24	3.35	3.98	3.72	10.01	5.60	6.14	5.36	5.56	3.64	6.82	8.96
Tb	0.84	0.54	0.54	0.68	0.65	1.76	1.02	1.20	0.97	0.97	0.64	1.20	1.63
Dy	5.23	3.33	3.26	4.28	4.02	11.07	6.47	7.94	6.22	5.92	3.98	7.73	10.57
Ho	1.11	0.68	0.67	0.89	0.85	2.33	1.35	1.66	1.31	1.23	0.84	1.62	2.17
Er	3.08	1.95	1.88	2.55	2.42	6.52	3.84	4.74	3.88	3.49	2.42	4.57	6.03
Tm	0.46	0.30	0.29	0.39	0.38	0.97	0.58	0.73	0.60	0.53	0.37	0.69	0.91
Yb	3.03	2.02	1.93	2.61	2.49	6.07	3.70	4.74	3.96	3.53	2.49	4.34	5.85
Lu	0.49	0.33	0.32	0.42	0.39	0.91	0.60	0.74	0.63	0.56	0.41	0.69	0.87

Table 2.3a: Whole rock XRF data of tholeiitic basalts and basaltic andesites from the Strawberry Volcanics

	Strawberry Volcanic Tholeiitic Basalt/Basaltic Andesite														
AS-SV-	287	109	11	217	47	203b	215	230	285c	285a	51	285d	253	195	198
XRF															
Wt.% normalized															
SiO_2	47.48	49.43	50.47	52.06	53.23	53.30	53.35	53.43	53.44	53.76	53.84	53.91	54.09	54.38	54.39
TiO_2	2.87	2.12	1.86	1.60	1.56	1.85	1.34	1.81	1.63	1.66	1.93	1.68	1.73	1.33	1.59
Al_2O_3	15.36	17.16	16.17	17.09	16.44	16.83	16.54	16.82	17.23	17.23	16.33	17.73	16.81	18.19	17.25
FeO*	13.74	11.78	10.65	9.61	9.20	9.78	10.40	9.59	9.37	9.29	9.83	9.72	9.41	8.62	8.98
MgO	7.22	5.93	6.69	5.82	5.23	4.53	5.01	5.00	4.41	4.22	4.72	2.99	4.26	4.11	4.12
CaO	9.77	9.28	9.52	8.41	9.15	8.09	8.66	8.26	7.60	7.45	8.01	7.74	7.91	7.32	7.22
Na_2O	2.39	3.09	3.09	3.27	3.49	3.52	3.40	3.27	3.55	3.85	3.41	3.76	3.70	3.72	3.92
K_2O	0.34	0.455	0.763	1.394	0.886	1.313	0.746	1.076	1.76	1.57	1.133	1.46	1.32	1.381	1.544
P_2O_5	0.622	0.569	0.592	0.581	0.559	0.605	0.333	0.597	0.830	0.794	0.634	0.824	0.597	0.780	0.813
MnO	0.209	0.193	0.194	0.167	0.260	0.170	0.211	0.158	0.177	0.177	0.164	0.184	0.157	0.173	0.172
ppm															
Ni	78.90	73.4	69.4	91.2	79.8	60	30.6	53.1	40.60	37.21	44.6	32.22	61.65	34.5	32.9
Cr	211.27	178.6	166.8	101.8	135.6	83.6	8.4	81.6	56.76	51.17	84.4	55.86	83.29	58.8	44.1
V	284.99	278.1	264.6	232.5	235.2	209.8	250.4	216.9	192.72	185.54	212.9	206.58	195.11	171	175.4
Ga	17.76	20.6	18.4	19.3	19.7	19.4	19.8	19.7	19.65	20.75	19	19.65	18.85	19.5	20.8
Cu	38.10	45.8	49.5	71.6	45.6	49.7	18.3	32.6	45.59	48.68	38.4	27.53	55.56	29.4	51.2
Zn	134.36	126	102.2	101.5	98.8	107.8	112	107	107.83	103.54	119.6	110.12	107.03	103.9	105.2

Table 2.3b: Whole rock ICP-MS data of tholeiitic basalts and basaltic andesites from the Strawberry Volcanics.

AS-SV-	287	109	11	217	47	203b	215	230	285c	285a	51	285d	253	195	198
ICP-MS															
Sc	31.8	29.96	29.09	23.26	23.72	22.78	28.10	24.11	21.0	21.3	22.19	21.7	21.8	20.54	19.89
Ba	415	484.95	431.03	576.77	511.22	636.40	336.68	578.22	757	694	701.91	841	646	615.57	676.00
Rb	2.5	4.07	8.67	12.83	9.80	14.09	14.37	13.19	21.1	19.0	13.06	19.4	12.6	18.67	20.22
Sr	343	522.99	527.15	564.36	512.17	575.28	384.23	498.13	611	609	477.36	628	586	712.35	603.26
Zr	166	163.91	118.99	143.46	125.80	205.43	116.29	171.93	196	182	197.56	195	201	138.07	182.18
Y	38.59	34.97	25.92	24.58	26.88	30.30	31.88	30.03	30.70	28.29	34.69	31.01	30.03	27.84	28.78
Nb	14.34	13.56	11.79	10.64	9.55	19.58	6.81	15.38	23.65	23.72	16.95	24.47	18.95	14.68	23.10
Pb	3.87	4.98	3.50	5.15	3.90	5.41	2.96	5.41	6.26	5.92	6.17	6.33	5.57	5.43	7.13
U	0.23	0.33	0.41	0.43	0.50	0.61	0.43	0.61	0.69	0.69	0.53	0.78	0.65	0.69	0.72
Th	0.89	1.37	1.23	1.22	1.42	2.04	1.18	2.00	2.00	2.13	1.62	2.14	2.06	1.99	2.10
Cs	0.12	0.13	0.18	0.19	0.23	0.31	0.63	0.33	0.56	0.37	0.40	0.37	0.22	0.29	0.32
Hf	4.17	4.02	2.85	3.41	3.15	4.75	3.03	4.01	4.47	4.19	4.89	4.53	4.70	3.46	4.26
Ta	0.88	0.80	0.68	0.60	0.58	1.19	0.40	0.89	1.36	1.41	0.99	1.43	1.13	0.81	1.37
La	22.53	26.97	19.63	22.22	18.01	28.20	13.89	27.07	32.88	29.43	31.00	32.94	28.15	27.58	29.90
Ce	53.82	56.13	42.55	45.59	40.13	58.57	31.52	55.37	68.23	61.54	65.26	67.64	58.04	57.23	62.73
Pr	7.40	7.78	5.67	5.94	5.46	7.77	4.40	7.40	8.71	7.92	8.75	8.69	7.57	7.75	8.16
Nd	33.29	32.99	24.50	24.90	23.51	31.78	18.77	30.67	35.76	32.32	36.79	35.56	31.38	31.43	32.89
Sm	8.16	7.62	5.61	5.46	5.44	7.04	4.62	6.83	7.43	6.80	8.01	7.53	7.00	6.48	7.03
Eu	2.66	2.47	1.90	1.75	1.76	2.19	1.55	2.12	2.35	2.13	2.47	2.30	2.12	1.93	2.16
Gd	8.21	7.50	5.46	5.08	5.59	6.59	5.08	6.39	6.72	6.16	7.77	6.72	6.47	5.82	6.35
Tb	1.32	1.18	0.84	0.82	0.90	1.03	0.90	1.02	1.04	0.93	1.20	1.03	1.02	0.91	0.97
Dy	7.96	7.05	5.06	4.69	5.35	6.01	5.78	5.87	6.02	5.61	7.19	6.03	5.91	5.27	5.70
Ho	1.57	1.42	1.01	0.95	1.09	1.19	1.22	1.19	1.19	1.11	1.42	1.19	1.17	1.06	1.12
Er	4.13	3.72	2.68	2.53	2.92	3.07	3.40	3.09	3.13	2.88	3.71	3.16	3.08	2.81	2.97
Tm	0.57	0.51	0.38	0.36	0.41	0.43	0.49	0.43	0.45	0.41	0.52	0.45	0.43	0.41	0.42
Yb	3.46	3.15	2.29	2.22	2.50	2.65	3.16	2.68	2.81	2.57	3.23	2.82	2.66	2.60	2.63
Lu	0.54	0.49	0.35	0.35	0.39	0.41	0.51	0.42	0.46	0.40	0.51	0.45	0.43	0.41	0.42

Table 2.3c: Whole rock XRF data of calc-alkaline basaltic andesites from the Strawberry Volcanics

	Strawberry Volcanic Calc-Alkaline Basaltic Andesite											
AS-SV-	15	16	14	289	291	81	55	17	39d	110b	43	283
XRF												
Wt.% normalized												
SiO_2	52.71	52.78	53.13	53.52	54.68	54.87	55.10	55.14	55.24	55.47	55.61	55.88
TiO_2	1.64	1.57	1.57	1.19	1.40	1.45	1.48	1.48	1.42	1.20	1.44	1.24
Al_2O_3	16.26	16.45	16.45	17.16	16.46	17.64	16.71	16.78	17.29	17.67	16.01	17.62
FeO*	9.44	9.18	9.11	8.44	8.39	8.31	8.39	8.18	8.10	8.24	8.75	7.83
MgO	6.15	6.24	5.83	5.89	4.77	4.55	4.98	4.87	4.58	4.69	5.32	4.30
CaO	8.24	8.38	8.51	9.41	8.70	7.64	7.63	7.75	7.97	7.36	7.42	7.71
Na_2O	3.55	3.33	3.44	3.09	3.72	3.68	3.71	3.44	3.83	3.61	3.15	3.63
K_2O	1.240	1.313	1.221	0.78	1.20	1.206	1.332	1.656	0.853	1.120	1.683	1.17
P_2O_5	0.597	0.592	0.562	0.355	0.494	0.493	0.516	0.553	0.552	0.480	0.455	0.486
MnO	0.162	0.159	0.160	0.168	0.188	0.153	0.148	0.147	0.159	0.158	0.164	0.134
ppm												
Ni	95.5	99.3	95.8	66.63	32.52	53.8	67.7	63.9	38.8	74	77.3	50.37
Cr	192.6	203.9	213.7	144.24	82.99	81	114.3	105.8	62	107.4	116.2	77.51
V	213.4	203.8	207.3	220.75	230.72	190.8	197.9	183.2	223.4	181.8	225.4	176.76
Ga	17.6	18.1	18.5	16.26	18.45	19.5	18.3	17.7	19.5	19.2	17.6	19.45
Cu	63	55.4	56	65.74	59.15	43.7	50.5	57.5	24.7	52.4	45.7	48.68
Zn	99.5	99	95.8	80.20	89.48	101.5	101.8	91.7	104.7	99.3	84.7	91.37

Table 2.3d: Whole rock ICP-MS of calc-alkaline basaltic andesites from the Strawberry Volcanics

AS-SV-	15	16	14	289	291	81	55	17	39d	110b	43	283
ICP-MS												
Sc	24.59	23.54	24.01	29.4	28.3	21.17	21.80	21.24	24.40	23.20	22.60	20.4
Ba	565.15	570.76	549.96	417	471	891.62	657.30	611.83	882.90	779.40	843.40	676
Rb	16.33	15.48	14.52	9.5	18.0	12.21	14.90	18.24	11.40	10.80	31.10	14.1
Sr	525.03	544.07	560.27	414	528	563.79	520.30	571.62	533.30	510.30	482.10	546
Zr	156.30	154.21	153.50	117	132	195.46	178.70	169.89	154.80	171.70	128.30	160
Y	27.03	26.31	26.21	23.61	24.41	27.58	27.80	25.13	31.10	28.10	26.10	23.72
Nb	16.47	16.23	16.21	8.60	9.99	15.02	16.00	15.89	11.10	12.50	11.10	12.48
Pb	5.35	4.77	4.78	3.88	4.47	7.12	5.90	5.51	6.00	7.30	6.50	5.95
U	0.52	0.55	0.55	0.48	0.52	0.65	0.90	0.62		1.00	2.20	0.65
Th	1.57	1.61	1.62	1.45	1.45	2.35	2.20	1.80	2.40	2.20	3.50	1.91
Cs	0.18	0.29	0.31	0.26	0.62	0.27		0.37				0.36
Hf	3.74	3.70	3.62	2.90	3.19	4.69		4.10				3.78
Ta	0.95	0.94	0.94	0.51	0.58	0.89		0.92				0.75
La	23.47	23.48	23.09	15.88	18.79	28.84	24.80	24.37	25.50	26.80	19.60	23.69
Ce	50.17	49.67	48.97	33.41	40.50	57.92	49.20	51.55	48.30	48.50	40.90	48.75
Pr	6.57	6.54	6.40	4.37	5.34	7.46		6.66				6.26
Nd	27.52	27.29	26.62	18.35	22.50	30.19	25.40	27.23	29.00	27.60	22.70	25.43
Sm	6.14	6.01	5.94	4.28	5.18	6.51		5.99				5.49
Eu	1.99	1.91	1.84	1.35	1.61	1.94		1.89				1.71
Gd	5.74	5.71	5.56	4.19	4.87	6.01		5.51				5.05
Tb	0.89	0.88	0.86	0.71	0.78	0.94		0.86				0.79
Dy	5.28	5.19	5.07	4.49	4.61	5.49		4.99				4.68
Ho	1.05	1.01	1.00	0.94	0.95	1.09		0.99				0.91
Er	2.76	2.67	2.60	2.58	2.46	2.94		2.57				2.45
Tm	0.38	0.38	0.37	0.38	0.35	0.41		0.36				0.35
Yb	2.36	2.36	2.31	2.36	2.21	2.60		2.28				2.14
Lu	0.39	0.37	0.37	0.39	0.35	0.41		0.37				0.35

Table 2.4a: Whole rock radiogenic Sr isotopes for mafic, intermediate, rhyolite lavas and crustal rocks.

Sample	**Rb** (ppm)	**Sr** (ppm)	**$^{87}Rb/^{86}Sr$**	**$^{87}Sr/^{86}Sr$** Present	**Age** (Ma)	**$^{87}Sr/^{86}Sr$** Initial
Mafic to intermediate lavas of the SV						
AS SV287*	2.49	343.46	0.0210	0.70527	14.5	0.70526
AS SV-11*	8.67	527.15	0.0476	0.70452	14.5	0.70451
AS SV203b*	14.09	575.28	0.0709	0.70409	14.5	0.70408
AS SV289	9.54	413.84	0.0667	0.70376	14.5	0.70375
AS SV39b*	4.23	509.56	0.0240	0.70435	14.5	0.70435
AS SV 56	22.02	510.95	0.1248	0.70441	14.5	0.70439
AS SV159c*	25.39	435.22	0.1688	0.70392	15.48	0.70388
AS SV231	32.21	435.63	0.2140	0.70397	14.5	0.70393
AS SV 188	37.47	410.48	0.2642	0.70404	14.5	0.70399
Rhyolite lavas of the SV						
AS-SV-151	86.65	231.02	1.0857	0.70429	16.06	0.70405
AS SV173	91.66	197.66	1.3422	0.70444	14.61	0.70416
AS-SV-190	90.49	76.82	3.4096	0.70499	14.7	0.70428
AS SV179	100.42	45.10	6.4450	0.70576	15.21	0.70437
AS SV179extra	100.42	45.10	6.4450	0.70583	15.21	0.70444
Crustal rocks surrounding the SV						
AS SV BAS RX01	21.70	539.00	0.1165	0.70384	200	0.70350
AS SV BAS RX-08	40.60	372.00	0.3159	0.70747	200	0.70658
MS-12-45	34.28	445.08	0.2229	0.70818	200	0.70755
MS-12-46	41.07	199.66	0.5953	0.70695	200	0.70526
AS-SV-288	47.14	425.64	0.3205	0.70384	19	0.70375

* tholeiitic lavas

$^{Sr}\lambda = 1.42E\text{-}11$

$^{Nd}\lambda = 6.54E\text{-}12$

Table 2.4b: Whole rock radiogenic Nd and Pb isotopes for mafic, intermediate, rhyolite lavas and crustal rocks.

Sample	**Sm** (ppm)	**Nd** (ppm)	**$^{147}Sm/^{144}Nd$**	**$^{143}Nd/^{144}Nd$** Present	**$^{143}Nd/^{144}Nd$** Initial	εNd Initial	**$^{208}Pb/^{204}Pb$**	**$^{207}Pb/^{204}Pb$**	**$^{206}Pb/^{204}Pb$**
Mafic to intermediate lavas of the SV									
AS SV287*	8.16	33.29	0.1483	0.512494	0.512480	-2.4	38.889	15.598	18.549
AS SV-11*	5.61	24.50	0.1386	0.512773	0.512760	3.0	38.544	15.593	18.826
AS SV203b*	7.04	31.78	0.1338	0.512787	0.512774	3.3	38.549	15.494	18.844
AS SV289	4.28	18.35	0.1410	0.512838	0.512825	4.3	38.512	15.604	18.873
AS SV39b*	6.67	29.60	0.1361	0.512822	0.512809	4.0	38.519	15.608	18.888
AS SV 56	5.44	25.03	0.1313	0.512826	0.512814	4.0	38.474	15.593	18.855
AS SV159c*	6.58	28.51	0.1395	0.512875	0.512861	5.0	38.466	15.600	18.856
AS SV231	3.90	18.18	0.1296	0.512839	0.512827	4.3	38.475	15.602	18.846
AS SV 188	4.59	20.86	0.1331	0.512796	0.512783	3.4	38.501	15.606	18.875
Rhyolite lavas of the SV									
AS-SV-151	3.82	19.62	0.1176	0.513046	0.513034	8.4	38.484	15.596	18.868
AS SV173	4.32	19.21	0.1360	0.512819	0.512806	3.9	38.801	15.715	19.046
AS-SV-190	5.67	26.15	0.1311	0.512892	0.512879	5.3	38.506	15.595	18.900
AS SV179	7.12	33.40	0.1290	0.512833	0.512820	4.2	38.558	15.620	18.994
AS SV179 extra	7.12	33.40	0.1290						
Crustal rocks surrounding the SV									
AS SV BAS RX01	2.96	14.11	0.1268	0.512911	0.512728	10.8	38.540	15.625	18.916
AS SV BAS RX-08	3.88	16.49	0.1423	0.51258	0.512375	4.4	38.617	15.639	19.048
MS-12-45	3.15	12.95	0.1468				38.656	15.644	19.036
MS-12-46	3.03	11.29	0.1625	0.51267	0.512457	5.6	38.698	15.654	19.116
AS-SV-288	4.65	24.68	0.1139				38.534	15.619	18.869

* tholeiitic lavas

$^{Nd}\lambda = 6.54E\text{-}12$

Table 3.1a: EMP data of cpx crystals from tholeiitic (Th) basalt and intermediate lavas

	AS-SV-203b										
	1.6	1.7	2.4	2.7	3.1	4.1	4.3	5.1	5.2	6.3	6.4
wt. %	*Th*										
SiO_2	49.27	50.34	47.62	49.45	51.16	50.71	48.77	50.87	49.09	51.41	50.99
MgO	14.62	15.54	14.16	15.04	15.87	15.62	14.75	15.81	14.89	15.82	15.95
FeO	8.96	8.07	10.02	8.44	8.07	8.31	9.11	8.11	8.57	10.96	11.37
CaO	19.93	20.32	18.68	19.72	20.03	19.67	18.49	19.90	19.49	17.68	16.85
Al_2O_3	4.24	3.51	5.36	3.90	2.83	2.87	4.90	2.74	4.58	1.74	2.10
TiO_2	1.39	0.98	1.84	1.19	0.83	0.86	1.37	0.85	1.21	1.01	1.11
Na_2O	0.34	0.33	0.43	0.38	0.30	0.35	0.37	0.34	0.43	0.31	0.30
MnO	0.24	0.21	0.26	0.20	0.22	0.20	0.19	0.18	0.19	0.36	0.39
Cr_2O_3	0.07	0.15	0.02	0.07	0.06	0.10	0.20	0.15	0.22	0.08	0.12
En	43	45	43	44	46	45	44	46	44	46	46
Fs	15	13	17	14	13	14	15	13	14	18	19
Wo	42	42	40	42	41	41	40	41	42	37	35
Mg#	74	77	72	76	78	77	74	78	76	72	71

	AS-SV-287				AS-SV-11						
	1.3	1.4	1.5	3.1	1.2	1.3	1.6	1.7	1.8	2.1	2.3
wt. %	*Th*				*Th*						
SiO_2	50.38	48.78	48.55	48.96	50.79	50.68	50.51	51.06	50.57	50.64	52.23
MgO	15.16	14.05	14.38	13.93	15.34	15.26	15.82	15.63	15.70	15.53	16.89
FeO	14.39	10.95	11.66	11.70	8.24	8.80	8.92	8.51	10.54	8.91	9.36
CaO	14.83	19.24	18.27	18.17	20.17	19.54	18.59	19.87	17.99	19.37	17.64
Al_2O_3	2.10	3.41	3.30	3.42	2.79	2.85	3.21	2.72	2.47	2.72	1.45
TiO_2	1.32	2.07	1.88	2.02	1.23	1.23	1.28	1.23	1.35	1.21	0.74
Na_2O	0.24	0.32	0.31	0.34	0.31	0.29	0.32	0.26	0.33	0.31	0.26
MnO	0.34	0.29	0.28	0.31	0.22	0.24	0.20	0.23	0.24	0.23	0.28
Cr_2O_3	0.06	0.14	0.04	0.10	0.45	0.41	0.54	0.34	0.16	0.40	0.29
En	45	41	42	42	45	45	46	45	45	45	49
Fs	24	18	19	20	13	14	15	14	17	15	15
Wo	31	41	39	39	42	41	39	41	37	40	36
Mg#	65	70	69	68	77	76	76	77	73	76	76

Table 3.1b: EMP data of cpx crystals from calc-alkaline (Ca) intermediate lavas

	AS-SV-155					AS-SV-281	
	1.2	1.1	2.1	2.5	3.5	1.1	1.4
wt. %	*Ca*					*Ca*	
SiO_2	50.89	52.14	53.16	51.69	50.98	52.01	52.02
MgO	16.69	16.90	17.93	16.13	15.04	15.61	16.30
FeO	6.59	6.96	6.77	8.54	9.15	8.10	7.75
CaO	19.96	20.33	19.95	20.00	20.36	20.33	20.46
Al_2O_3	3.23	2.61	1.65	2.58	2.74	2.90	2.28
TiO_2	0.53	0.48	0.34	0.53	0.68	0.56	0.45
Na_2O	0.27	0.24	0.17	0.30	0.33	0.35	0.27
MnO	0.17	0.23	0.22	0.26	0.25	0.24	0.25
Cr_2O_3	0.45	0.12	0.09	0.12	0.02	0.17	0.15
En	48	48	50	46	43	45	46
Fs	11	11	11	14	15	13	12
Wo	41	41	40	41	42	42	42
Mg#	82	81	83	77	75	77	79

	AS-SV-21					
	1.3	1.5	2.5	3.2	3.4	3.6
wt. %	*Ca*					
SiO_2	52.64	51.86	52.57	52.80	52.26	52.18
MgO	14.43	14.10	16.52	14.16	15.24	13.65
FeO	9.48	9.97	6.77	10.47	9.49	11.53
CaO	21.22	20.73	20.44	20.70	20.22	20.01
Al_2O_3	1.25	1.65	2.43	1.46	1.97	1.44
TiO_2	0.25	0.36	0.38	0.28	0.59	0.31
Na_2O	0.34	0.34	0.26	0.32	0.30	0.36
MnO	0.30	0.39	0.21	0.46	0.33	0.52
Cr_2O_3	0.00	0.00	0.20	0.00	0.02	0.02
En	48	41	47	41	43	40
Fs	11	16	11	17	15	19
Wo	41	43	42	43	41	42
Mg#	73	72	81	71	74	68

Table 3.1c: EMP data of opx crystals from calc-alkaline (Ca) intermediate lavas

	AS-SV-155									
Ca	1.5	1.6	2.3	2.4	3.3	3.4	3.7	4.2	4.3	4.4
Wt. %	*Ca*									
SiO_2	54.21	54.98	54.44	54.66	54.71	53.13	53.74	53.60	55.23	54.76
MgO	29.47	27.85	28.85	27.72	29.18	22.56	25.68	25.81	30.06	29.79
FeO	11.17	14.21	12.23	14.36	11.55	20.75	16.71	15.75	10.29	10.43
CaO	1.83	1.56	1.83	1.65	1.88	1.59	1.28	1.58	1.68	1.68
Al_2O_3	2.11	1.36	2.14	1.50	2.18	0.82	1.19	1.44	1.84	2.33
TiO_2	0.20	0.24	0.23	0.22	0.22	0.18	0.29	0.16	0.13	0.20
Na_2O	0.03	0.02	0.03	0.02	0.01	0.04	0.01	0.00	0.03	0.01
MnO	0.26	0.35	0.29	0.33	0.26	0.45	0.58	0.35	0.25	0.25
Cr_2O_3	0.43	0.06	0.14	0.05	0.25	0.08	0.02	0.32	0.38	0.49
En	80	75	78	75	79	75	71	72	81	81
Fs	17	22	19	22	18	22	26	25	16	16
Wo	4	3	4	3	4	3	3	3	3	3
Mg#	82	78	81	77	82	66	73	75	84	84

	AS-SV-281						AS-SV-21				
Ca	1.2	1.3	2.3	2.4	2.6	2.8	1.1	1.4	2.2	2.3	2.4
Wt. %	*Ca*						*Ca*				
SiO_2	55.04	55.12	54.30	54.51	54.05	54.00	52.87	51.38	54.99	53.56	55.86
MgO	28.17	27.53	27.19	26.43	27.00	27.70	23.22	17.46	28.58	24.19	29.32
FeO	13.44	14.63	14.88	15.30	14.82	13.94	20.15	28.70	13.05	18.84	12.14
CaO	1.52	1.53	1.54	1.86	1.88	1.62	1.34	1.14	1.66	1.43	1.67
Al_2O_3	1.23	1.03	1.58	1.27	1.44	1.74	1.64	0.41	1.48	1.43	1.67
TiO_2	0.19	0.18	0.26	0.28	0.28	0.25	0.28	0.12	0.17	0.27	0.20
Na_2O	0.02	0.04	0.04	0.03	0.02	0.04	0.03	0.02	0.01	0.01	0.02
MnO	0.35	0.47	0.38	0.39	0.34	0.38	0.59	0.70	0.31	0.53	0.28
Cr_2O_3	0.17	0.08	0.12	0.09	0.10	0.32	0.02	0.00	0.11	0.01	0.18
En	77	75	74	73	74	76	65	51	77	68	79
Fs	20	22	23	24	23	21	32	47	20	30	18
Wo	3	3	3	4	4	3	3	2	3	3	3
Mg#	79	77	77	75	76	78	67	52	80	70	81

Table 3.1d: EMP data of olivine crystals from tholeiitic (Th) basalt and intermediate lavas

	AS-SV-203b											
Th	1.1	2.3	3.1	3.4	4.3	5.1	5.2	5.4	7.5	8.2	8.3	9.1
Wt. %	*Th*											
SiO_2	36.94	36.32	36.74	36.17	35.97	37.73	37.44	37.48	36.00	35.87	35.57	37.48
MgO	37.21	32.14	33.13	30.46	31.29	37.79	37.44	36.82	30.94	30.32	29.24	35.91
FeO	24.17	30.43	28.98	31.82	31.40	23.51	23.72	24.31	31.27	32.33	33.23	25.40
CaO	0.18	0.18	0.22	0.23	0.22	0.17	0.19	0.17	0.24	0.18	0.24	0.19
Al_2O_3	0.02	0.02	0.02	0.01	0.02	0.02	0.02	0.02	0.02	0.01	0.02	0.02
TiO_2	0.04	0.02	0.02	0.03	0.02	0.02	0.01	0.01	0.03	0.03	0.01	0.04
Na_2O	0.02	0.00	0.01	0.00	0.00	0.01	0.00	0.01	0.00	0.00	0.03	0.00
MnO	0.38	0.48	0.52	0.51	0.53	0.39	0.33	0.39	0.52	0.52	0.54	0.39
Cr_2O_3	0.01	0.03	0.00	0.00	0.00	0.02	0.01	0.02	0.02	0.00	0.00	0.01
NiO	0.13	0.11	0.12	0.09	0.08	0.07	0.13	0.07	0.03	0.09	0.05	0.08
Fo#	73	65	67	63	64	74	74	73	64	63	61	72

	AS-SV-287											
Th	19.1	20.1	20.2	20.3	20.4	21.1	21.3	21.4	22.1	22.2	22.3	22.4
Wt. %	*Th*											
SiO_2	37.11	37.40	36.79	36.64	33.96	34.09	37.14	37.20	34.55	37.53	37.08	34.88
MgO	35.05	36.09	35.14	32.49	21.01	21.87	35.11	34.54	23.43	35.49	35.10	26.28
FeO	26.71	24.95	26.35	29.40	42.98	40.99	26.09	26.80	40.09	25.94	26.69	36.54
CaO	0.28	0.27	0.26	0.27	0.31	0.34	0.25	0.26	0.28	0.25	0.26	0.28
Al_2O_3	0.03	0.03	0.02	0.02	0.02	0.08	0.03	0.03	0.02	0.02	0.02	0.03
TiO_2	0.02	0.03	0.03	0.04	0.06	0.06	0.03	0.04	0.05	0.02	0.00	0.02
Na_2O	0.02	0.01	0.02	0.01	0.00	0.01	0.01	0.00	0.00	0.00	0.00	0.01
MnO	0.43	0.35	0.39	0.48	0.64	0.68	0.39	0.37	0.61	0.36	0.38	0.61
Cr_2O_3	0.04	0.04	0.04	0.02	0.00	0.02	0.02	0.02	0.00	0.02	0.02	0.00
NiO	0.08	0.08	0.07	0.03	0.05	0.00	0.09	0.06	0.05	0.15	0.08	0.05
Fo#	70	72	70	66	47	49	71	70	51	71	70	56

Table 3.1e: EMP data of olivine crystals from calc-alkaline (Ca) intermediate lavas

	AS-SV-167							
	10.2	10.3	10.4	11.1	11.3	11.4	11.5	11.6
Wt. %	*Ca*							
SiO_2	40.07	39.80	40.49	40.28	40.39	40.08	39.99	39.18
MgO	43.29	42.35	44.13	43.91	44.76	43.70	43.38	39.92
FeO	16.32	17.64	15.73	16.02	15.22	15.39	15.40	20.39
CaO	0.17	0.15	0.17	0.16	0.17	0.16	0.17	0.20
Al_2O_3	0.02	0.02	0.03	0.02	0.02	0.02	0.02	0.02
TiO_2	0.01	0.02	0.01	0.00	0.01	0.02	0.00	0.01
Na_2O	0.00	0.01	0.00	0.00	0.01	0.00	0.00	0.01
MnO	0.24	0.27	0.24	0.24	0.23	0.22	0.24	0.35
Cr_2O_3	0.01	0.04	0.00	0.01	0.01	0.01	0.02	0.01
NiO	0.29	0.26	0.30	0.26	0.30	0.30	0.30	0.25
Fo#	83	81	83	83	84	84	83	78

Table 3.2: Partition coefficient used in calculations for FC and AFC models**.** Ree (Nd, La Sm and Ce), Pb and Rb partition coefficients in plagioclase are from McKenzie and O'Nions (1991). Th and Nb are from Rollinson (1993), Cs from Villemant, B. (1988), Ba from Matsui et al (1977) and K from Philpotts & Schnetzler (1970). Ree (Nd, La Sm and Ce), and Pb partition coefficients in olivine are from McKenzie and O'Nions (1991). Rb, Cs, Ba, and Th are from Fujimaki et al. (1984) and Nb and K are from Zanetti et al (2004). Ree (Nd, La Sm and Ce), Pb, Rb, Ba and Nb partition coefficients in cpx are from Foley et al (1996)). Th from Rollinson (1993) and K from Philpotts & Schnetzler (1970). All reported partition coefficients for magnetite are from Rollinson (1993) and K-spar Cs and Pb partition coefficients are from Larsen (1979) and K from Philpotts & Schnetzler (1970).

	plag	*cpx*	*ol*	*mag*	*k-feldspar*	*ap*
Th	0.0100	0.0300	0.0400	NA	NA	NA
Nd	0.1400	0.1730	0.0010	1.0000	NA	NA
Rb	0.1000	0.0047	0.0020	NA	NA	NA
Nb	0.0100	0.0027	0.0017	0.4000	NA	NA
Pb	0.3600	0.0056	0.0001	NA	0.2080	NA
La	0.2700	0.0435	0.0006	1.5000	NA	NA
K	0.1560	0.0072	0.0130	0.0450	1.4900	NA
Sm	0.1100	0.2830	0.0013	1.1000	NA	NA
Cs	0.1300	0.1300	0.0004	NA	0.0440	NA
Ba	0.3000	0.0006	0.0020	NA	NA	NA
Ce	0.2000	0.0843	0.0005	1.3000	NA	NA

Table 3.3a: Whole rock XRF analysis of crustal rock which crop out within the Strawberry Volcanics

	Local Crust											
AS-SV-	BASE-01	BASE-02	BASE-03	BASE-04	BASE-05	BASE-06	BASE-07	BASE-08	BASE-09	12-45	12-46	228
XRF												
Wt.% normalized												
SiO_2	67.85	67.24	66.48	41.02	54.20	55.93	74.97	56.70	69.49	60.90	70.98	67.05
TiO_2	0.645	0.559	0.553	0.000	0.143	0.278	0.043	0.685	0.600	0.599	0.596	0.59
Al_2O_3	15.44	16.25	16.22	0.12	2.58	19.63	15.68	13.23	13.66	14.09	13.66	15.38
FeO*	3.67	3.61	3.48	7.54	5.40	4.24	0.97	6.06	5.58	5.13	4.36	4.05
MgO	2.46	1.90	2.18	51.13	19.15	4.69	0.14	2.39	3.12	1.95	2.36	2.08
CaO	3.86	3.95	4.48	0.05	17.88	8.93	1.61	16.39	3.37	11.82	2.97	4.20
Na_2O	4.66	4.73	5.30	0.01	0.46	5.81	5.08	2.41	2.64	3.72	3.38	3.82
K_2O	1.16	1.50	1.08	0.01	0.05	0.22	1.40	1.73	1.36	1.44	1.52	2.564
P_2O_5	0.169	0.192	0.150	0.004	0.008	0.186	0.070	0.174	0.139	0.171	0.131	0.208
MnO	0.070	0.068	0.076	0.119	0.124	0.084	0.048	0.216	0.054	0.178	0.047	0.062
ppm												
Ni	30	15	19	2605	390	41	7	38	31	22	16	32.9
Cr	46	24	25	2297	2536	16	4	52	52	43	37	49.1
V	78	74	77	11	137	82	5	153	156	123	126	81.1
Ga	17	19	18	1	4	12	20	11	15	12	13	16.8
Cu	5	10	31	7	4	6	5	67	81	52	64	34.4
Zn	41	57	172	83	41	33	49	138	71	96	74	60.7

Table 3.3b: Whole rock ICP-MS analysis of crustal rock which crop out within the Strawberry Volcanics

	Local Crust											
AS-SV-	BASE-01	BASE-02	BASE-03	BASE-04	BASE-05	BASE-06	BASE-07	BASE-08	BASE-09	12-45	12-46	228
ICP-MS												
Sc	8.7	8.3	9.1	2.8	58.1	17.8	1.1	16.9	15.3	16.5	15.8	10.31
Ba	664	728	534	4	12	15	593	426	846	1909	1004	1069.11
Rb	21.7	29.4	16.3	0.4	0.3	1.6	30.1	40.6	39.0	34.3	41.1	47.14
Sr	539	545	544	2	24	130	403	372	413	445	200	425.64
Zr	142	116	103	1	6	25	42	75	96	67	69	140.01
Y	13.85	12.46	14.92	0.10	5.02	8.69	13.44	25.76	21.17	20.01	18.64	17.18
Nb	8.77	5.24	4.23	0.03	0.08	0.13	8.51	3.05	4.67	2.48	2.44	9.83
Pb	8.04	5.62	13.53	0.68	0.71	0.16	9.28	8.45	4.03	7.13	4.83	9.43
U	0.89	1.12	1.07	0.02	0.03	0.10	0.81	1.93	1.90	1.11	1.30	1.76
Th	2.63	2.58	2.30	0.03	0.08	0.26	2.18	2.92	4.05	2.24	2.72	5.38
Cs	3.03	2.61	0.75	0.07	0.05	0.03	1.10	3.20	2.65	3.57	4.22	1.14
Hf	3.68	3.04	2.76	0.02	0.25	0.78	1.93	2.14	2.69	1.93	2.05	3.61
Ta	0.72	0.38	0.33	0.01	0.02	0.02	0.62	0.23	0.35	0.18	0.18	0.78
La	15.67	14.34	12.31	0.126	1.77	1.59	13.25	16.98	15.52	11.94	7.55	30.32
Ce	29.98	27.90	24.01	0.235	2.80	3.48	26.36	26.12	28.59	20.90	16.08	48.72
Pr	3.64	3.44	2.96	0.027	0.59	0.52	3.53	3.98	4.04	3.06	2.53	6.68
Nd	14.11	13.25	11.95	0.093	2.68	2.77	14.07	16.49	16.34	12.95	11.29	24.68
Sm	2.96	2.74	2.70	0.021	0.78	0.98	2.90	3.88	3.85	3.15	3.03	4.65
Eu	0.92	0.84	0.90	0.003	0.27	0.58	0.78	1.04	0.87	0.90	0.86	1.11
Gd	2.79	2.47	2.64	0.019	0.94	1.37	2.51	4.02	3.65	3.30	3.29	3.95
Tb	0.45	0.39	0.44	0.003	0.16	0.25	0.40	0.67	0.61	0.56	0.56	0.60
Dy	2.66	2.37	2.72	0.019	0.98	1.66	2.36	4.33	3.85	3.56	3.47	3.45
Ho	0.53	0.47	0.55	0.004	0.19	0.36	0.46	0.90	0.79	0.74	0.71	0.65
Er	1.42	1.28	1.48	0.011	0.54	0.99	1.21	2.53	2.20	1.98	1.96	1.72
Tm	0.21	0.19	0.22	0.002	0.07	0.15	0.18	0.38	0.33	0.28	0.28	0.25
Yb	1.33	1.19	1.35	0.015	0.44	0.89	1.16	2.44	2.06	1.71	1.73	1.52
Lu	0.21	0.19	0.21	0.003	0.07	0.15	0.19	0.40	0.33	0.28	0.27	0.23

Table 3.4a: Results of trace element FC models of the Strawberry Volcanics.

	Fractional Crystallization									
F	1	0.9	0.8	0.7	0.6	0.5	0.4	0.3	0.2	0.1
ppm										
Cs	0.18	0.19	0.21	0.24	0.28	0.33	0.4	0.51	0.74	1.37
Rb	8.67	9.57	10.7	12.14	14.04	16.68	20.6	27.03	39.64	76.28
Ba	431	471	520	581	661	770	929	1182	1660	2966
Sr	527	521	515	507	499	489	477	463	443	411
Pb	3.5	3.8	4.18	4.64	5.25	6.07	7.24	9.1	12.55	21.75
Th	1.23	1.36	1.53	1.74	2.03	2.43	3.02	4.01	5.97	11.81
U	0.41	0.45	0.51	0.58	0.67	0.8	1	1.33	1.98	3.9
Zr	119	131	147	166	192	227	280	366	534	1019
Hf	2.85	3.08	3.35	3.68	4.11	4.69	5.5	6.76	9.03	14.84
Ta	0.68	0.73	0.79	0.87	0.96	1.09	1.26	1.53	2.02	3.22
Y	25.92	28.33	31.29	35.02	39.89	46.52	56.15	71.58	100.78	180.86
Nb	11.79	13.05	14.63	16.66	19.34	23.08	28.66	37.88	56.13	109.92
La	19.63	21.25	23.21	25.66	28.81	33.05	39.08	48.51	65.8	110.77
Ce	42.55	46.24	50.75	56.39	63.69	73.55	87.72	110.09	151.62	262.08
Pr	5.67	6.22	6.89	7.74	8.86	10.39	12.62	16.22	23.1	42.28
Nd	24.5	26.69	29.38	32.75	37.13	43.07	51.65	65.28	90.82	159.68
Sm	5.61	6.1	6.7	7.45	8.42	9.72	11.61	14.58	20.1	34.81
Eu	1.9	2	2.12	2.26	2.43	2.66	2.95	3.39	4.12	5.74
Gd	5.46	5.98	6.63	7.44	8.5	9.96	12.09	15.51	22.04	40.2
Tb	0.84	0.92	1.01	1.12	1.27	1.47	1.76	2.21	3.06	5.34
Dy	5.06	5.54	6.14	6.89	7.87	9.21	11.17	14.33	20.35	37.07
Ho	1.01	1.1	1.22	1.37	1.57	1.83	2.22	2.85	4.05	7.37
Er	2.68	2.94	3.25	3.66	4.19	4.91	5.97	7.68	10.96	20.12
Tm	0.38	0.41	0.45	0.51	0.58	0.67	0.81	1.03	1.44	2.58
Yb	2.29	2.51	2.77	3.09	3.52	4.1	4.95	6.29	8.84	15.81
Lu	0.35	0.39	0.43	0.49	0.56	0.67	0.82	1.06	1.53	2.88

F = fraction of melt remaining

Table 3.4b: Results of trace element AFC models of the Strawberry Volcanics.

	Assimilation Fractional Crystallization									
F	1	0.94	0.88	0.82	0.76	0.7	0.64	0.58	0.52	0.46
ppm										
Cs	0.18	0.19	0.21	0.24	0.26	0.29	0.33	0.37	0.43	0.49
Rb	8.67	9.52	10.48	11.58	12.85	14.33	16.08	18.18	20.74	23.95
Ba	431	461	495	533	576	627	685	755	839	944
Sr	527	523	518	513	507	502	496	489	482	474
Pb	3.5	3.74	4	4.3	4.64	5.04	5.49	6.03	6.68	7.48
Th	1.23	1.34	1.47	1.62	1.79	2	2.24	2.52	2.88	3.33
U	0.41	0.45	0.49	0.54	0.6	0.66	0.74	0.84	0.95	1.1
Zr	119	127	136	146	158	172	188	208	232	262
Hf	2.85	3	3.17	3.35	3.56	3.81	4.08	4.41	4.8	5.27
Ta	0.68	0.71	0.75	0.79	0.84	0.89	0.95	1.02	1.1	1.2
Y	25.92	27.4	29.07	30.95	33.11	35.6	38.51	41.97	46.15	51.32
Nb	11.79	12.58	13.48	14.52	15.71	17.1	18.75	20.73	23.17	26.22
La	19.63	20.74	21.98	23.38	24.97	26.78	28.89	31.37	34.33	37.95
Ce	42.55	44.96	47.66	50.7	54.16	58.14	62.78	68.25	74.82	82.89
Pr	5.67	6.03	6.43	6.89	7.41	8.02	8.73	9.57	10.6	11.87
Nd	24.5	25.9	27.48	29.26	31.3	33.64	36.37	39.61	43.51	48.31
Sm	5.61	5.92	6.26	6.65	7.09	7.6	8.19	8.89	9.72	10.75
Eu	1.9	1.96	2.03	2.1	2.17	2.26	2.36	2.47	2.6	2.76
Gd	5.46	5.79	6.15	6.56	7.04	7.59	8.23	8.99	9.92	11.07
Tb	0.84	0.89	0.94	1	1.06	1.14	1.23	1.33	1.46	1.61
Dy	5.06	5.36	5.69	6.07	6.51	7.01	7.6	8.3	9.15	10.21
Ho	1.01	1.07	1.13	1.21	1.29	1.39	1.51	1.65	1.82	2.03
Er	2.68	2.84	3.01	3.22	3.45	3.72	4.04	4.41	4.87	5.44
Tm	0.38	0.4	0.42	0.45	0.48	0.52	0.56	0.61	0.67	0.74
Yb	2.29	2.42	2.57	2.74	2.93	3.14	3.4	3.7	4.07	4.52
Lu	0.35	0.38	0.4	0.43	0.46	0.5	0.54	0.6	0.66	0.74

F = fraction of melt remaining

Table 3.5a: Results of XRF generated data mixing models between calc-alkaline andesite (AS-SV-33) and Canyon Mountain crust (AS-BASE-04).

Intermediate calc-alkaline mixed with Canyon Mountain Dunite												
wt.%	0%	5%	10%	20%	30%	40%	50%	60%	70%	80%	90%	100%
SiO_2	63.87	62.73	61.58	59.30	57.01	54.73	52.44	50.16	47.87	45.59	43.30	41.02
TiO_2	0.68	0.65	0.61	0.55	0.48	0.41	0.34	0.27	0.20	0.14	0.07	0.00
Al_2O_3	16.81	15.98	15.15	13.48	11.81	10.14	8.47	6.80	5.13	3.46	1.79	0.12
FeO*	5.04	5.16	5.29	5.54	5.79	6.04	6.29	6.54	6.79	7.04	7.29	7.54
MgO	1.96	4.42	6.87	11.79	16.71	21.63	26.54	31.46	36.38	41.29	46.21	51.13
CaO	5.58	5.31	5.03	4.48	3.92	3.37	2.82	2.26	1.71	1.16	0.60	0.05
Na_2O	3.83	3.64	3.45	3.06	2.68	2.30	1.92	1.54	1.15	0.77	0.39	0.01
K_2O	1.90	1.81	1.71	1.52	1.34	1.15	0.96	0.77	0.58	0.39	0.20	0.01
P_2O_5	0.24	0.23	0.22	0.19	0.17	0.14	0.12	0.10	0.07	0.05	0.03	0.00
MnO	0.09	0.09	0.09	0.09	0.10	0.10	0.10	0.11	0.11	0.11	0.12	0.12
ppm												
Ni	19	148	277	536	795	1053	1312	1571	1829	2088	2347	2605
Cr	25	138	252	479	706	934	1161	1388	1615	1843	2070	2297
V	112	107	102	92	82	72	62	51	41	31	21	11
Ga	18	17	16	14	13	11	9	8	6	4	3	1
Cu	36	35	33	31	28	25	22	19	16	13	10	7
Zn	68	68	69	71	72	74	75	77	78	80	81	83

Table 3.5b: Results of ICP-MS generated data mixing models between calc-alkaline andesite (AS-SV-33) and Canyon Mountain crust (AS-BASE-04).

Intermediate calc-alkaline mixed with Canyon Mountain Dunite												
ppm	0%	5%	10%	20%	30%	40%	50%	60%	70%	80%	90%	100%
ICP-MS												
Sc	14.4	13.8	13.2	12.1	10.9	9.7	8.6	7.4	6.3	5.1	3.9	2.8
Ba	904	859	814	724	634	544	454	364	274	184	94	4
Rb	34	32	31	27	24	20	17	14	10	7	4	0
Sr	394	374	355	315	276	237	198	159	120	80	41	2
Zr	170	162	153	136	119	102	85	68	51	35	18	1
Y	20.97	19.92	18.88	16.79	14.71	12.62	10.53	8.45	6.36	4.27	2.19	0.10
Nb	8.31	7.89	7.48	6.65	5.82	5.00	4.17	3.34	2.51	1.69	0.86	0.03
Pb	8.15	7.78	7.40	6.66	5.91	5.16	4.41	3.67	2.92	2.17	1.43	0.68
U	1.14	1.09	1.03	0.92	0.81	0.69	0.58	0.47	0.36	0.25	0.13	0.02
Th	3.09	2.94	2.79	2.48	2.17	1.87	1.56	1.25	0.95	0.64	0.33	0.03
Cs	1.59	1.51	1.44	1.28	1.13	0.98	0.83	0.68	0.53	0.37	0.22	0.07
Hf	4.17	3.96	3.76	3.34	2.92	2.51	2.09	1.68	1.26	0.85	0.43	0.02
Ta	0.55	0.52	0.49	0.44	0.38	0.33	0.28	0.22	0.17	0.11	0.06	0.01
La	22.96	21.82	20.68	18.39	16.11	13.83	11.54	9.26	6.98	4.69	2.41	0.13
Ce	43.10	40.96	38.82	34.53	30.24	25.96	21.67	17.38	13.10	8.81	4.52	0.24
Pr	5.42	5.15	4.88	4.34	3.80	3.26	2.72	2.18	1.65	1.11	0.57	0.03
Nd	21.04	19.99	18.95	16.85	14.76	12.66	10.57	8.47	6.38	4.28	2.19	0.09
Sm	4.46	4.24	4.01	3.57	3.13	2.68	2.24	1.80	1.35	0.91	0.47	0.02
Eu	1.24	1.18	1.12	1.00	0.87	0.75	0.62	0.50	0.38	0.25	0.13	0.00
Gd	4.10	3.89	3.69	3.28	2.87	2.47	2.06	1.65	1.24	0.83	0.43	0.02
Tb	0.66	0.63	0.60	0.53	0.47	0.40	0.33	0.27	0.20	0.14	0.07	0.00
Dy	3.89	3.70	3.51	3.12	2.73	2.34	1.96	1.57	1.18	0.79	0.41	0.02
Ho	0.81	0.77	0.73	0.65	0.57	0.49	0.41	0.33	0.25	0.17	0.08	0.00
Er	2.19	2.09	1.98	1.76	1.54	1.32	1.10	0.88	0.67	0.45	0.23	0.01
Tm	0.33	0.31	0.29	0.26	0.23	0.20	0.16	0.13	0.10	0.07	0.03	0.00
Yb	2.07	1.97	1.86	1.66	1.45	1.25	1.04	0.84	0.63	0.43	0.22	0.01
Lu	0.32	0.31	0.29	0.26	0.23	0.20	0.16	0.13	0.10	0.07	0.03	0.00

Table 3.6a: Result of XRF generated data mixing model between basalt and rhyolite.

Mixing between basalt and rhyolite												
wt.%	0%	5%	15%	25%	35%	45%	55%	65%	75%	85%	95%	100%
SiO_2	50.47	51.61	53.88	56.15	58.42	60.69	62.97	65.24	67.51	69.78	72.05	73.19
TiO_2	1.86	1.79	1.64	1.49	1.33	1.18	1.03	0.88	0.73	0.58	0.43	0.35
Al_2O_3	16.17	16.09	15.93	15.77	15.61	15.45	15.29	15.13	14.97	14.81	14.65	14.57
FeO*	10.65	10.23	9.39	8.55	7.70	6.86	6.02	5.18	4.34	3.50	2.66	2.23
MgO	6.69	6.37	5.72	5.08	4.43	3.78	3.14	2.49	1.85	1.20	0.55	0.23
CaO	9.52	9.14	8.39	7.64	6.88	6.13	5.38	4.63	3.87	3.12	2.37	1.99
Na_2O	3.09	3.13	3.21	3.28	3.36	3.44	3.51	3.59	3.67	3.75	3.82	3.86
K_2O	0.76	0.90	1.16	1.43	1.69	1.96	2.23	2.49	2.76	3.02	3.29	3.42
P_2O_5	0.59	0.57	0.52	0.47	0.42	0.37	0.32	0.27	0.22	0.17	0.12	0.10
MnO	0.19	0.19	0.17	0.16	0.14	0.13	0.12	0.10	0.09	0.07	0.06	0.05
ppm												
Ni	69	66	59	53	46	39	33	26	19	13	6	3
Cr	167	159	143	126	110	94	78	62	46	30	13	5
V	265	253	229	206	182	159	135	112	89	65	42	30
Ga	18	18	18	18	17	17	17	17	16	16	16	16
Cu	50	47	43	39	35	30	26	22	18	14	9	7
Zn	102	100	94	89	83	78	73	67	62	57	51	49

Table 3.6b: Result of ICP-MS generated data mixing model between basalt and rhyolite.

Mixing between basalt and rhyolite												
ppm	0%	5%	15%	25%	35%	45%	55%	65%	75%	85%	95%	100%
Sc	29.1	27.9	25.6	23.3	21.0	18.6	16.3	14.0	11.6	9.3	7.0	5.8
Ba	431	483.7	589.1	694.5	800	905.4	1011	1116	1222	1327	1432	1485
Rb	9	13	20	28	36	44	52	59	67	75	83	87
Sr	527.2	512.3	482.7	453.1	423.5	393.9	364.3	334.7	305.1	275.4	245.8	231
Zr	119	121.6	126.8	132	137.2	142.4	147.6	152.8	158	163.2	168.4	171
Y	25.92	25.52	24.72	23.92	23.12	22.32	21.52	20.72	19.93	19.13	18.33	17.93
Nb	11.79	11.64	11.33	11.03	10.73	10.43	10.13	9.83	9.53	9.23	8.93	8.78
Pb	3.50	4.02	5.06	6.10	7.14	8.18	9.22	10.27	11.31	12.35	13.39	13.91
U	0.41	0.57	0.90	1.22	1.55	1.88	2.20	2.53	2.86	3.18	3.51	3.67
Th	1.23	1.55	2.20	2.85	3.49	4.14	4.79	5.43	6.08	6.73	7.38	7.70
Cs	0.18	0.38	0.78	1.18	1.59	1.99	2.39	2.79	3.20	3.60	4.00	4.20
Hf	2.85	2.94	3.11	3.29	3.46	3.64	3.81	3.98	4.16	4.33	4.50	4.59
Ta	0.68	0.68	0.69	0.70	0.70	0.71	0.71	0.72	0.72	0.73	0.74	0.74
La	19.63	19.92	20.50	21.07	21.65	22.23	22.81	23.39	23.96	24.54	25.12	25.41
Ce	42.55	42.74	43.10	43.47	43.84	44.21	44.57	44.94	45.31	45.68	46.05	46.23
Pr	5.67	5.66	5.63	5.60	5.56	5.53	5.50	5.47	5.44	5.41	5.37	5.36
Nd	24.50	24.25	23.76	23.28	22.79	22.30	21.82	21.33	20.84	20.35	19.87	19.62
Sm	5.61	5.52	5.34	5.16	4.99	4.81	4.63	4.45	4.27	4.09	3.91	3.82
Eu	1.90	1.85	1.75	1.65	1.55	1.44	1.34	1.24	1.13	1.03	0.93	0.88
Gd	5.46	5.36	5.14	4.93	4.72	4.51	4.30	4.09	3.87	3.66	3.45	3.35
Tb	0.84	0.83	0.80	0.77	0.74	0.71	0.68	0.64	0.61	0.58	0.55	0.54
Dy	5.06	4.97	4.79	4.61	4.43	4.25	4.07	3.89	3.71	3.53	3.35	3.26
Ho	1.01	0.99	0.96	0.92	0.89	0.86	0.82	0.79	0.75	0.72	0.69	0.67
Er	2.68	2.64	2.56	2.48	2.40	2.32	2.24	2.16	2.08	2.00	1.92	1.88
Tm	0.38	0.37	0.36	0.36	0.35	0.34	0.33	0.32	0.31	0.30	0.30	0.29
Yb	2.29	2.28	2.24	2.20	2.17	2.13	2.10	2.06	2.02	1.99	1.95	1.93
Lu	0.35	0.35	0.35	0.35	0.34	0.34	0.34	0.33	0.33	0.33	0.32	0.32

Table 3.6c: Result of XRF generated data mixing model between basalt and crust.

Mixing between basalt and crust												
wt.%	0%	5%	15%	25%	35%	45%	55%	65%	75%	85%	95%	100%
SiO_2	50.47	51.50	53.55	55.60	57.65	59.70	61.75	63.80	65.85	67.90	69.95	70.98
TiO_2	1.86	1.80	1.67	1.55	1.42	1.29	1.17	1.04	0.91	0.79	0.66	0.60
Al_2O_3	16.17	16.04	15.79	15.54	15.29	15.04	14.79	14.54	14.29	14.04	13.79	13.66
FeO*	10.65	10.33	9.71	9.08	8.45	7.82	7.19	6.56	5.93	5.30	4.68	4.36
MgO	6.69	6.48	6.04	5.61	5.18	4.74	4.31	3.88	3.44	3.01	2.58	2.36
CaO	9.52	9.19	8.54	7.88	7.23	6.57	5.92	5.26	4.61	3.95	3.30	2.97
Na_2O	3.09	3.10	3.13	3.16	3.19	3.22	3.25	3.28	3.30	3.33	3.36	3.38
K_2O	0.76	0.80	0.88	0.95	1.03	1.10	1.18	1.26	1.33	1.41	1.48	1.52
P_2O_5	0.59	0.57	0.52	0.48	0.43	0.38	0.34	0.29	0.25	0.20	0.15	0.13
MnO	0.19	0.19	0.17	0.16	0.14	0.13	0.11	0.10	0.08	0.07	0.05	0.05
ppm												
Ni	69	67	61	56	51	45	40	35	29	24	19	16
Cr	167	160	147	134	121	108	95	82	69	56	43	37
V	265	258	244	230	216	202	189	175	161	147	133	126
Ga	18	18	18	17	17	16	15	15	14	14	13	13
Cu	50	50	52	53	55	56	57	59	60	62	63	64
Zn	102	101	98	95	92	90	87	84	81	78	75	74

Table 3.6d: Result of ICP-MS generated data mixing model between basalt and crust.

Mixing between basalt and crust												
ppm	0%	5%	15%	25%	35%	45%	55%	65%	75%	85%	95%	100%
Sc	29.09	28.43	27.1	25.77	24.44	23.11	21.78	20.44	19.11	17.78	16.45	15.79
Ba	431	459.7	517	574.3	631.6	689	746.3	803.6	860.9	918.2	975.6	1004
Rb	8.668	10.29	13.53	16.77	20.01	23.25	26.49	29.73	32.97	36.21	39.45	41.07
Sr	527.2	510.8	478	445.3	412.5	379.8	347	314.3	281.5	248.8	216	199.7
Zr	119	116.5	111.6	106.6	101.7	96.7	91.75	86.79	81.84	76.89	71.94	69.46
Y	25.92	25.56	24.83	24.1	23.37	22.64	21.91	21.19	20.46	19.73	19	18.64
Nb	11.79	11.32	10.38	9.45	8.515	7.581	6.646	5.712	4.777	3.843	2.908	2.441
Pb	3.499	3.566	3.699	3.833	3.966	4.1	4.233	4.367	4.5	4.634	4.767	4.834
U	0.408	0.452	0.541	0.631	0.72	0.809	0.898	0.987	1.076	1.165	1.254	1.299
Th	1.227	1.302	1.451	1.6	1.75	1.899	2.048	2.198	2.347	2.496	2.646	2.72
Cs	0.176	0.378	0.783	1.187	1.592	1.996	2.4	2.805	3.209	3.614	4.018	4.22
Hf	2.854	2.814	2.733	2.652	2.571	2.49	2.409	2.328	2.247	2.166	2.086	2.045
Ta	0.681	0.656	0.606	0.556	0.506	0.456	0.406	0.357	0.307	0.257	0.207	0.182
La	19.63	19.02	17.82	16.61	15.4	14.19	12.99	11.78	10.57	9.363	8.155	7.551
Ce	42.55	41.23	38.58	35.93	33.29	30.64	27.99	25.35	22.7	20.05	17.41	16.08
Pr	5.674	5.517	5.203	4.889	4.574	4.26	3.946	3.632	3.317	3.003	2.689	2.532
Nd	24.5	23.84	22.51	21.19	19.87	18.55	17.23	15.91	14.59	13.27	11.95	11.29
Sm	5.614	5.485	5.227	4.969	4.711	4.453	4.195	3.937	3.679	3.421	3.163	3.034
Eu	1.905	1.853	1.748	1.644	1.54	1.436	1.331	1.227	1.123	1.019	0.914	0.862
Gd	5.462	5.353	5.136	4.918	4.701	4.483	4.266	4.048	3.83	3.613	3.395	3.287
Tb	0.843	0.829	0.8	0.772	0.744	0.716	0.688	0.66	0.631	0.603	0.575	0.561
Dy	5.059	4.979	4.82	4.661	4.502	4.343	4.184	4.025	3.866	3.707	3.548	3.468
Ho	1.007	0.993	0.963	0.934	0.904	0.875	0.845	0.816	0.786	0.757	0.727	0.712
Er	2.676	2.64	2.568	2.496	2.424	2.352	2.28	2.208	2.135	2.063	1.991	1.955
Tm	0.377	0.373	0.363	0.354	0.344	0.335	0.325	0.316	0.306	0.297	0.288	0.283
Yb	2.294	2.266	2.21	2.154	2.098	2.042	1.986	1.931	1.875	1.819	1.763	1.735
Lu	0.354	0.35	0.342	0.333	0.325	0.316	0.308	0.3	0.291	0.283	0.274	0.27

Table 3.6e: XRF data of 55 % mixture of basalt and rhyolite mixed with crust.

55% mixture of basalt and rhyolite mixed with crust												
wt.%	0%	5%	15%	25%	35%	45%	55%	65%	75%	85%	95%	100%
SiO_2	62.97	63.37	64.17	64.97	65.77	66.57	67.37	68.17	68.97	69.77	70.57	70.98
TiO_2	1.03	1.01	0.97	0.92	0.88	0.84	0.79	0.75	0.70	0.66	0.62	0.60
Al_2O_3	15.29	15.21	15.04	14.88	14.72	14.56	14.39	14.23	14.07	13.91	13.74	13.66
FeO*	6.02	5.94	5.77	5.61	5.44	5.27	5.11	4.94	4.78	4.61	4.44	4.36
MgO	3.14	3.10	3.02	2.94	2.87	2.79	2.71	2.63	2.55	2.48	2.40	2.36
CaO	5.38	5.26	5.02	4.78	4.54	4.30	4.06	3.81	3.57	3.33	3.09	2.97
Na_2O	3.51	3.51	3.49	3.48	3.47	3.45	3.44	3.42	3.41	3.40	3.38	3.38
K_2O	2.23	2.19	2.12	2.05	1.98	1.91	1.84	1.77	1.70	1.63	1.56	1.52
P_2O_5	0.32	0.31	0.29	0.27	0.25	0.23	0.22	0.20	0.18	0.16	0.14	0.13
MnO	0.12	0.11	0.11	0.10	0.09	0.09	0.08	0.07	0.06	0.06	0.05	0.05
ppm												
Ni	33	32	30	28	27	25	24	22	20	19	17	16
Cr	78	76	72	68	64	60	55	51	47	43	39	37
V	135	135	134	133	132	131	130	129	129	128	127	126
Ga	17	17	16	16	16	15	15	14	14	14	13	13
Cu	26	28	32	36	39	43	47	51	54	58	62	64
Zn	73	73	73	73	73	73	73	74	74	74	74	74

Table 3.6f: ICP-MS data of 55 % mixture of basalt and rhyolite mixed with crust.

55% mixture of basalt and rhyolite mixed with crust												
ppm	0%	5%	15%	25%	35%	45%	55%	65%	75%	85%	95%	100%
Sc	16.30	16.27	16.22	16.17	16.12	16.07	16.02	15.97	15.92	15.86	15.81	15.79
Ba	1011	1010	1010	1009	1008	1008	1007	1007	1006	1005	1005	1004
Rb	52	51	50	49	48	47	46	45	44	43	42	41
Sr	364	356	340	323	307	290	274	257	241	224	208	200
Zr	148	144	136	128	120	112	105	97	89	81	73	69
Y	21.52	21.38	21.09	20.80	20.51	20.22	19.94	19.65	19.36	19.07	18.78	18.64
Nb	10.13	9.75	8.98	8.21	7.44	6.67	5.90	5.13	4.36	3.59	2.83	2.44
Pb	9.22	9.01	8.57	8.13	7.69	7.25	6.81	6.37	5.93	5.49	5.05	4.83
U	2.20	2.16	2.07	1.98	1.89	1.80	1.71	1.62	1.52	1.43	1.34	1.30
Th	4.79	4.68	4.48	4.27	4.06	3.86	3.65	3.44	3.24	3.03	2.82	2.72
Cs	2.39	2.48	2.67	2.85	3.03	3.21	3.40	3.58	3.76	3.95	4.13	4.22
Hf	3.81	3.72	3.54	3.37	3.19	3.02	2.84	2.66	2.49	2.31	2.13	2.05
Ta	0.71	0.69	0.63	0.58	0.53	0.47	0.42	0.37	0.31	0.26	0.21	0.18
La	22.81	22.05	20.52	18.99	17.47	15.94	14.42	12.89	11.37	9.84	8.31	7.55
Ce	44.57	43.15	40.30	37.45	34.60	31.75	28.90	26.06	23.21	20.36	17.51	16.08
Pr	5.50	5.35	5.06	4.76	4.46	4.16	3.87	3.57	3.27	2.98	2.68	2.53
Nd	21.82	21.29	20.24	19.18	18.13	17.08	16.03	14.97	13.92	12.87	11.82	11.29
Sm	4.63	4.55	4.39	4.23	4.07	3.91	3.75	3.59	3.43	3.27	3.11	3.03
Eu	1.34	1.32	1.27	1.22	1.17	1.12	1.08	1.03	0.98	0.93	0.89	0.86
Gd	4.30	4.25	4.15	4.05	3.94	3.84	3.74	3.64	3.54	3.44	3.34	3.29
Tb	0.68	0.67	0.66	0.65	0.64	0.62	0.61	0.60	0.59	0.58	0.57	0.56
Dy	4.07	4.04	3.98	3.92	3.86	3.80	3.74	3.68	3.62	3.56	3.50	3.47
Ho	0.82	0.82	0.80	0.79	0.78	0.77	0.76	0.75	0.74	0.73	0.72	0.71
Er	2.24	2.22	2.20	2.17	2.14	2.11	2.08	2.05	2.03	2.00	1.97	1.96
Tm	0.33	0.33	0.32	0.32	0.31	0.31	0.30	0.30	0.29	0.29	0.29	0.28
Yb	2.10	2.08	2.04	2.01	1.97	1.93	1.90	1.86	1.83	1.79	1.75	1.73
Lu	0.34	0.33	0.33	0.32	0.31	0.31	0.30	0.29	0.29	0.28	0.27	0.27

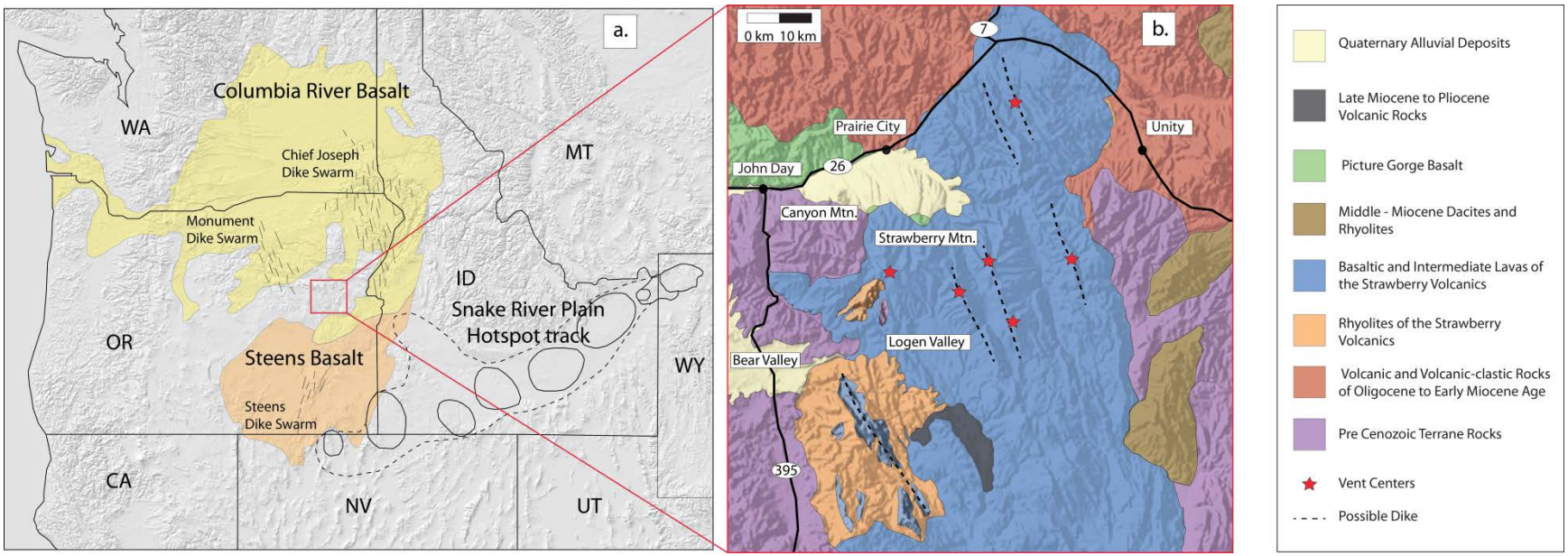

Figure 1.1: Regional map and simplified geologic map. a) Regional map showing the location of Columbia River Basalt Group (CRBG) lavas including Steens Basalt in relation to study area (red square) with the Strawberry Volcanics. The solid circles are presumed rhyolitic centers associated with the Yellowstone hotspot, (modified after Camp and Ross, 2004. b) Simplified geologic map from 44° to 44° 30´ latitude and 118° to 119° longitude of the Strawberry Volcanics and surrounding units. The geologic units surrounding the Strawberry Volcanics are based on: Brooks and Ferns, 1979; Brown and Thayer, 1966; Brown and Thayer, 1977; Crowley, 1960; Ferns et al., 1983; Green et al., 1972; Mullen, 1983; Robyn, 1977; Thayer, 1956; Thayer et al., 1967.

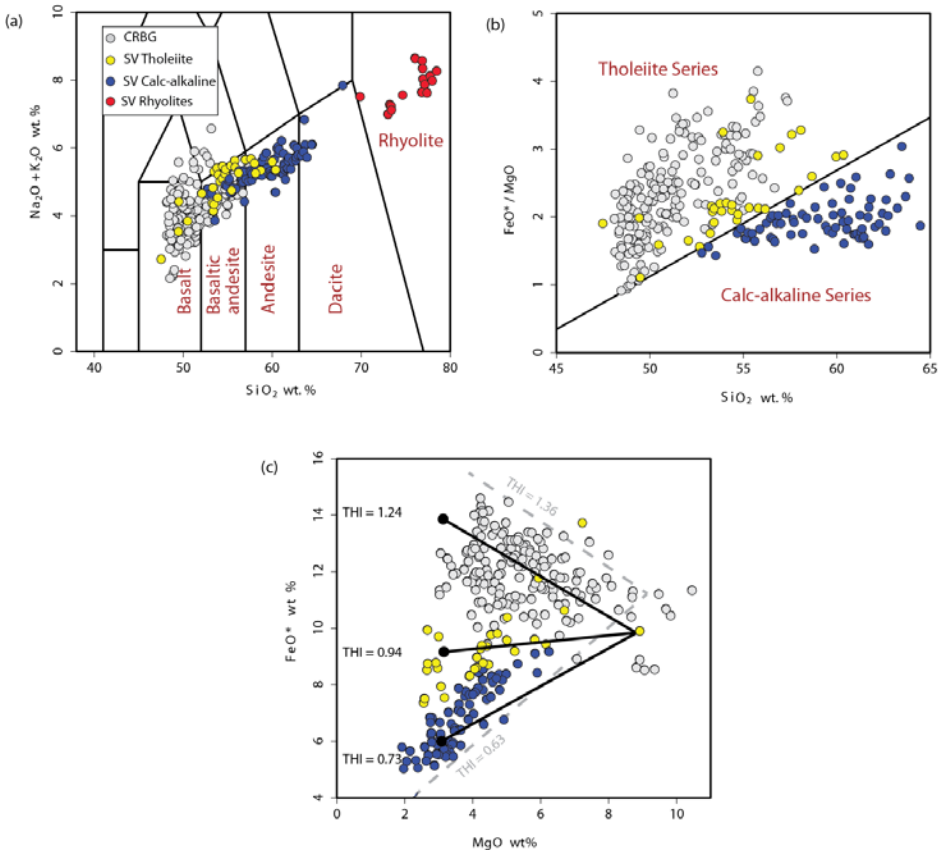

Figure 1.2: TSA, FeO* vs SiO_2 wt % and FeO* vs MgO wt % with calculated THI of the Strawberry Volcanics and the CRBG. Compositional spread of lavas of the Strawberry Volcanics (this study) and of the Columbia River Basalt Group (CRBG) (Wolff et al. (2008). a) Total alkali-silica diagram (Le Bas et al., 1986). Yellow circles indicate tholeiitic compositions while blue circles are calc-alkaline compositions according to scheme of Miyashiro (1974). Red circles are for rhyolites of the Strawberry Volcanics; b) FeO*/MgO versus SiO_2 diagram with tholeiitic/calc-alkaline fields as based on Miyashiro (1974). c) FeO* vs. MgO wt.% diagram. Overall, FeO* wt.% decreases with decreasing MgO wt.% in the tholeiitic and calc-alkaline lavas of the Strawberry Volcanics, yet the tholeiitic lavas decrease less than the calc-alkaline. The most mafic tholeiitic lavas of the Strawberry Volcanics overlap considerably with the CRBG and transition towards calc-alkaline compositions as MgO wt.% decreases. Calc-alkaline lavas of the Strawberry Volcanics have a Tholeiitic Index (THI) of 0.73 while tholeiitic basalt and intermediate lavas have a THI of 0.94. The tholeiitic index (THI) was developed by Zimmer et al. (2010) and is defined in the following way: THI = $Fe_{4.0}$ / $Fe_{8.0}$ where $Fe_{4.0}$ is the average FeO* wt.% concentration of samples with 4 ± 1 wt.% MgO, and $Fe_{8.0}$ is the average FeO* wt.% concentration at 8 ± 1 wt.% MgO thus, samples with THI>1 are tholeiitic and samples with THI<1 are calc-alkaline. The three solid lines correspond with calculated THI values for the various suites, i.e. calc-alkaline and tholeiitic suites of the Strawberry Volcanic and the tholeiitic lavas of the CRBG if we use the composition of a primitive basalt of the Strawberry Volcanics for $Fe_{8.0}$. Alternatively, if we use an initially higher FeO* at 8 wt.% MgO, this will lead to a reduced THI value for the Strawberry lavas (dashed gray line) and consequently to a stronger calc-alkaline signature.

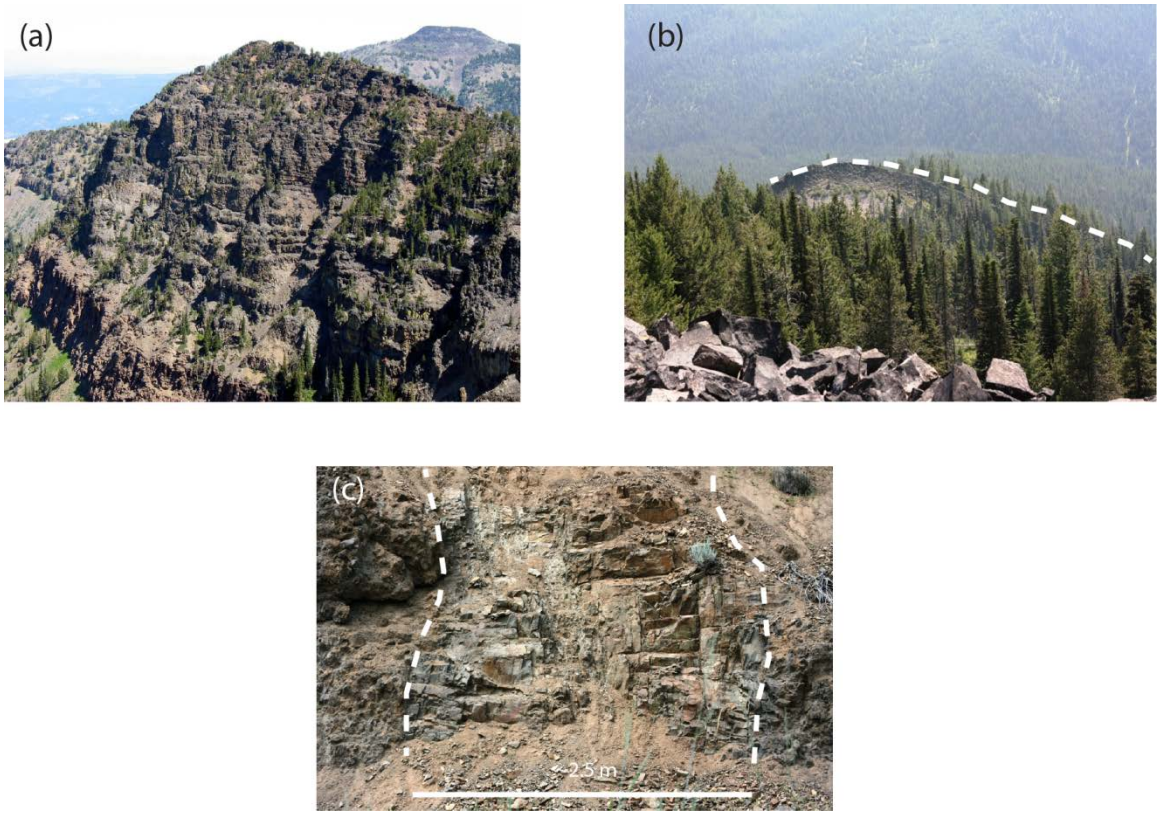

Figure 1.3: Field photographs of lavas and dikes of the Strawberry Volcanics. a) Section of >1000 m in thickness of lava flows of the Strawberry Volcanics exposed in the glaciated wall of Strawberry Mountain (44°17’44’’N, 118°40’41’’W); b) NNW-SSE trending dike of the Strawberry Volcanics (44°16’54’’N, 118°31’18’’W) that follows a regional dike trend; c) close up of a Strawberry Volcanics dike cross-cutting other volcanic rocks (44°22’04’’N, 118°26’30’’W).

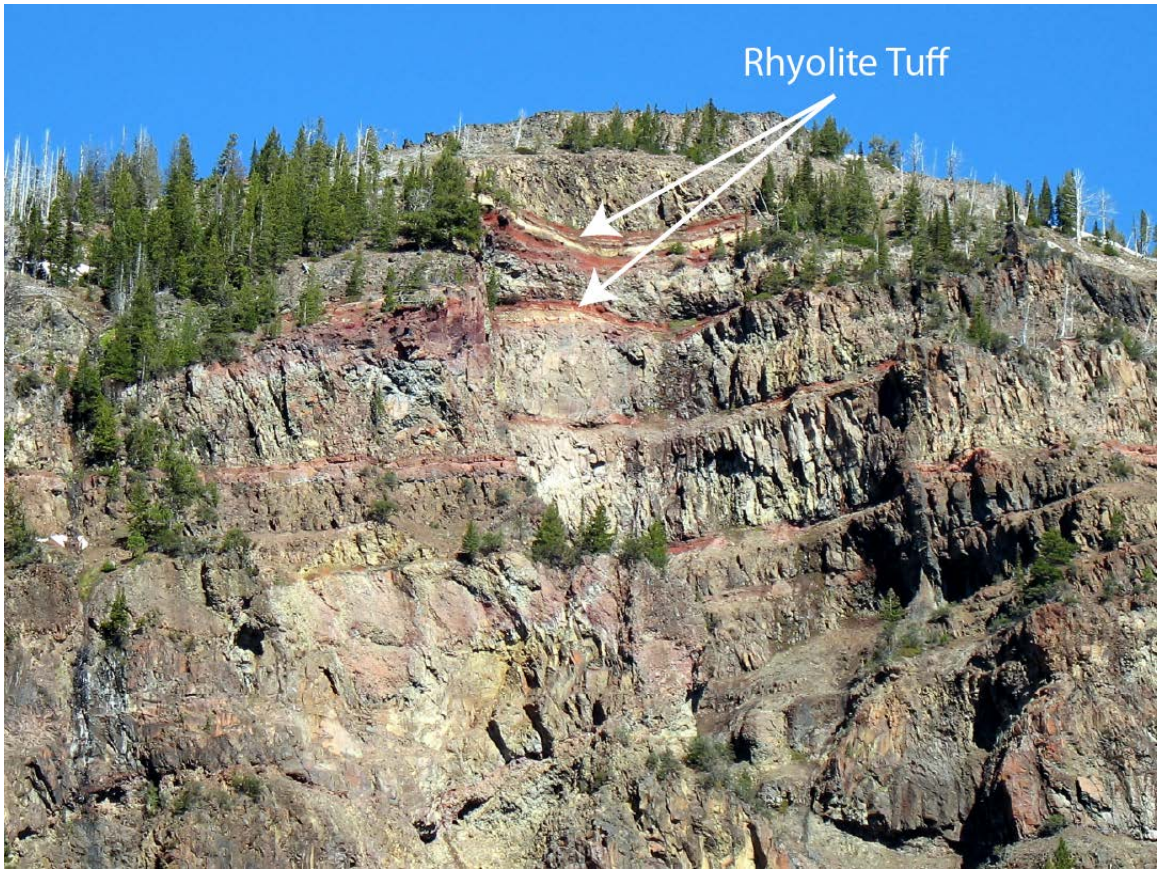

Figure 1.4: Field photograph of lavas with rhyolite tuff between lavas. Two ~8 m thick rhyolitic ash-flow tuffs intercalated with lava flows of the Strawberry Volcanics (44°18’52’’N, 118°41’32’’W). These tuffs are correlated with the Dinner Creek Tuff which erupted between 15.9-15.4 Ma (Streck et al., 2011). This stratigraphic evidence indicates that activity of the Strawberry Volcanics likely started at ≥ 16 Ma.

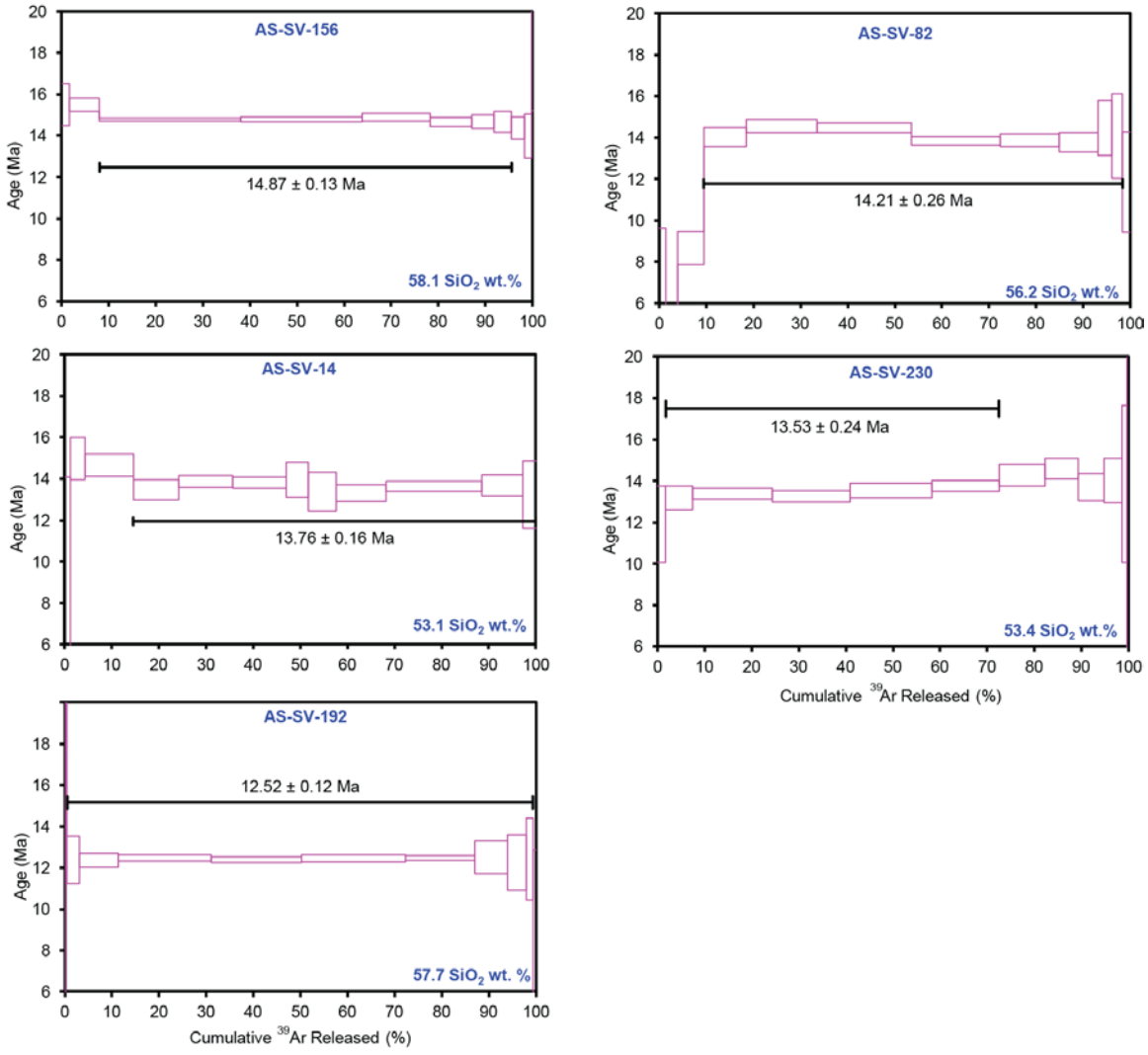

Figure 1.5: $^{40}Ar/^{39}Ar$ analysis of lavas of the Strawberry Volcanics. Results of $^{40}Ar/^{39}Ar$ dating experiments indicating that the Strawberry Volcanics were at least active between 14.87±0.13 Ma to 12.52±0.12 Ma, see text for discussion. SiO_2 content of dated sample is given in right hand corner.

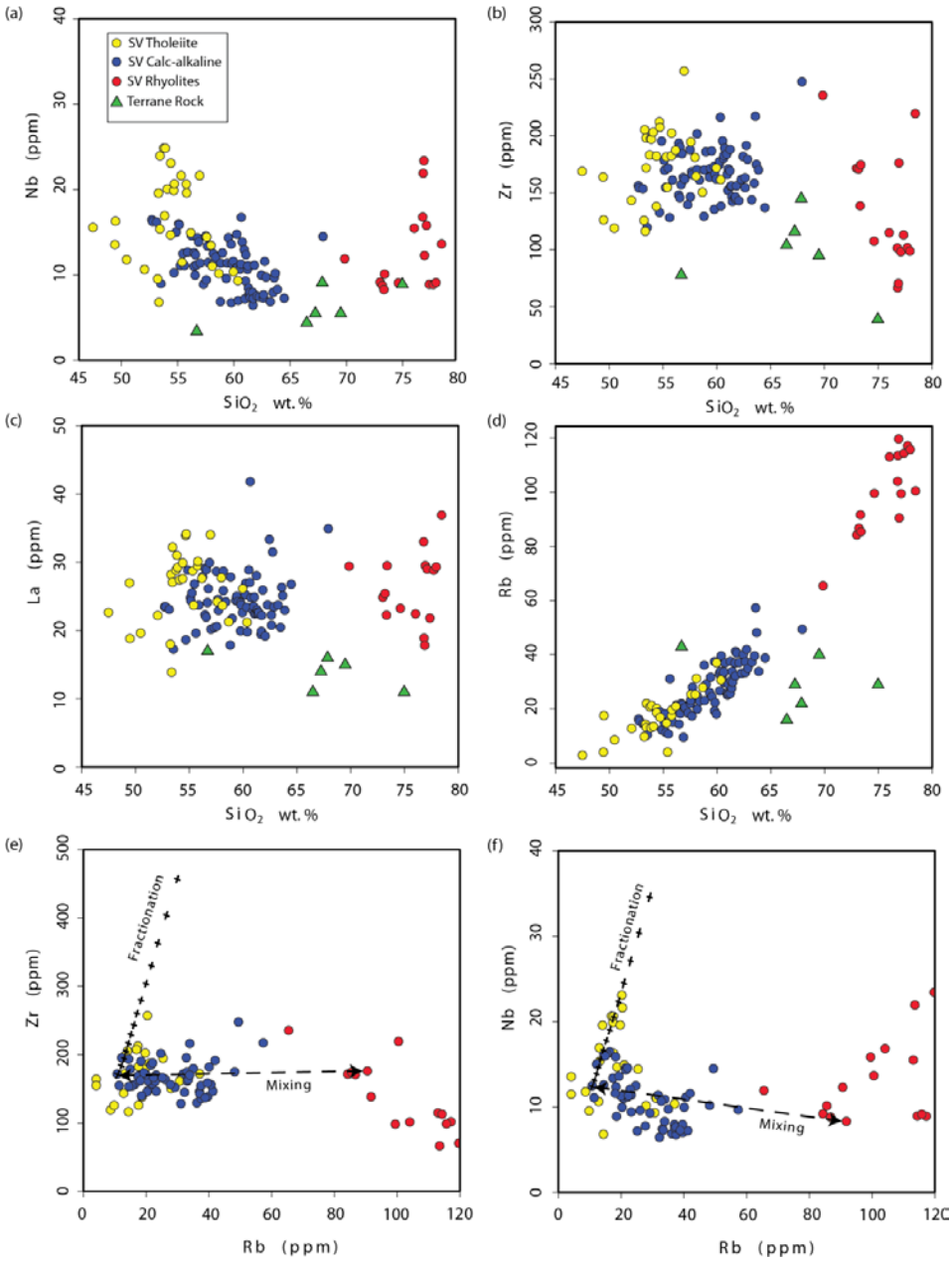

Figure 1.6: Harker diagrams for selected trace elements vs SiO_2 wt % and calculated fractional crystallization models for selected trace elements. Variation diagrams of Nb (a), Zr (b), La (c), and Rb vs. SiO_2 (d). Observed trends among incompatible elements towards increased silica rule out fractional crystallization as main process to generate calc-alkaline andesites. Diagrams e and f include mixing and fractionation models. Fractionation models are based on partition coefficients for Rb of 0.071, 0.031, 0.02, for Zr of 0.048, 0.10, 0.18 and for Nb of 0.01, 0.15, and 0.005 for plagioclase, clinopyroxene and othropyroxene, respectively. The modal proportions used are based on observed mineral assemblages and are as follows; 68 % plagioclase, 17% clinopyroxene and 15% orthopyroxene. The composition of the liquid has been calculated in intervals of 5% as illustrated by + marks.

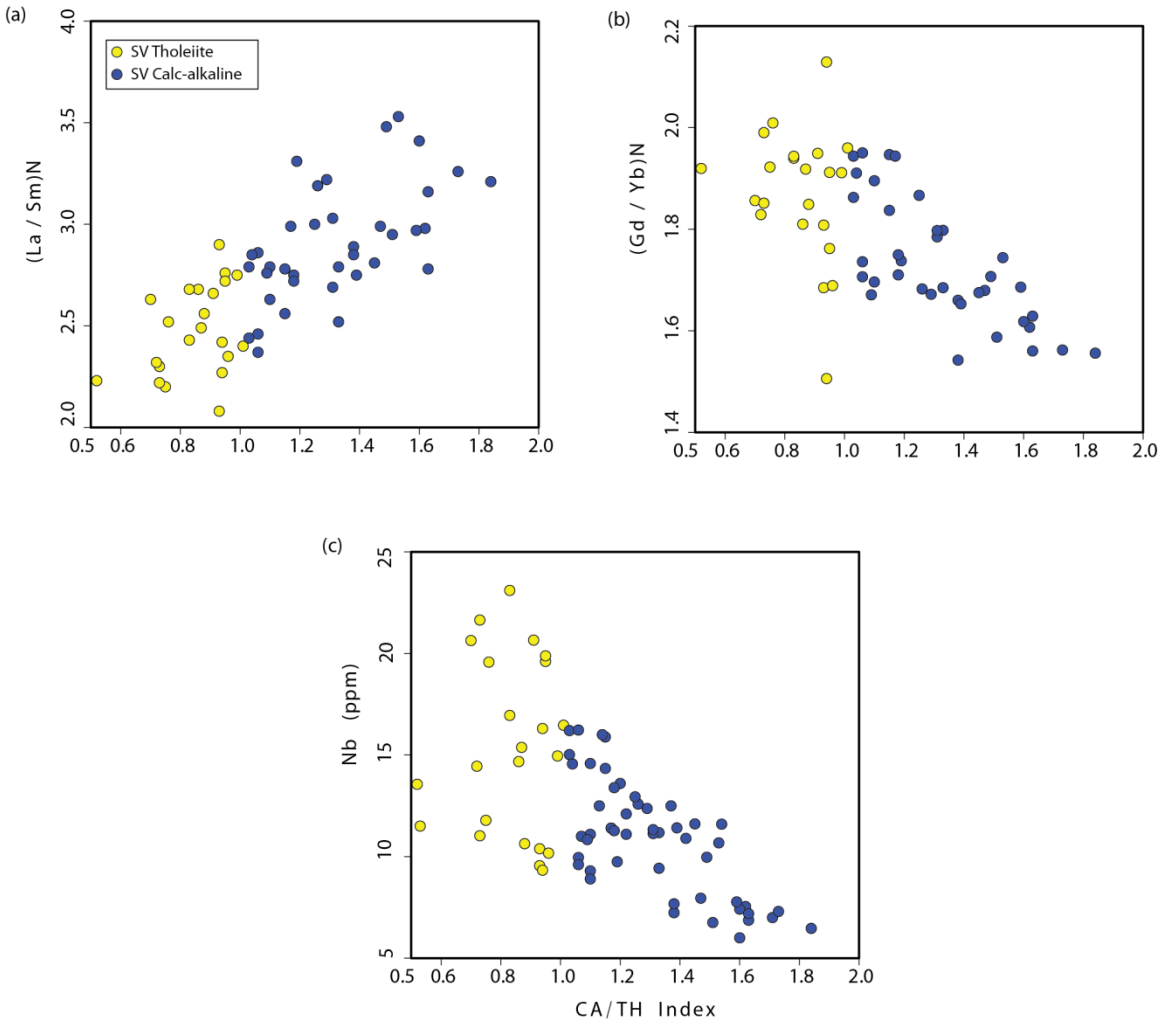

Figure 1.7: Selected trace element ratios and trace elements vs tholeiitic index. Ratios of $(La/Sm)_N$ and $(Gd/Yb)_N$, and concentrations of Nb plotted versus calc-alkaline/tholeiite (CA/TH) index of Hora et al. (2009) determined for each sample. CA/TH index = (wt.% SiO_2 -42.8)/(6.4 x FeO*/MgO). A CA/TH index of <1 indicates tholeiitic character and of >1 calc-alkaline character. We are using the CA/TH index here because it allows to assign a value of calc-alkaline/tholeiitic character to individual samples as opposed to the THI index that describes the trend within a suite of samples. On average, tholeiitic lavas of the Strawberry Volcanics have a flatter LREE $(La/Sm)_N$ slope but a steeper HREE $(Gd/Yb)_N$ slope than calc-alkaline lavas. Nb concentrations are higher in the tholeiitic lavas and decrease with increasing calc-alkalinity.

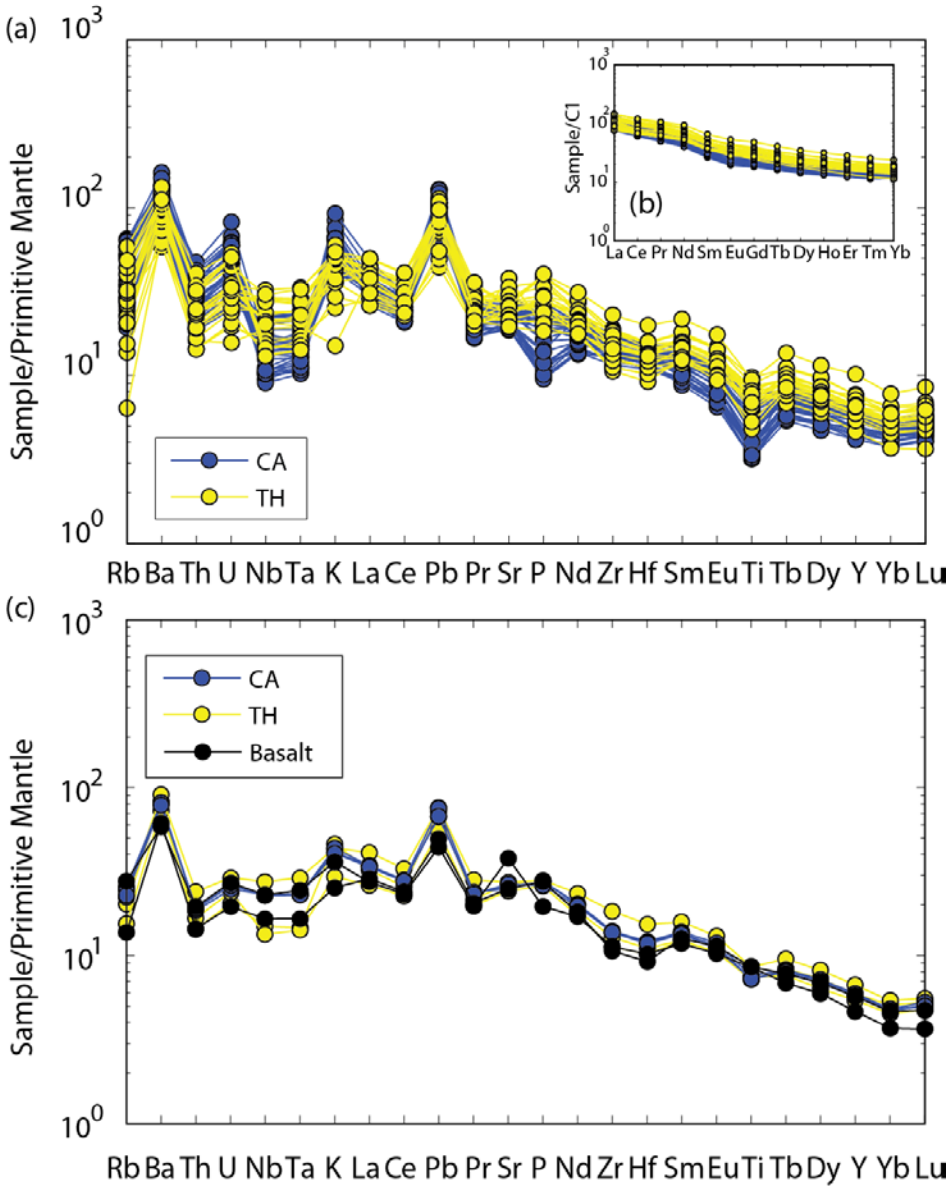

Figure 1.8: Primitive mantle and C1 normalized multi-variable diagrams. Primitive mantle normalized incompatible element diagram (a) and chondrite normalized REE diagram (b) of select andesites (<62 SiO_2 wt.%) of Strawberry Volcanics showing similarities as well as difference towards more evolved compositions. Normalization values are taken from Sun and McDonough (1989) for (a) and McDonough and Sun (1995) for (b). Diagram c) is a primitive mantle normalized incompatible element diagram of selected basalts and basaltic andesites with compositions of ≤53 wt.% SiO_2 wt.% showing similarity of both tholeiitic (yellow) and calc-alkaline (blue) basaltic andesites and tholeiitic basalts.

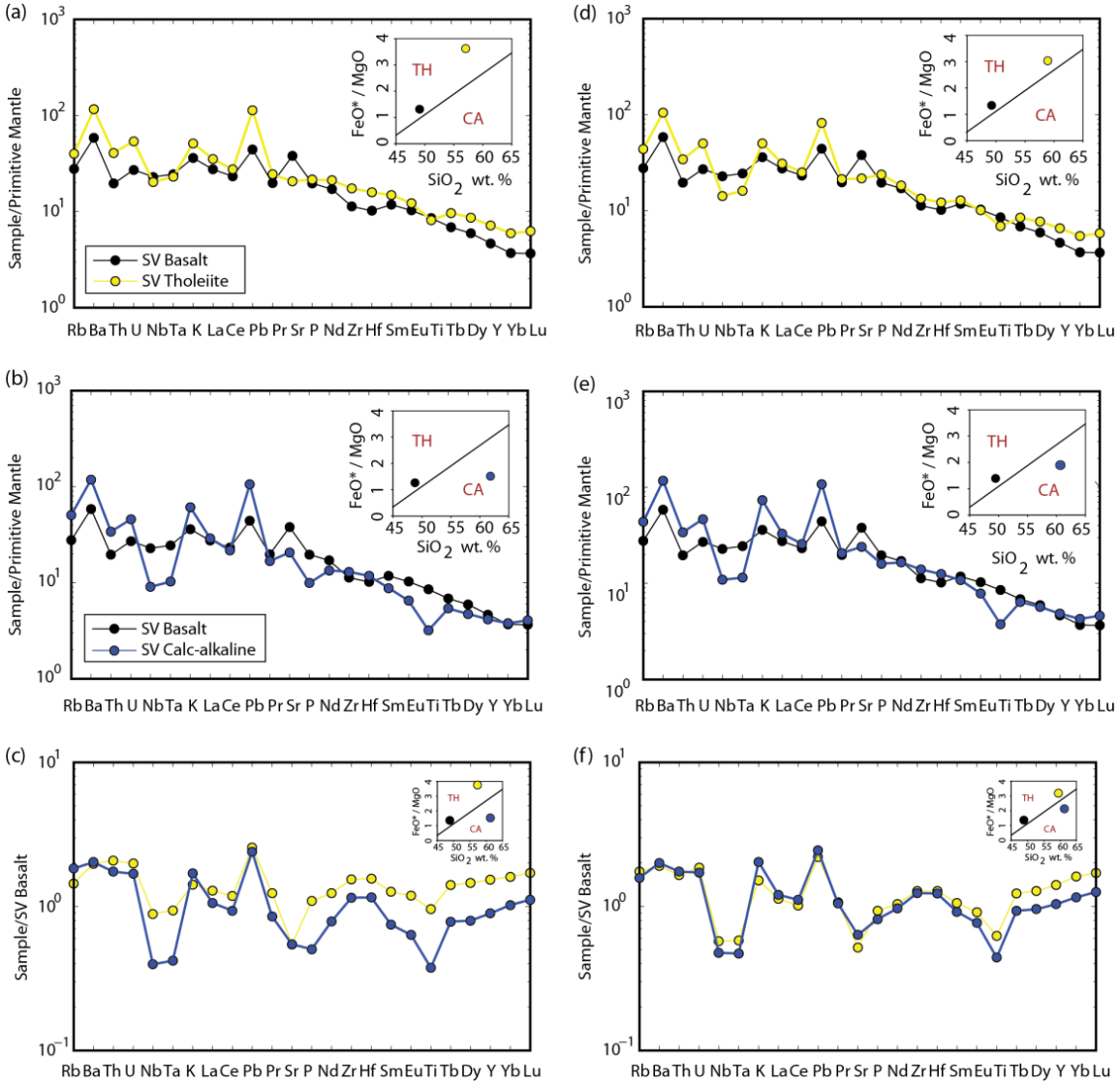

Figure 1.9: Primitive mantle multi-variable diagrams comparing basalts to increasing THI of various tholeiites and calc-alkaline lavas. Primitive mantle normalized (Sun and McDonough, 1989) incompatible element diagrams of select samples of Strawberry Volcanics comparing primitive tholeiite (AS-SV-171) to single intermediate composition members of the tholeiitic (a and d) and calc-alkaline (b and e) suites within a narrow silica range (57-61 wt.%). Figures a) and b) compare samples that are most tholeiitic and most calc-alkaline and figures d) and e) compare samples that are tholeiitic and calc-alkaline but are closer in their Fe*O/MgO ratios and straddle the tholeiitic/calc-alkaline divide. Figure c) and f) show normalization diagrams using elemental concentrations of basalt (AS-SV-171) of the Strawberry Volcanics; c) displays differences between andesites of panel a) and b) and f) shows differences between andesites of panel d) and e). Insets show position of samples relative to tholeiitic/calc-alkaline divide of Miyashiro (1974). Differences in incompatible element compositions between tholeiitic and calc-alkaline samples are notable the more different samples are in terms of their FeO*/MgO ratio (or CA/TH index) but are less notable as samples converge in their FeO*/MgO ratio (see text for discussion).

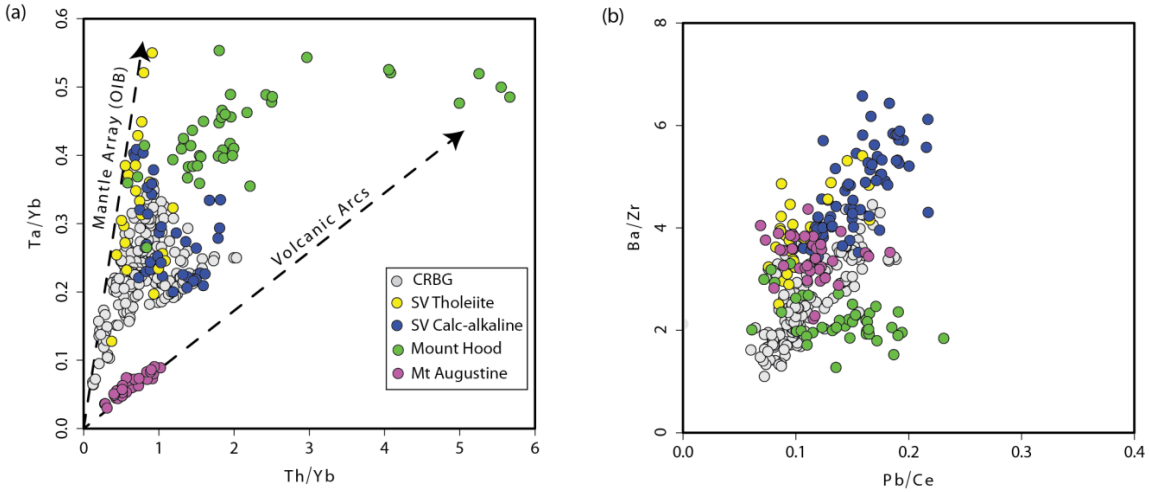

Figure 1.10: Comparison of selected trace element ratios of the Strawberry Volcanics with lavas of the CRBG and typical 'orogenic' andesites. Lavas of the Strawberry Volcanics relative to lavas of CRBG and typical continental arcs represented by Mt. Hood and Mt. Augustine: a) Th/Yb vs. Ta/Yb diagram; dashed arrows indicate typical volcanic arcs and a "mantle array" (OIB) trajectories taken from Leeman et al. (1990); b) Pb/Ce vs. Ba/Zr diagram. Significant overlap between lavas of the Strawberry Volcanics and the CRBG and their compositional spread indicate derivation from a similar mantle source that has been previously metasomatized. Data for Mt. Hood taken from Wood (2004) and for Mt. Augustine from Steiner et al. (2012).

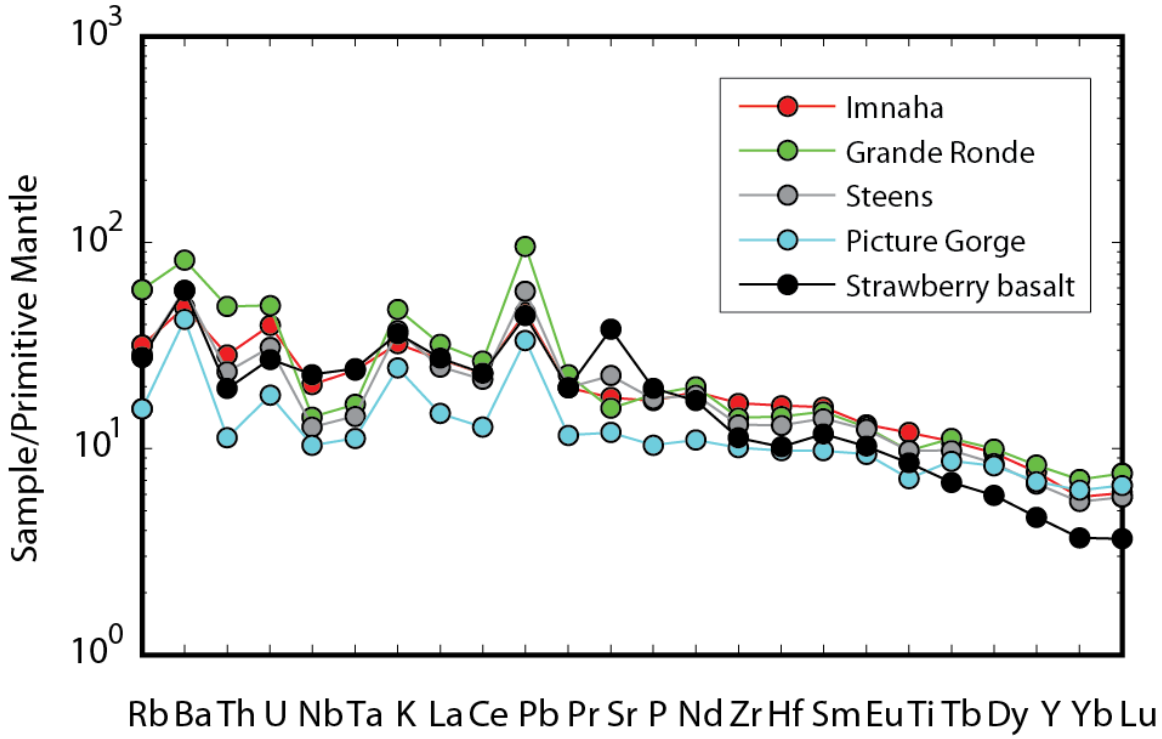

Figure 1.11: Comparison of primitive mantle normalized multi-variable diagram and the average analysis of lavas of the CRBG. Primitive mantle normalized (Sun and McDonough, 1989) incompatible element diagram comparing one basalt of the Strawberry Volcanics (black) with select lavas of the CRBG (Wolff et al. (2008) representing following members: Imnaha Basalt (red), Grande Ronde Basalt (green), Steens Basalt (gray), and Picture Gorge Basalt (blue). The tholeiite of the Strawberry Volcanics is lightly depleted in HREE relative to CRBG lavas but otherwise indicate a very similar pattern. Best match is found with Steens type basalt.

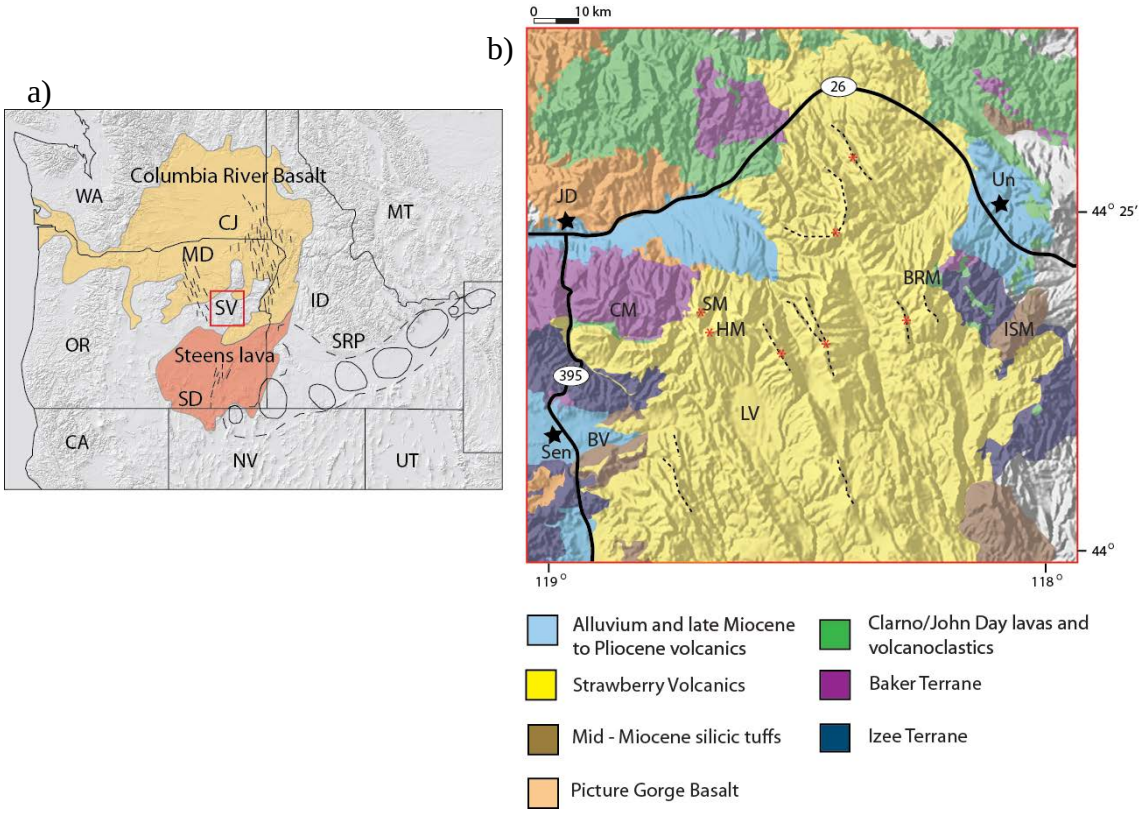

Figure 2.1: Regional map and simplified geologic map. a) Location of the Strawberry Volcanics and regional lavas of the CRB. b) The larger map shows the geology surrounding the Strawberry Volcanics and the boundary of the volcanic field (yellow). Field observations identified volcanic centers (red stars) and dikes (dashed lines) are included on map. BRM (Bull Run Mtn.), BV (Bear Valley), CA (California), CJ (Chief Joseph Dikes), CM (Canyon Mtn.), HM (High Mtn.), ID (Idaho), ISM (Ironside Mtn.), LV (Logan Valley), MD (Monument Dikes), MT (Montana), NV (Nevada), OR (Oregon), SD (Steens Dikes), SM (Strawberry Mtn.), SRP (Snake River Plains – Yellowstone Hotspot), SV (Strawberry Volcanics)UT (Utah), WA (Washington), WY (Wyoming). Black stars represent towns JD (John Day), Sen (Seneca), Un (Unity). Figure of the CRBG lavas is molded after Camp and Ross, (2004). The geological units surrounding the Strawberry Volcanics are based on Thayer (1956), Crowley (1960), Brown and Thayer (1966a, b, 1977), Thayer et al. (1967), Greene et al. (1972), Robyn (1977), Brooks and Ferns (1979), Ferns et al. (1983) and Mullen (1983).

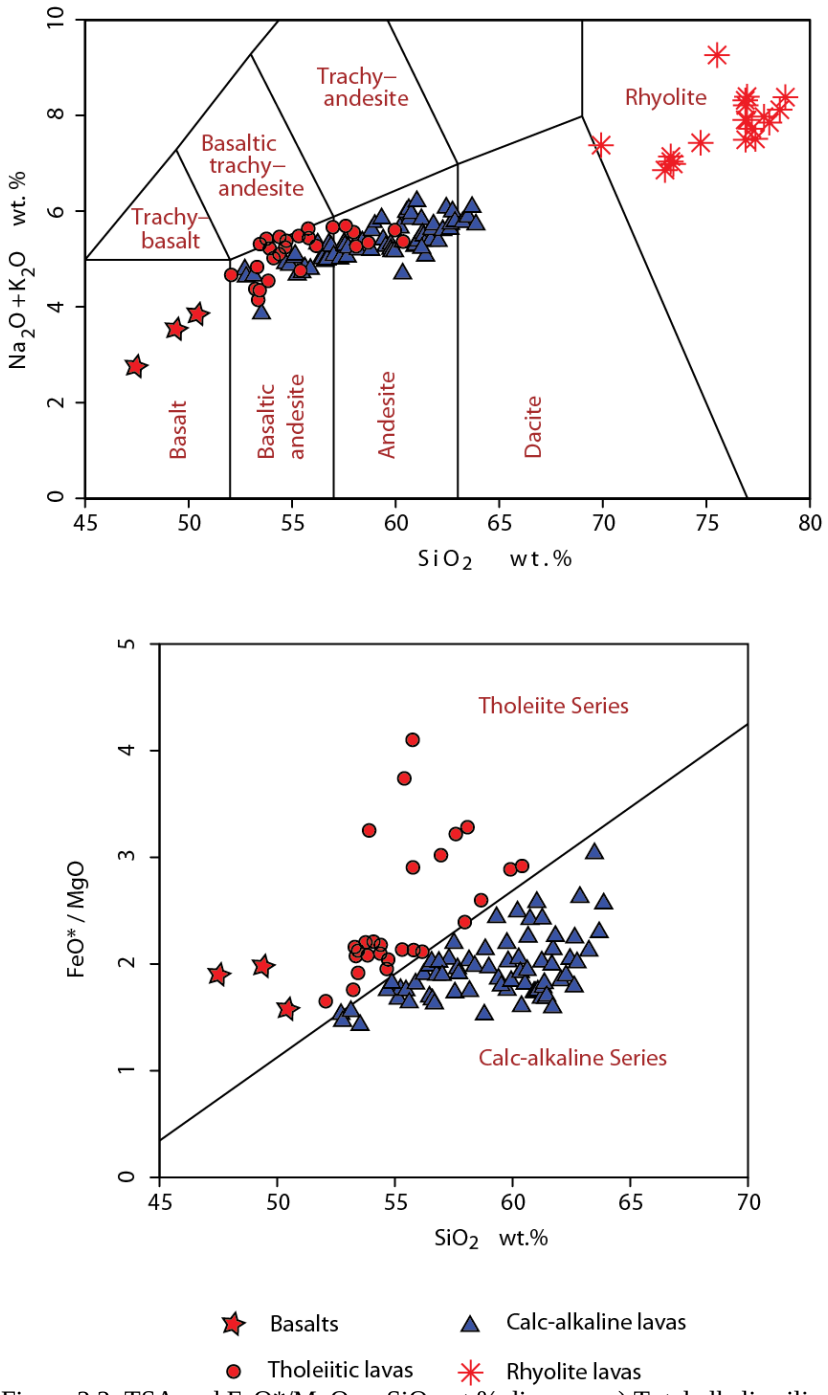

Figure 2.2: TSA and FeO*/MgO vs SiO_2 wt % diagram. a) Total alkali– silica diagram (Le Bas et al. 1986) with all SV data showing diversity of the volcanic suite and b) Miyashiro (1974) tholeiitic and calc-alkaline diagram showing that mafic to intermediate compositions of Strawberry Volcanics display both tholeiites and calc-alkaline affinities.

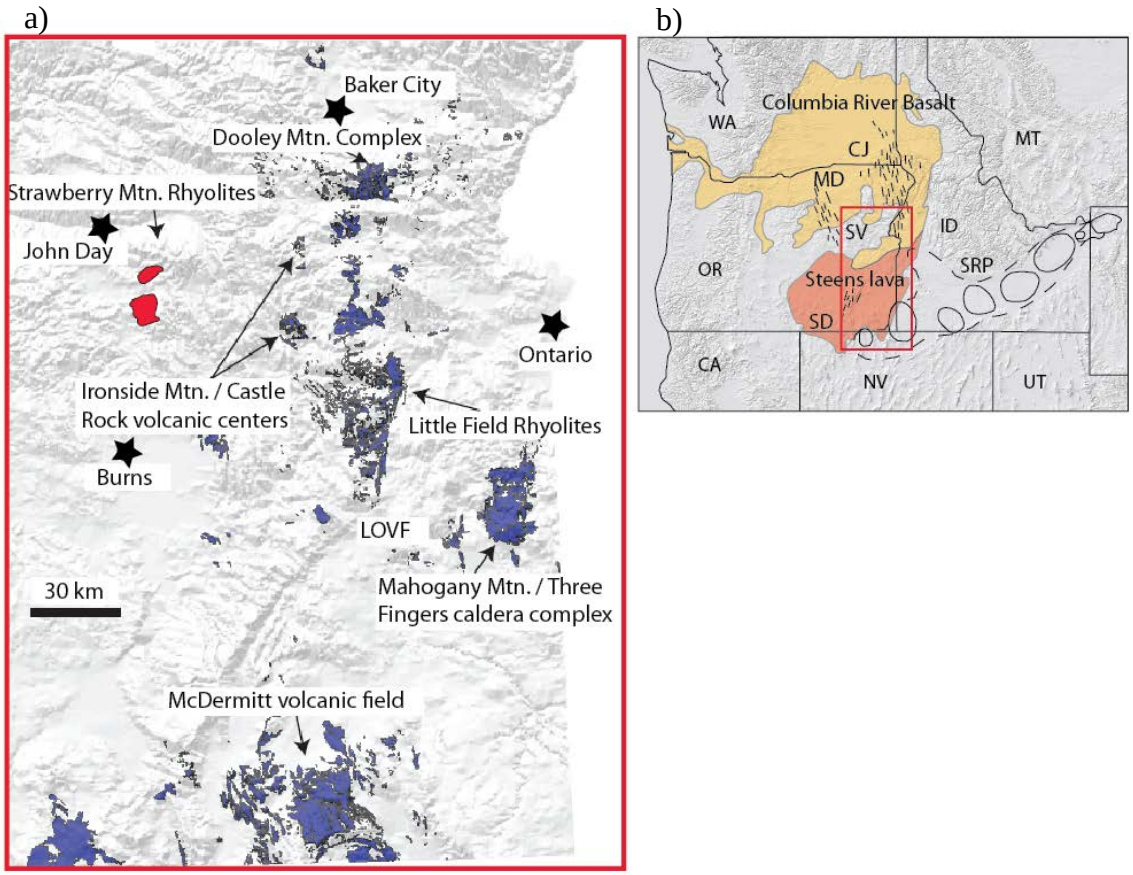

Figure 2.3: Regional map of the distribution of mid-Miocene rhyolitic centers. a) Location map of mid-Miocene rhyolites of eastern OR related to the onset of the Yellowstone-Snake River Plains Hotspot. b) Location of the area in a).

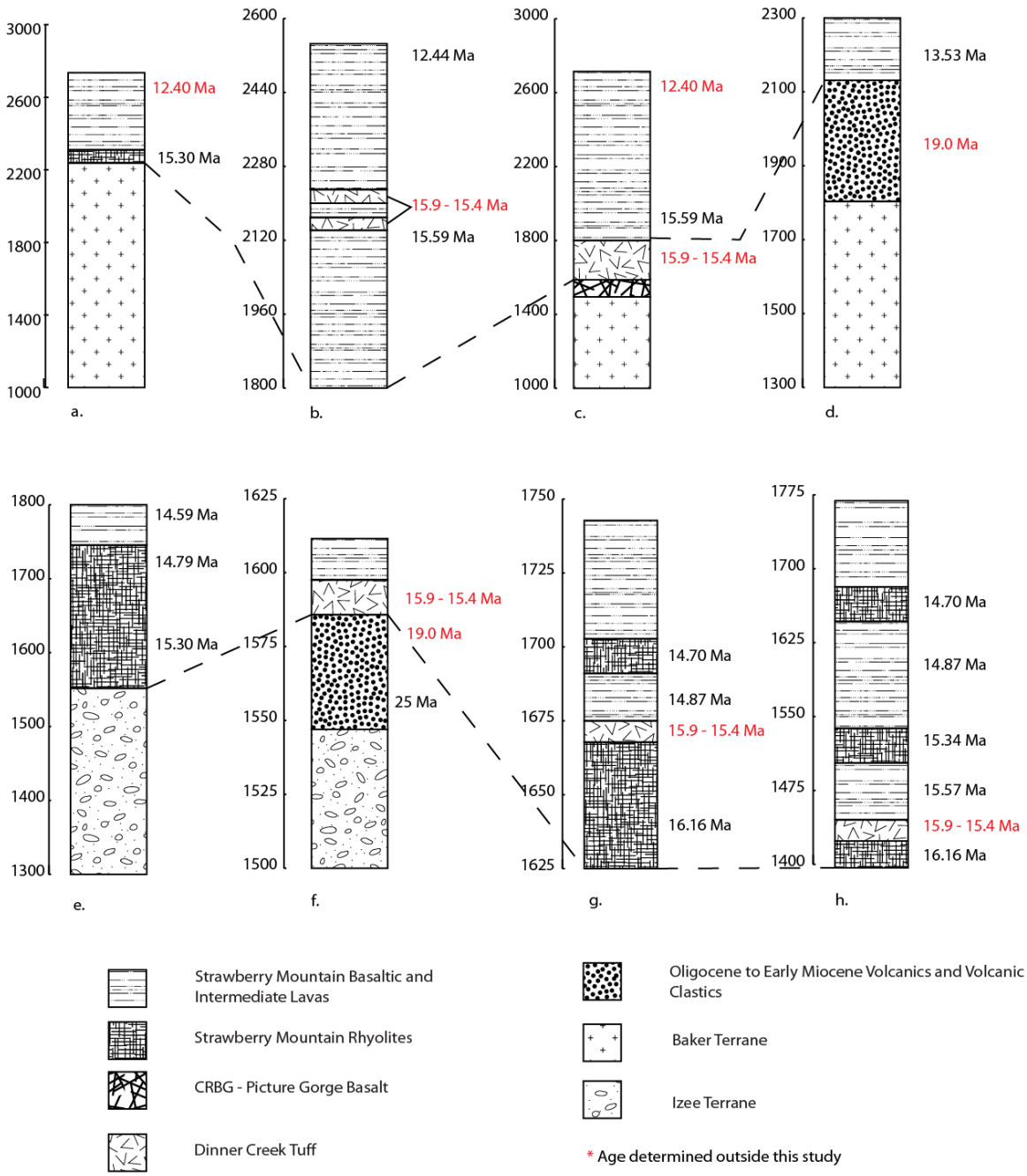

Figure 2.4: Fence diagram of the Strawberry Volcanics. Sections through the Strawberry Volcanics and other important geologic units in the surrounding area. Sections are labeled a-h and can be correlated to locations on Figure 5. Ages of specific units are labeled to the right of the diagram. All ages in black are determined by this study. In red are ages associated with specific units determined outside of this study (Streck et. al., 2011 and Robyn, 1977). Numbers on left of diagram are in meters.

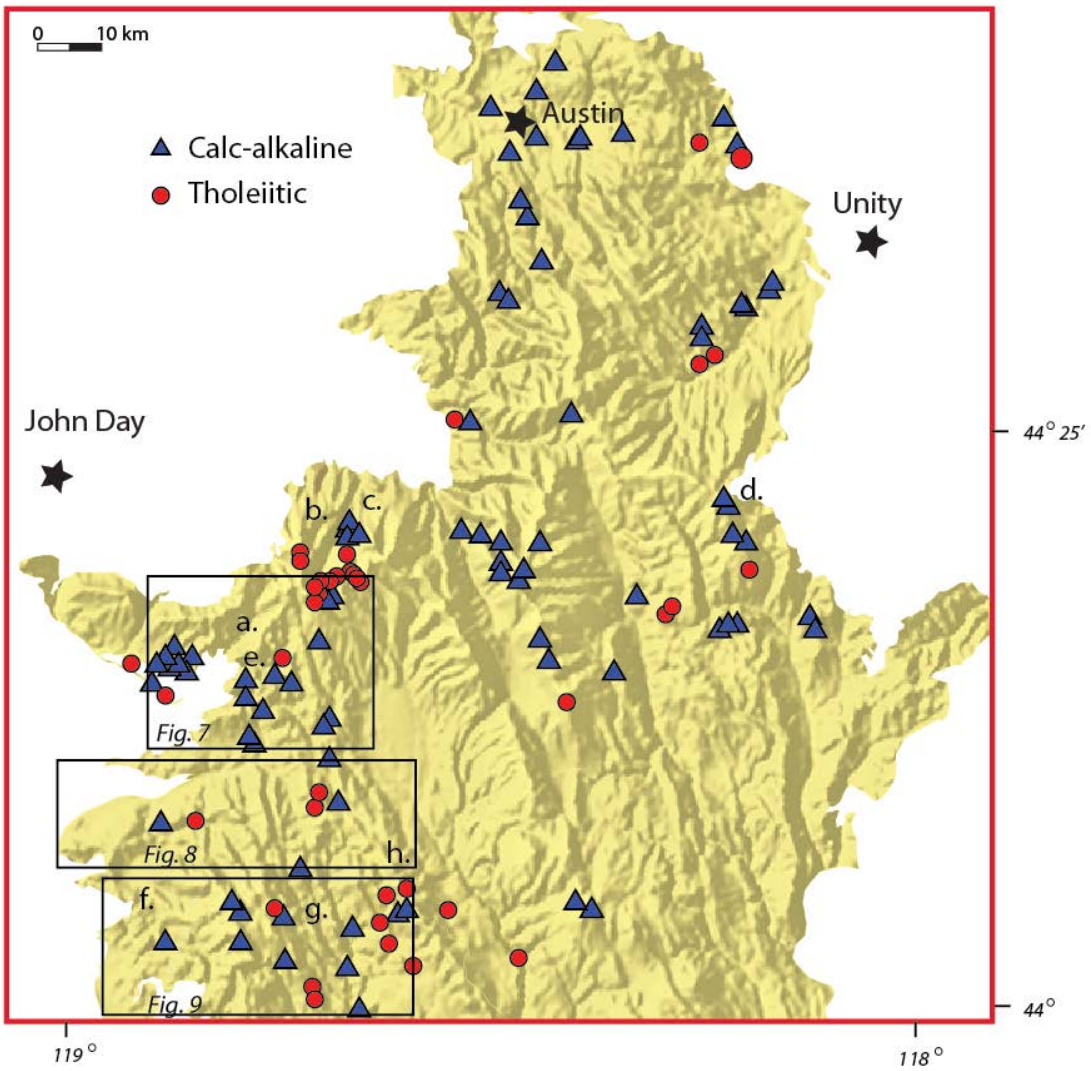

Figure 2.5: Sample location map of lavas analyzed by whole rock XRF and ICP-MS analysis. a to h are locations of schematic sections of Figure 4. Black frames indicate arial coverage of geology maps in figures 7, 8, and 9.

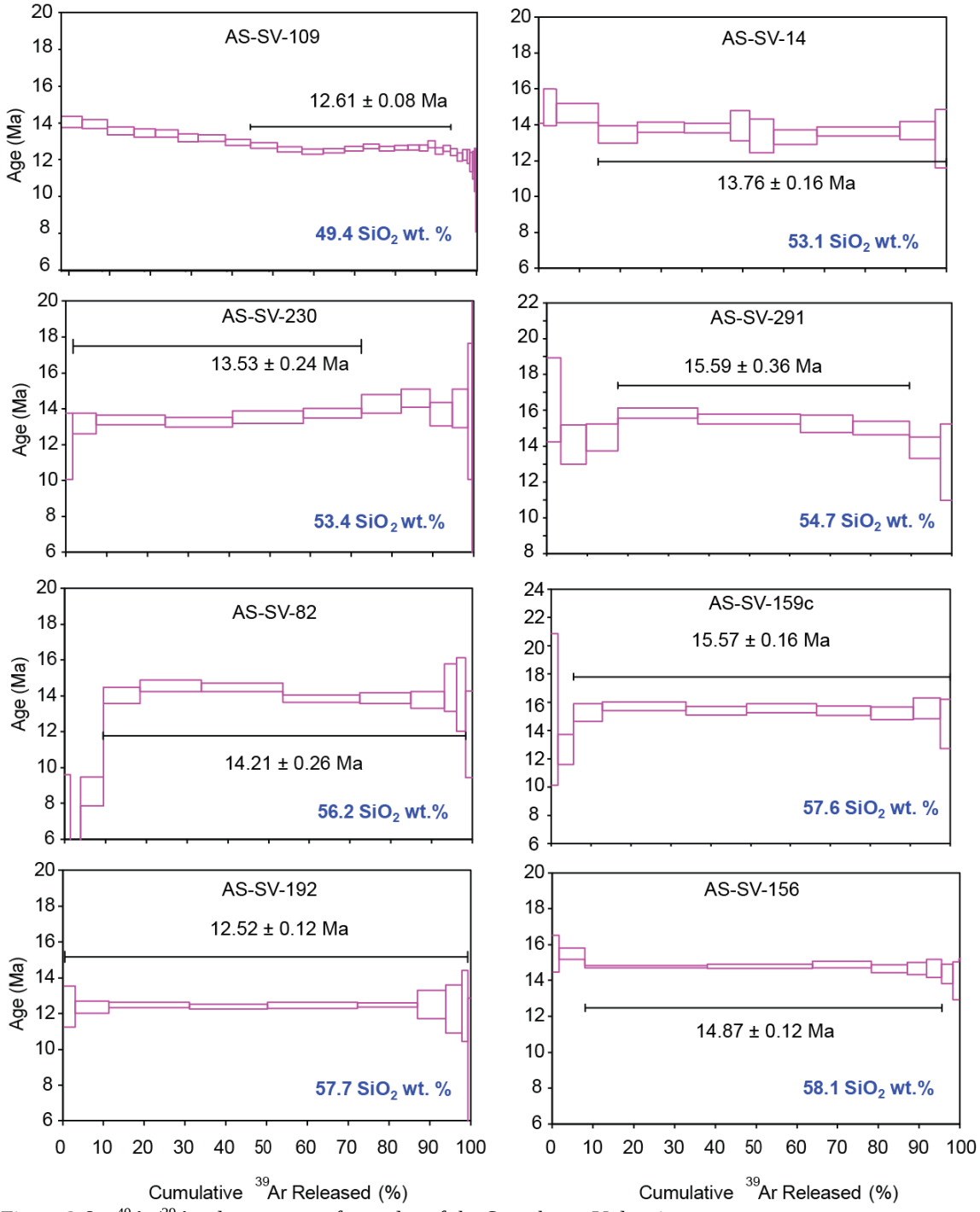

Figure 2.6a: $^{40}Ar/^{39}Ar$ plateau ages of samples of the Strawberry Volcanics.

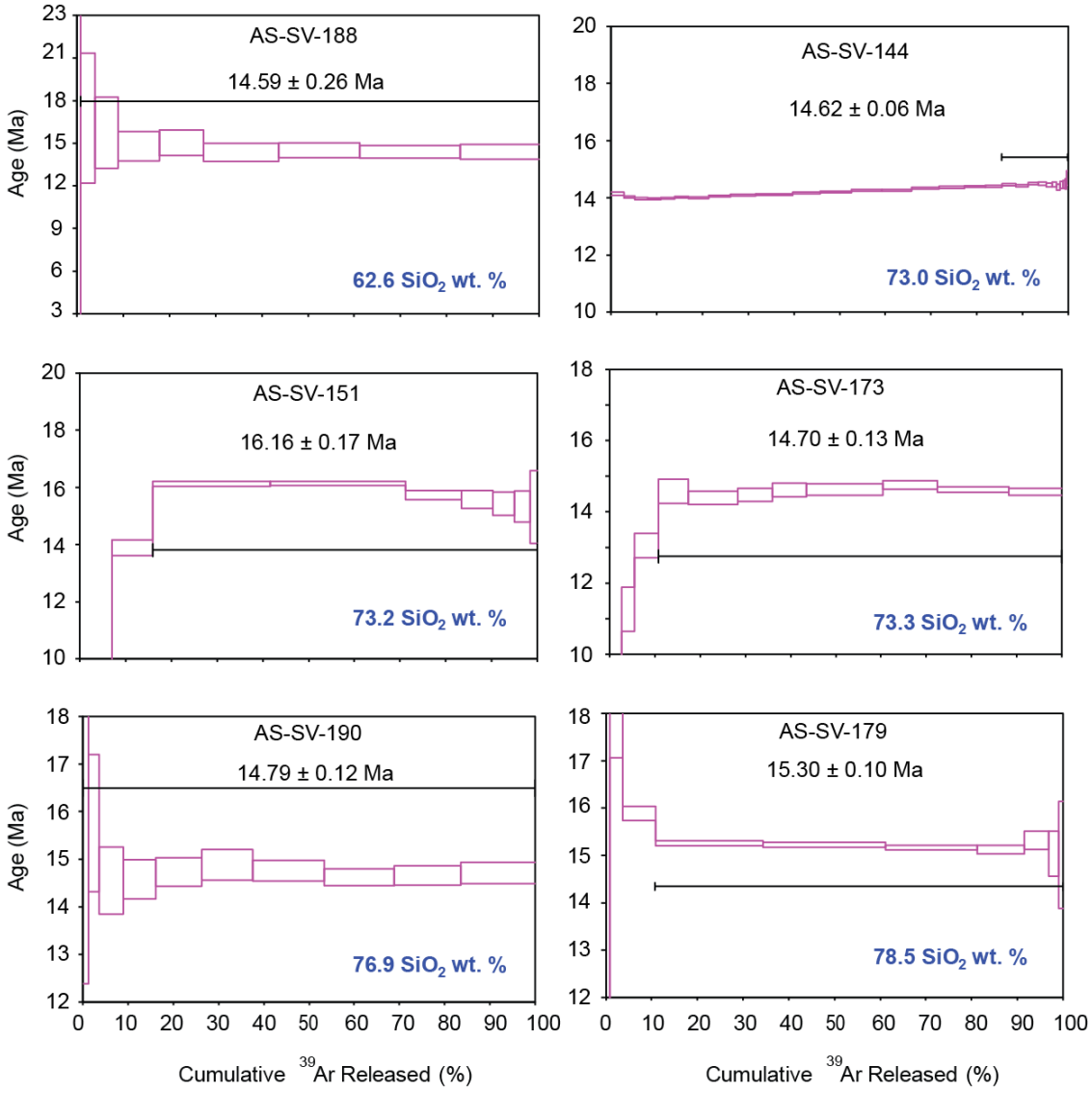

Figure 2.6b: $^{40}Ar/^{39}Ar$ plateau ages of samples of the Strawberry Volcanics (continued).

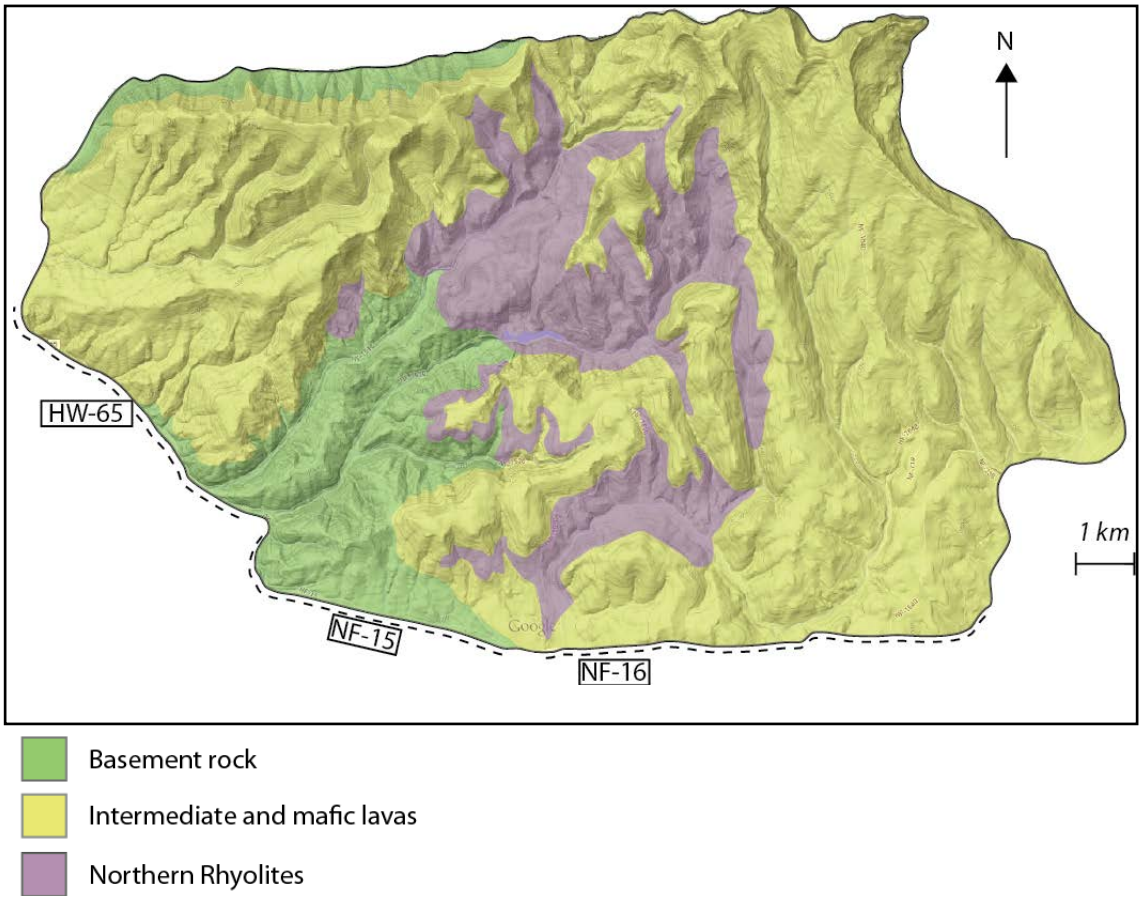

Figure 2.7: Geologic map of the northern rhyolites section and surrounding units.

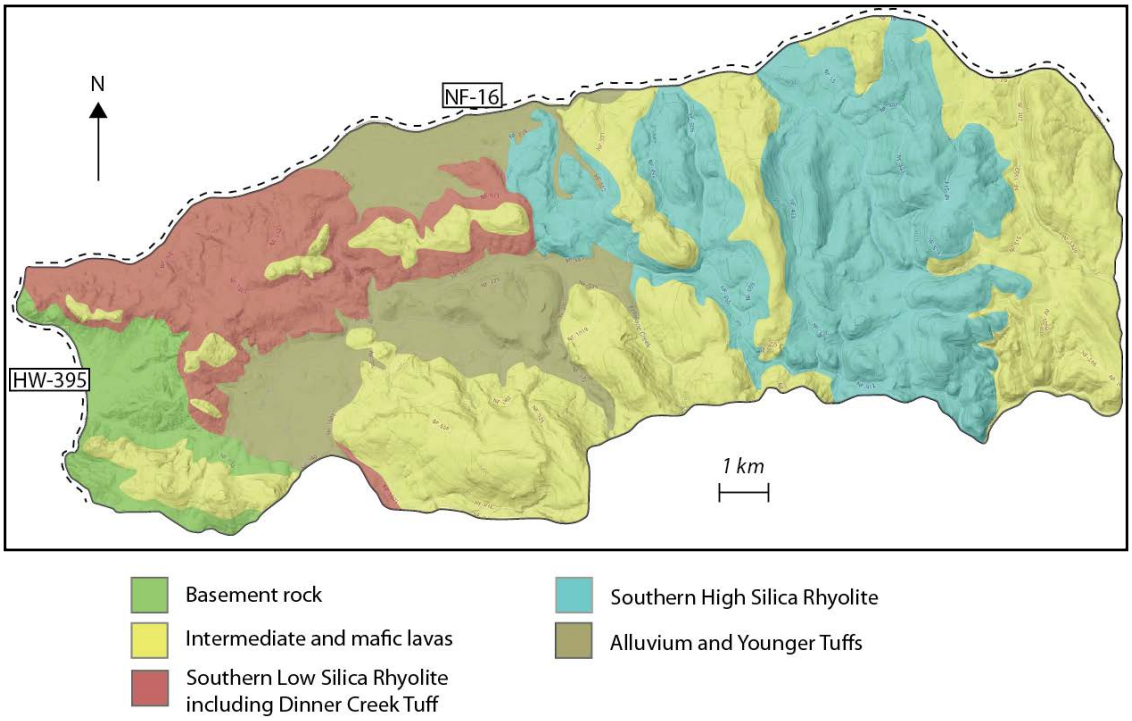

Figure 2.8: Geologic map of the north section of the southern rhyolites section and surrounding units.

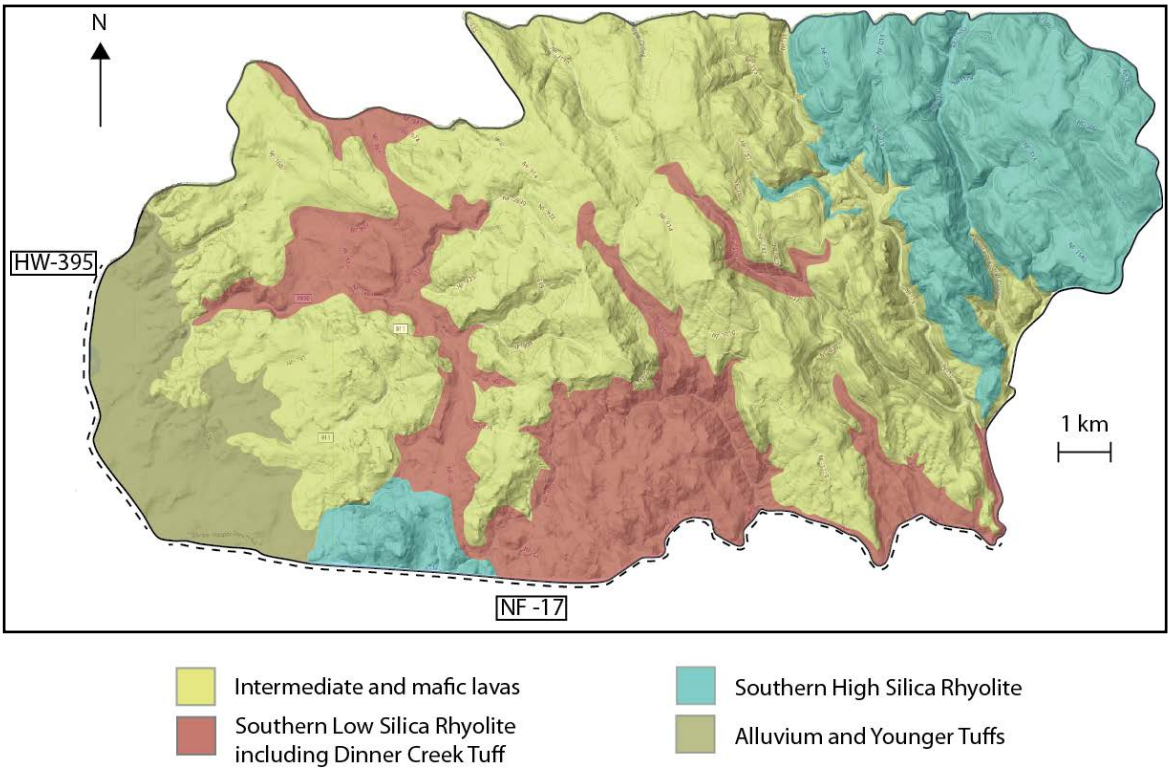

Figure 2.9: Geologic map of the south section of the southern rhyolites section and surrounding units.

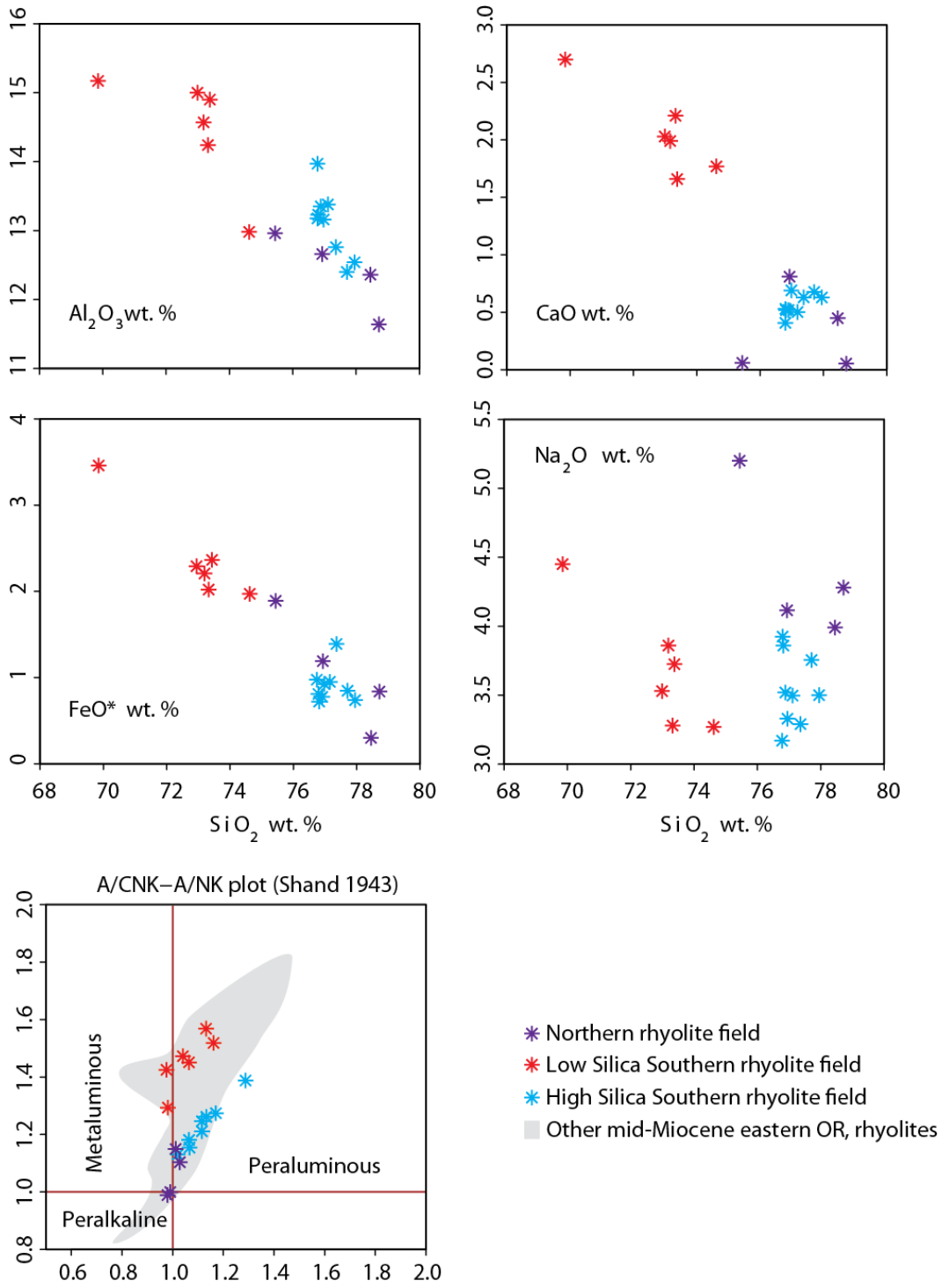

Figure 2.10: Major element Harker diagrams of rhyolites of the Strawberry Volcanics.

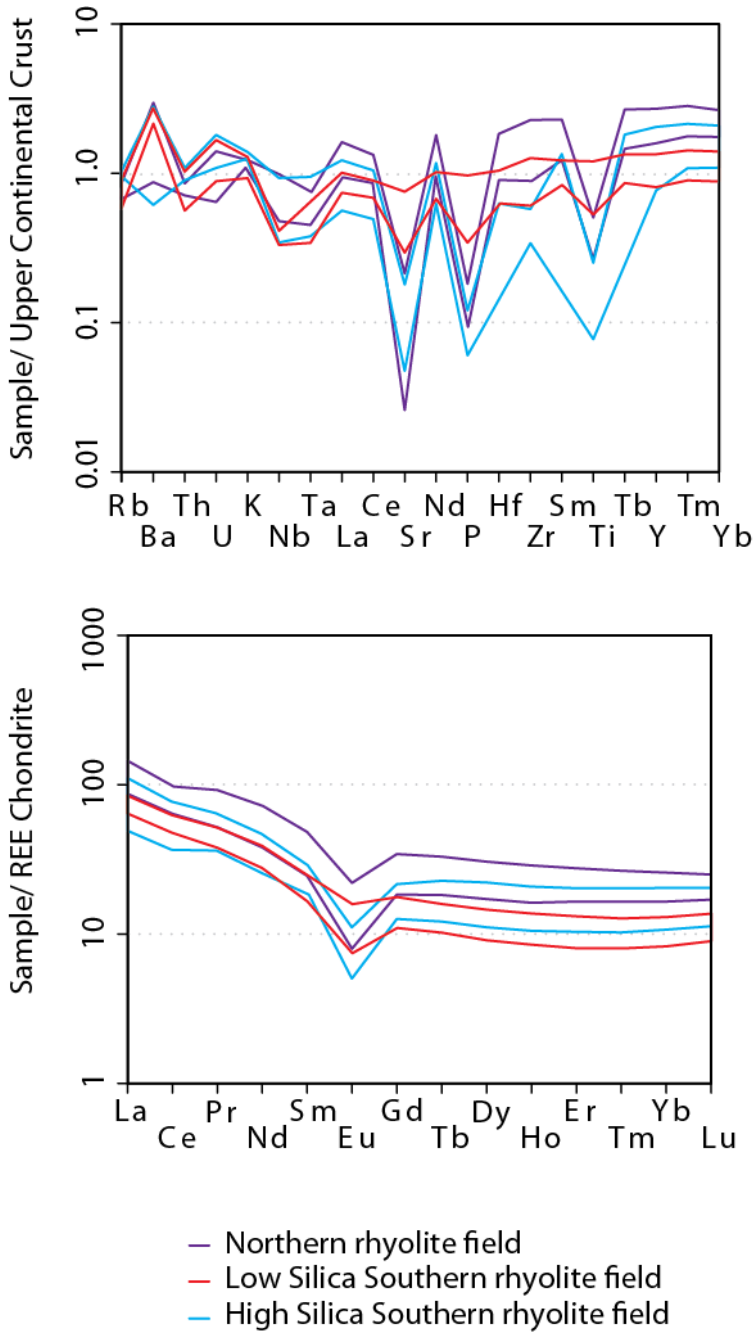

Figure 2.11: Normalized upper continental crust and normalized chondrite multi-variable diagrams of rhyolite units of the Strawberry Volcanics. Samples used in this diagram are the upper and lower concentration limits for each group. Normalized values for upper continental crust are from Taylor and McLennan (1995) and REE chondrite is from Boynton (1984).

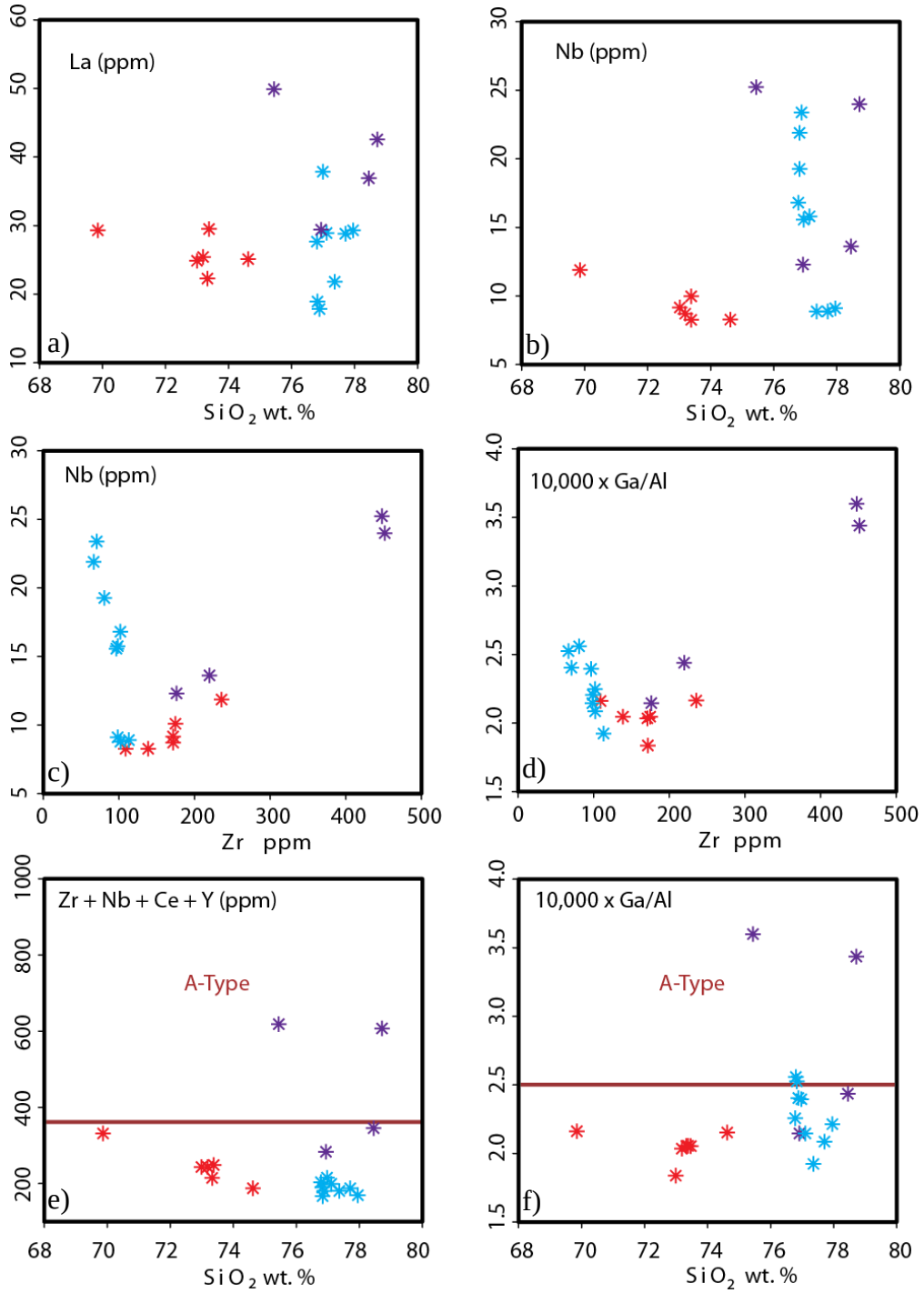

Figure 2.12: Selected trace elements including A-Type rhyolite discrimination diagram vs SiO_2 wt % and Zr (ppm) for rhyolites. La and Nb vs SiO_2 wt % (a and b), Nb, 10,000 x Ga/Al vs Zr (ppm) (c and d) and Zr+Nb+Ce+Y and 10,000 x Ga/Al vs SiO_2 wt % (e and f). Solid line represents the dividing line for A-Type rhyolites from Whalen et al., 1987.

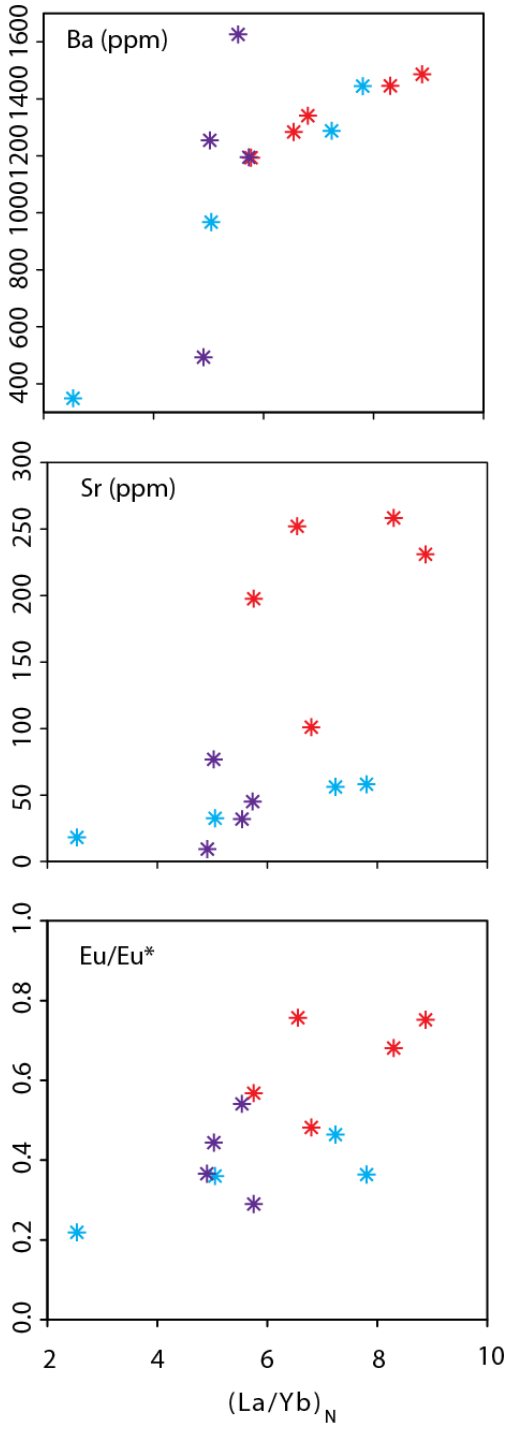

Figure 2.13: Ba, Sr, and Eu/Eu* vs $(La/Yb)_N$ plots for rhyolites. Slope of REE $(La/Yb)_N$ of rhyolites showing weak positive correlation with Ba (ppm), Sr (ppm), and Eu/Eu*.

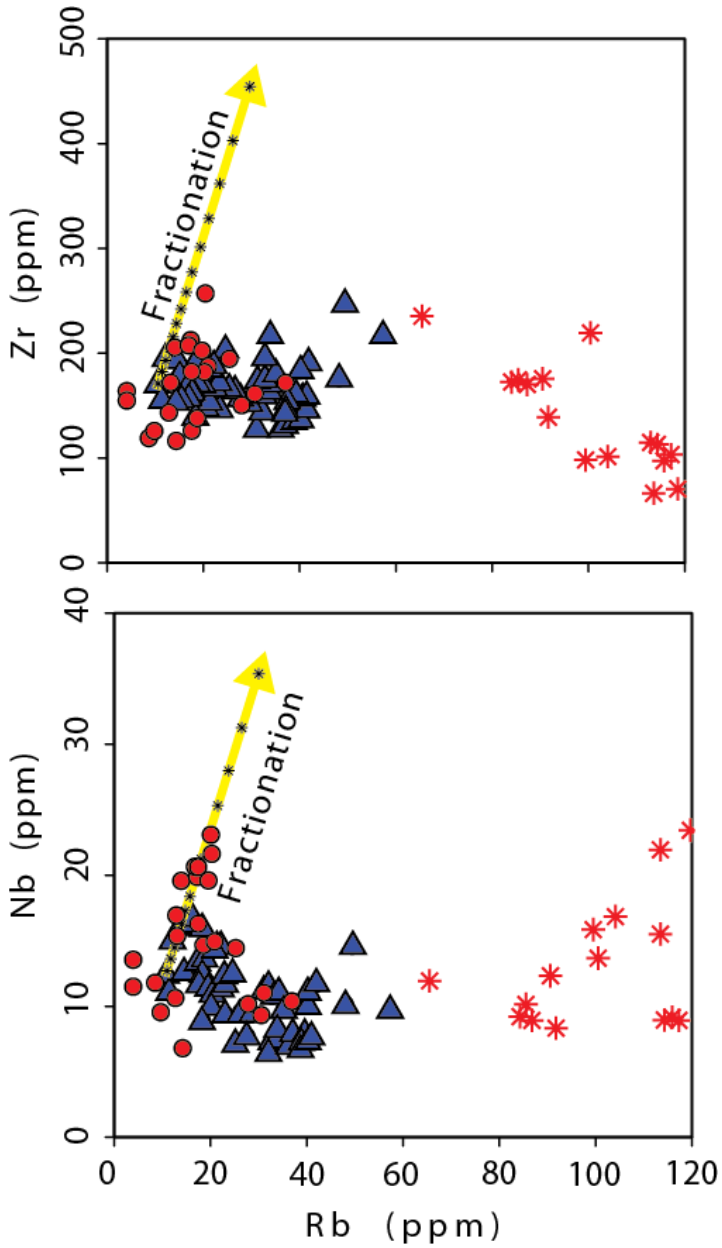

Figure 2.14: Selected trace element Harker diagrams with model fractional crystallization trend. Model diagrams show the path of fractionation crystallization from a mafic lava to 65% crystallization with 5% increments. These diagrams show the trend among incompatible elements towards increased silica of the Strawberry Volcanics and rules out fractional crystallization as the main process of generating the silicic lavas. These rhyolites are likely products of partial melting of the basement lithology during input of mafic magmas from the mantle. Fractionation models are based on partition coefficients for Rb of 0.071, 0.031, 0.02, for Zr of 0.048, 0.10, 0.18 and for Nb of 0.01, 0.15 and 0.005 for plagioclase, clinopyroxene and othropyroxene, respectively. The modal proportions used are based on observed mineral assemblages and are as follows; 68% plagioclase, 17% clinopyroxene and 15% orthopyroxene.

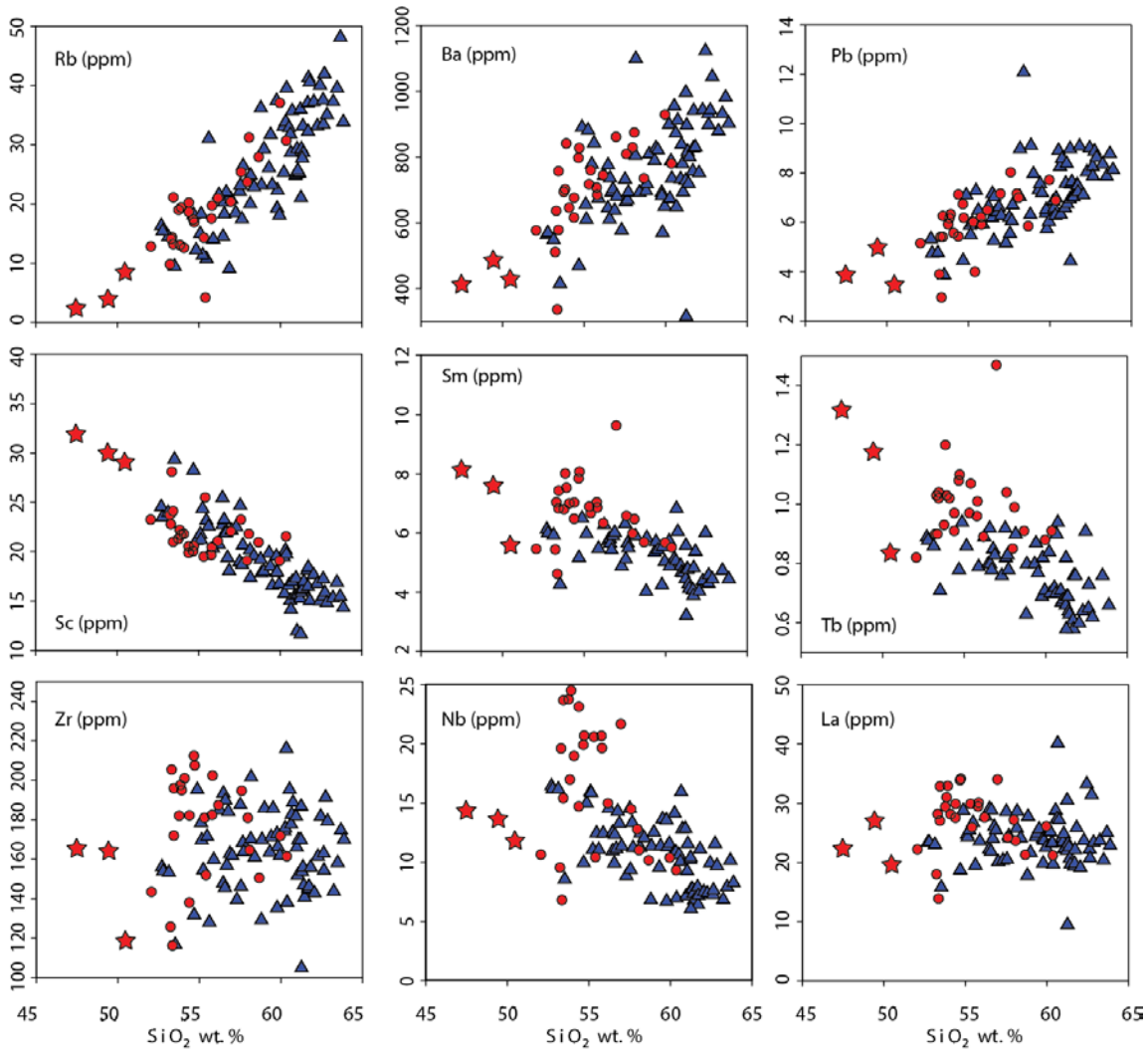

Figure 2.15: Selected trace and Rare earth element diagrams for basalt to intermediate lavas vs SiO_2 wt%. Enrichment trends occur with Rb, Ba, and Pb and depletion trends in Sc, Sm, and Tb with increased SiO_2. Elements which little to no enrichment or flat trends with silica enrichment include Zr, Nb, and La. This pattern cannot be explained by fractional crystallization and is likely produced through mixing of magmas and/or AFC processes.

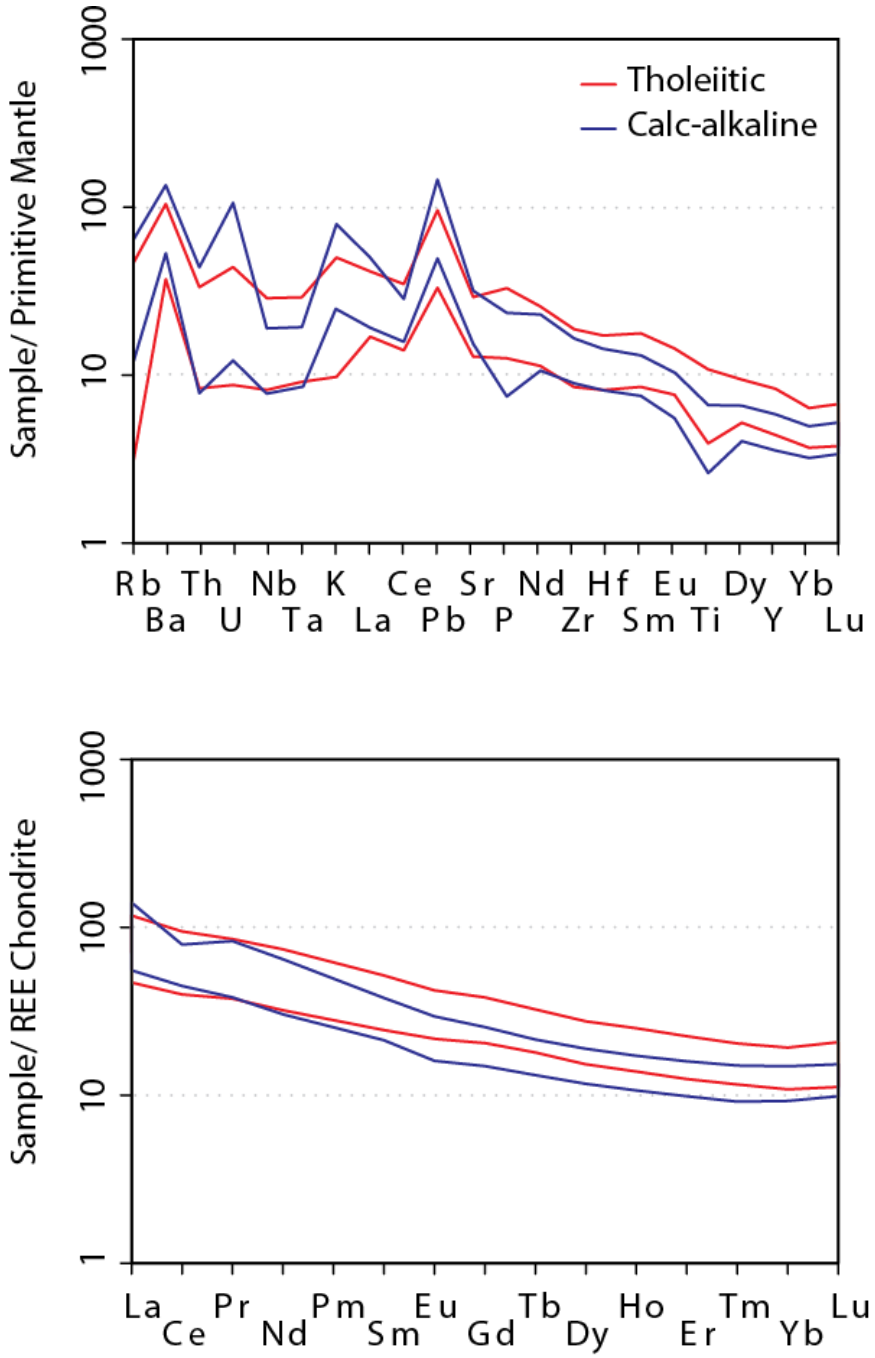

Figure 2.16: Normalized trace element and REE multi-variable diagrams using the maximum and minimum values for the calc-alkaline and tholeiitic suite of lavas analyzed. Normalized values are from Sun and McDonough, 1989 and Boynton, 1984.

Figure 2.17: Field photographs of mafic dikes. The dash lines are indication of where the dike is located or outline the dike as it crosscuts other lavas.

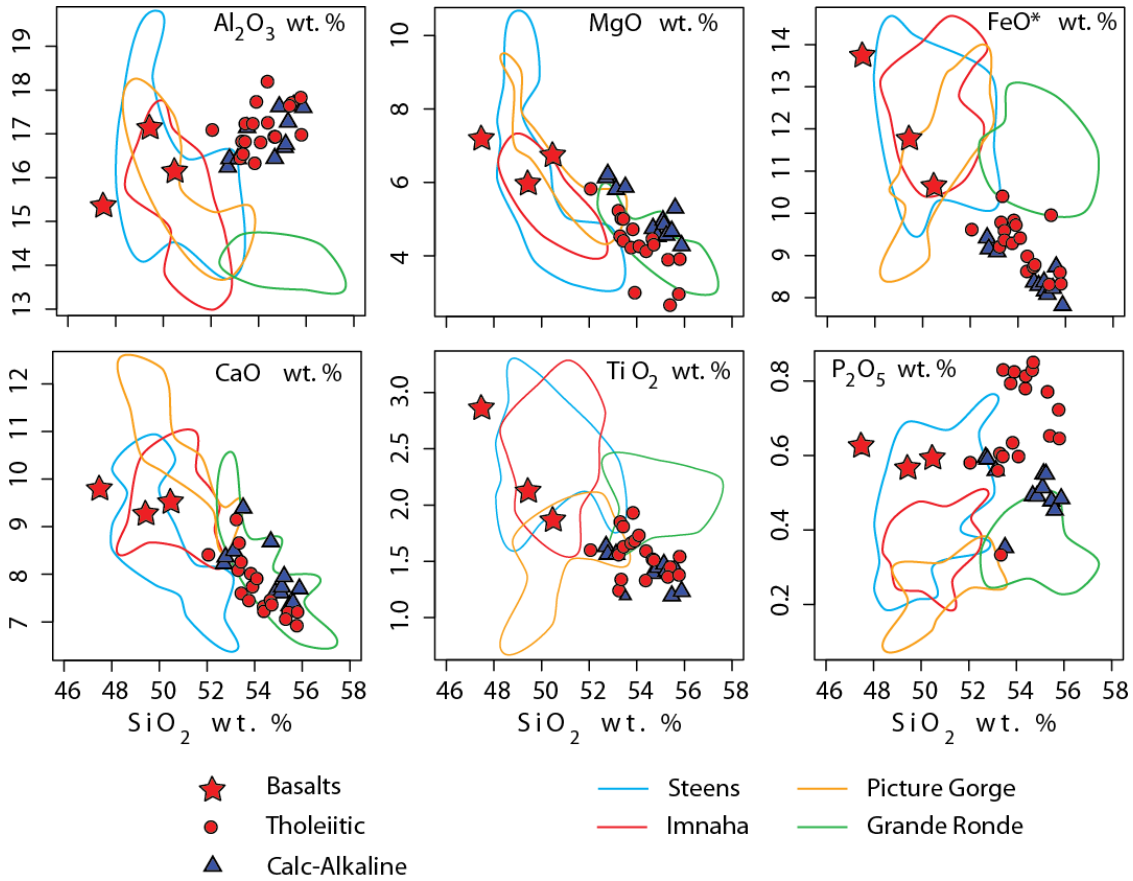

Figure 2.18: Major element geochemistry of selected lavas of ≤ 56 SiO_2 wt. % of the Strawberry Volcanics and the CRBG for comparison. The Strawberry Volcanics appear to overlap mostly with the Steens lavas and some with Picture Gorge lavas. Geochemical data of the CRBGs is from Wolff et. al. (2008).

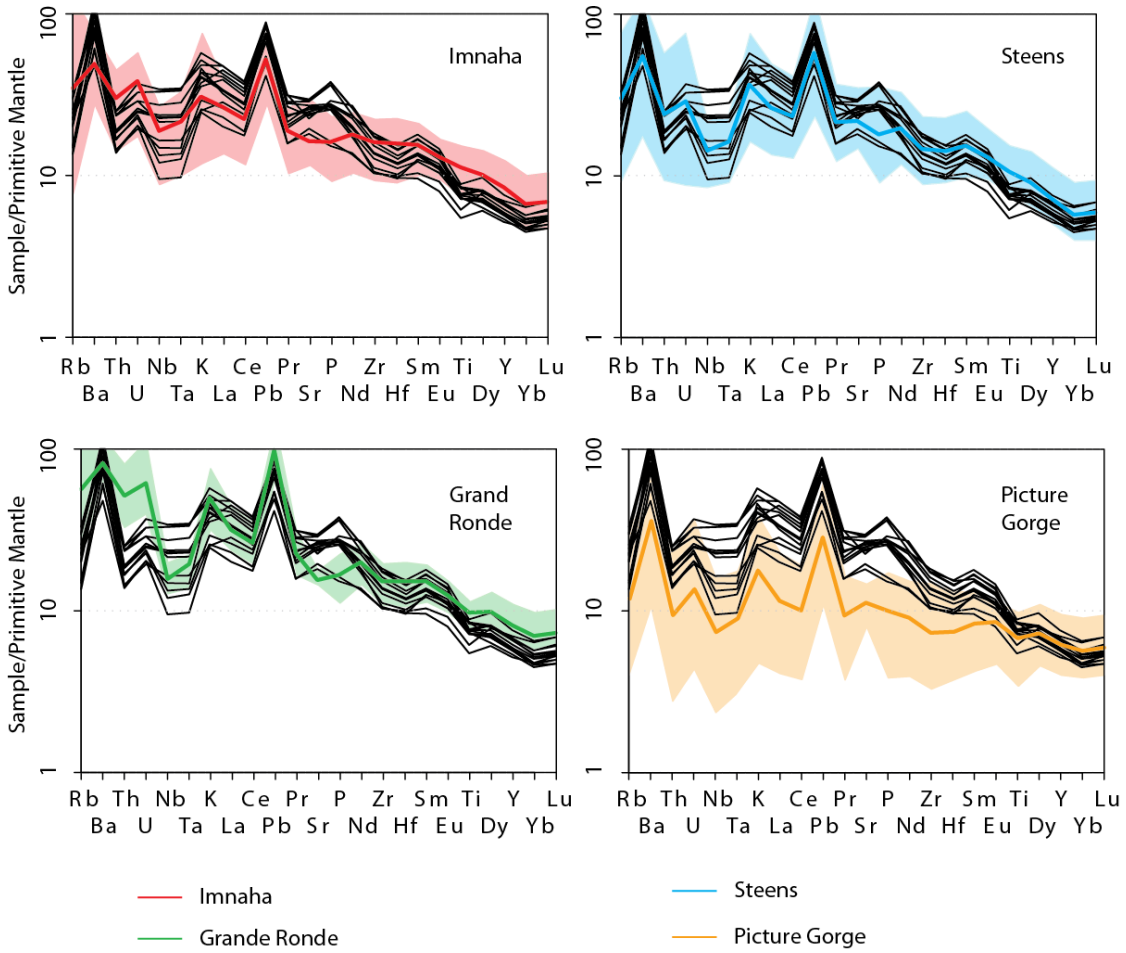

Figure 2.19a: A comparison of normalized to primitive mantle trace and REE multi-variable diagrams of the mafic Strawberry Volcanic tholeiites and calc-alkaline lavas (≤ 54 SiO_2 wt. %) (black lines) and lavas of the CRBG.

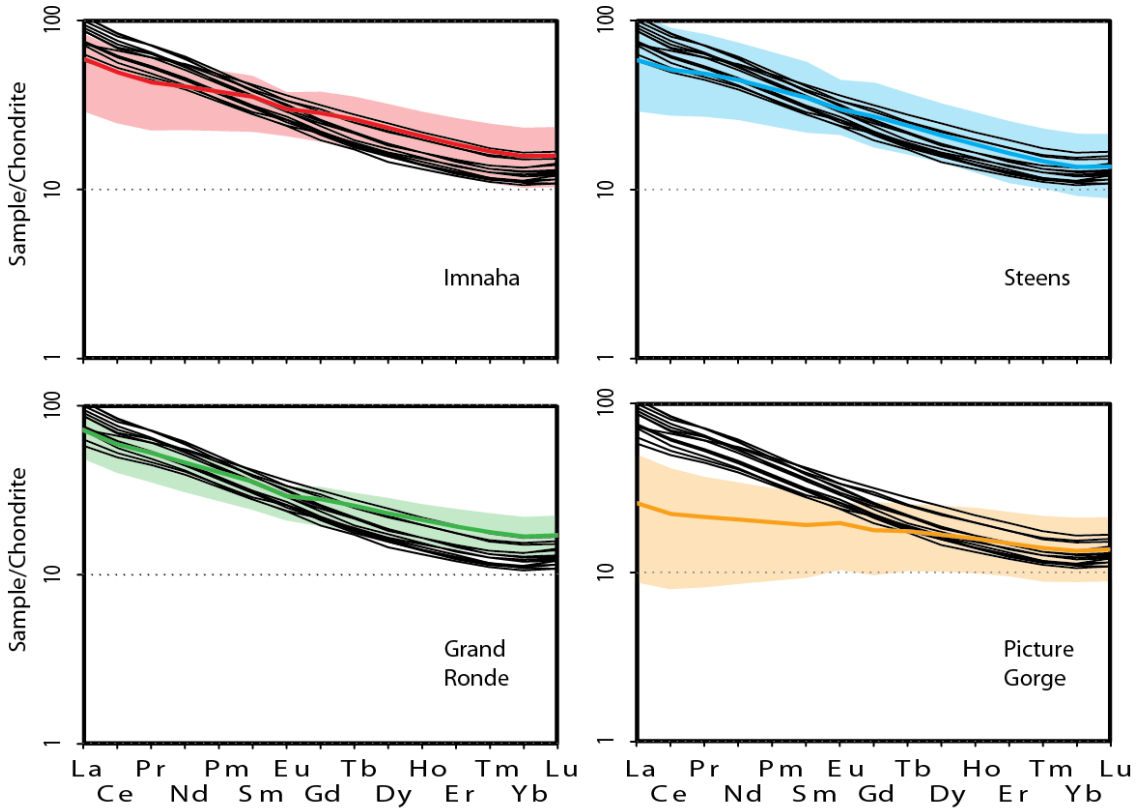

Figure 2.19b: A comparison of normalized to chondrite trace and REE multi-variable diagrams of the mafic Strawberry Volcanic tholeiites and calc-alkaline lavas (≤ 54 SiO_2 wt. %) (black lines) and lavas of the CRBG. The transparent color indicates the groups range and the solid colored line is the groups average. The Strawberry Volcanics mostly overlap with the Steens lava (light blue) and Imnaha (red). Normalized values are from Sun and McDonough, (1989) and Boynton, (1984).

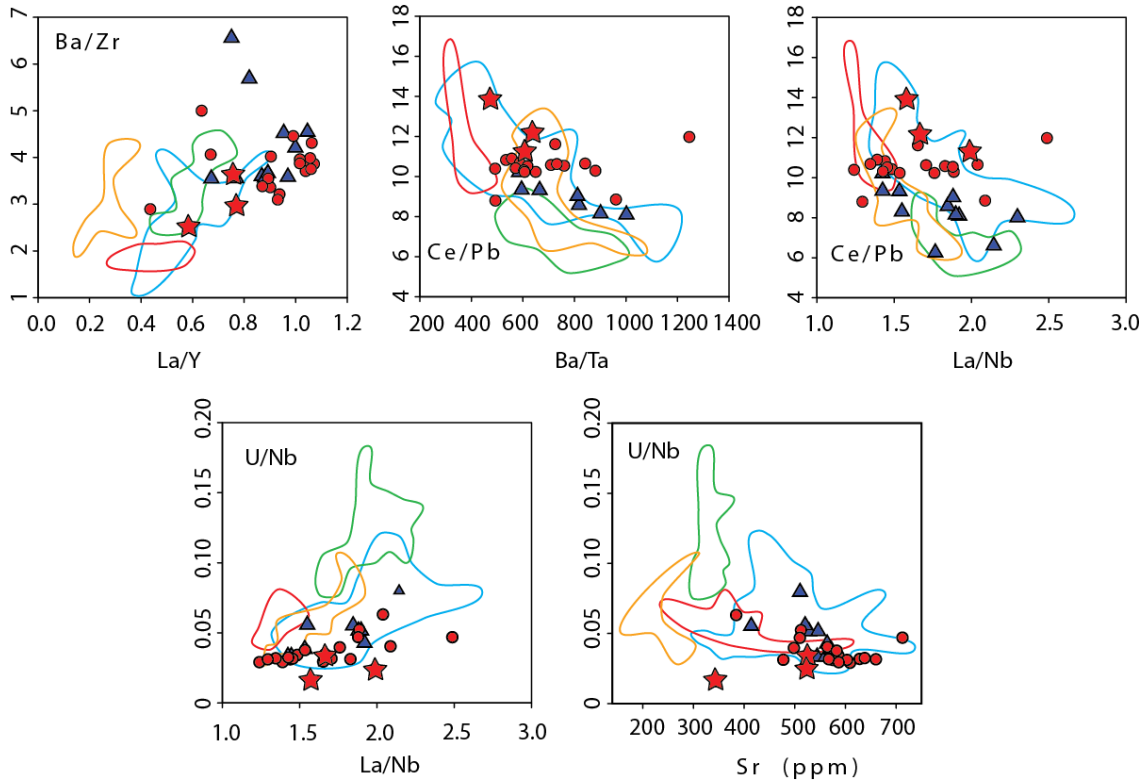

Figure 2.20: A comparison of selected trace element ratios of the Strawberry Volcanic lavas (≤ 54 SiO_2 wt. %) and lavas of the CRBG. Significant overlap is apparent with the Strawberry Volcanics and Steens lavas (light blue). Legend is the same as in 2.18.

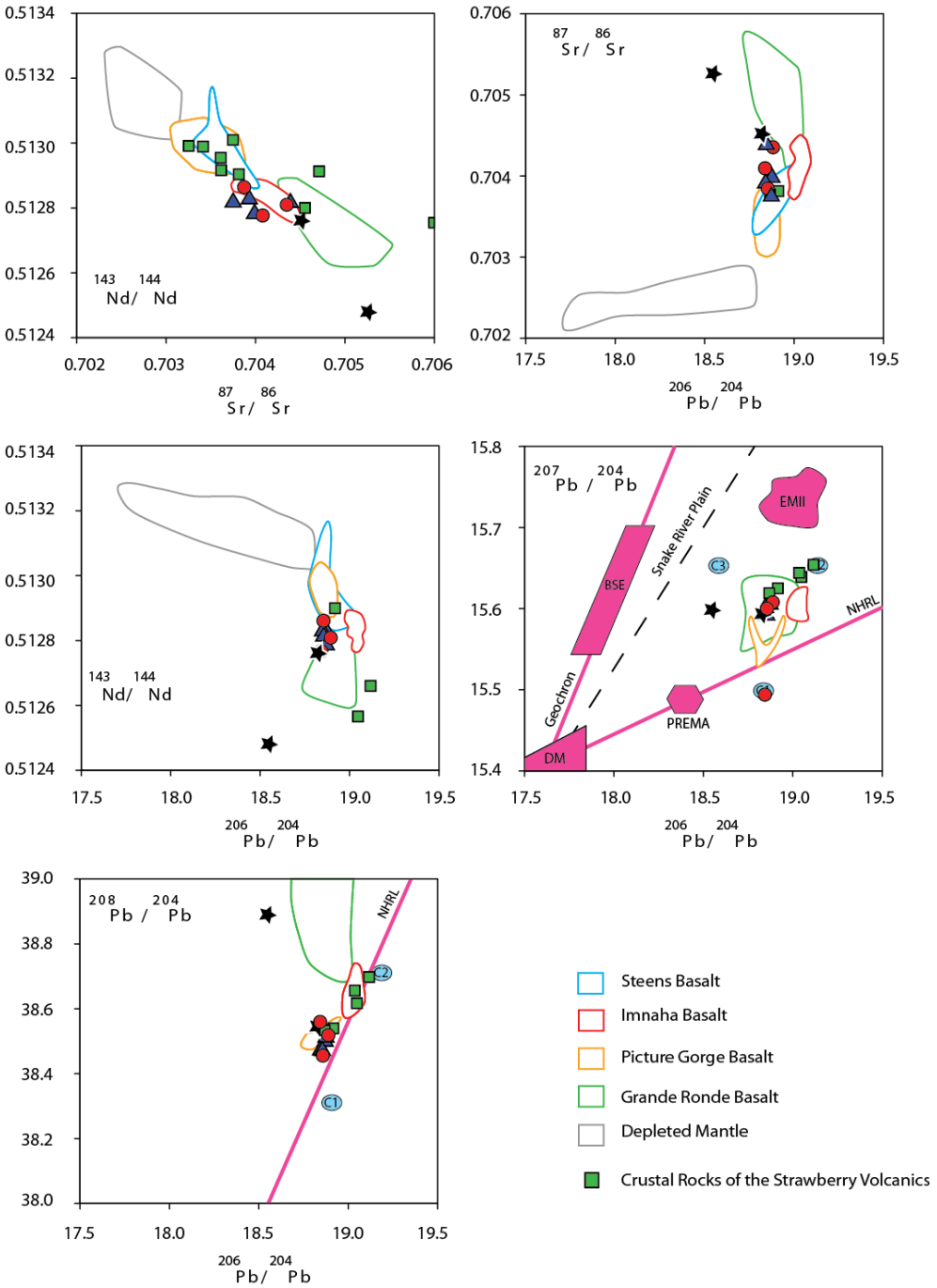

Figure 2.21: Radiogenic isotopes of the Strawberry Volcanics and fields for the CRBG (Wolff et. al., 2008). The isotopes of the Strawberry Volcanics overlap with lavas of the CRBGs specifically with lavas of Steens and Imnaha. C1, C2, and C3 are end-member composition of the plume hotspot of the CRBG from Carlson (1984). ^{207} Pb/^{204}Pb vs ^{206}Pb/^{204}Pb figure molded after Wilson (1989). NHRL (Northern Hemisphere Reference Line) for reference, DM (depleted mantle), EMII (enriched mantle II), BSE (bulk silica Earth), PREMA (prevalent mantle). Fields are after Zindler and Hart (1986), Staudigel et al. (1984), Hamelin et al. (1986) and Wilson (1989).

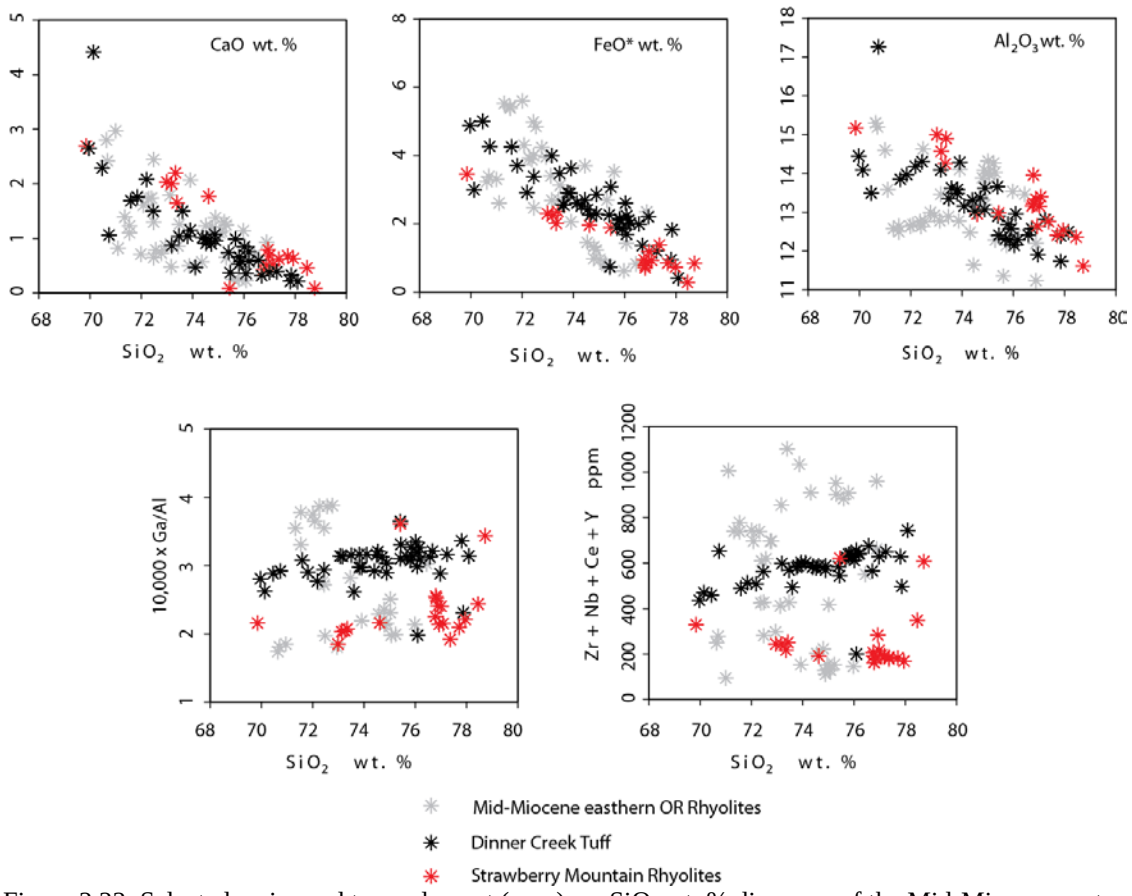

Figure 2.22: Selected major and trace element (ppm) vs. SiO_2 wt. % diagrams of the Mid-Miocene eastern OR, rhyolitic volcanic centers (gray) including Dinner Creek Tuff (blue) and the Strawberry Volcanic rhyolites (red).

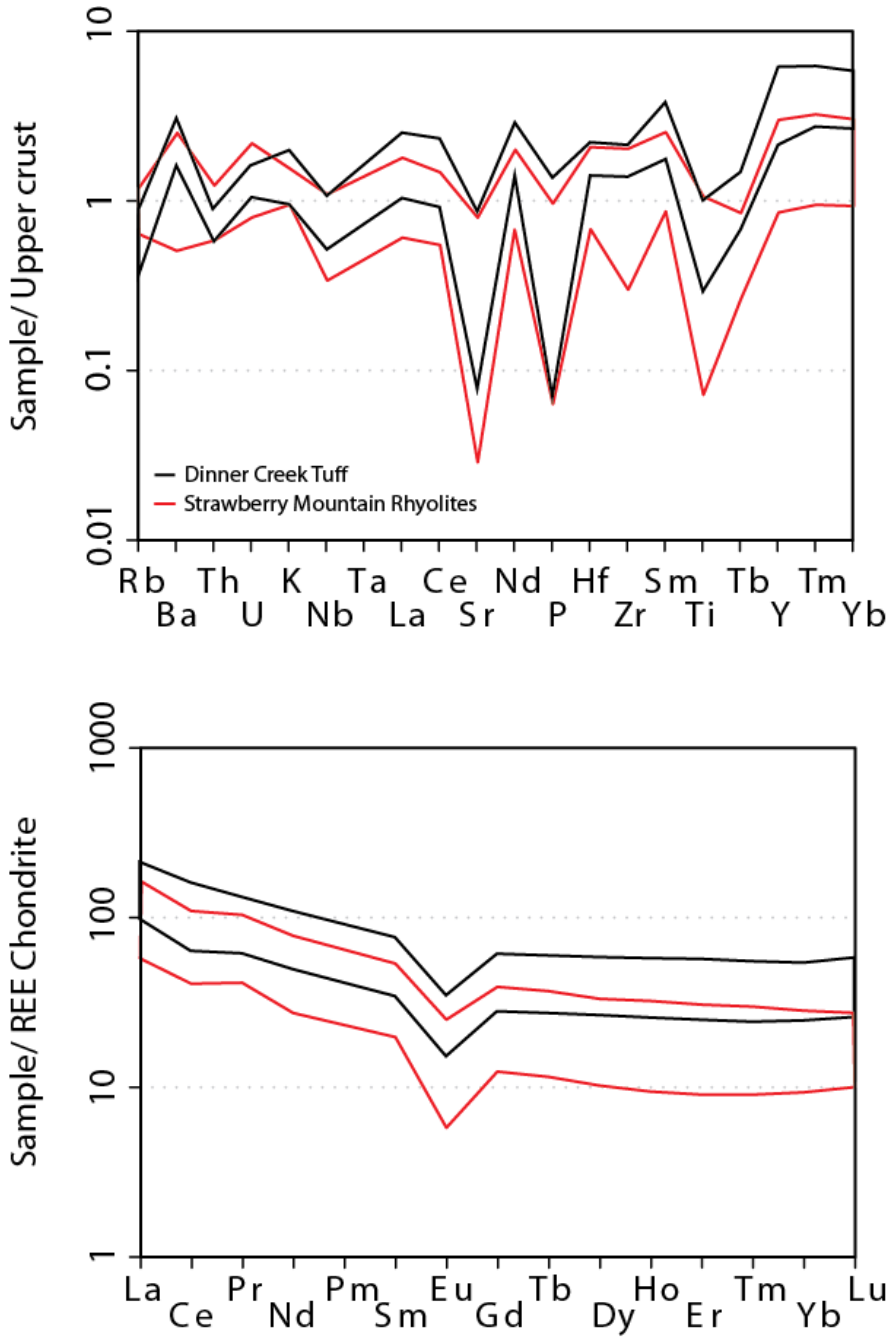

Figure 2.23: Normalized multi-variable diagrams of the Strawberry Mountain rhyolites and Dinner Creek Tuff for comparison.

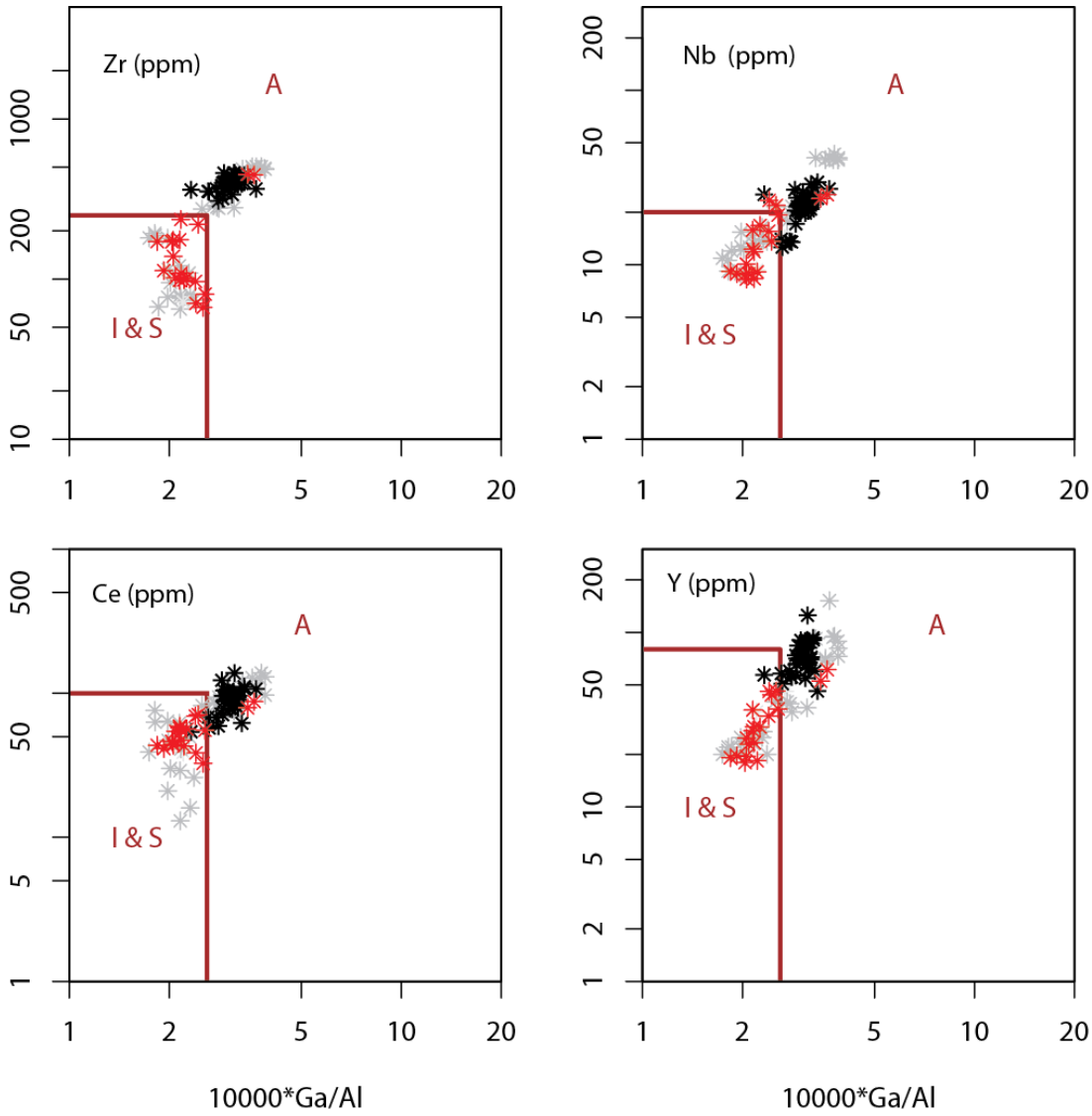

Figure 2.24: I-S-A-type rhyolite discrimination diagram (Whalen et al., 1987) for the strawberry volcanic rhyolites and Dinner Creek Tuff. Dinner Creek Tuff is predominately considered an A- Type rhyolite while the rhyolites of the Strawberry Volcanics are mostly I/S-Type.

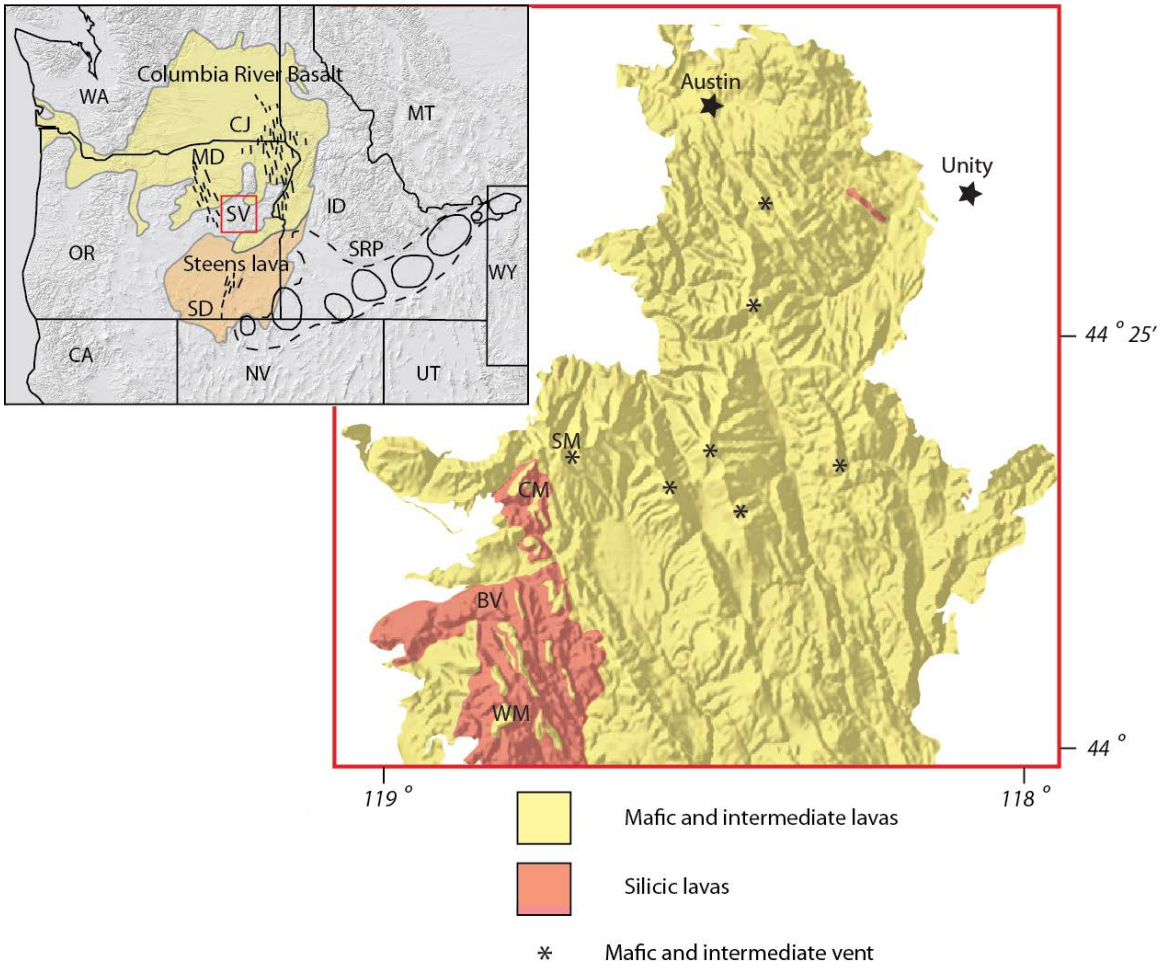

Figure 3.1: Location of the Strawberry Volcanics and regional lavas of the CRB and simplified geologic map. The larger inset shows the area defined as the Strawberry Volcanics including a general geologic map showing the location of mafic and intermediate lavas (yellow) and rhyolitic lavas (red). Field observations identified volcanic centers and are included on map. BV (Bear Valley), CA (California), CJ (Chief Joseph Dikes), CM (Canyon Meadows), ID (Idaho), MD (Monument Dikes), MT (Montana), NV (Nevada), OR (Oregon), SD (Steens Dikes), SM (Strawberry Mountain), SRP (Snake River Plains – Yellowstone Hotspot), SV (Strawberry Volcanics), UT (Utah), WA (Washington), WM (Wolf Mountain), WY (Wyoming)

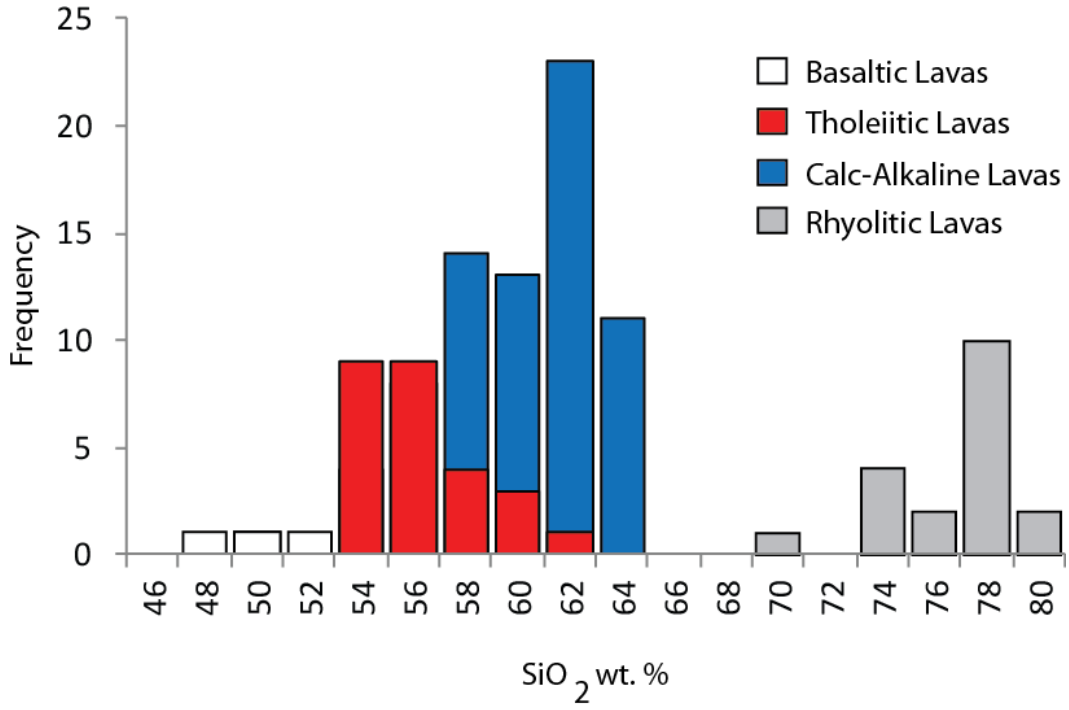

Figure 3.2: The frequency of various lavas and SiO_2 wt. % analyzed by XRF of the Strawberry Volcanics. These data show that the majority of the Strawberry Volcanics are calc-alkaline andesite composition.

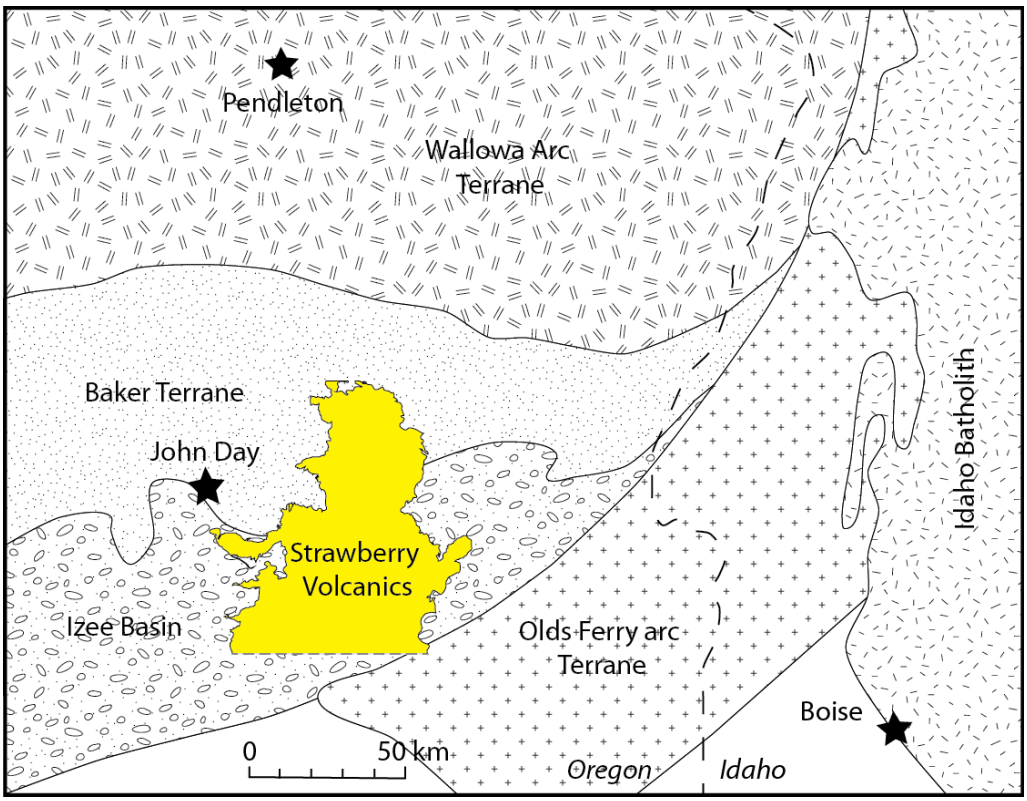

Figure 3.3: Location of the Strawberry Volcanics (yellow) and the terrane rocks of the surrounding area. Dashed line represent state boarder. Other dashed line under the area outlined as the Strawberry Volcanics is the 44° latitude and the furthest south of this research. Modified map from Schwartz et al, 2010.

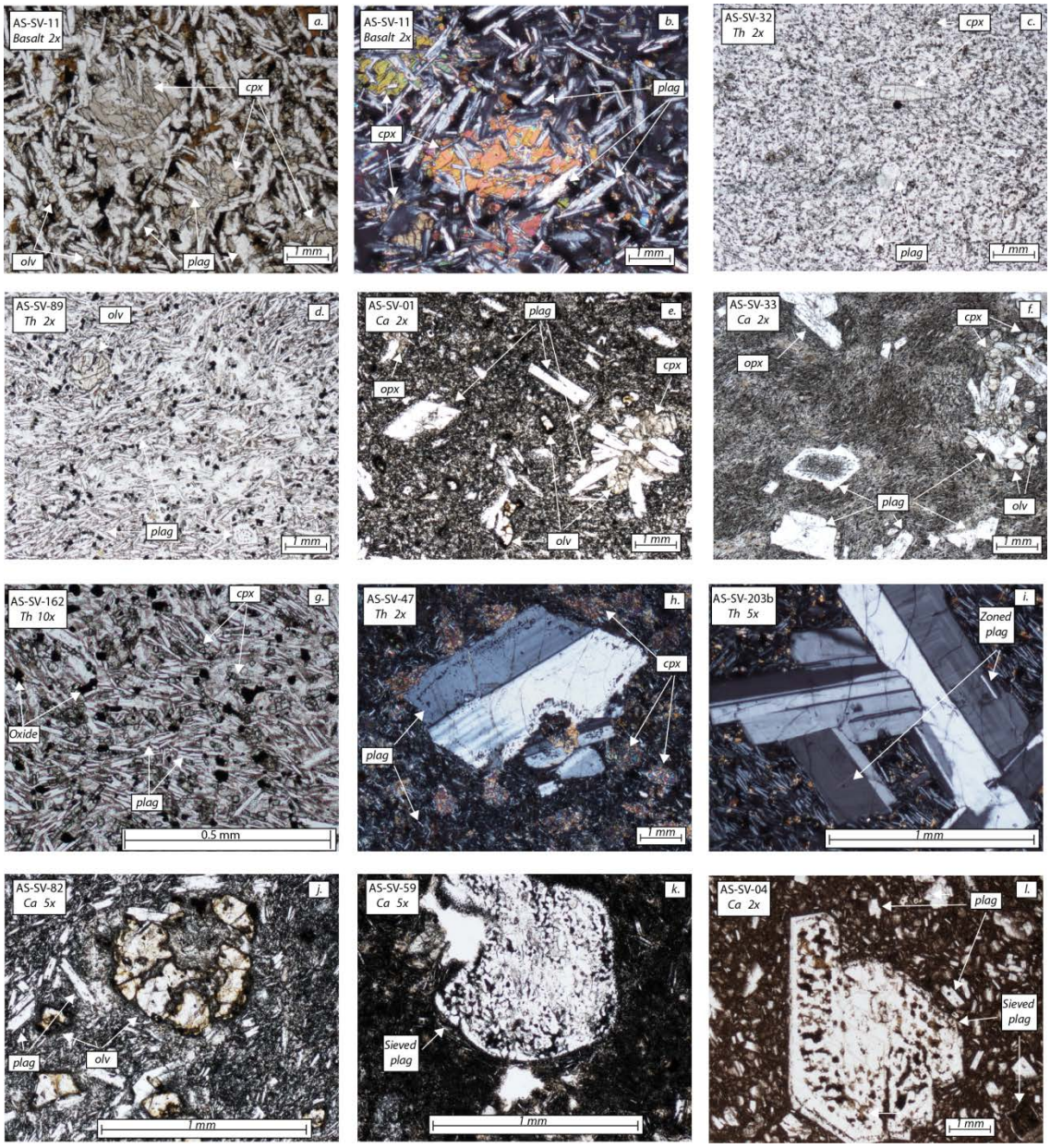

Figure 3.4: Photomicrographs of thin-sections from lavas of the Strawberry Volcanics including composition type. a) and b) basalt; c) and d) tholeiite and e) and f) calc-alkaline and photomicrographs of groundmass and phenocryst textures including: g – i) tholeiites and j-l) calc-alkaline type lavas. Basalts have and ophitic groundmass and lack phenocrysts (a and b) while tholeiites have a similar groundmass to the basalts but can contain phenocrysts of plagioclase + cpx + oxides ± olivine (g-i) and the calc-alkaline lavas are display both phenocryst poor lavas and phenocryst rich lavas (j-l). Phenocrysts can include plagioclase + cpx +opx + oxides ± olivine.

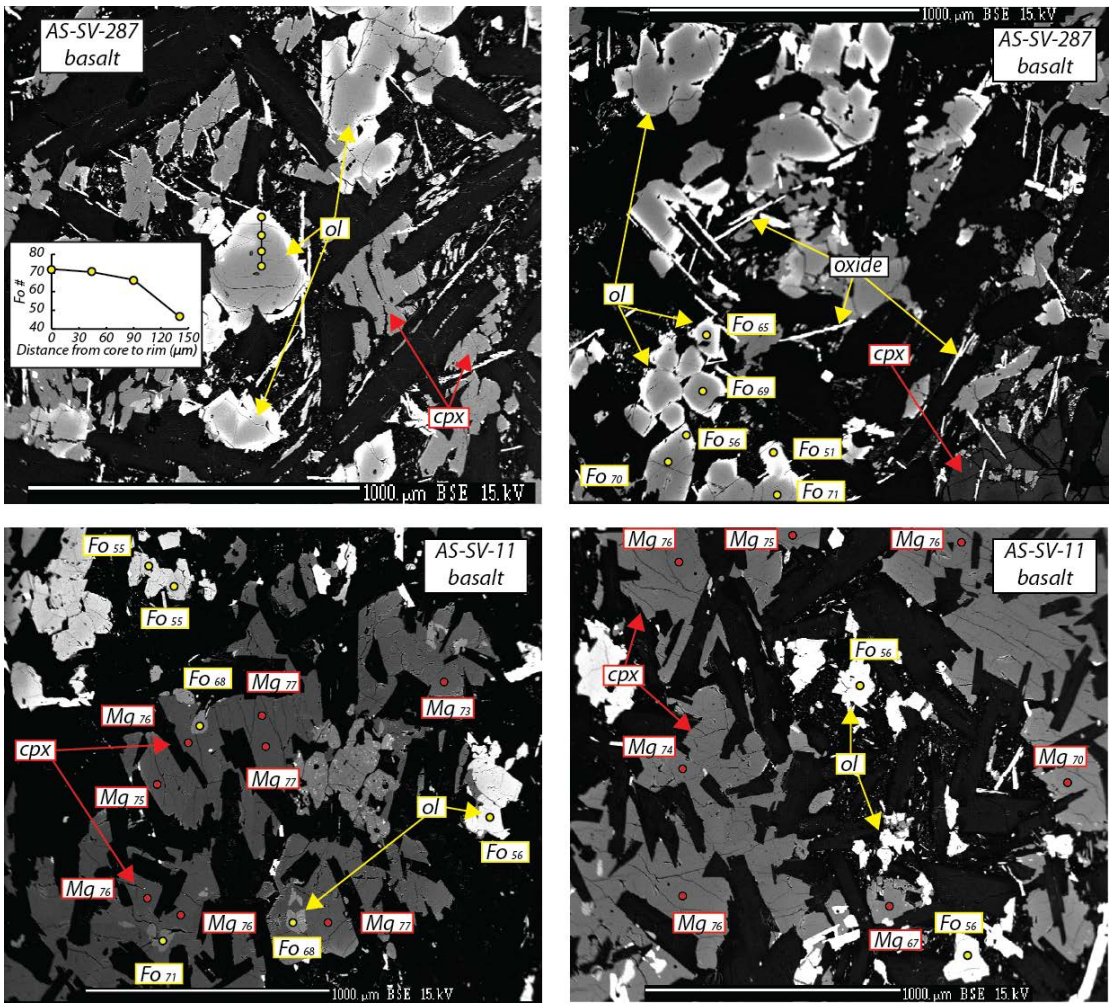

Figure 3.5: Backscatter image of basalt lavas analyzed with Fo and Mg numbers for olivines (yellow) and cpx (red) respectively analyzed by EMP.

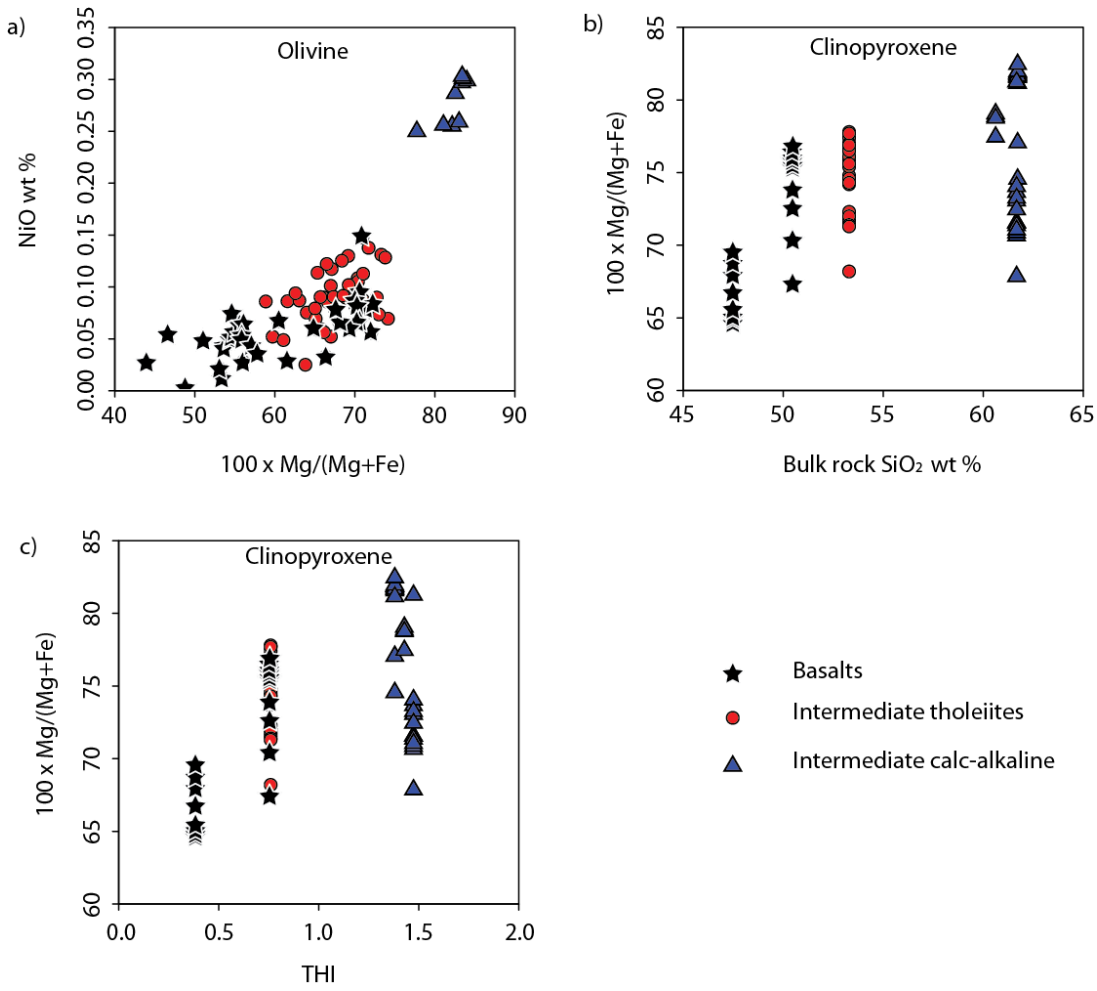

Figure 3.6:EMP mineral data of olivines, and clinopyroxene of various lava types from the Strawberry Volcanics.

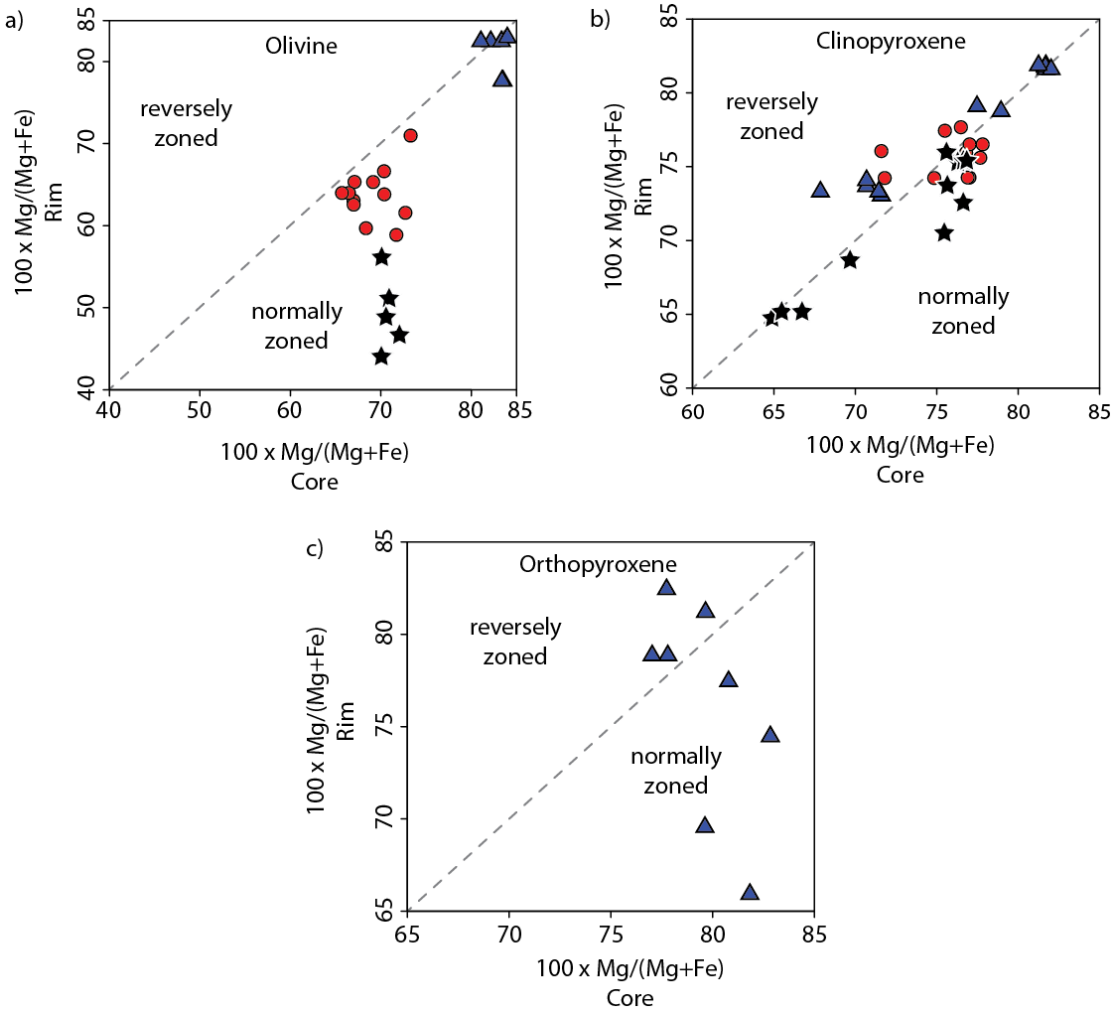

Figure 3.7: Core to rim analysis of EMP mineral data of olivine, clinopyroxene and orthopyroxene in various lava types from the Strawberry Volcanics. Symbols are same as in Figure 3.6.

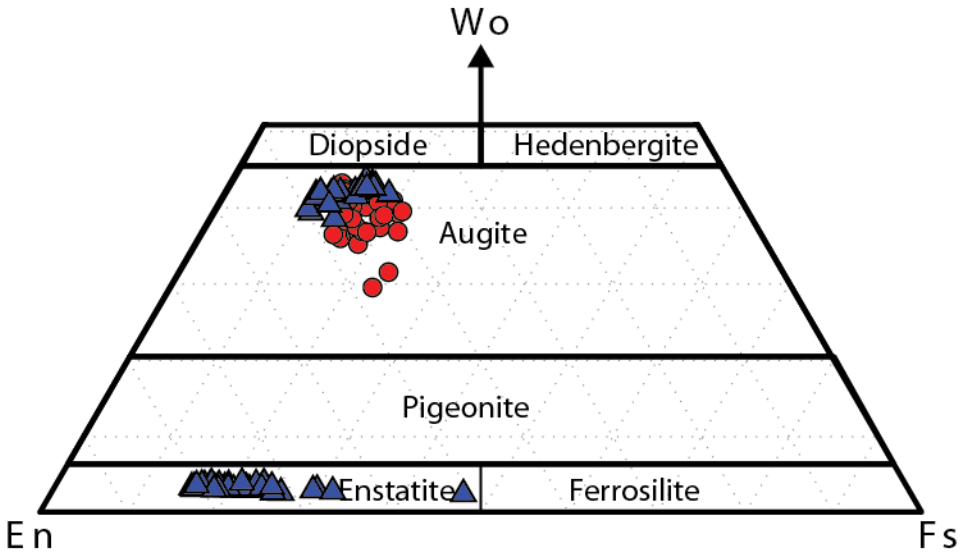

Figure 3.8: Pyroxene ternary diagram. Pyroxene composition of crystals in both tholeiitic (red circles) and calc-alkaline (blue triangles) lavas collected by EMP. Data shows that tholeiites contain a single cpx crystal phase while the calc-alkaline contain both cpx and opx. Symbols are same as in Figure 3.6.

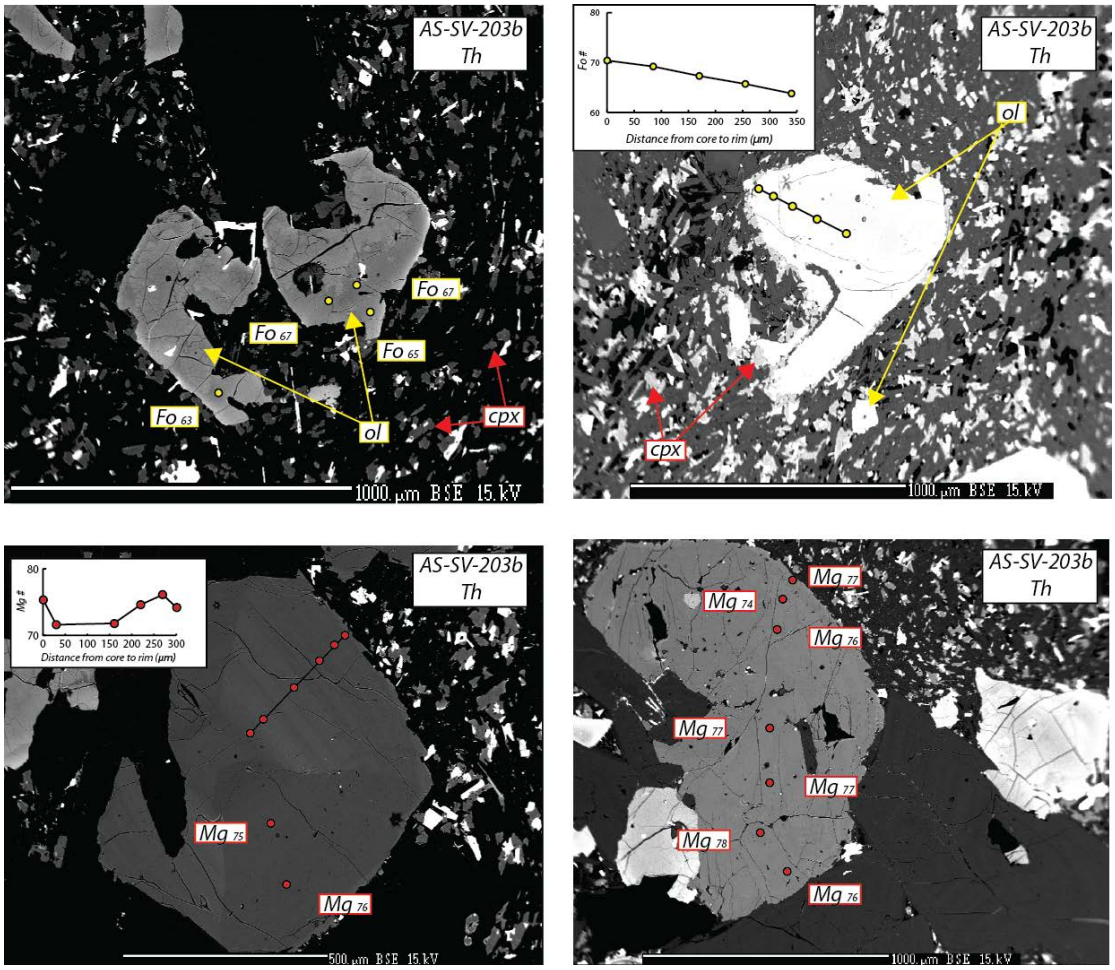

Figure 3.9: Backscatter image and EMP results of intermediate tholeiitic lavas. Olivines (yellow),cpx (red).

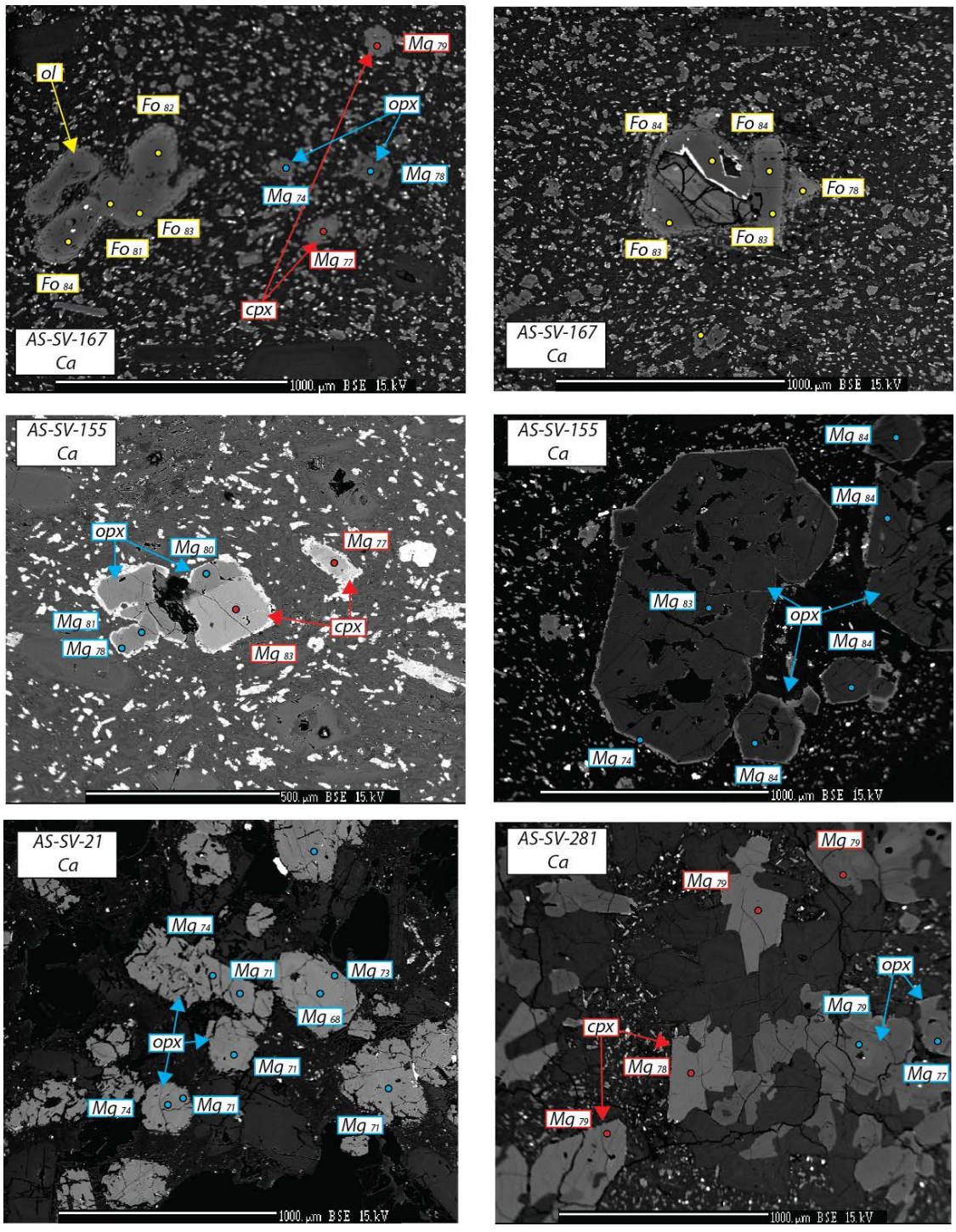

Figure 3.10: Backscatter image and EMP results of intermediate calc-alkaline lavas. Fo and Mg numbers for olivines (yellow), cpx (red) and opx (blue) respectively.

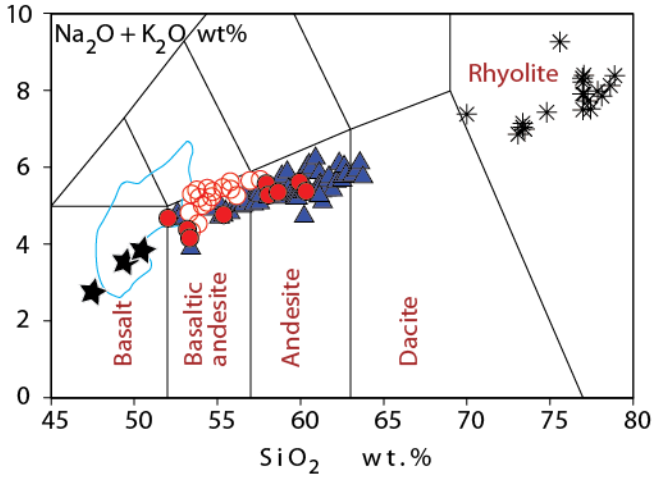

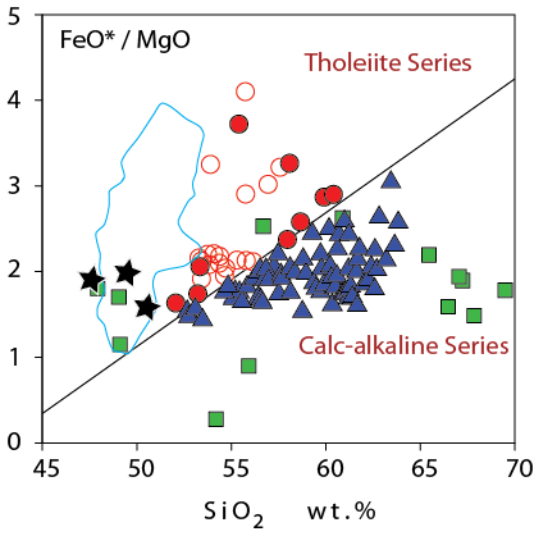

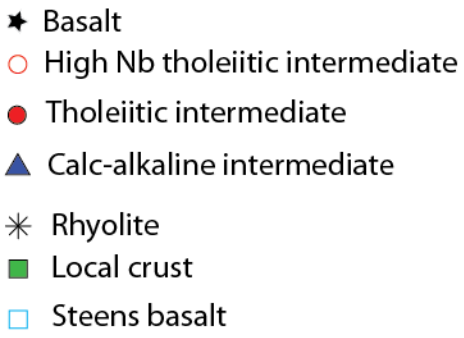

Figure 3.11: TSA and FeO*/MgO vs SiO_2 wt % diagram. Whole rock major element analysis of the Strawberry Volcanic lavas including Steens basalt (Wolff et al., 2008) and local crustal rocks (this study and Schwartz et al., 2010)

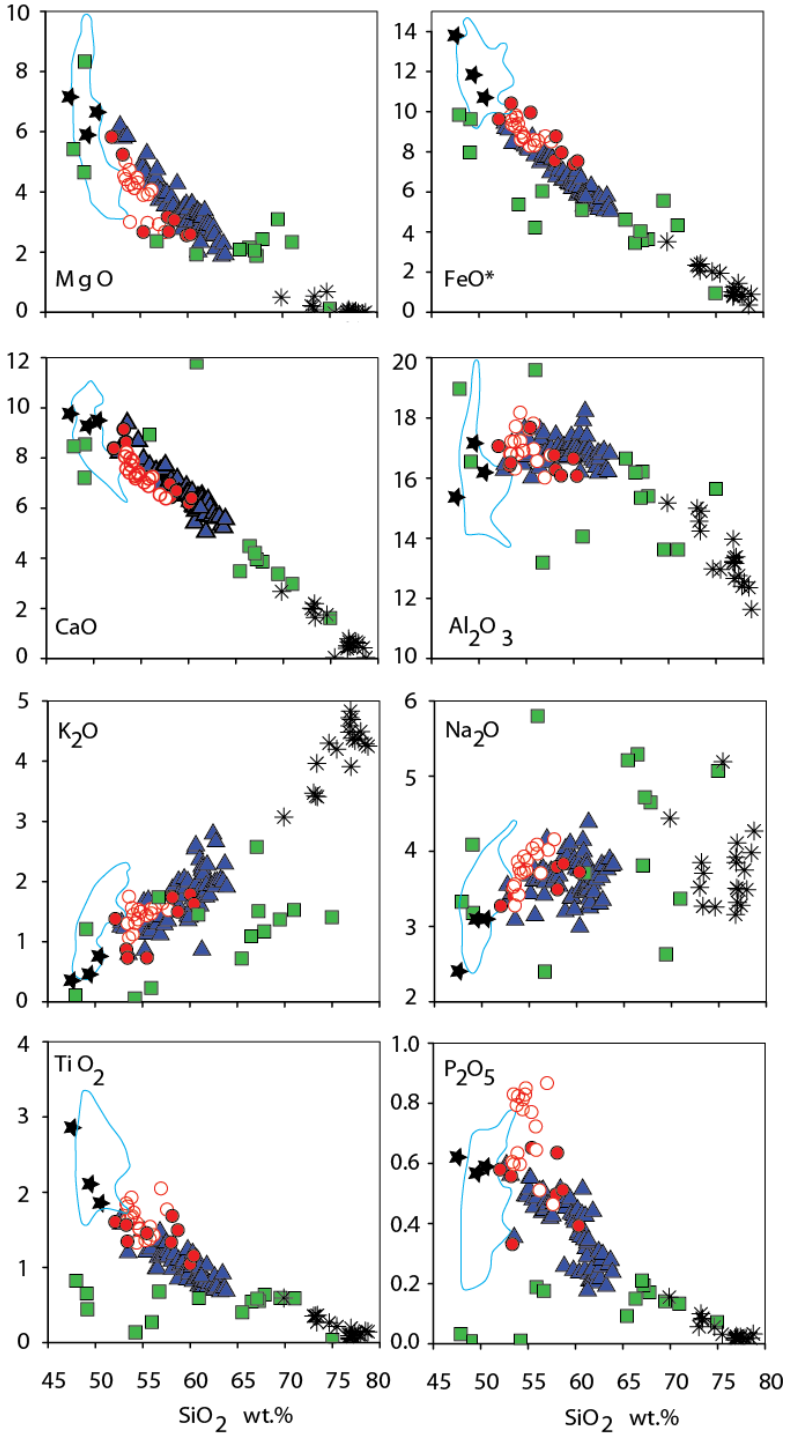

Figure 3.12: Whole rock major element chemistry. Diagram includes Strawberry Volcanic lavas, Steens and basement lithologies for reference.

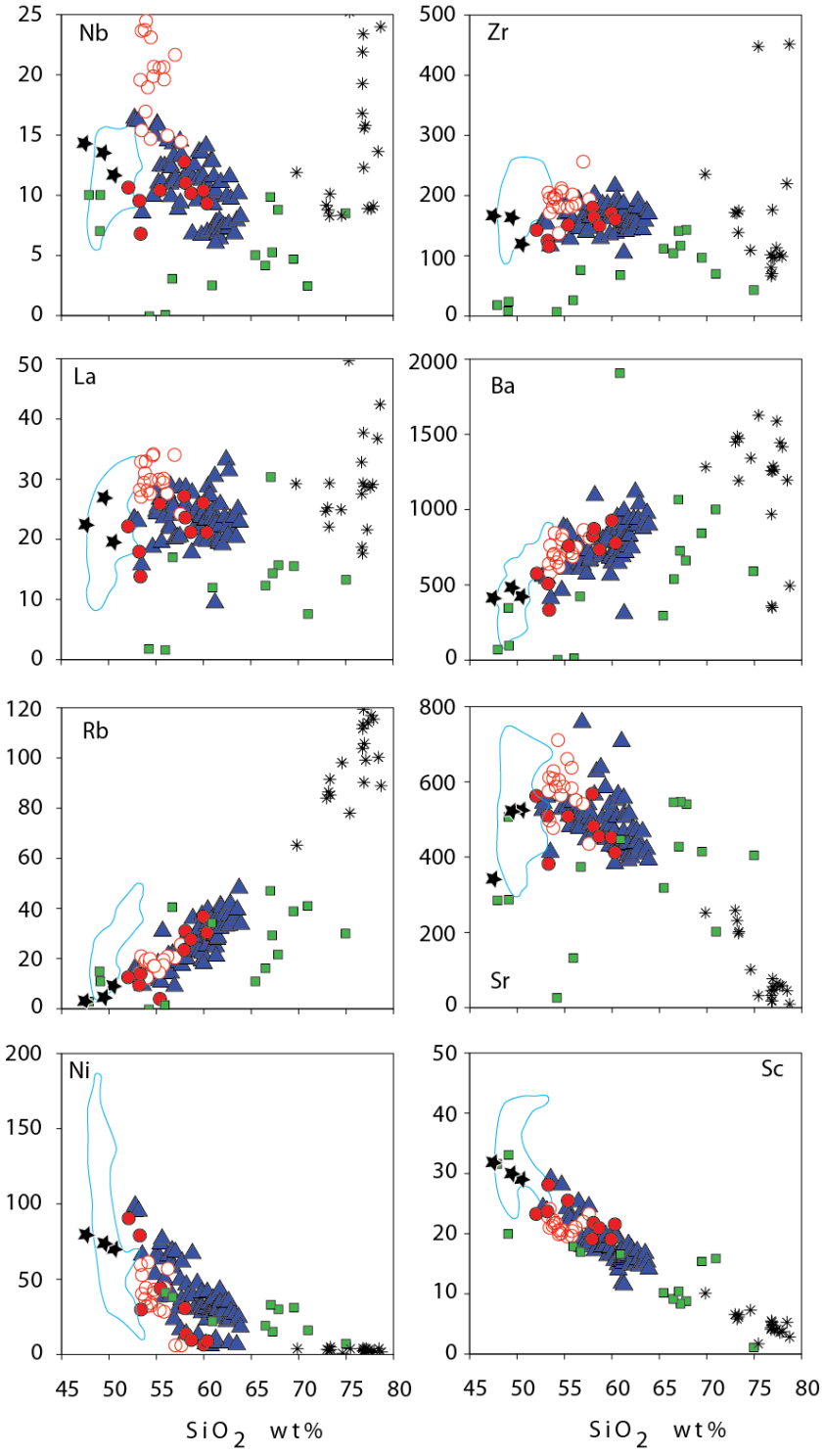

Figure 3.13: Whole rock trace element chemistry. Strawberry Volcanics, Steens and local basement rocks for comparison.

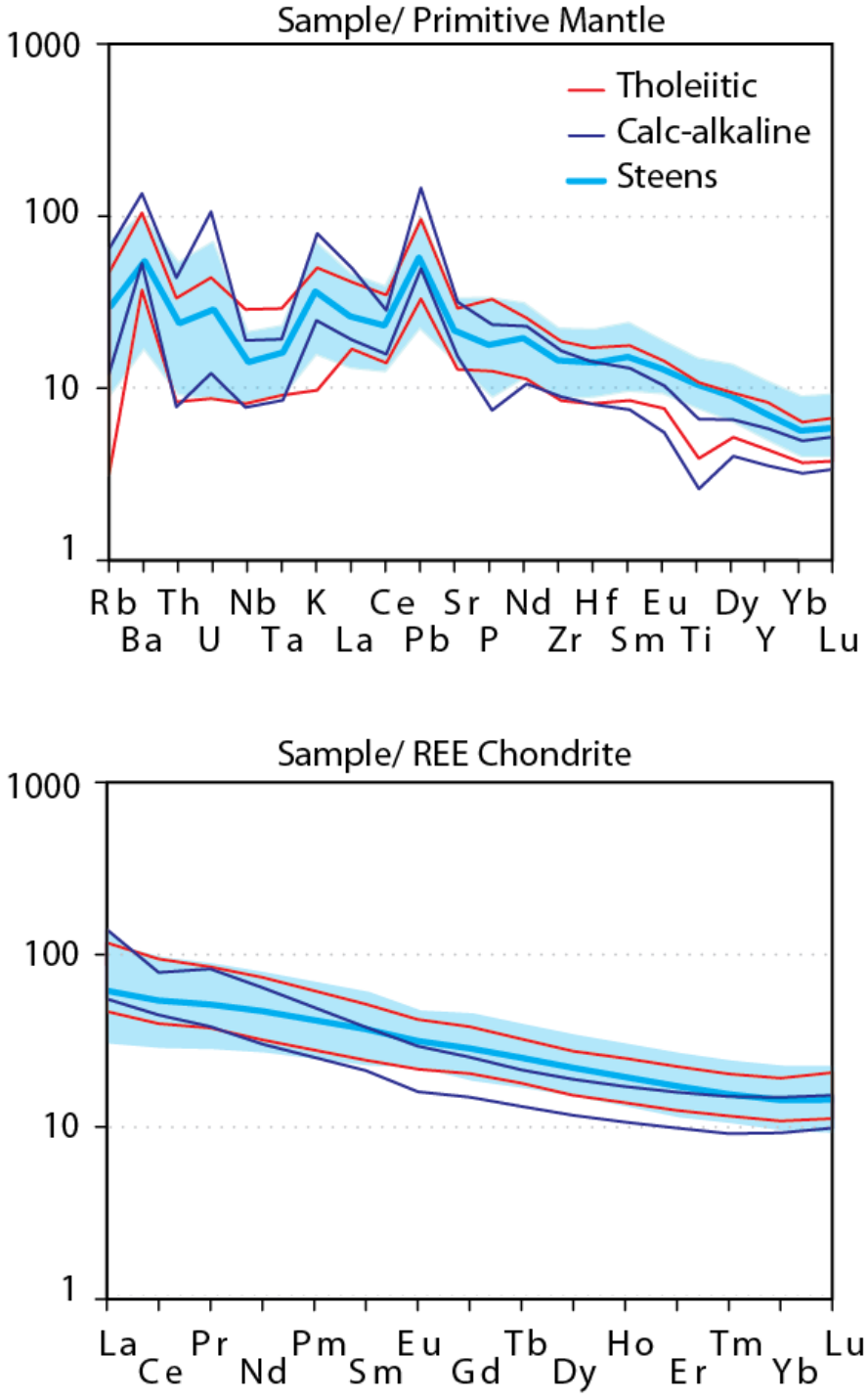

Figure 3.14: Primitive mantle (Sun McDonough, 1989) and chondrite (Boynton, 1984) normalized multivariable trace and REE diagrams of various lava groups of the Strawberry Volcanics and Steens lava (Wolff et al., 2008). Shaded area is the maximum and minimum concentrations for Steens lavas and solid line represents the average.

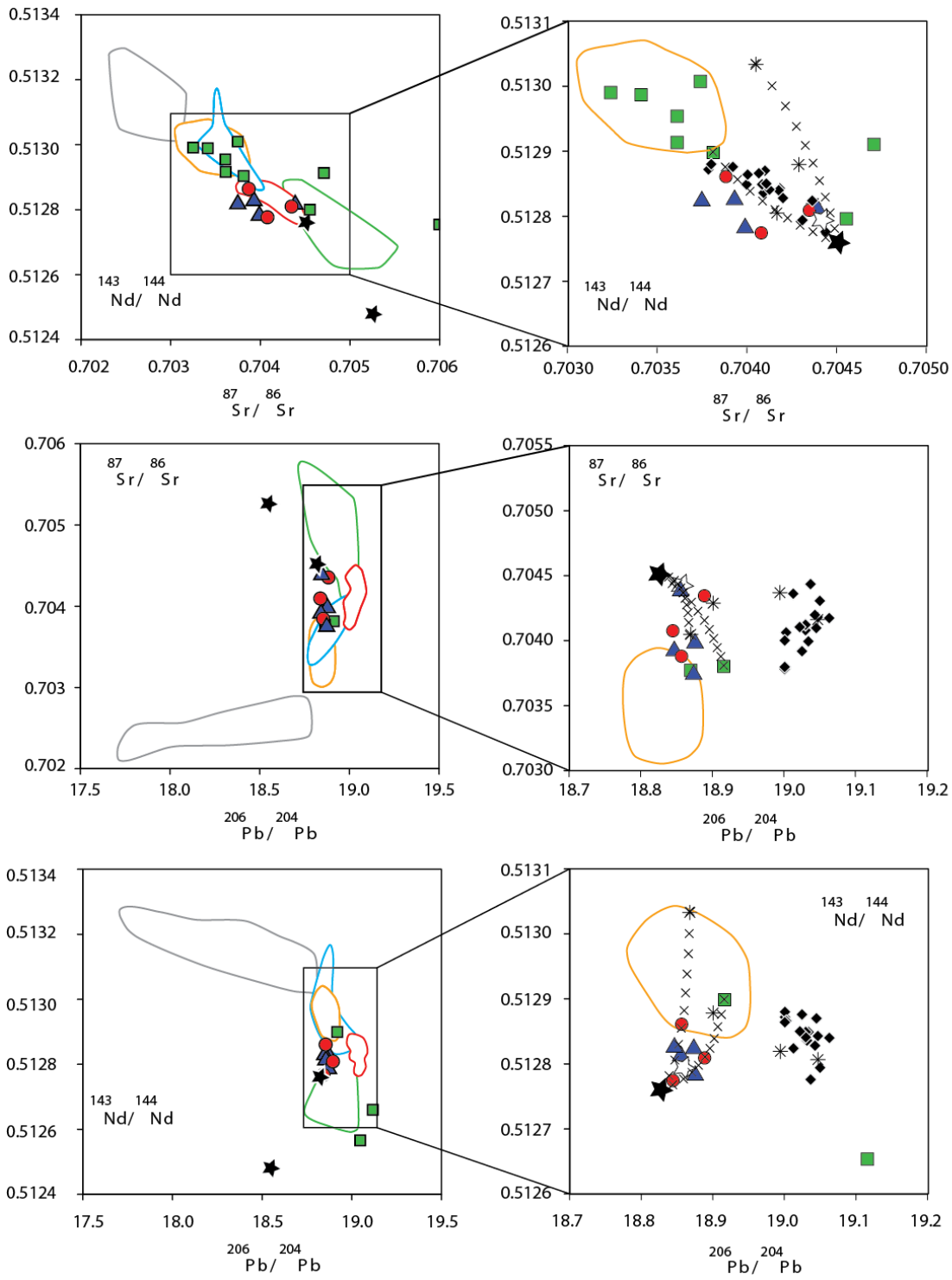

Figure 3.15a: Whole rock radiogenic isotopes of the various groups of lavas of the Strawberry Volcanics and lavas of theCRBG (Wolff et al., 2008).

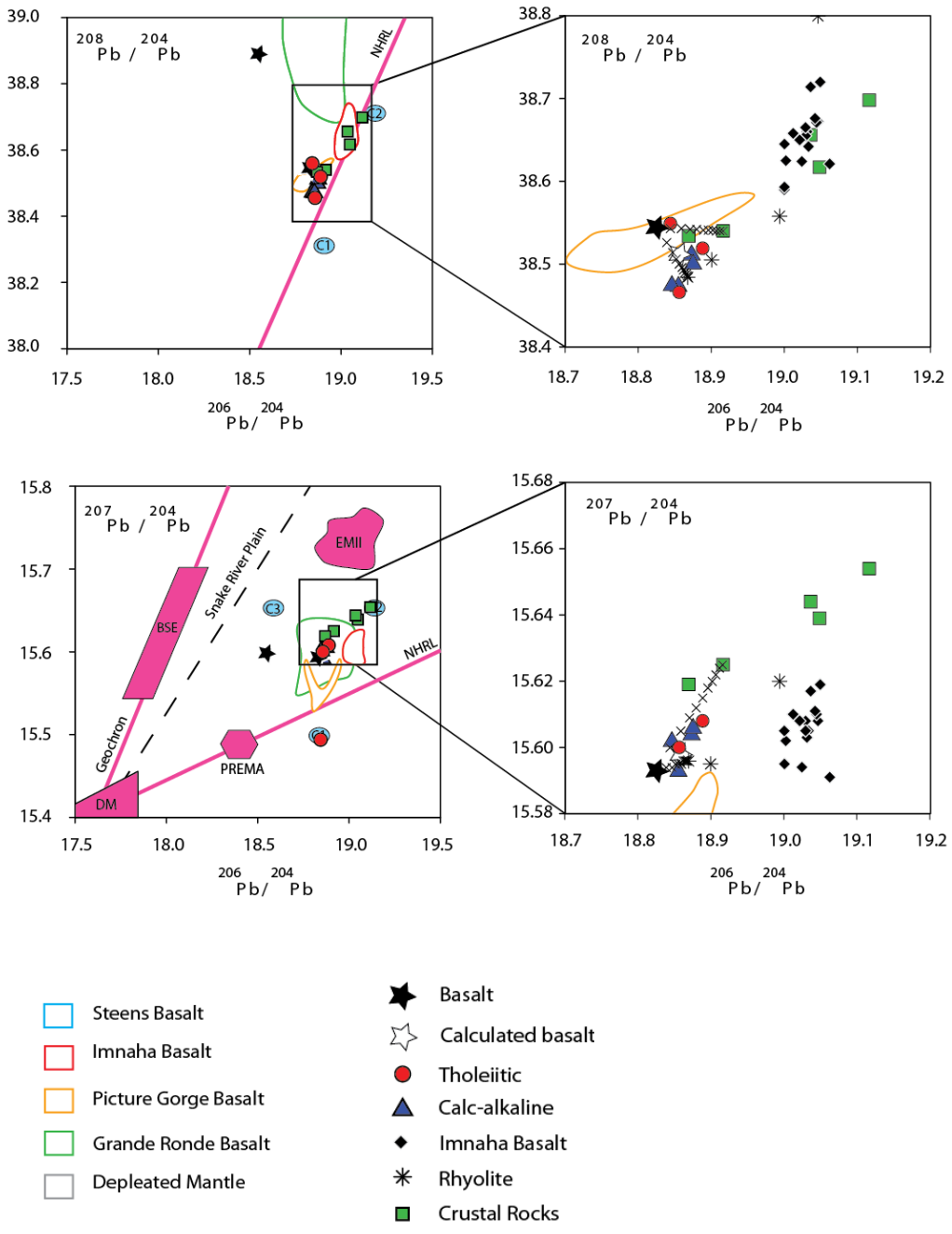

Figure 3.15b: Whole rock radiogenic isotopes of the various groups of lavas of the Strawberry Volcanics and lavas of the CRBG (Wolff et al., 2008) (continued). Tick marks represent calculated mixing line with the Strawberry Volcanic basalt (AS-SV-11) and crustal rock (AS-BASRX-01) and rhyolite (AS-SV-151). NHRL (Northern Hemisphere Reference Line) for reference, DM (depleted mantle), EMII (enriched mantle II), BSE (bulk silica Earth), PREMA (prevalent mantle). Fields are after Zindler and Hart (1986), Staudigel et al. (1984), Hamelin et al. (1986) and Wilson (1989).

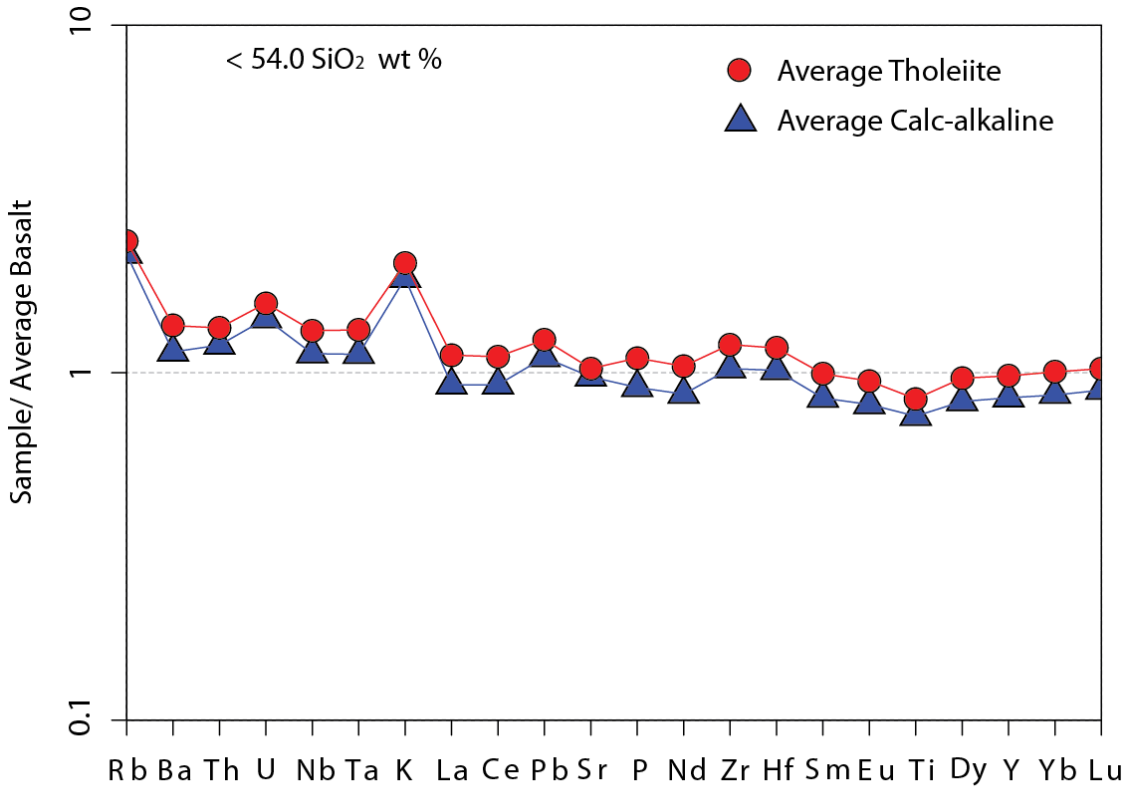

Figure 3.16: Multi-variable diagram of average samples of < 54.0 SiO_2 wt % normalized to the average basalt for a comparison.

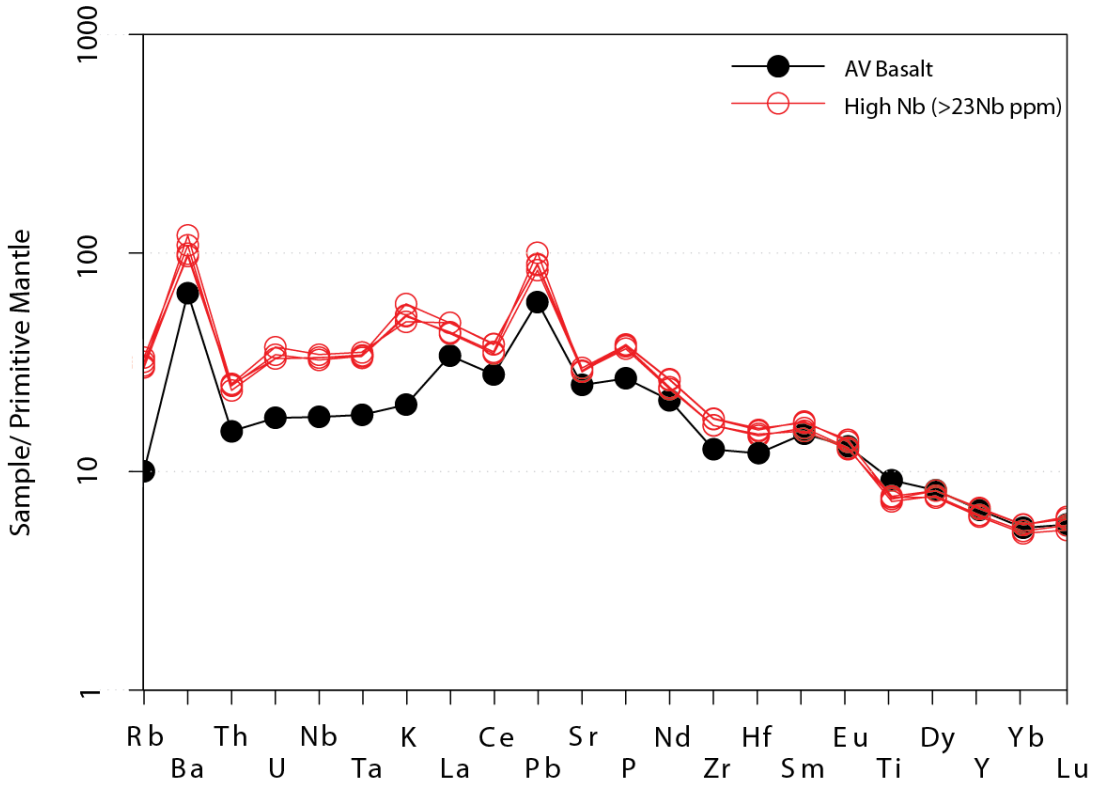

Figure 3.17: Normalized to primitive mantle multi-variable diagram with highest Nb concentrations (>23 Nb ppm) of tholeiitic intermediate lavas and average basalt for comparison.

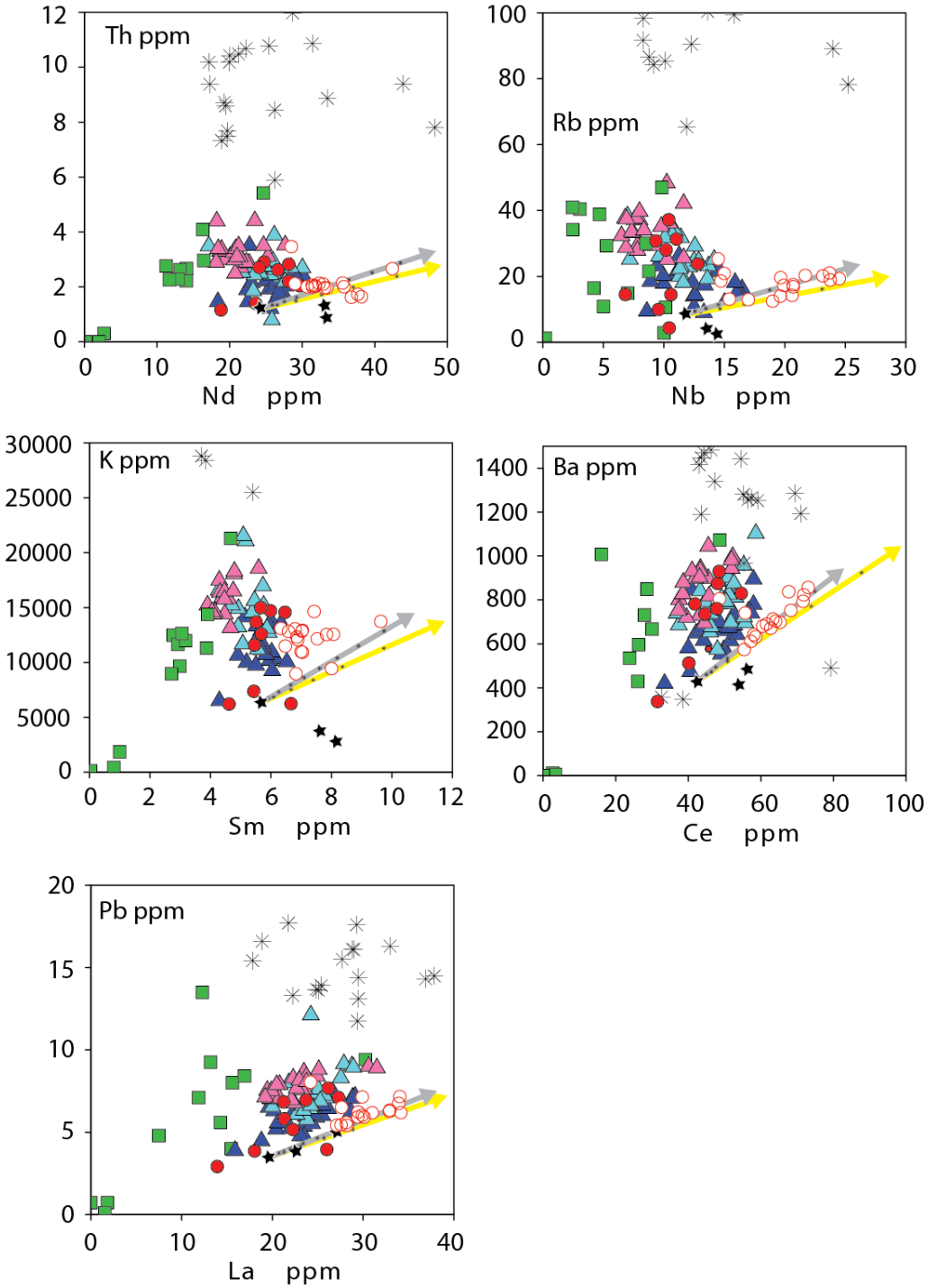

Figure 3.18: Whole rock trace and REE diagrams of the various groups of lavas of the Strawberry Volcanics. Included are FC (yellow arrow) and AFC (light gray arrow) lines. The AFC line ends at 54% crystallization and the FC line has hash marks every 5% increase. Also included is a color scale of various SiO_2 wt. % of the calc-alkaline lavas (triangles). Dark blue triangles are lavas between 52 and 56 SiO_2 wt. %, light blue triangle are 56 and 60 SiO_2 wt. %, and pink triangles are 60 and 63 SiO_2 wt. %. See text for further information.

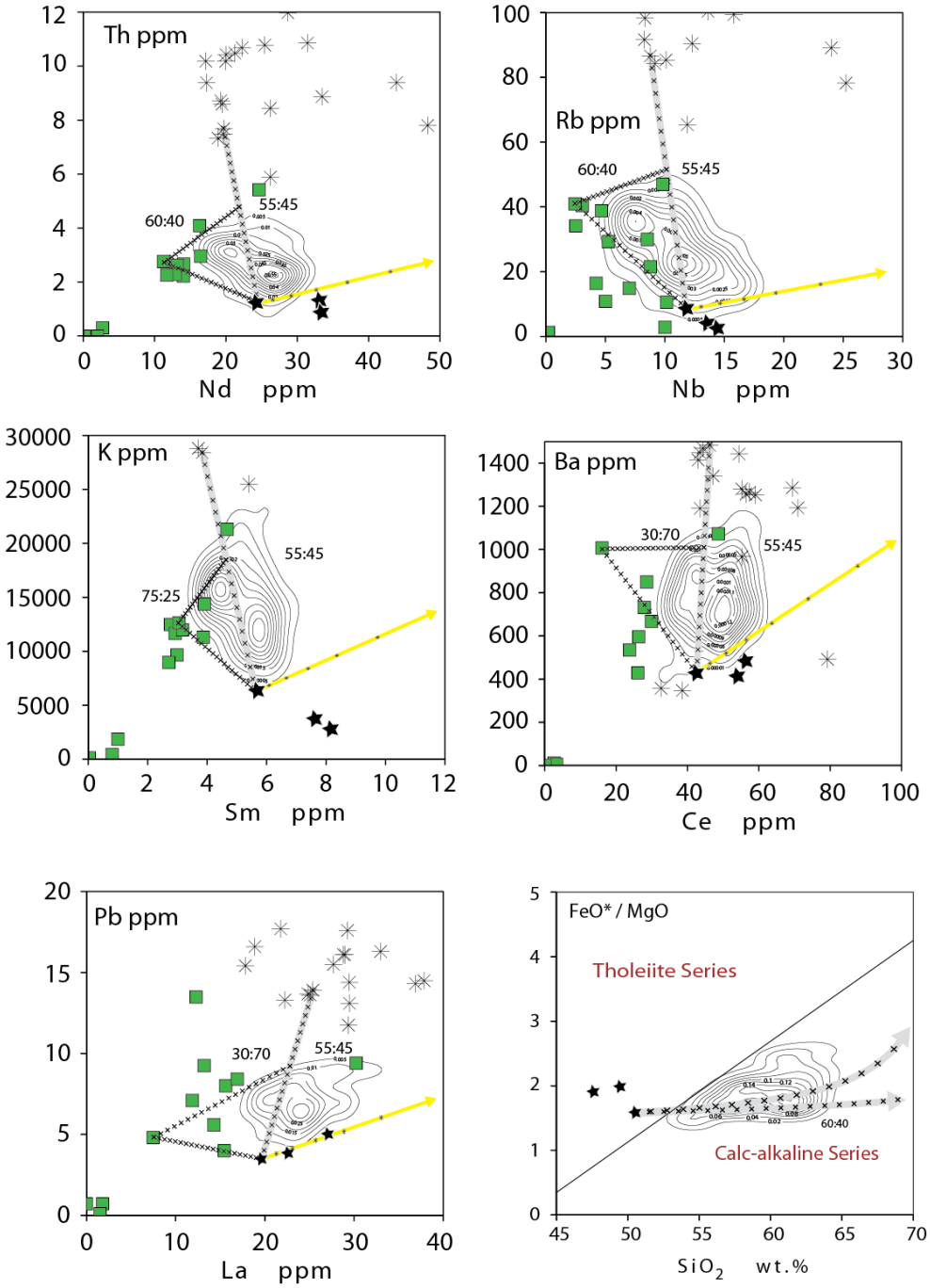

Figure 3.19: Selected incompatible trace element Harker diagrams with calculated paths of three component mixing. Selected trace element diagrams include probability density contours of the calc-alkaline lavas shown in Figure 3.18. Along with the observed data are mixing lines between three different end-members including: 1) a basalt, 2) a rhyolite, and 3) local crust. Also plotted is the same FC path in Figure 3.18 for reference. Mixing lines are also plotted for FeO*/MgO vs SiO2 wt. % the mixing line which curves upwards is mixing with the rhyolite end-member and the straight path is mixing with the basement end-member

REFERENCES

Arculus, R. J. 2003. Use and Abuse of the Terms Calcalkaline and Calcalkalic. *Journal of Petrology,* 44, 929-935.

Askren, D.R. Roden. M.F. & Whitney, J.A. 1997. Petrogenesis of Tertiary andesite lava flows interlayered with large-volume felsic ash-flow tuffs of the western USA. *Journal of Petrology,* 38, 1021-1046.

Bacon, C. R. & Druitt, T. H. 1988. Compositional evolution of the zoned calcalkaline magma chamber of Mount Mazama, Crater Lake, Oregon. *Contributions to Mineralogy and Petrology*, 98, 224–256.

Baksi, A. K. 1989. Reevaluation of the timing and duration of extrusion of the Imnaha, Picture Gorge, and Grande Ronde Basalts, Columbia River basalt group. *Geological Society of America Special Papers*, 239, 105-112.

Barry, T. L. Self, S. Kelley, S.P. Reidel, S. Hooper, P. Widdowson. M. 2010. New $^{40}Ar/^{39}Ar$ dating of the Grande Ronde lavas, Columbia River Basalts, USA: Implications for duration of flood basalt eruption episodes. *Lithos,* 118 (3–4) 213-222. http://dx.doi.org/10.1016/j.lithos.2010.03.014

Barry, T. L. Kelley, S. P. Reidel, S. P. Camp, V. E. Self, S. Jarboe, N. A. and Renne, P. R. 2013. Eruption chronology of the Columbia River Basalt Group, *Geological Society of America Special Papers*, 497, 45-66.

Bowen, N. L. 1928. The Evolution of the Igneous Rocks. Princeton, NJ: Princeton University Press.

Boynton, W.V. 1984. Cosmochemistry of the rare earth elements; meteorite studies. In: Rare earth element geochemistry. Henderson, P. (Editors), Elsevier Science Publication Co., Amsterdam. 63-114.

Brandon, A. D. Goles, G. G. 1988. A Miocene subcontinental plume in the Pacific Northwest: geochemical evidence. *Earth and Planetary Science Letters*, 88(3–4), 273-283. http://dx.doi.org/10.1016/0012-821X(88)90084-2

Brandon, A. D. Hooper, P. R. Goles, G. G. & Lambert, R. St. J. 1993. Evaluating crustal contamination in continental basalts: The isotopic composition of the Picture Gorge Basalt of the Columbia River Basalt Group. *Contributions to Mineralogy and Petrology,* 114, 452–464.

Brandon, A.D. Goles, G.G. 1995. Assessing subcontinental lithospheric mantle sources for basalts: Neogene volcanism in the Pacific Northwest, USA as a test case. *Contributions to Mineralogy and Petrology,* 121, 364–379.

Brooks, H.C. & Ferns, M.L. 1979. Geologic map of the Bull Run Rock quadrangle, Oregon. *Oregon Department of Geology and Mineral Industries, Portland, OR. Open-File Report O*-79-6, scale 1:24,000.

Brown, C.E. & Thayer, T.P. 1966a. Geologic map of the Canyon City quadrangle, northeastern Oregon. *Washington D.C. U.S. Geological Survey Miscellaneous Investigations Map* 447, scale 1:250,000.

Brown, C.E. & Thayer, T.P. 1966b. Geologic map of the Mount Vernon quadrangle, Grant County. *Washington D.C. U.S. Geological Survey* Geologic *Quadrangle Map* GQ-548, scale 1:62,500.

Brown, C.E. &Thayer, T.P. 1977. Geologic map of pre-Tertiary rocks in the eastern Aldrich Mountains and adjacent areas to the south, Grant County, Oregon. *Reston, VA. U.S. Geological Survey Miscellaneous Investigations Map* 1021, scale 1:62,500.

Brown, R.J. Blake, S. Thordarson, T. and Self, S. 2014. Pyroclastic edifices record vigorous lava fountains during the emplacement of a flood basalt flow field, Roza Member, Columbia River Basalt Province, USA. *Geological Society of America Bulletin*, 126, 875-891. doi:10.1130/B30857.1.

Brueseke, M.E. and Hart, W.K. 2008. Geology and Petrology of the Mid-Miocene Santa Rosa–Calico Volcanic Field, Northern Nevada. *Nevada Bureau of Mines and Geology Bulletin*, 113, 44.

Brueseke, M.E. & Hart, W.K. 2009. Intermediate composition magma production in an intracontinental setting: Unusual andesites and dacites of the mid-Miocene Santa Rosa–Calico volcanic field, Northern Nevada. *Journal of Volcanology and Geothermal Research*, 188, 197-213.

Brueseke, M. E. Callicoat, J. S. Hames, W. and Larson, P. B. 2014. Mid-Miocene rhyolite volcanism in northeastern Nevada: The Jarbidge Rhyolite and its

relationship to the Cenozoic evolution of the northern Great Basin (USA). *Geological Society of America Bulletin,* 126(7-8), 1047-1067.

Camp, V. E. & Hooper, P. R. 1981. Geologic studies of the Columbia Plateau: Part I. Late Cenozoic evolution of the southeast part of the Columbia River Basalt Province. *Geological Society of America Bulletin,* 92, 659–668.

Camp, V. E. Ross, M. E. & Hanson, W. E. 2003. Genesis of flood basalts and Basin and Range volcanic rocks from Steens Mountain to the Malheur River Gorge, Oregon. *Geological Society of America Bulletin,* 115, 105–128.

Camp, V. E. and Ross, M. E. 2004. Mantle dynamics and genesis of mafic magmatism in the intermontane Pacific Northwest. *Journal of Geophysical Research,* 109. doi:10.1029/2003JB002838.

Camp, V. E. Ross, M. E. Duncan, R. A. Jarboe, N. A. Coe, R. S. Hanan, B. B. and Johnson, J. A. 2013. The Steens basalt: Earliest lavas of the Columbia River basalt group. *Geological Society of America Special Papers*, 497, 87-116.

Carlson, R.W. 1984. Isotopic constraints on Columbia River flood basalt genesis and the nature of the subcontinental mantle. *Geochimica et Cosmochimica Acta*, 48, 2357-2372.

Christiansen R.L. 2001. The Quaternary and Pliocene Yellowstone Plateau Volcanic Field of Wyoming, Idaho, and Montana. *U.S. Geological Survey Professional Paper*, 729-G. 145.

Christiansen, E.H. & McCurry, M. 2008. Contrasting origins of Cenozoic silicic volcanic rocks from the western Cordillera of the United States. *Bulletin of Volcanology*, 70, 251–267.

Clemens, J. D. & Wall, V. J. 1984. Origin and evolution of a peraluminous ignimbrite suite: the Violet Town Volcanics. *Contributions to Mineralogy and Petrology*, 88, 354–371.

Clemens, J. D. 2003. S-type granite—petrogenetic issues, models and evidence. *Earth-Science Reviews,* 61, 1–18.

Clynne, M. A. 1999. A complex magma mixing origin for rocks erupted in 1915, Lassen Peak, California. *Journal of Petrology,* 40, 105-132.

Coble, M.A. & Mahood, G.A. 2012. Initial impingement of the Yellowstone plume located by widespread silicic volcanism contemporaneous with Columbia River flood basalts. *Geology,* 40, 655-658.

Crowley, K.C. 1960. Geology of the Seneca-Silvies area, Grant County, Oregon. *University of Oregon, Eugene, Unpublished thesis map*, scale 1:55,000.

DePaolo, D. J. 1981. Trace element and isotopic effects of combined wallrock assimilation and fractional crystallization. *Earth and planetary science letters*, 53(2), 189-202.

DePaolo, D. J. Perry, F. V. & Baldridge, W. S. 1992. Crustal versus mantle sources in granitic magmas: a two-parameters model based on Nd isotope studies. *Transactions of the Royal Society of Edinburgh*, 83, 439–446.

Duncan, R. A. and Keller, R. A. 2004. Radiometric ages for basement rocks from the Emperor Seamounts, ODP Leg 197. *Geochemistry Geophysics Geosystems,* 5. http://dx.doi.org/10.1029/2004GC000704.

Dungan, M.A. and Davidson, J.P. 2004. Partial assimilative recycling of the mafic plutonic roots of arc volcanoes: An example from the Chilean Andes. *Geology,* 32, 773–776. doi: 10.1130/G20735.1.

Eichelberger, J. C. 1975. Origin of andesite and dacite: evidence of mixing at Glass Mountain in California and at other Circum- Pacific volcanoes. *Geological Society of America Bulletin,* 86, 1381-1391.

Ewart, A. Schön, R.W. & Chappell, B.W. 1982. The Cretaceous volcanic-plutonic province of the central Queensland (Australia) coast - a rift-related 'calc-alkaline' province. *Transactions of the Royal Society of Edinburgh,* 83, 327-346.

Fenner, C. N. 1929. The crystallization of basalts. *American Journal of Science* 18, 225-253.

Ferns, M.L. Brooks, H.C. & Avery, D.G. 1983. Geology and gold deposits of the Greenhorn quadrangle, Baker and Grant Counties, Oregon. *Oregon Department of Geology and Mineral Industries, Portland, OR,* GMS-28, scale 1:24,000.

Ferns, M. L. Madin, I. P. & Taubeneck, W. H. 2001. Reconnaissance Geologic Map of the La Grande 30’ x 60’ quadrangle, Baker, Grant, Umatilla, and Union Counties, Oregon. *Oregon Department of Geology and Mineral Industries Reconnaissance Map,* RMS-1, scale 1:100,000.

Ferns, M.L. & McClaughry, J.D. 2013. Stratigraphy and volcanic evolution of the middle Miocene to Pliocene La Grande – Owyhee eruptive axis in eastern Oregon. *Geological Society of America Special Paper*, 497, 401-427.

Foley, S.F. Jackson, S.E. Fryer, B.J. Greenough, J.D. and Jenner, G.A. 1996. Trace element partition coefficients for clinopyroxene and phlogopite in an alkaline lamprophyre from Newfoundland by LAM-ICP-MS. *Geochimica et Cosmochimica Acta*, 60(4): 629-638. doi: 10.1016/0016-7037(95)00422-X.

Fruchter, J. S. and Baldwin, S. F. 1975. Correlations between dikes of the Monument swarm, central Oregon, and Picture Gorge Basalt flows. *Geological Society of America Bulletin*, 86(4), 514-516.

Fujimaki, H. Tatsumoto, M. and Aoki, K.-i. 1984. Partition coefficients of Hf, Zr, and REE between phenocrysts and groundmasses. *Journal of Geophysical Research*, 89: 662-672.

Gill, J.B. 1981. Orogenic Andesites and Plate Tectonics, Springer, Berlin, 390.

Greene, R.C. Walker, G.W. & Corcoran, R.E. 1972. Geologic map of the Burns quadrangle, Oregon. *United States Geological Survey, Interpretive Map* I-680, scale 1:250,000.

Green, R.C. 1973. Petrology of the welded tuff of Devine Canyon, southeastern Oregon. *United States Geological Survey, Professional Paper*, 797, 1-26.

Grove, T. L. and Baker, M. B. 1984. Phase equilibrium controls on the tholeiitic versus calc-alkaline differentiation trends. *Journal of Geophysical Research,* 89: 3253-3274.

Goles, G.G. Brandon, A.D. & Lambert, R. St. J. 1989. Miocene basalts of the Blue Mountains province in Oregon: Part 2, Sr isotopic ratios and trace element features of little-known Miocene basalts of central and eastern Oregon. In: Volcanism and Tectonism in the Columbia River Flood Basalt Province. *Geological Society of America, Special Paper,* 239, 357-365.

Gunnarsson, B. Marsh, B. D. & Taylor, H. P. U. R. Jr. 1998. Generation of Icelandic rhyolites: silicic lavas from the Torfajokull central volcano. *Journal of Volcanology and Geothermal Research,* 83, 1–45.

Harangi, S. Downes, H. Thirlwall, M. & Gméling, K. 2007. Geochemistry, Petrogenesis and Geodynamic Relationships of Miocene Calc-alkaline Volcanic Rocks in the Western Carpathian Arc, Eastern Central Europe. *Journal of Petrology,* 48, 2261-2287.

Hawkesworth, C. Turner, S. Gallagher, K. Hunter, A. Bradshaw, T. & Rogers, N. 1995. Calc-alkaline magmatism, lithospheric thinning and extension in the Basin and Range. *Journal of Geophysical Research,* 100, 10271-10286.

Hildreth, W. 1981. Gradients in silicic magma chambers: implications for lithospheric magmatism. *Journal of Geophysical Research,* 86, 10153–10192.

Hildreth, W. and Moorbath, S. 1988. Crustal contributions to arc magmatism in the Andes of central Chile: *Contributions to Mineralogy and Petrology*, 98, 455–489.

Hildreth, W. & Fierstein. J. 2000. Katmai volcanic cluster and the great eruption of 1912. *Geological Society of America Bulletin*, 112, 1594–1620.

Hooper, P.R. and Hawkesworth, C.J. 1993. Isotope and geochemical constraints on the origins and evolution of the Columbia River Basalt. *Journal of Petrology*, 34, 1203-1246.

Hooper, P.R. Bailey, D.G. McCarley Holder, G.A. 1995. Tertiary calc-alkaline magmatism associated with lithospheric extension in the Pacific Northwest. *Journal of Geophysical Research*, 100, 10,303–10,319.

Hooper, P.R. Binger, G.B. & Lee, K.R. 2002. Ages of the Steens and Columbia River flood basalts and their relationship to extension-related calc-alkalic volcanism in eastern Oregon. *Geological Society of America, Bulletin*, 114, 43-50.

Hora, J. M. Singer, B. S. Wörner, G. Beard, B. L. Jicha, B. R. & Johnson, C. M. 2009. Shallow and deep crustal control on differentiation of calc-alkaline and tholeiitic magma. *Earth and Planetary Science Letters*, 285, 75-86.

Irvine,T. N. & Baragar,W. R. A. 1971. A guide to the chemical classification of the common volcanic rocks. *Canadian Journal of Earth Sciences*, 8, 523-548.

Jakes, P. & Gill, J. 1970. Rare earth elements and the island arc tholeiitic series. *Earth and Planetary Science Letters*, 9, 17-28.

Jarboe, N.A. Coe, R.S. Renne, P.R. Glen, J.M.G. and Mankinen, E.A. 2008. Quickly erupted volcanic sections of the Steens Basalt, Columbia River Basalt Group: Secular variation, tectonic rotation, and the Steens Mountain reversal. *Geochemistry Geophysics Geosystems,* 9, 1525-2027. doi:10.1029/2008GC002067.

Jarboe, N. A. Coe, R. S. Renne, P. R. & Glen, J. M. 2010. The age of the Steens reversal and the Columbia River Basalt Group. *Chemical Geology*, 274(3), 158-168.

Jordan, B.T. Grunder, A.L. Duncan, R.A. & Deino, A.L. 2004. Geochronology of age-progressive volcanism of the Oregon High Lava Plains: Implications for the plume interpretation of Yellowstone. *Journal of Geophysical Research,* 109(B10), 1978-2012. doi: 10.1029/2003JB002776.

Koppers, A.A.P. 2002. ArArCALC – software for Ar-40/Ar-39 age calculations. *Computers & Geosciences*, 28(5), 605-619.

Kuiper, K. F. Deino, A. Hilgen, F. J., Krijgsman, W., Renne, P. R. and Wijbrans, J. R. 2008. Synchronizing rock clocks of Earth history. *Science*, 320(5875), 500-504.

Kuno, H. 1950. Petrology of Hakone volcano and the adjacent areas, Japan. *Geological Society of America Bulletin*, 61, 957-1014.

Kuno, H. 1959. Origin of Cenozoic petrographic provinces of Japan and surrounding areas. *Bulletin of Volcanology*, 20, 37-76.

Kuno, H. 1968. Differentiation of basalt magmas. In: Hess, H. H. & Poldervaart, A. (eds) Basalts, The Poldervaart Treatise on Rocks of Basaltic Composition,Volume 2. NewYork*: Interscience*, 623-688.

Kürkcüoglu, B.S. Sen, E. Temel, A. Aydar, E. & Gourgaud, A. 2001. Trace-element modeling and source constraints for tholeiitic and calc-alkaline basalts from a depleted ashenospheric mantle source, Mt. Erciyes Stratovolcano, Turkey. *International Geology Review*, 43, 508-522.

LaMaskin, T.A., Schwartz, J.J., Dorsey, R.J., Snoke, A.W., Johnson, K., and Vervoort, J.D., 2009b, Mesozoic sedimentation, magmatism, and tectonics in the Blue Mountains Province, northeastern Oregon, Volcanoes to Vine. Geology Field Trips *Geological Society of America*, *Field Guide 15*, p. 187–202.

LaMaskin, T. A. Vervoort, J. D. Dorsey, R. J. Wright, J. E. 2011. Early Mesozoic paleogeography and tectonic evolution of the western United States: Insights from detrital zircon U-Pb geochronology, Blue Mountains Province, northeastern Oregon. *Geological Society of America Bull*etin, 123 (9-10), 1939-1965.

Langer, V. 1991. Geology and petrologic evolution of the silicic to intermediate volcanic rocks underneath Steens Mountain basalt, southeastern Oregon. *Oregon State University, Corvallis, OR, Unpublished MS thesis*, 109.

Large, A.M. Streck, M. J. Hess, E.N. Janzen, R.D. and Ferns, M.L. 2015. Rhyolites of Dooley Mountain and Buchanan, Oregon: Silicic Volcanism at the Northern and

Western Extension of the Columbia River Basalt Rhyolite Flair-Up. *Geological Society of America,* Abstracts with Programs. 47 (4), 47**.**

Larsen, L.M. 1979. Distribution of Ree and Other Trace-Elements between Phenocrysts and Peralkaline Undersaturated Magmas, Exemplified by Rocks from the Gardar Igneous Province, South Greenland. *Lithos*, 12(4): 303-315. doi: 10.1016/0024-4937(79)90022-7.

Le Bas, M. J. Le Maitre, R. W. Streckeisen, A. & Zanettin, B. 1986. A chemical classification of volcanic rocks based on the total alkali–silica diagram. *Journal of Petrology,* 27, 745–750.

Leeman, W. P. Smith, D.R. Hildreth, W. Palacz, Z. & Rogers, N. 1990. Compositional diversity of Late Cenozoic basalts in a transect across the southern Washington Cascades: Implications for subduction zone magmatism. *Journal of Geophysical Research,* 95(B12), 19561–19582.

Lindsay, J. M. Schmitt, A. K. Trumbull, R. B. De Silva, S. L. Siebel, W. & Emmermann, R. 2001. Magmatic evolution of the La Pacana caldera system, Central Andes, Chile: compositional variation of two cogenetic, large-volume felsic ignimbrites. *Journal of Petrology,* 42, 459–486.

Lipman, P. W. Prostka, H. J. & Christiansen, R. L. 1972. Cenozoic volcanism and plate-tectonic evolution of the Western United States. I. Early and Middle Cenozoic. *Royal Society of London Philosophical Transactions,* 271, 217-248.

Lipman, P.W. 2000. The central San Juan caldera cluster: Regional volcanic framework. In P.M. Bethke and R.L. Hay, Eds., Ancient Lake Creede: Its Volcano- Tectonic Setting, History of Sedimentation, and Relation of Mineralization in the Creede Mining District. *Geological Society of America Special Paper,* 346, 9–69.

Mahood, G. A. & Halliday, A. N. 1988. Generation of high-silica rhyolite: a Nd, Sr, and O isotopic study of Sierra La Primavera, Mexican neovolcanic belt. *Contributions to Mineralogy and Petrology,* 100, 183–191.

Matsui, Y. Onuma, N. Nagasawa, H. Higuchi, H. and Banno, S. 1977. Crystal structure control in trace element partition between crystal and magma. *Tectonics,* 100: 315-324.

McDonough, W. F. & Sun, S.S. 1995. The composition of the Earth. *Chemical Geology,* 120, 223-253.

McKenzie, D. and O'Nions, R.K. 1991. Partial melt distributions from inversion of rare Earth element concentrations. *Journal of Petrology,* 32, 1,021-1,091.

Michael, P. J. 1984. Chemical differentiation of the Cordillera Paine granite (Southern Chile) by in situ fractional crystallization. *Contributions to Mineralogy and Petrology,* 87, 179–195.

Miyashiro, A. 1974. Volcanic rock series in island arcs and active continental margins. *American Journal of Science,* 274, 321–355.

Mullen, E.D. 1983. Petrology and regional setting of peridotite and gabbro of the Canyon Mountain complex, northeast Oregon. *University of Oregon, Eugene, OR unpublished Ph.D. dissertation*, map scale 1:12,000.

Munksgaard, N. C. 1984. High $d^{18}O$ and possibly pre-eruptional Rb–Sr isochrons in cordierite-bearing Neogene volcanics from SE Spain. *Contributions to Mineralogy and Petrology*, 87, 351–358.

Pichavant, M. Kontak, D. J. Briqueu, L. Herrera, J. V. & Clark, A. H. 1988a. The Miocene–Pliocene Macusani Volcanics, SE Peru, 1. Mineralogy and magmatic evolution of a two-mica aluminosilicate bearing ignimbrite suite. *Contributions to Mineralogy and Petrology*, 100, 300–324.

Pichavant, M. Kontak, D. J. Briqueu, L. Herrera, J. V. & Clark, A. H. 1988b. The Miocene–Pliocene Macusani Volcanics, SE Peru, 2. Geochemistry and origin of felsic peraluminous magma. *Contributions to Mineralogy and Petrology*, 100, 325–338.

Pierce, K. L. & Morgan, L. A. 1992. The track of the Yellowstone Hotspot: Volcanism, faulting, and uplift. *Geological Society of America, Memoir*, 179, 1-52.

Plank, T. & Langmuir, C. H. 1988. An evaluation of the global variations in the major element chemistry of arc basalts. *Earth and Planetary Science Letters*, 90, 349-370.

Reidel, S. P. Camp, V. E. Tolan, T. L. and Martin, B. S. 2013. The Columbia River flood basalt province: Stratigraphy, areal extent, volume, and physical volcanology. *Geological Society of America Special Papers*, 497, 1-43.

Renne, P. R. Swisher, C.C. Deino, A.L. Karner, D.B. Owens, T.L. & DePaolo, D.J. 1998. Intercalibration of standards, absolute ages and uncertainties in $^{40}Ar/^{39}Ar$ dating. *Chemical Geology,* 145, 117-152.

Robyn, T. L. 1977. Geology and petrology of the Strawberry Mountain volcanic series, Central Oregon. *University of Oregon, Eugene, OR, Unpublished PhD thesis*.

Robyn, T. L. 1979. Miocene volcanism in eastern Oregon—An example of calc-alkaline volcanism unrelated to subduction. *Journal of Volcanology and Geothermal Research*, 5, 149-161.

Rogers, J.W. Novitsky, J.M. and Evans, 1977. The Clarno Formation of central Oregon, U.S.A. Volcanism on a thin continental margin. *Earth and Planetary Science Letter*, 34 (1), 56-66.

Rollinson, H. 1993. Using Geochemical Data: Evaluation, Presentation, Interpretation: New York, Longman Scientific & Technical.

Rudnick, R. L. 1995. Making continental crust. *Nature*, 378, 571-578.

Rudnick, R. L. & Gao, S. 2003. The composition of the continental crust. *The Crust,* Oxford: Pergamon, pp. 1-64.

Schnetzler, C.C. and Philpotts, J.A. 1970. Partition coefficients of rare-earth elements between igneous matrix material and rock-forming mineral phenocrysts; II.

Geochimica et Cosmochimica Acta, 34(3), 331-340. doi: 10.1016/0016-7037(70)90110-9.

Schwartz, J. J. Snoke, A. W. Frost, C. D. Barnes, C. G. Gromet, L. P. 2010. Analysis of the Wallowa-Baker terrane boundary: Implications for tectonic accretion in the Blue Mountains province, northeastern Oregon. *Geological Society of America Bulletin*, 122 (3-4), 517-536.

Shervais, J. W. and Hanan, B. B. 2008. Lithospheric topography, tilted plumes, and the track of the Snake River–Yellowstone hot spot. *Tectonics*, 27(5).

Smith, D. R. & Leeman, W. P. 1987. Petrogenesis of Mount St. Helens dacitic magmas. *Journal of Geophysical Research*, 92, 10,313-10,334.

Smith, I. E. M. Stewart, R. B. & Price, R. C. 2003. The petrology of a large intra-oceanic silicic eruption: the Sandy Bay Tephra, Kermadec Arc, Southwest Pacific. *Journal of Volcanology and Geothermal Research*, 124, 173–194.

Steiger, R. H. & Jäger, E. 1977. Subcommision on geochronology: Convention on the use of decay constants in geo- and cosmochronology. *Earth Planetary Sciences Letters*, 36, 359–362.

Steiner, A.R. & Streck, M.J. 2011. Strawberry Rhyolites, Oregon: Northwestern extent of mid-Miocene flood basalt related rhyolites of the Pacific Northwest. *2011, Fall Meeting, American Geophysical Union, San Francisco, CA,* Abstract T51H-2473, Dec 5-9.

Steiner, A.R. Browne, B.L. & Nye, C.J. 2012. Quenched mafic inclusions in ≤ 2200 years B.P. deposits at Augustine Volcano, Alaska. *International Geology Review,* 54(11), 1241-1270. doi:10.1080/00206814.2011.636641.

Steiner, A. R., & Streck, M. J. 2013. The Strawberry Volcanics: generation of 'orogenic' andesites from tholeiite within an intra-continental volcanic suite centered on the Columbia River flood basalt province, USA. *Geological Society, London, Special Publications*, 385(1), 281-302.

Streck, M.J. & Grunder A.L. 1995. Crystallization and welding variations in a widespread ignimbrite sheet: The Rattlesnake Tuff, eastern Oregon. *Bulletin of Volcanology*, 57, 151-169.

Streck, M.J. Ferns, M. Ricker, C. 2011. The Dinner Creek Tuff and other mid-Miocene rhyolites at the magmatic focal zone of the Columbia River Basalt group. *Geological Society of America,* Abstracts with Programs, 43(4), 5.

Streck, M.J. & Grunder A.L. 2012. Temporal and crustal effects on differentiation of tholeiite to calcalkaline and ferro-trachytic suites, High Lava Plains, Oregon, USA. *Geochemical, Geophysical, Geosystems*, 13(11). doi:10.1029/2012GC004237.

Streck, M. J. 2014. Evaluation of crystal mush extraction models to explain crystal-poor rhyolites. *Journal of Volcanology and Geothermal Research*, 284, 79-94.

Streck, M. J. Ferns, M. L. and McIntosh, W. 2015. Large, persistent rhyolitic magma reservoirs above Columbia River Basalt storage sites: The Dinner Creek Tuff Eruptive Center, eastern Oregon. *Geosphere*, 11(2), 226-235.

Sisson, T. W. and Grove, T.L. 1993. Experimental investigations of the role of H2O in calc-alkaline differentiation and subduction zone magmatism. *Contribution to Mineralogy and Petrology,* 113 (2), 143–166.

Sun, S.-S. & McDonough, W.F. 1989. Chemical and isotopic systematics of oceanic basalts: implications for mantle composition and processes. *Geological Society of London Special Publication,* 42(1), 313-345.

Swanson, D. A. and Robinson, P. T. 1968. Base of the John Day Formation in and near the Horse Heaven mining district, north-central OR, Geological Survey research 1968: U.S. *Geological Survey Professional Paper*, 600, 154-161.

Swanson, D.A. Wright, T.L. and Helz, R.T. 1975. Linear vent systems and estimated rates of magma production and eruption for the Yakima Basalt on the Columbia Plateau. *American Journal of Science,* 275 (8), 877–905. doi:10.2475/ajs.275.8.877.

Tatsumi, Y. Takahashi, T. Hirahara, Y. Chang, Q. Miyazaki, T. Kimura, J. I. & Sakayori, A. 2008. New insights into andesite genesis: the role of mantle-derived calc-alkalic and crust-derived tholeiitic melts in magma differentiation beneath Zao Volcano, NE Japan. *Journal of Petrology,* 49(11), 1,971-2,008.

Taylor, S. R. 1995. Cosmochemistry; potassium tells a tale. *Nature*, 376, 20-21.

Thayer, T.P. 1956. Preliminary geologic map of the John Day quadrangle, Oregon. *U.S. Geological Survey, Washington, D.C. Miscellaneous Field Studies Map* MF-51, scale 1:62,500.

Thayer, T.P. 1957. Some relations of later Tertiary volcanology and structure in eastern Oregon. *International Geological Congress 20th*, Mexico, Sec. 1, Volcanologia del Cenozoico, 1, 231.

Thayer, T.P. Brown, C.E. & Hay, R.L. 1967. Preliminary geologic map of the Prairie City quadrangle, Grant County, Oregon. *U.S. Geological Survey Open File Map,* scale 1:62,500.

Thordarson, T. and Self, S. 1998. The Roza Member, Columbia River Basalt group: A gigantic pahoehoe lava flow field formed by endogenous process?. *Journal of Geophysical Research: Solid Earth*, 103(B11), 1,978-2,012.

Villemant, B. 1988. Trace-Element Evolution in the Phlegrean Fields (Central-Italy) - Fractional Crystallization and Selective Enrichment. *Contributions to Mineralogy and Petrology*, 98(2), 169-183.

Wager, L. R. & Deer,W. A. 1939. Geological investigations in East Greenland. Part III. The petrology of the Skaergaard intrusion, Kangerdlugssuaq, East Greenland. *Meddelelser om Gronland,* 105, 352.

Whalen, J. B. Currie, K. L. and Chappell, B. W. 1987. A-type granites: geochemical characteristics, discrimination and petrogenesis. *Contributions to Mineralogy and Petrology,* 95(4), 407-419.

Wilcox, R. E. & Fisher, R. V. 1966. Geologic map of the Monument quadrangle, Grant County, Oregon. *U.S. Geological Survey,* Geology Quadrangle Map GQ-541.

Wolff, J.A. Ramos, F.C. Hart, G.L. Patterson, J.D. & Brandon, A.D. 2008. Columbia River flood basalts from a centralized crustal magmatic system. *Nature geoscience,* 1, 177 -180.

Zanetti, A. Tiepolo, M. Oberti, R. and Vannucci, R. 2004. Trace-element partitioning in olivine: modeling of a complete data set from a synthetic hydrous basanite melt. *Lithos,* 75, 39-54.

Zielinski, R. A. & Lipman, P. W. 1976. Trace-element variations at Summer Coon volcano, San Juan Mountains, Colorado, and the origin of continental-interior andesite. *Geological Society of America, Bulletins,* 87(10), 1477-1485.

Zimmer, M. M. Plank, T. Hauri, E. H. Yogodzinski, G. M. Stelling, P. Larsen, J. Singer, B. Jicha, B. Mandeville, C. & Nye, C. J. 2010. The Role of Water in Generating the Calc-alkaline Trend: New Volatile Data for Aleutian Magmas and a New Tholeiitic Index. *Journal of Petrology*, 51, 2411-2444

APPENDIX A

XRF

XRF analysis attached as supplementary file. File name: Appendix_A_XRF.csv, File Type: .csv, File Size: 116 KB, Special Hardware: None

APPENDIX B

ICP-MS

ICP-MS analysis attached as supplementary file. File name: Appendix_B_ICP-MS.csv, File Type: .csv, File Size: 27 KB, Special Hardware: None

APPENDIX C

NORMS

Calculated NORMS attached as supplementary file. File name:

Appendix_C_NORMS.csv, File Type: .csv, File Size: 18 KB, Special Hardware: None

APPENDIX D

ISOTOPES

Isotope analysis attached as supplementary file. File name: Appendix_D_ISOTOPES.csv, File Type: .csv, File Size: 8 KB, Special Hardware: None

APPENDIX E

EMP-CPX

EMP analysis on CPX attached as supplementary file. File name: Appendix_E_EMP-CPX.csv, File Type: .csv, File Size: 8 KB, Special Hardware: None

APPENDIX F

EMP-OPX

EMP analysis of OPX attached as supplementary file. File name: Appendix_F_EMP-OPX.csv, File Type: .csv, File Size: 4 KB, Special Hardware: None

APPENDIX G

EMP-OLV

EMP analysis of Olivines attached as supplementary file. File name: Appendix_G_EMP-OLV.csv, File Type: .csv, File Size: 7 KB, Special Hardware: None

APPENDIX H

$^{40}Ar/^{39}Ar$ AGE ANALYSIS

$^{40}Ar/^{39}Ar$ age analysis attached as supplementary file. File name: Appendix_H_Age Analysis.pdf, File Type: .pdf, File Size: 1,614 KB, Special Hardware: None